MAX-PLANCK-INSTITUT FÜR POLYMERFORSCHUNG IN MAINZ

Synthesis of Polyphenylene Cylinders with Different Sizes and Connectivity Patterns as well as Study of their Linear Congeners

Dissertation zur Erlangung des Grades

„Doktor der Naturwissenschaften“

Am Fachbereich Chemie, Pharmazie und Geowissenschaften

der Johannes Gutenberg-Universität Mainz

Florian Ernst Golling
geboren in Gießen
Mainz im Jahr 2014

Dekan: Prof. Dr. Holger Frey

1. Berichterstatter: Prof. Dr. Klaus Müllen

2. Berichterstatter:

Tag der mündlichen Prüfung:

Die vorliegende Arbeit wurde in der Zeit vom Januar 2011 bis November 2014 am Max-Planck-Institut für Poylmerforschung in Mainz unter Betreuung von Prof. Dr. K. Müllen durchgeführt.

Ich danke Prof. Dr. Klaus Müllen für seine unterstützende und unermüdliche Diskussionsbereitschaft zur wissenschaftlichen Bearbeitung dieses interessanten Themas.

Meinen Eltern und Großeltern

“They are ill discoverers that think there is no land when they can see nothing but sea.”
(Francis Bacon)

Table of Contents

Index of Abbreviations

CNT	carbon nanotubes
COSY	correlation spectroscopy
CPP	cycloparaphenylene
CVD	chemical vapor deposition
DLS	dynamic light scattering
DDQ	2,3-dichlor-5,6-dicyano-1,4-benzoquinone
DMF	dimethyl formamide
EMPA	Eidgenössische Materialprüfungs- und Forschungsanstalt
FET	field effect transistor
GNR	graphene nanoribbons
HMBC	heteronuclear single quantum coherence
HR-MS	high resolution mass spectrometry
HPB	hexaphenylbenzene
HBC	hexa-*peri*-benzocoronone
HSQC	heteronuclear single quantum coherence
LWH	length, width, height
MALDI-MS	matrix-assisted laser desorption ionization mass spectrometry
MS	mass spectrometry
NMR	nuclear magnetic resonance
NOE	nuclear *Overhauser* effect
NOESY	nuclear *Overhauser* enhancement and exchange spectrocopy
PPC	polyphenylene cylinder
r	distance between nuclei
rGO	reduced graphene oxide
S/N	signal to noise ratio
TfOH	trifluoromethanesulfonic acid
THF	tetrahydrofuran
r.t.	room temperature

UHV	ultra-high vacuum

I. Introduction

We live in a materials world, constantly thriving for and experiencing new and improved applications. To fuel and continue technological advances, the discovery, development and processing of novel materials plays an important role. Otherwise, e.g., integrated circuits for microprocessors could not have experienced a steady miniaturization and thus an improved performance, following Moore's law;[1] also, new applications based on organic components such as organic light emitting diodes (OLEDs) would not have been realized without tailored molecular systems and novel manufacturing processes; the decrease in material's weight while maintaining or even improving its intrinsic properties, such as flexibility or ductility, serves as another example of beneficial technological developments, leading to more sustainable, efficient, cheaper or even completely new applications. This progress equally holds true for the different disciplines of material science – whether they are based on organic or inorganic matter. By combining the complementary forces of this diverse field, significant progress has been achieved and increasingly continues to do so.

To accurately obtain desired material properties, special emphasis has been put on "precision synthesis" throughout the past decades. This term refers to the preparation and development of defined target structures by means of *organic synthesis* that exactly match with the design guidelines on a molecular level and dimensions. Such defined structures enable one to carefully adjust the physical, electronic and chemical properties of the material. In *organic electronics* (OE) – part of the wide field of materials science –, electronic circuits are based on molecular systems[2] and polymers.[3] Prominent examples, representing organic devices, are OLEDs,[4-6] organic photovoltaics (OPV)s[7-10] and organic field effect transistors (OFET)s.[11] Owing to the careful molecular design in combination with sophisticated processing, electronic properties, performance, and overall lifetime could be adjusted in a way that OLEDs have already reached a commercial stage, whereas other devices require further understanding and improvement. This shows, on the one hand, that such novel materials can fulfill high hopes; however, on the other hand, they still do require further scientific efforts to bring about their full potential – on the molecular, processing and fabrication level.

The research in the field of OE has gained additional momentum, since the discovery of *graphene* by *Novoselov* and *Geim*[12] in 2004, who developed an easy preparation and, as a consequence, could elucidate its remarkable electronic and materials properties. These findings have also spurred the synthesis and investigation of polycyclic polyaromatic hydrocarbons (PAH)s which are regarded as molecular precursors and cut-outs of graphene.

Graphene can either be obtained *via* physical as well as chemical methods, using graphite or graphene oxide as precursors – among others. These methods are referred to as *top-down* approaches. By adjusting the reaction protocol and post-treatment, the physical and electronic properties can be varied. However, these methods lead to defects on the molecular level, which can pose a challenge or even severe drawback for electronic applications. Therefore, a different approach has been developed by synthetic organic chemists, where small aromatic building blocks are connected by chemical transformations which can give rise to large overstructures – the so called *bottom-up* approach. This method gives access to molecular graphenic structures with defined shape, length, width and edge structure that can also encompass solubility.[13-14] This precision synthesis enables the design of new materials[15] and paves the way for new electronic devices.[16]

Carbon Nanotubes (CNT)s, as a different carbon allotrope, are built of rolled-up graphene and have been of scientific interest since their discovery[17-19] in the early 90s, because of their interesting physical and electronic properties. CNTs can be made *via* various high temperature methods, such as arc-discharge, laser ablation, or CVD methods using gaseous carbon sources. These methods, similar to the above described top-down approaches, yield CNTs with different diameter, length and edge structure, but also defects. In addition, CNTs can also be contaminated by amorphous carbon as well as catalysts particles which require additional purification.

To overcome these drawbacks, a concise bottom-up synthesis of short segments is of high interest. The research in this area has been fueled by the seminal work of *Jasti* and *Bertozzi* in 2008, when they achieved the synthesis of cycloparaphenylenes (CPP)s.[20] This has spurred the research on the bottom-up synthesis of such structures by the groups of *Itami*, *Jasti*, *Yamago* and the *Müllen*. Suitable π-extended structural precursors for the bottom-up synthesis of CNTs are currently under investigation.

1.1. Graphene

Graphene is a carbon allotrope that consists of sp^2-hybridized carbon atoms forming a honey-comb-shaped lattice. This arises from its smallest subunit: benzene. The preparation and elucidation of its remarkable electronic properties was first achieved by *Novoselov* and *Geim* in 2004.[12] This two-dimensional material can be regarded as a precursor of CNTs and fullerenes:[21] CNTs can be obtained by rolling-up a graphene sheet, whereas fullerene is obtained by forming a sphere, however, also containing five-membered rings.

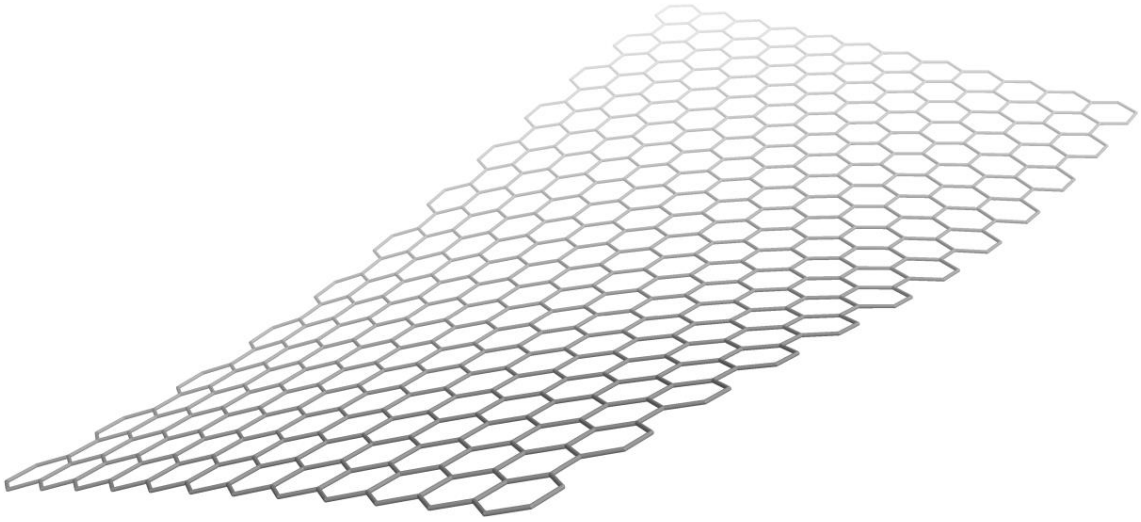

Figure 1: graphene sheet.

Graphene is neither a metal nor a semiconductor, but rather a half metal with a vanishing band gap, i.e., a zero gap semiconductor.[22] Due to its structure, it was expected to show high charge carrier mobilities, which were first theoretically predicted[23] and later on experimentally verified.[24] By suspending single layer graphene above a Si/SiO_2 gate electrode, mobilities of 200.000 $cm^2(V \cdot s)^{-1}$ were achieved. In addition, Graphene shows thermal conductivities of 3.000 -5.000 W/m·K,[25-26] which lies in the range of SW- and MWCNTs. The thermal conductivities of graphene in comparison to graphite are 30-fold higher (5000 W/m·K) and still exceed pure copper (401 W/m·K) by one order of magnitude.[27-30] Its Young's modulus is ca. 1 TPa (steel = 1.8 MPa) and it shows an intrinsic tensile strength of ca 140 GPa.[24] Its transparency to incident light is 97.7% over a wide visible range (450 nm – 720 nm). Several groups have therefore suggested the use of graphene as a transparent window electrode.[31-32]

The production of graphene can be achieved *via* mechanical exfoliation, reduction of graphene oxide or chemical vapour deposition (CVD). Mechanical exfoliation, which led to the groundbreaking results of Geim and coworkers, gives access to high quality graphene, however, its preparation is tedious and affords only small amounts. An alternative approach is to exfoliate graphene in solution which yields graphene dispersions, containing few layered-graphene or even single sheets.[33-35] They can be used for standard deposition techniques, such as spray-coating, drop-casting or ink-jet printing.[36-38]

Graphene can also be produced from graphene oxide. First, graphite is oxidized by strong oxidation agents. Several methods have been developed, starting in the mid of the 19th century by *Brodie*.[39] Nowadays, the *Hummer's* method is most widely applied: a mixture of concentrated sulfuric acid, sodium nitrate, and potassium chlorate is used.[40] Second, graphene oxide is exfoliated by ultrasonication in water or polar organic solvents, such as DMF or THF, to give single sheets. As the oxidation renders the material an insulator, the material needs to be reduced after deposition to recover its properties. Therefore, third, graphene oxide (GO) is reduced to reduced graphene oxdide (rGO) by thermal treatment or the use of reducing agents.[37, 41]

Graphene can also be produced *via* CVD processes, which is usually performed at high temperatures under low pressure or ultra-high vacuum (UHV). Gaseous carbon sources such as methane or acetylene are used which react at the catalytically active metal surface (platinum,[42] iridium,[43-44] ruthenium,[45]) to give monolayers of graphene. This methods has been improved by so much that a large-area fabrication on copper foils is possible.[46] Such approaches can pave the way for an industrial applicability.[32] Though, the transfer from the metal to an insulating layer still remains very challenging.[47]

1.2. Graphene Nanoribbons

The application of graphene for electronic devices is limited due to its intrinsic materials properties as zero-band gap conductor. Hence, the fabrication of electronic devices, such as field-effect transistor (FET)s, is generally not feasible,[48-49] since they require semiconducting materials, which exhibit a current dependent conductivity. The bandgap of graphene can be opened by heteroatom-doping or introduction of structural defects. Another approach in order to do so, is based on Graphene nanoribbons (GNR)s, that is, graphene stripes with a high aspect ratios. The synthesis of GNRs can be either achieved *via top-down* or *bottom-up* approaches. Top-down methods encompass etching of graphene films or unzipping of CNTs.[50] Since these methods generally require harsh methods, a regular edge-structure cannot be preserved, which, however, crucially influences the electronic properties of the material.

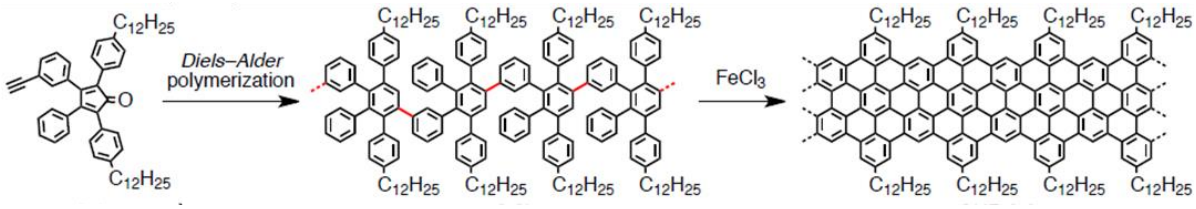

Figure 2: bottom-up solution synthesis of GNRs.

In our group, we have therefore developed several approaches for the bottom-up synthesis of GNRs[51-53] that were performed in solution, rendering short GNRs. The first GNR with high aspect ratios was achieved in collaboration with Fasel by polymerization and dehydrogenation of small molecule precursors on metal-surfaces.[54-55] Despite the feasibility and structural perfectness, they processing remains challenging. For applications as FETs, these ribbons need to be transferred onto insulators. It was until *A. Narita* achieved the synthesis of long GNRs in solution via a *Diels-Alder* approach and subsequent oxidative cyclodehydrogenation. Due to solubilizing alkyl chains, the GNRs can afterwards still be solution processed (see *Figure 2*).[13]

1.3. CNT

Carbon Nanotubes (CNT)s are rolled up single or multilayered graphene sheets, referred to as either single-walled (SWCNT)s or multi-walled CNTs (MWCNT)s, respectively. The latter were synthesized by S. IIjima in 1991, for the first time.[18] Shortly after, also SWCNTs were synthesized.[17, 19] These initial syntheses were achieved, using an arc-discharge evaporation method. Since then, also laser ablation and chemical vapor deposition are applied for the production of CNTs.

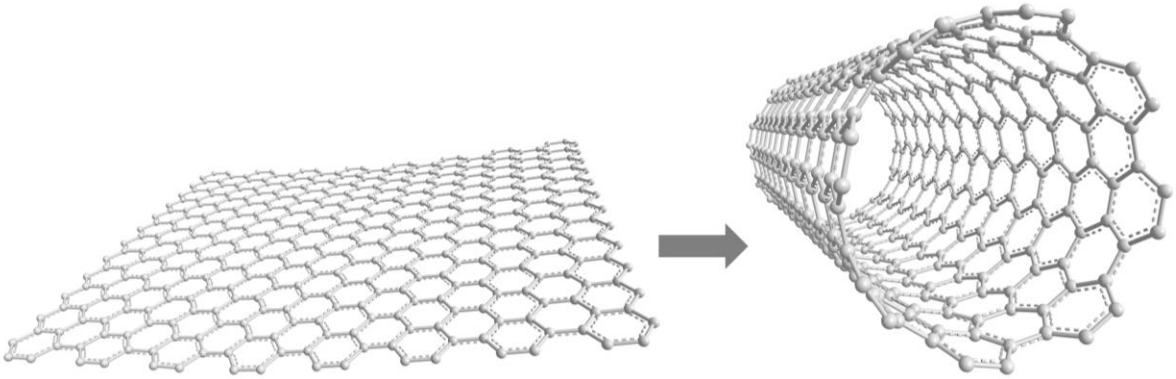

Figure 3: Roll-up of a graphene sheet into a [8,8]CNT.

For arc-discharge production, usually a direct current (DC) between two graphite electrodes is employed, yielding CNTs at temperature of around 1700 °C.[19] For laser ablation, the fundamental mechanism of generating CNTs is similar: a laser pulse is used to provide the energy to form CNT. By that, the carbon source and the transition metals, preferably nickel and cobalt,[56] are vaporized by the impinging radiation of the laser. This method was introduced by R. Smalley in 1995[57]. Both, arc-discharge and laser ablation yield CNTs of very high quality. However, these two methods are very expensive and cannot be used for scale-up. In addition, this process usually affords highly entangled CNTs.

Chemical vapor deposition (CVD) has become the standard method for the synthesis of CNTs, which gives rise to large scale production in fluidized bed reactors.[58] CVD grown SWCNT can be easily separated from the catalyst yielding tubes with purities > 99.98% under optimized conditions.[59] Commercially available as-grown high-pressure carbon monoxide (HiPco) CNT usually contain 5-35 wt% metal impurities, [60] depending on purification.[61] Intense purification of CNTs is usually avoided as this can lead to further structural defects.

The synthesis of CNTs – independent of the process – gives CNTs with different lengths, diameters and structural features. Depending on the chrial vector, i.e , which direction a graphene sheet is rolled-up to form CNTs, one can obtain armchair (n = m), zigzag (n = 0; m = 0) or chiral (any other n and m) varieties (see *Figure 4*). Depending on the edge structure and chirality, either semiconducting or metallic CNTs are observed.

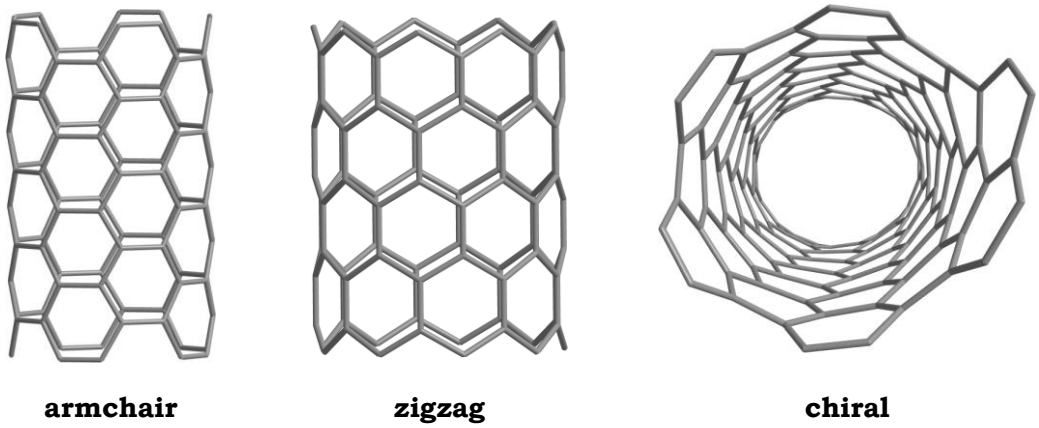

Figure 4: armchair, zigzag and chiral CNTs.

In this regard, all armchair nanotubes are metals (m-CNT). Tubes with n – m = 3k, where *k* is an integer, are semiconductor with a tiny band gap.[62] All other combinations result in semiconducting CNTs (sc-CNT)s that exhibit band gaps that inversely depend on the radius.[63] These fundamental properties render CNTs interesting building blocks for *organic electronics*. For example, they have a charge carrier mobility of ca. 10.000 $cm^2V^{-1}s^{-1}$ and can carry an electrical current density of ca $4 \cdot 10^9$ A cm^{-2}, which is three orders of magnitude higher than of copper or aluminium.[64] To make use of these properties, one faces, in fact, three problems: first, CNTs contain impurities;[65] second, depending on the electronic device, either metallic or semiconducting CNTs are required; third, the fabrication of devices is challenging, i.e., SWCNTs are synthesized as powders and, ideally, require a specific positioning to realize their full potential as conducting or semiconducting material.[64] As an example, an impurity of 1% m-SWCNT in a FET can decrease the on/off ratio by three orders of magnitude.[66]

After production, purification is often necessary, as CNTs can contain amorphous carbon as well as metal impurities from the catalyst, which can influence the desired electronic properties. To reduce impurities, CNTs are often treated with acid, which, however, can

induce further structural defects. Second, the production facilitates a mixture of CNTs, as stated above. For FET, for instance, only semiconducting CNTs are of use, whereas metallic CNTs need to be removed. Different approaches to take this hurdle have been reported in the literature and are continuously being reported. There are physical and chemical as well as combined approaches.[65] One strategy is to optimize the reaction conditions of the production to obtain defined CNTs (size, length, edge-structure), which has been achieved for metallic[67] and semiconducting CNTs likewise, enabling a preferential enrichment.[68] Another approach was pioneered by *Dai* using methane plasma etching for the production of *m*-SWCNTs.[69] A common method for post deposition removal of m-SWCNTs bundles is a so called "electrical burning". The sc-SWCNTs are switched off by a positive gate voltage. In the next step a high drain/source voltage (> 30 V) is applied to selectively destroy the m-SWCNTs.[70-72] This treatment, however, is a slow process that also leads to collateral damage if CNTs bundles are too closely packed. Another method to avoid shorted transistors by mixed SWCNT is the *strip method*.[70, 73] For that, the SWCNTs are aligned into stripes by lithography and conventional reactive-ion etching. The percolation pathway of the m-SWCNT is disrupted by the stripping. By that, the on/off ratio can be greatly enhanced without reducing the mobility.[74] Third, for a densely packed device, the transistor, i.e. the transistor needs to be arranged. However, as nanotubes form bundles, additional afford is required for alignment. In addition, most of the currently available methods for mass productions give SWCNTs with relatively low mobility (ca. 10-30 $cm^2 V^{-1} cm^{-2}$).[75]

Despite the outlined concepts, the preparation and purification of CNTs still remains challenging, as the above stated techniques and methods can be employed to enrich metallic or semiconducting tubes or used to remove or reduce the impact of one or the other. Therefore, new preparative methods are of great need. A bottom-up synthesis of short CNTs based on cycloparaphenylenes (CPP)s could therefore be an interesting approach to tackle the above outlined issues. The synthesis, properties and characterization of CPPs will be discussed in the next chapter.

1.4. Cycloparaphenylenes

CPPs are the smallest subunits of armchair CNTs (see *Figure 5*). They have been foreseen and allegedly synthesized as early as 1934.[76] *Vögtle* fueled the research in this area in 1993, when they published a study on their attempts to synthesize macrocyclic *para*-phenylenes.[77] In their work they showed four different approaches, where they synthesized and characterized different precursor structures; the desired CPPs were unfortunately not obtained. In 1996, *Herges* and coworkers were the first to report the bottom-up synthesis of a fully conjugated CPP with a radial π-system, the so-called "picotube", which is built of four 9-10-bridged anthracenes that form a central [4]CPP ring.[78]

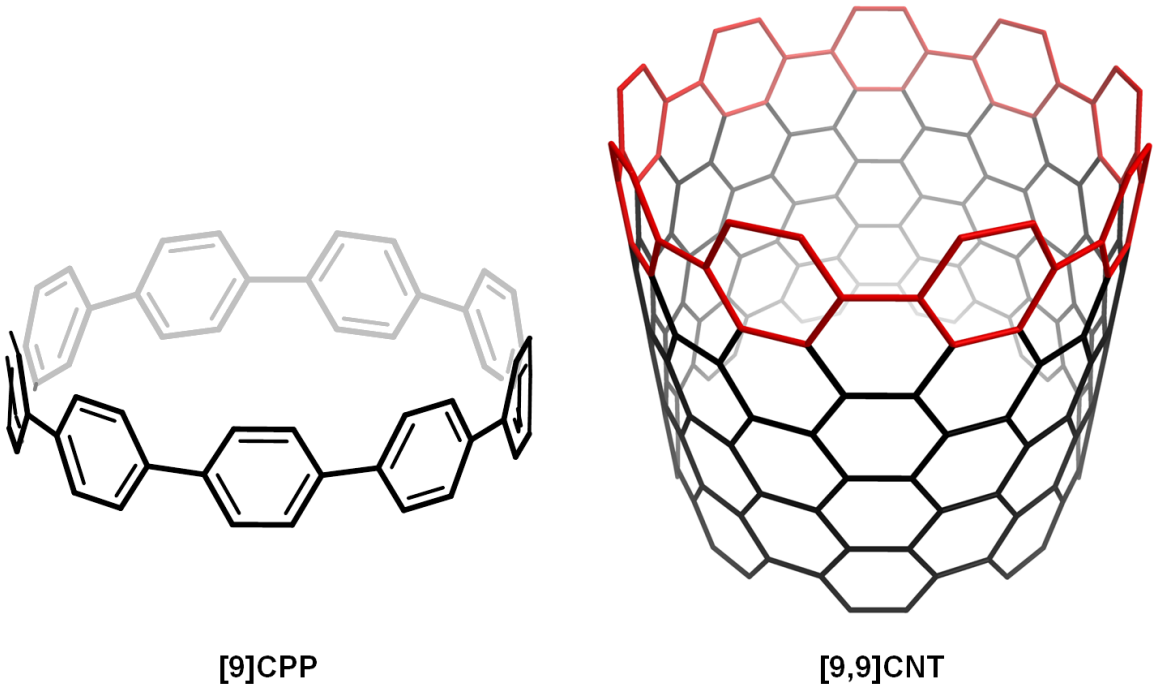

Figure 5: CPP as a segment of CNTs.

It was until 2008 when *Jasti* and *Bertozzi* realized the first bottom-up synthesis of these enticing rings (see *Figure 6*).[20] Their synthesis is based on *cis*-1,4-substituted cyclohexa-2,5-dienes that are used as V-shaped precursors, enabling the macrocyclization of these building blocks. The kinked macrocycle can contain 3 to 6 kinks. For that, Jasti developed a reductive aromatization with sodium napthalenide (NaNp) that circumvents a 1,2-phenyl shift, which is otherwise observed under *Brønsted* or *Lewis* acid conditions. For the first time, CPPs with 9, 12 and 18 phenylenes were synthesized. Short after, *Itamis* group published the synthesis of CPPs, using a different route, which is based on a kinked building

block developed by *Vögtle*.[79] *Yamago* entered the field of CPP synthesis in 2010, pursuing an organometallic approach, which prior to that, had been applied by *Bäuerle* et al. to synthesize a *cyclic*-2,5-connected *octa*-thiophene.[80-81] A platinum(II) complex was prepared containing for linear precursor to give square-shaped CPP precursors.[82] Reductive elimination of the platinum complex affords the strained CPPs. Recently, a fourth approach has been published in the literature, in which *Wang* and coworkers modified a Diels-Alder approach from *Vögtle*: they synthesized a kinked precursor from a butadiene and benzoquinone derivative. The kinked precursor is cyclized and oxdatively cyclodehyrogenated with DDQ to give a strained CPP.[83]

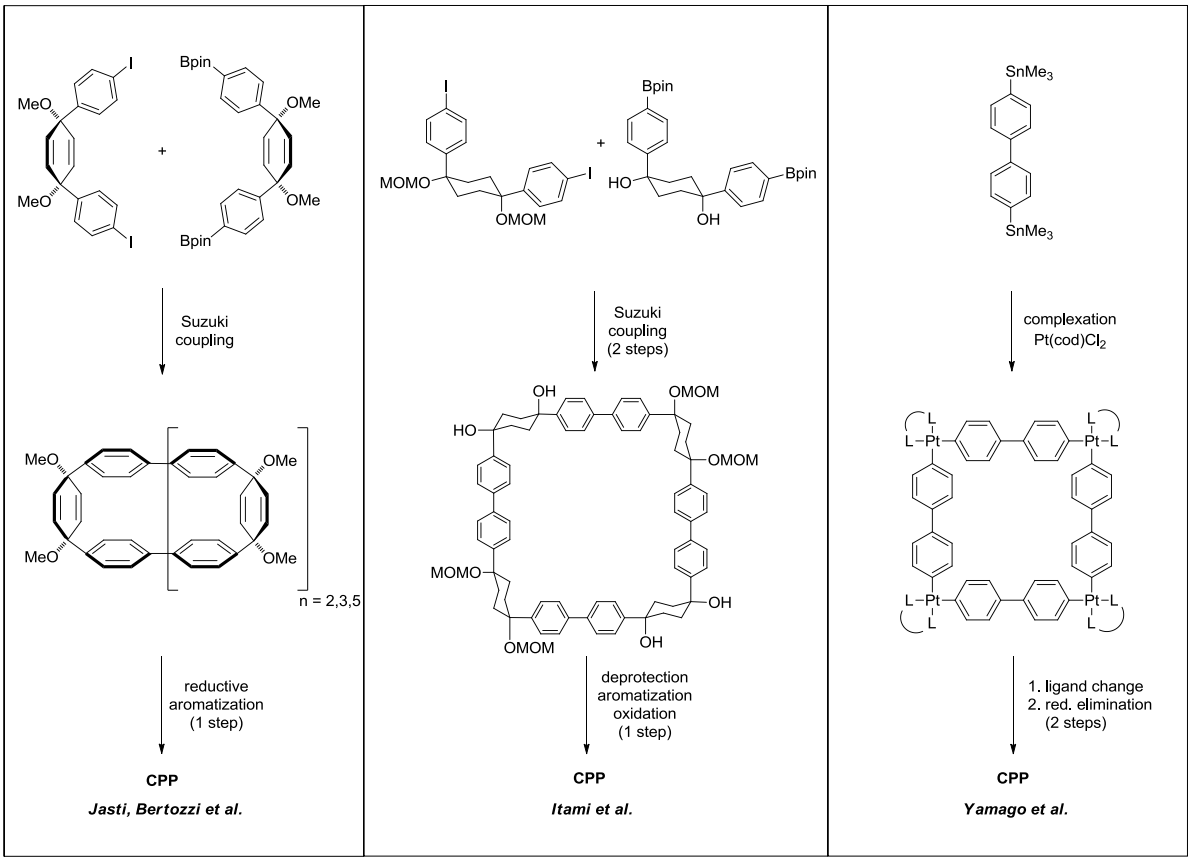

Figure 6: different routes for the synthesis of CPPs

To date, CPPs ranging from n 6 to 18 have been synthesized;[84-95] only [17] has not yet been prepared. Recently, the groups of *Yamago* and *Jasti* achieved the synthesis of the shortest CPP ring, encompassing five phenylene units.[90-91] Nitrogen containing CPPs have been published by the *Itami* group.[96]

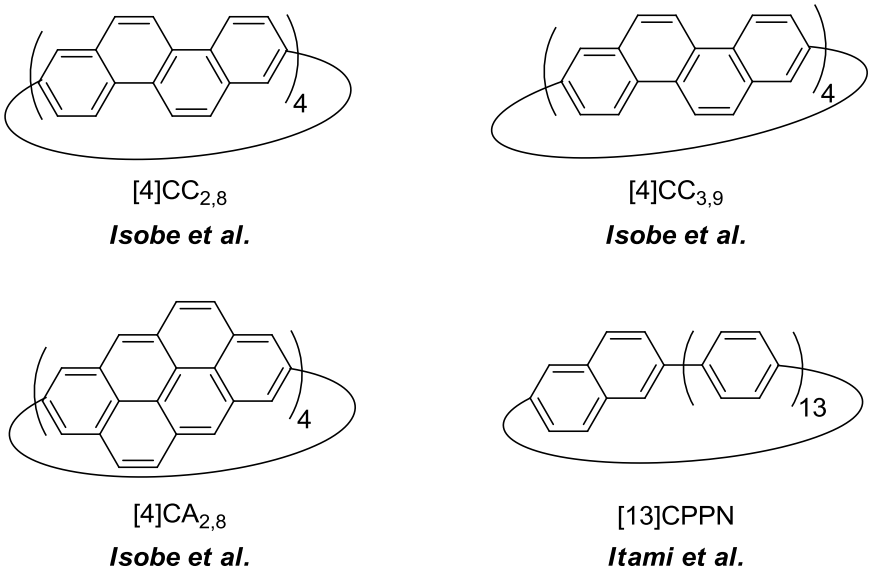

Figure 7: chiral shortest segments of CNTs

Isobe and coworkers have also introduced chiral carbon nanohoops that are based on [4]cyclochrysenylenes ([4]$CC_{2,8}$, [4]$CC_{3,9}$).[97-100] For preparation, they applied the organometallic approach from *Yamago* and coworkers. They were even able to introduce [4]cyclo-2,8-anthanthrenylene ([4]$CA_{2,8}$) to give π-lenghtened finite SWNT segments with armchair and helical structures.[101] *Itami* and coworker synthesized a *cyclo-p*-napthalene CPP, rendering this structure the shortest sidewall segment of a chiral [15,14]CNT.[102]

1.4.2. Bottom-Up Synthesis of CNT segments

CPPs are regarded as ideal building for the bottom-up synthesis of CNTs. Since the seminal work by *Jasti* and *Bertozzi*, CPPs of different size have been synthesized. The structural features of these novel macrocycles were studied. In addition, also photophysical as well as host guest properties have been studied.[97-101, 103-104] The concise bottom-up synthesis of short CNT segments in solution has so far not been achieved. On a sapphire surface, the *Itami* group used a CPP segment as a template to grow CNTs, which show a small size distribution.[105] A solution approach, in contrast, would enable the preparation of soluble and monodisperse CNTs, which contain a defined edge structure, which is a crucial premise for electronic applications.

The synthesis of CNTs from CPP requires a π-extension of the nanohoop toward a belt-like structure. Several approaches for a concise bottom-up synthesis have been reported in the

literature. Thus far, only cycloparaphenylene-2,7-pyrenylene,[106] [4]cyclo-2,7-pyrenylene (see *Figure 8, left*)[107] 1,4-phenylene bridged dimers (see *Figure 8, middle*),[108] arylated CPP,[109] and polyarylated CPP([3]CHBP, see *Figure 8, right*) [110] have been synthesized. None of these π-extended molecules can be regarded as structural precursors of CNTs.

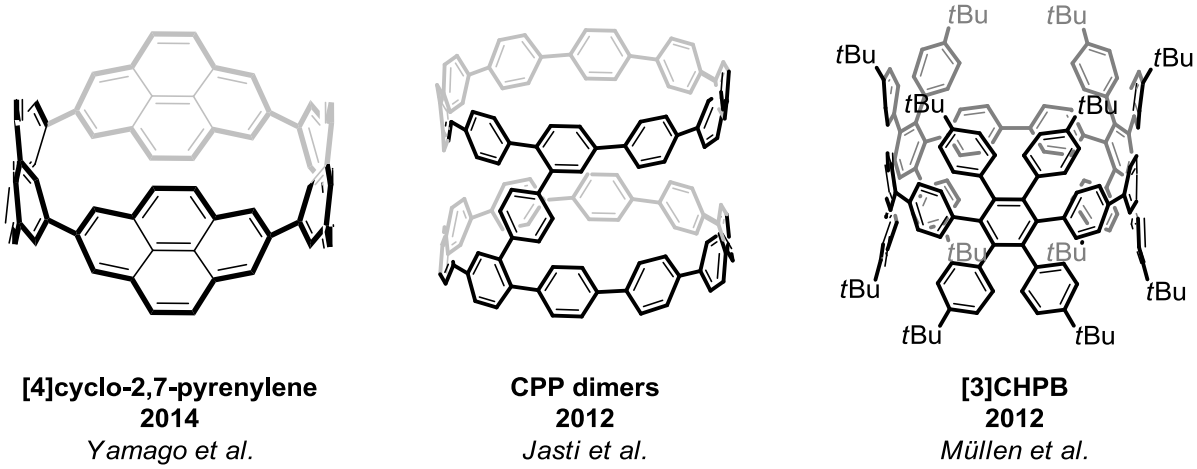

Figure 8: π-extended CPP by different groups.

[9]Cyclo-1,4-napthylene[111] and the CPP dimer,[112] shown in *Figure 9*, resemble structural precursors for a bottom-up synthesis of a CNT. However, neither the *peri*-condensation nor the *cata*-condensation approach has afforded annulated dimers.

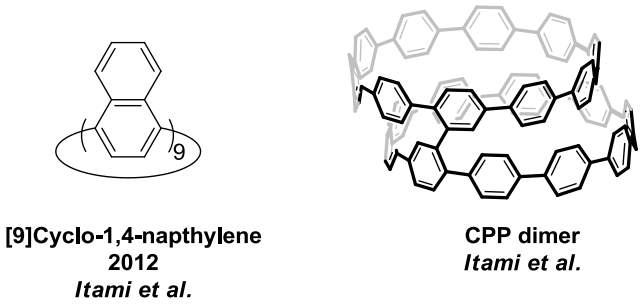

Figure 9: first structural precursor of short CNT segments.

All of the above described π-extended structures have one thing in common: the limiting factor for the CNT synthesis is that all of these structures have at least three or more single bonds, i.e., bridged or *cata*-fused CPP have not yet been reported. This work aims at overcoming this limit, to approach a concise bottom-up synthesis of CNTs.

II. Objectives & Motivation

In this work, the synthesis of polyphenylene cylinders (PPC) (see *Figure 10, bottom right*) as structural precursors of CNTs is investigated. This approach is to give synthetic access toward a concise bottom-up synthesis of size- and edge-defined CNT segments, which has hitherto not yet been achieved.

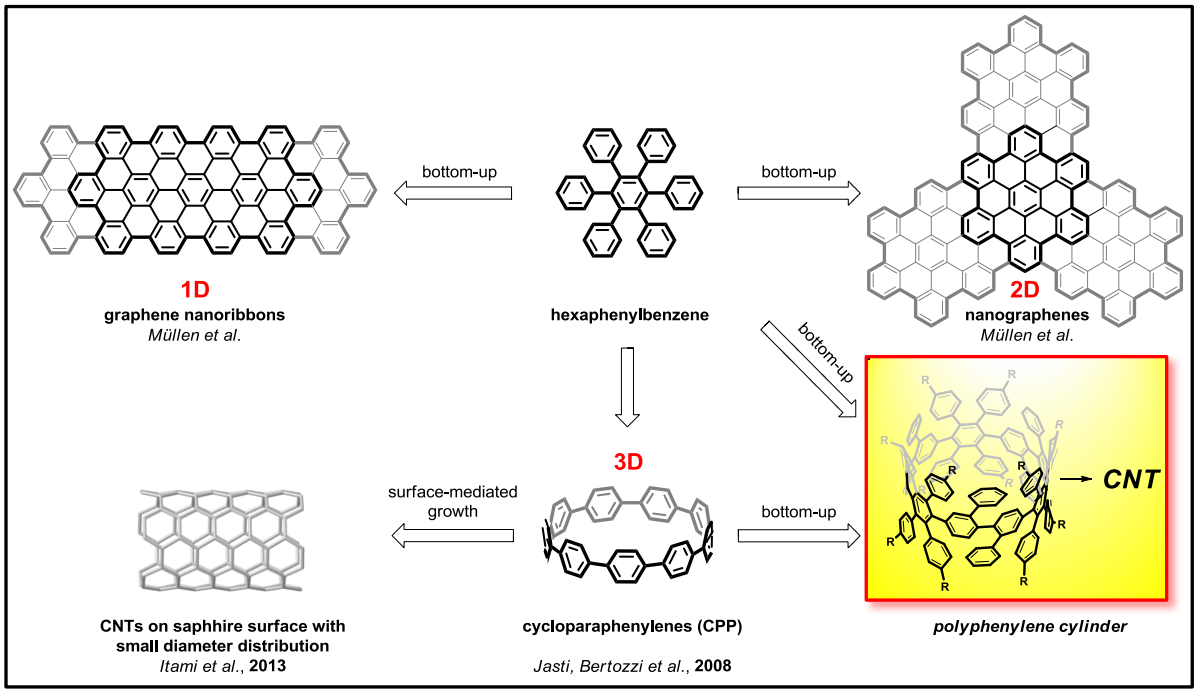

Figure 10: Overview of synthetic congeners derived from hexaphenylbenzene.

Our research is originating from *hexaphenylbenzene* (HPB) and *cycloparaphenylene* (CPP), as the two central building blocks. The first structure is the precursor of one of the most fundamental polyaromatic hydrocarbons (PAH), namely, hexa-*peri*-benzocoronene (HBC).[113-115] Hexaphenylbenzene was and still is applied as a building block for the bottom-up synthesis of a wide range nanographenes (NG)s[116-119] and graphene nanoribbons (GNR)s.[13, 51, 120-122]. Such graphenic structures are of great interest since edge-structures (zigzag, armchair, cove) and aspect ratios sensitively influence their electronic properties. The oxidative cyclodehydrogenation[123-124] is generally applied to transform polyphenylene precursors by an intramolecular C-C-coupling into the annulated target molecules. CPPs[20, 79, 82, 88, 97-101, 109, 111, 125-127] resemble the smallest unit of an armchair CNT and are envisioned as precursor structures for a bottom-up synthesis of CNTs.[78, 128-133] They have

already been used as a template for a surface-mediated growth of CNTs on sapphire surfaces (see *Figure 10, bottom, left*).[105]

On the basis of these two concepts (*vide supra*), a successful π-extension of CPPs to give a cyclic hexaphenylbenzene trimer [3]CHPB has been realized in our group.[110] Having proved the synthetic accessibility of this enticing molecule, we opted for the synthesis of PPCs (see *Figure 11, goal 1*) that resemble the connectivity pattern of a CNT. This precursor is then foreseen to be converted into a CNT *via* an oxidative cyclodehydrogenation, giving rise to edge- and size-defined and soluble CNT segments.

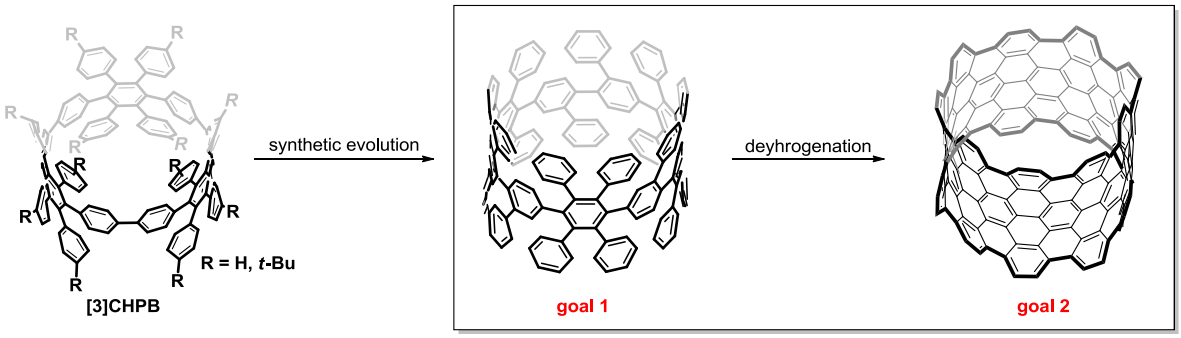

Figure 11: conceptual evolution arising from [3]CHPB

The synthesis of PPCs and - after another synthetic transformation - of CNTs will be investigated, since it could answer the question whether a bottom-up approach can be realized by means of synthetic organic chemistry. Such a strategy would enable the preparation of sized-defined CNTs being soluble in organic solvents. This is of interest because of several reasons: first, one could study their fundamental electronic properties, for instance, does a short CNT exhibit the same properties as its larger homologue? Do they, as expected from its armchair structure, reveal metallic properties? If so, could such molecules give rise for electronic applications? Second, can these molecules be used as templates for the growth of CNTs? Third, does this molecule display a host-guest-type chemistry. If so, could an energy transfer between, for instance, a fullerene or a smaller CNT be observed? Fourth, such defined and defect-free CNTs could allow for more detailed studies on oxygen reduction for the hydrogen peroxide (H_2O_2) synthesis. Lately, a study was published by *Unwin* and coworkers where they could visualize the electrocatalytic activity of pristine, kinked and oxidized sites on individual CNTs. In their summary, they venture an outlook, saying that the "activity can be tailored (enhanced) by building in particular architectures

(kinks) or through surface modification (sidewall oxidation)".[134] Bottom-up synthesized CNTs would serve as ideal candidates for such studies, as they could give rise to defined chemical modifications.

III. Results & Discussion

3.1. Retrosynthetic Analysis of CNT

The bottom-up synthesis of CNTs requires the preparation of cyclic pre-structures that resemble the necessary connectivity pattern of phenylene and phenyl rings to form CNTs by fusing the remaining bonds *via* an intramolecular C-C coupling. To develop such precursors, we conducted a retrosynthetic analysis, starting from a short CNT segment, which gives rise to several strategies (see *Figure 12*).

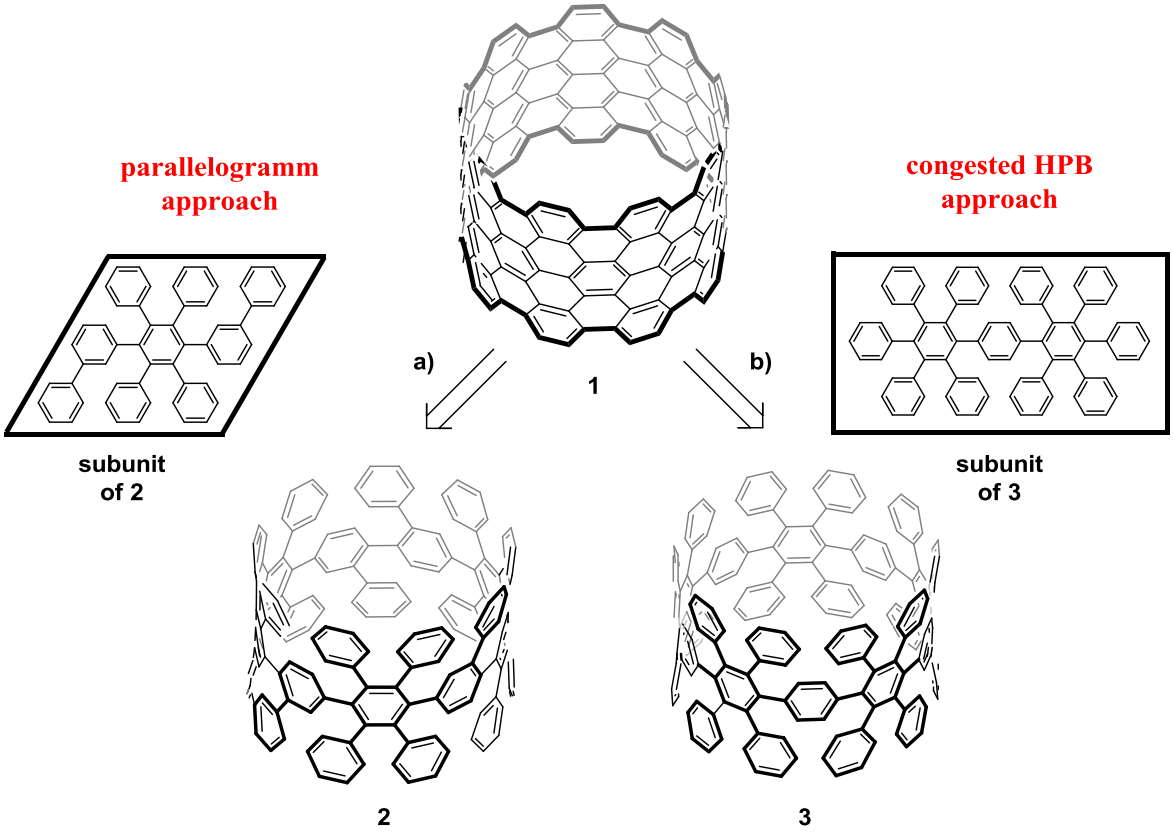

Figure 12: Retrosynthetic analysis of CNTs. Route a) parallelogram approach (left); b) congested HPB approach (right).

Here, two retrosynthetic approaches are presented: a) the CNT structure was broken down into three identical subunits that contain a hexaphenylbenzene core which is extended by two phenyl rings, resembling a *parallelogram-shaped* structure, to be called *parallelogram* approach (see *Figure 12, route a)*). This structural motif is embedded into a macrocycle to give PPC **2**. As stated before, the necessary structural premise, to account as a CNT precursor, needs to be fulfilled. This can be clearly seen from the indicative drawing of **2**;

route b) is also structurally derived from a hexaphenylbenzene motif. The structure, however, differs from a hexaphenylbenzene dimer in terms of the bridging phenylene unit which is shared by two hexaphenylbenzenes, leading to *congested* hexaphenylbenzenes **3**, to be called *congested HPB approach*.

As the π-extension of a [9]CPP to give a [3]CHPB was achieved in our group to access 3D structures,[110] we wanted to built upon this precursor, since it *only* required the addition of six phenyl rings to the [3]CHPB structure. Therefore, the parallelogram approach will be discussed first (see *chapter III, p.18*). Later on, the *congested HPB approach* is described which, however, requires a complete redesign of the synthetic precursor (see *chapter III, p. 68*). Both strategies yield target structures that can be possibly converted into short CNT segments.

3.2. Parallelogram Approach

In this chapter, the parallelogram approach is employed to synthesize PPCs with [9], [15], and [21]CPP rings as central cores. A kinked precursor **7** was developed as the monomeric unit, which evolves from the [3]CHPB, designed by Dr. T. Nishiuchi (see precursor **6**, *Figure 13*). This new structure contains two additional phenyl rings to render the new macrocycles precursors for a solution-mediated synthesis of CNTs. Thus, the target structure **7**, as shown in *Figure 13*, contains six additional phenyl rings, in comparison to the [3]CHPB **6**.

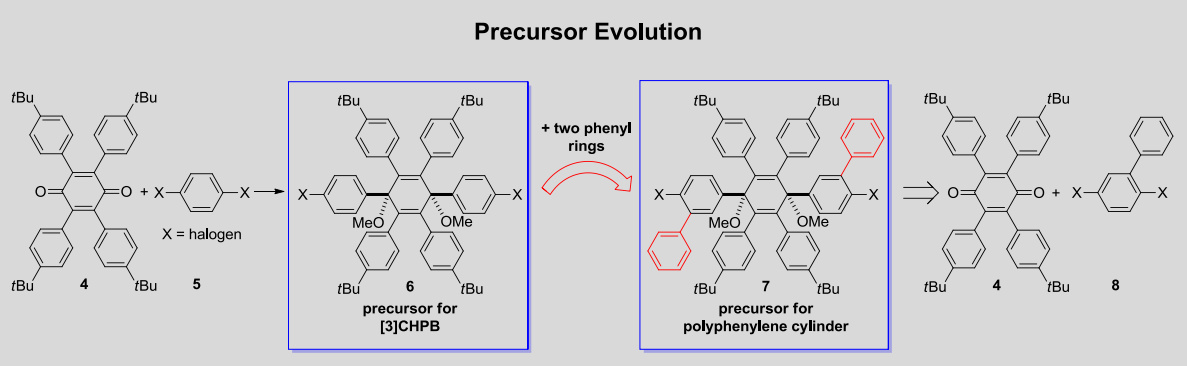

Figure 13: Precursor evolution: structural difference between precursor **6** and **7** and synthetic analogies.

In order to synthetically and structurally achieve the CNT precursor synthesis, the following premises must be fulfilled: a) the starting material, i.e., the central 1,4-dimethoxycyclohexa-2,5-diene should feature a suitable kinking angle to enable macrocyclization; b) the molecule needs to bear reactive groups to enable coupling of the kinked monomers; c) the precursor molecule needs to resemble the necessary bonding pattern, that is, a respective connectivity of a CNT precursor. Compounds **2** and **3** were designed to meet these criteria. Such structures will also be referred to as *polyphenylene cylinders* (PPC)s throughout this Ph.D. thesis.

Here, the introduction of *t*-butyl groups into the respective precursor structures shall be highlighted as they serve two crucial purposes: first, they increase the solubility of the precursors which enables purification and eases handling. Second, *t*-butyl groups still allow for the growth of single crystals while providing solubility. Methyl groups, in contrast to *t*-butyl groups, would not have provided enough solubility, on the one hand, even though they are ideally suited for growth of crystals; on the other hand, *n*-butyl chains or longer alkyl

chains, increase solubility strongly, but their high structural flexibility renders them difficult to crystallize. As a consequence, all structures throughout this PhD. thesis bear *t*-butyl groups. This criterion is very important, since the presented molecules exhibit a high structural complexity and cannot always be unambiguously proven by NMR spectroscopy in conjunction with other methods. Therefore, we opted for the use of single crystal X-ray crystallography to get full structural insights into the synthesized molecules.

3.2.1. [9]CPP based Polyphenylene Cylinder

3.2.1.1. Introduction

The synthesis of the [9]CPP based PPC **38** is described in this chapter. In addition to the identical features of the precursor for [3]CHPB in terms of geometry and reactivity, the new precursor **7** contains two more phenyl rings. Therefore, the previously used 1,4-dihalobenzene **5** was substituted by a correspondingly functionalized biphenyl.

3.2.1.2. The Kinked Precursor

In order to synthesize title compound **11**, the readily available silylether protected 3-bromobiphenyl **9** was lithiated using *n*-BuLi and subsequently reacted with the literature known compound 1,4-benzoquinone derivative **4** (see *Scheme 1*).[135] Mass spectrometry indicated the formation of trace amounts of **10**; **22** could not be observed. After purification, 95% of the starting material **A** was recovered. Depending on the experimental conditions (*Table 1*), **9** was partially or fully desilylated which hinted at an insufficient stability of the (dimethyl)*iso*-propylsilylether protecting group in the presence of *n*-BuLi.

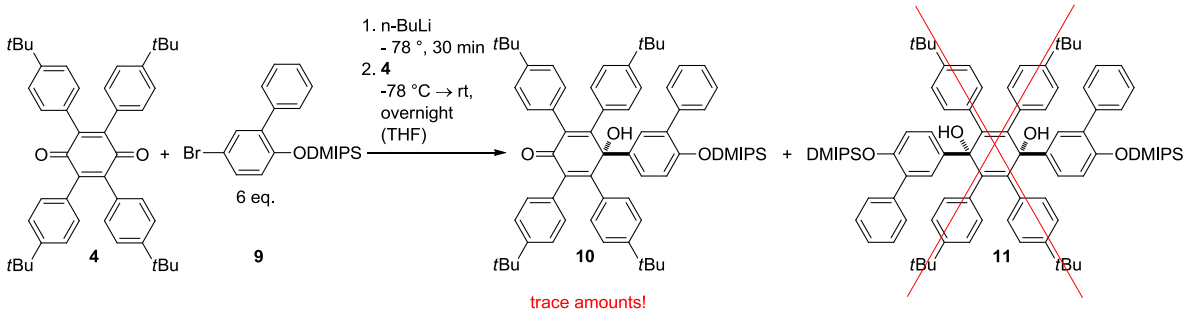

Scheme 1: Studies towards the 1,4-dihydro[quinquephenyl]-1,4-diol **11**.

To improve the reactions conditions, $LaCl_3 \cdot 2LiCl$ was used as an oxophilic *Lewis* acid, which is especially used for a selective 1,2-addition of sterically demanding α,β-unsaturated ketons (see *Table 1*, *entry B*).[136] However, no product formation was observed. Also, the *Grignard* formation of 3-bromobiphenyl was investigated, using *i*PrMgCl in the presence of LiCl which, according to literature,[137] is known to yield fast transmetallations. Though, no Mg/Br exchange was observed and both starting materials could be fully recovered. The above described synthetic approaches did not give title compound **11**. Thus, a different biphenyl was prepared.

To synthesize compound **17**, the dihalobiphenyl **16** was prepared (see *Scheme 2*). After *Curtius* rearrangement of **12** and deprotection of the carbamate **13**, liberating the aniline derivative **15**, 4-bromo-3-iodoaniline (**16**) was obtained. *Suzuki* coupling[138] and modified *Sandmeyer* reaction conditions[139] furnished the desired product **16** in good yields.

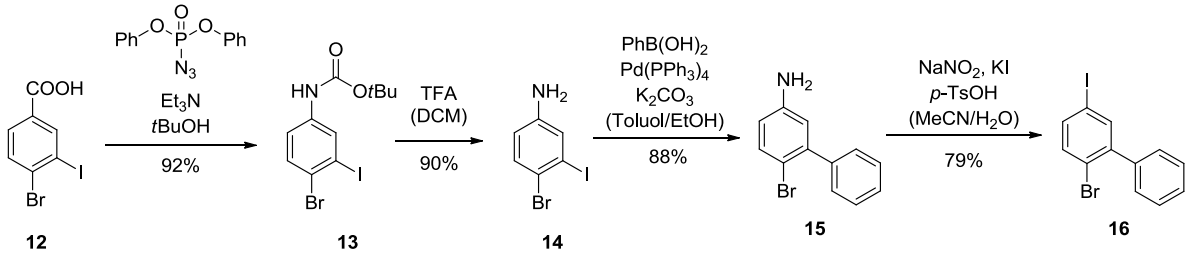

Scheme 2: Synthesis of 2-bromo-5-iodo-1,1'-biphenyl (**10**).

For the synthesis of the *V*-shaped precursor **17**, biphenyl **16** was reacted with benzoquinone **4**. After lithiation, **16** was subjected to **4** affording **17**. However, mass spectrometry (MALDI-TOF) revealed the formation of a mono-debrominated side product (~10%), which could not be separated by flash chromatography: lithiation did not only occur in the *5*-position but also in the *2*-position, possibly due to stabilizing effects of the phenyl substituent.

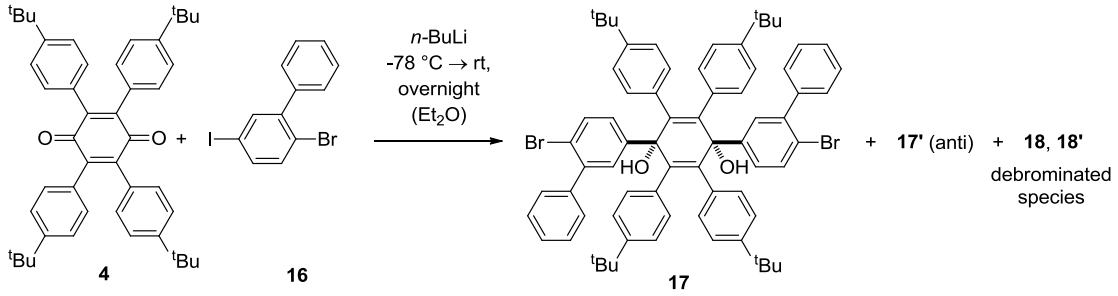

Scheme 3: Synthesis of diol **17**.

To suppress byproduct formation, a 2-chloro-5-iodo-1,1'-biphenyl (**19**) precursor was synthesized. The exchange of bromine against chlorine atoms surpresses dehalogenation, as lithiation takes exclusively place at the 5-position. Therefore, **15** was prepared analogously to **16** (*vide supra*) in similar yields (see *Scheme 4*).

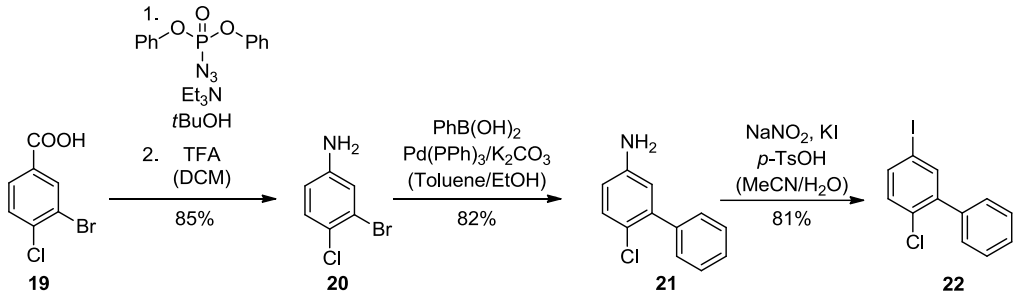

Scheme 4: Synthesis of 2-chloro-5-iodo-1,1'-biphenyl (**22**).

22 was reacted with **4** to give syn-diol **23** (34%). As compound **23** readily decomposes, it was methylated directly after purification affording **24** (84%) (see *Scheme 5).*

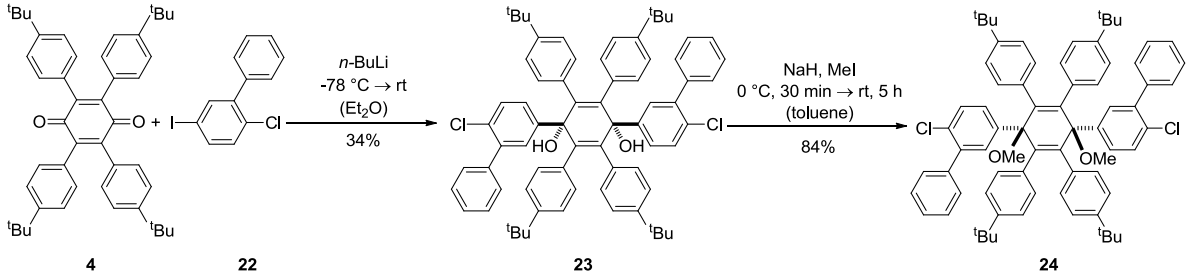

Scheme 5: Synthesis of *V*-shaped precursor **24**.

In *Figure 14*, the MALDI-TOF spectrum of compound **24** is depicted. The main peak shows the monodemethoxylated product, whereas the higher mass depicts the product mass and the lower mass results from the doubly demethoxylated product. Such mass pattern were observed for all 1,4-dimethoxycyclohexa-2,5-dienes derivates studied with MALDI- and FD-MS throughout this work. NMR-spectroscopy always proved symmetric strcutures with the appropriate integration for the methoxy groups.

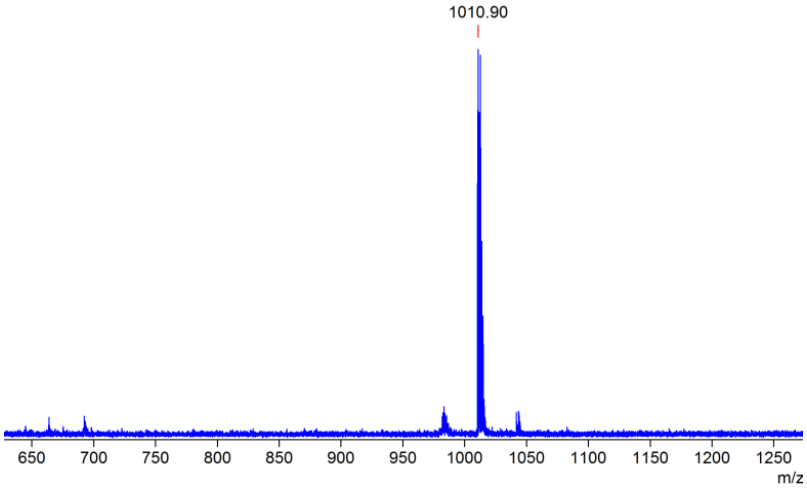

Figure 14: MALDI-TOF spectrum of **24** showing the its title mass, its mono- and dimethoxylated product. Intensity given in a.u.

After the successful synthesis of compound **24**, macrocyclization *via Yamamoto* coupling (see *Scheme 6*) was investigated. The reaction, however, did not afford the desired macrocycle: initially, the *Yamamoto* coupling was performed at concentrations of 6 mM. After 24 h, only a small amount (< 5%) of dimer **27** was observed by mass spectrometry (MALDI-MS). The low conversion is due to sparsely reactive aryl chlorides in conjunction with an increased sterical demand of the substrates during coupling, in contrast to the homocoupling of unsubstituted phenyls. Comparison of the results with *Yamamoto* cross couplings of similarily sterically demanding aryl chlorides showed that these reactions were performed at prolonged reaction times as well as tenfold higher concentrations.[140]

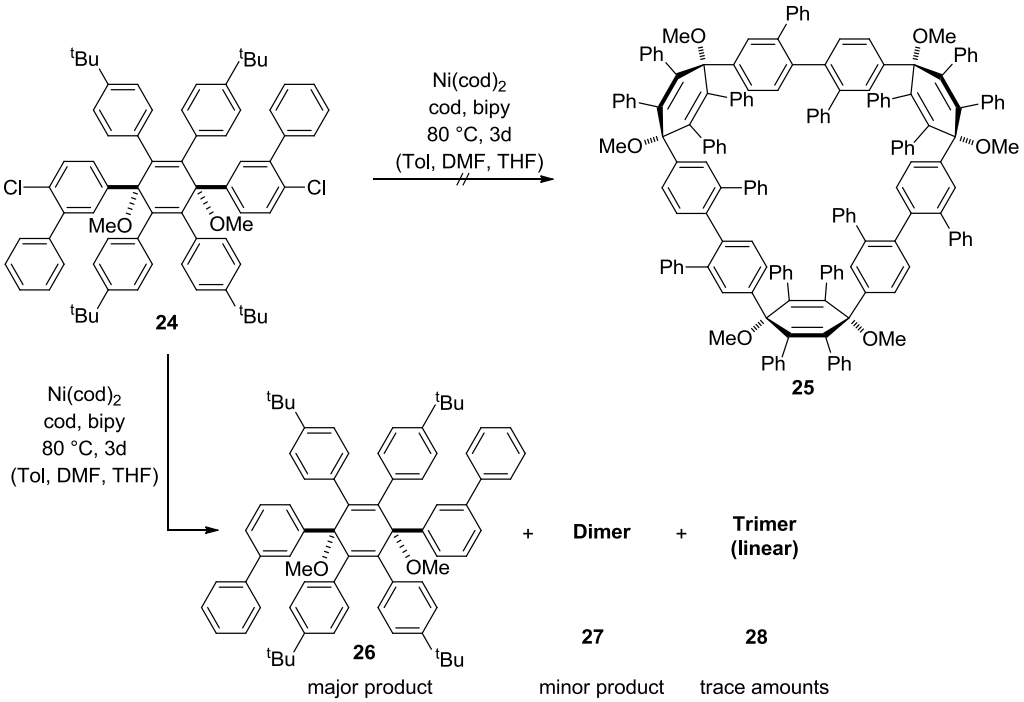

Scheme 6: Studies towards macrocycle **25**.

As a consequence, the cross-coupling reaction was surveyed at concentrations of 60 mM. After 3d at 80 °C, the coupling yielded dimer **27** and trimer **28**. Microwave-assisted coupling at the same concentration gave similar results. As shown in *Figure 15*, primarily dechlorinated starting material **24** was obtained. Besides, small amounts of monodichlorinated dimer were observed, too, also tiny fractions of still dichlorinated trimer were obtained, which could not be isolated for a repeated coupling.

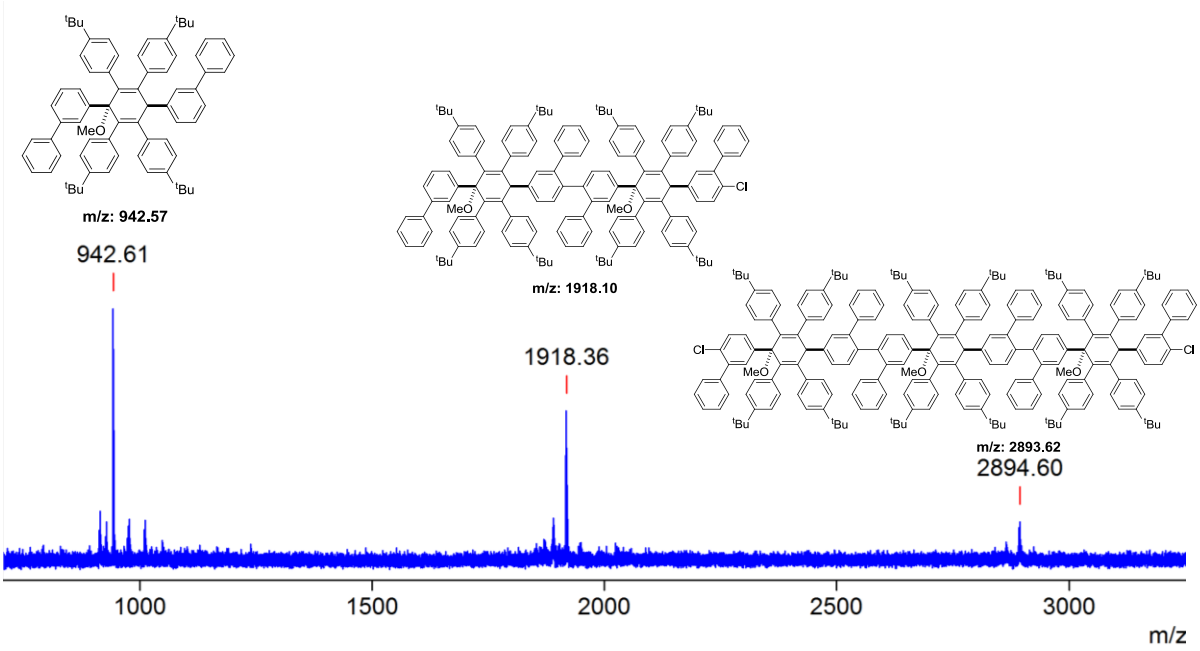

Figure 15: MALDI-MS spectrum of the homocoupling reaction of **24**. Demethoxylation is generally observed for these structures. Intensity given in a.u.

As the macrocyclization of aryl chloride **24** *via Yamamoto* was not possible, a new building block was designed. Molecule **35** (see *next section*) paved the way for a successful and efficient synthesis of all macrocycles following the *parallelogramm* approach, since it enabled the use of a powerful oxidative homocoupling *via* a *Lipshutz* cuprate intermediate. The synthesis of aryl iodides in comparison to aryl chlorides as reactive groups became necessary, as the reaction conditions of the homocoupling require lithiation of the kinked dihalide as an initial step. Since aryl chlorides cannot be lithiated under standard reactions conditions, a synthesis of a new kinked precursor was developed.

3.2.1.3. Synthesis and Characterization

The new precursor is prepared *via* a multistep synthesis starting from the commercially available [1,1'-biphenyl]-2-amine (**29**). After selective bromination in *para*-position, **30** was iododeaminated *via* a modified *Sandmeyer* reaction and subsequently silylated with chlorotrimethylsilane to give **32** in good yields (92%). For the preparation of **33**, the TMS-protected biphenyl **32** was lithiated and reacted with quinone **4**, yielding the *cis*- and *trans*-isomers in a 1:1 ratio. The two isomers can be separated by column chromatography to give the *cis*-isomer **33** (44%) as the distinctively more polar compound, which is necessary for

macrocycle synthesis. The *trans*-isomer was also isolated and used for polymerization studies (see *p. 99*). Diol **8** decomposes at temperatures above 40 °C, after standing in solution for prolonged times or under acidic conditions. Thus, a rapid purification and immediate methylation with MeI was found to give best results (90%). Subsequently, iododesilylation of **34** was performed to cleanly afford **35** in very good yields (89%).

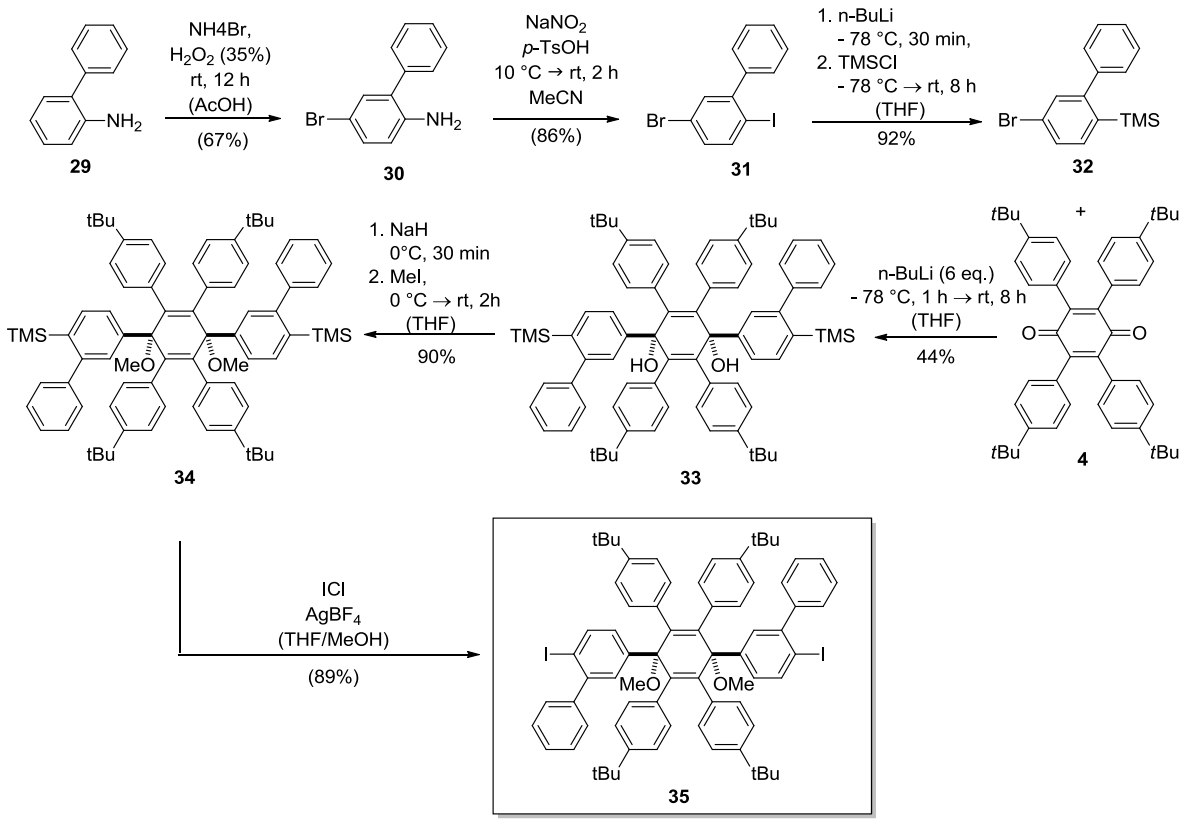

Scheme 7: synthesis of diiodide **35**

Throughout the first attempts, we discovered that the TMS groups could not be converted to the diiodide without irreversibly dimethylating the methoxy groups (see *Scheme 8*). In the presence of the soluble silver salt $AgBF_4$, these difficulties could by overcome, by trapping free chloride anions and iodide, present from *in situ* formed iodine. These findings will now be discussed in greater detail.

Due to the irreversible demethylation of the diol **33**, the reaction mechanism of the 1,2-shift[141] is depicted in *Scheme 8*. The reaction mechanism is emphasized in such detail here, since this side reaction could not be suppressed when harsher reaction conditions were applied to iododesilylate sterically more crowded substrates (see *p. 71*).

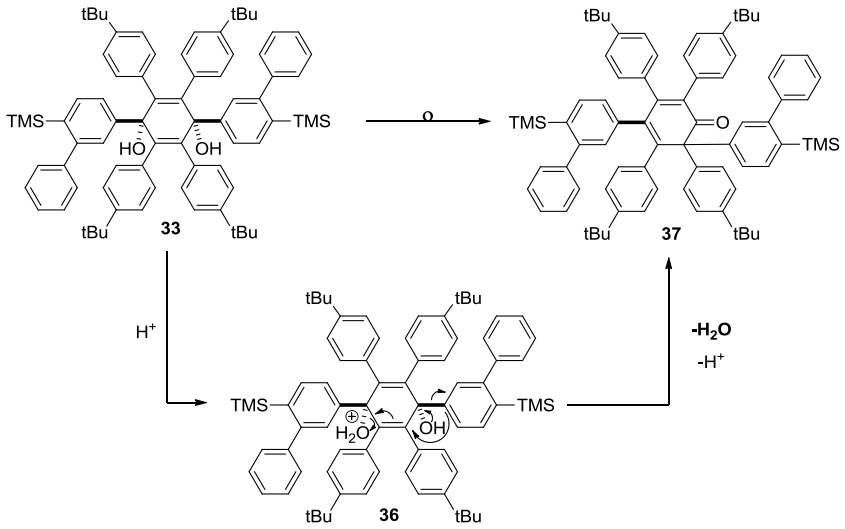

Scheme 8: 1,2-phenyl-shift of cyclohexa-2,5-diene-1,4-diol known from literature.[141]

The 1,2-phenyl-shift, which has been reported for similar structures,[141] is described in *Scheme 8*. Acidic conditions, either *Lewis* or *Brønsted* acids, induce an intramolecular 1,2-phenyl shift. On non-subsititued quinones, the cyclohexadienone is rearomatized to form phenol derivatives. Here, the remethylation did not give an anisol derivative.

After synthesis of the kinked building block **35**, the macrocyclization was investigated. *Yamamoto* coupling was studied for **35**, since this reaction was also applied for the macrocyclization of the kinked dichloride **24** (see *Scheme 6*), which failed, as reported before. Nonetheless, we decided to perform *Yamamto* coupling, as it is known that halides such a bromine and iodine lead to increased reactivity; on the other hand, such substrates are even more prone to undergo dehalogenation than aryl chlorides.

Unfortunately, *Yamamoto* coupling of the kinked diiodide **35** did not yield macrocycle **25** (see *Scheme 9*). The reaction exclusively gave deiodinated starting material which was primarily assigned to the increased sterical hindrance, arising from the *o*-phenyl substituents as well as the use of iodide. In contrast, the coupling of the sterically less hindered kinked precursors (phenyl-phenyl coupling) for the synthesis of the [3]CHPB by Dr. T. Nishiuchi in our group gave the title compound in satisfactory yields.[110] Therefore, another homocoupling method was investigated: an oxidative homocoupling *via* a *Lipshutz* cuprate, which is known to be a very robust aryl-aryl coupling, especially regarding sterically hindered and strained systems.[142]

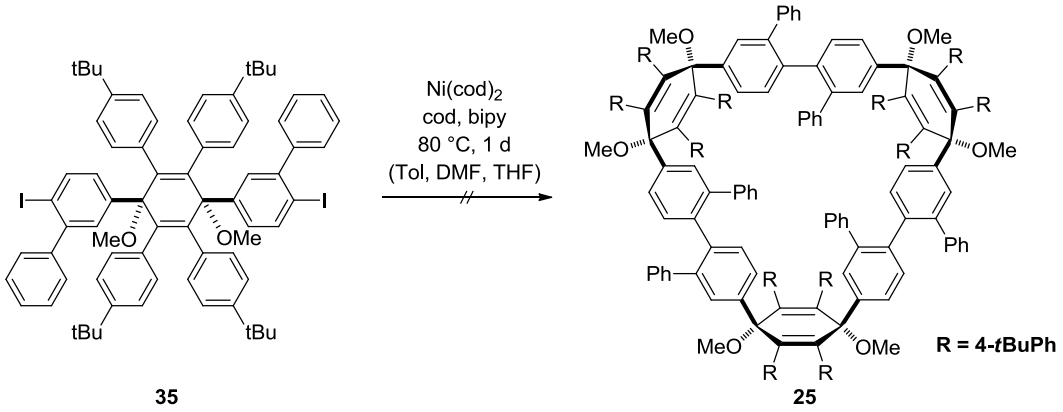

Scheme 9: unsuccessful Yamamoto coupling of the kinked diiodide **35**.

To this end (see *Scheme 10*), **35** was lithiated with *t*-BuLi to form the corresponding lithium organyl. A *Lipshutz* cuprate was *in situ* generated upon addition of CuCN. Subsequent oxidation with duroquinone gave the aryl-aryl coupled product **25**. To preferentially form entropically less favored macrocycles over linear oligmers, the cyclization was performed at high dilutions (5 mM). Nonetheless, the reaction afforded the desired cyclic trimer **25** only in very moderate yields (10%).[142-144] This was partly due to the formation of higher linear homologues, but mostly due to dedihalogenated monomer, linear dimers and trimers; these side products were observed by MALDI-MS, which could not be avoided under the given reaction conditions. The separation of the linear homologues could be achieved by a serendipitous discovery: the title compound **10** precipitated from chloroform whereas the linear homologues remained in solution; surprisingly, all compounds are soluble in DCM.

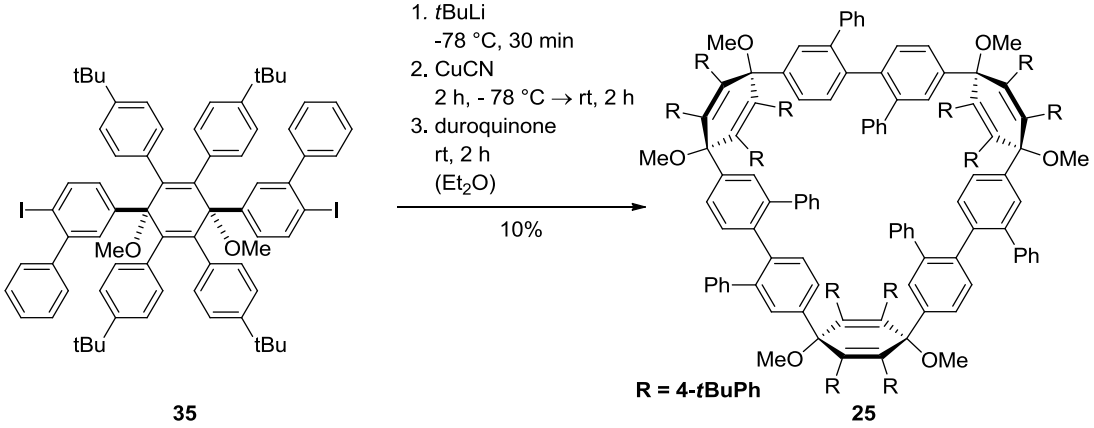

Scheme 10: macrocyclization of **35** yielding triangular macrocycle **25**.

The cyclic structure of **25** could be verified by mass spectrometry and NMR spectroscopy. In addition, single crystals could be obtained by slow diffusion of hexane or acetonitrile into

DCM. The crystal structure (see *Figure 16*) depicts the kinked 9-membered macrocycle **25** which contains four disordered DCM and two disordered water molecules (not shown for clarity). The molecule resembles a triangular structure with C_2-geometry. The angles between the plane of the cyclohexadiene unit and the biphenyl substituents *versus* cyclohexadiene and the methoxy groups is slightly increased to 56.5° (ideally 54.5 °). As a consequence, the angle between the plane of the cyclohexadiene and the methoxy group is diminished to 50°. Due to the triangular geometry and the thus weakly enforced ring strain, the tetrahedral angels between the methoxy group and the bridging biphenyl are slightly reduced by 4°. The low ring-strain is due to the kinking angle of the *cis*-3,6-dimethoxycyclohexa-1,4-diene. This is supported by the bond length between the biphenyl units which are 1.482 Å (2x) and 1.503 Å. They are in good agreement with bond lengths of unsubstituted biphenyls (1.507 Å) and prove that the geometry of the macrocycle does not influence bond lengths.[145] Apparently, the tetraphenyl units exert sufficient sterical hindrance – in the solid state – on the neighbouring phenyl rings of the bridging biphenyl moieties to be arranged in a staggered fashion; this alignment could be advantageous during C-H-activated C-C bond coupling of chlorinated kinked macrocycles (see *3.3 parallelogram approach, p. 63*), since a preordering of the neighbouring moieties is required to obtain parallelogram-shaped units.

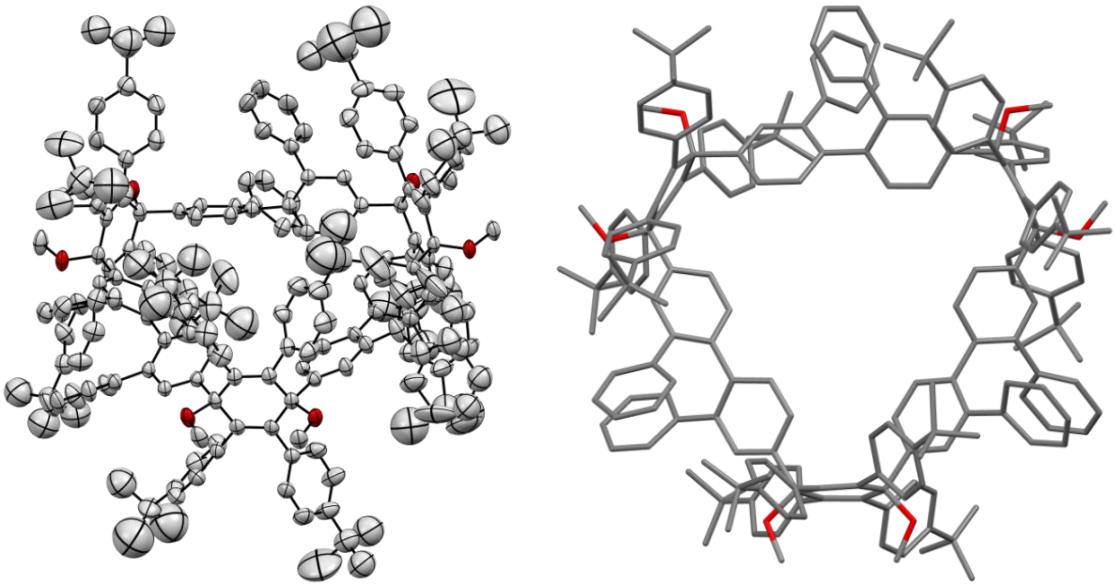

Figure 16: X-ray structure of the kinked 9-membered macrocycle **25**. ORTEP drawing at 50% probability level front view (left), wireframe model on top (right). Oxygen atoms are labeled in red. Solvent molecules are omitted for clarity.

Reductive aromatization of **25**, using low-valent titanium at 80 °C, was performed to give **38** in comparable yields (55%). The title compound could be characterized by MALDI-MS, NMR and single crystal X-ray crystallography.

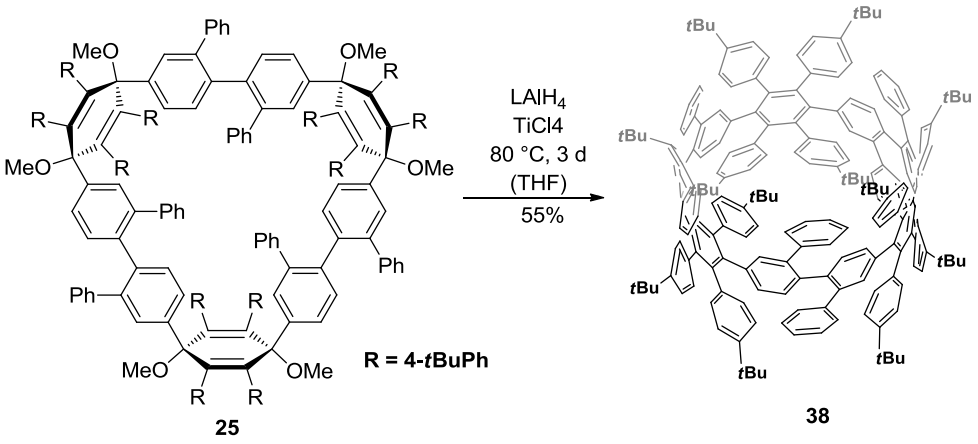

Scheme 11: Synthesis of [9]PPC.

The HR-MALDI-MS measurement and ^{1}H NMR spectroscopy at 100 °C were in agreement with expectations. Prolonged NMR measurements at elevated temperature, however, led to decomposition of **38**. Fortunately, single crystals could be grown from DCM/acetonitrile mixtures, to give insights into this fascinating structure (see *Figure 17*).

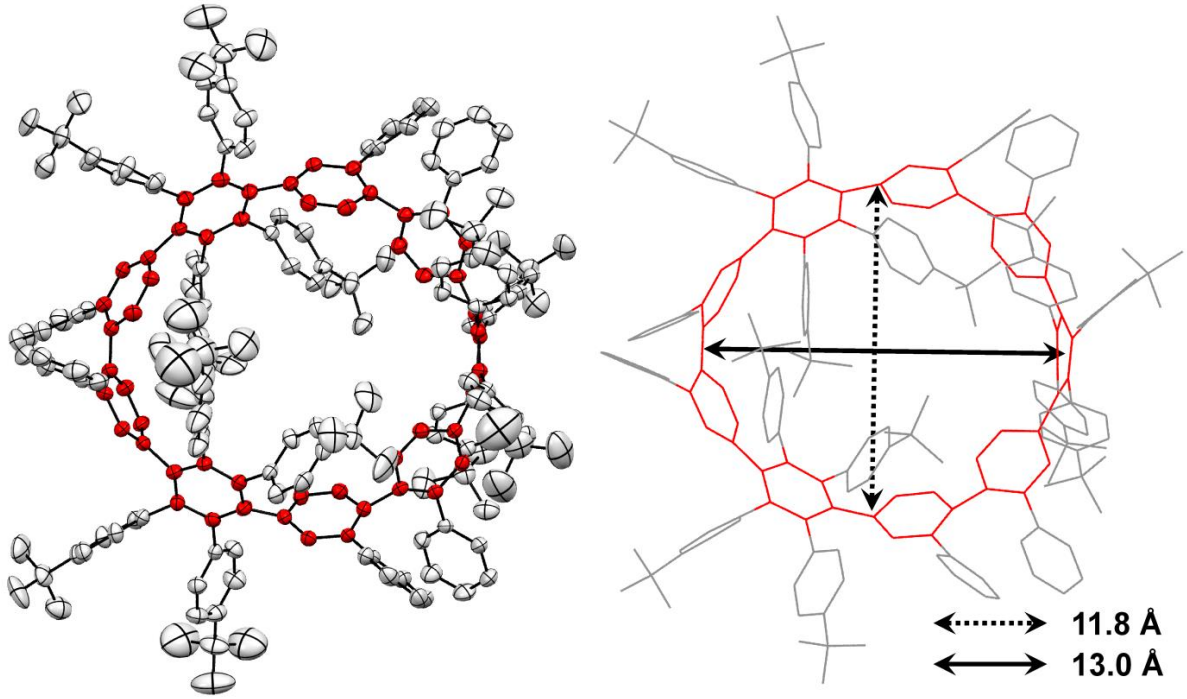

Figure 17: X-ray crystal structure of **38** a) ORTEP drawing at 50% probability level and b) wireframe model. Hydrogen atoms and solvent molecules are omitted for clarity. The CPP ring is labeled in red.

The X-ray structure shows an ellipsoidal macrocycle with a length of 13.0 Å and a width of 11.8 Å (see *Figure 17*). The unit cell contains six MeCN, and six DCM molecules and one H_2O molecule (omitted for clarity). The ellipsoidal structure stems from the odd number ("9") of phenylene units of the CPP ring. Ellipsoidal-shaped CPPs were observed for [9]CPP[126] and [3]CHPB[110] where no or significantly less sterical hindrance of phenyl substituents is present. In addition, even numbered CPPs display circular structures.[87] The ellipsoidal shape can be explained by a repulsion-induced alternating twisting of the phenylene units. Generally, neighboring phenylenes point in an alternating pattern to the outside and inside of the ring to minimize repulsion of hydrogen atoms. For an even-numbered ring, this positioning is feasible without inducing additional ring strain. [87, 127, 146] In the case of odd-numbered rings, however, one phenylene moiety experiences significantly higher sterical repulsion, as the in- and outside positions (*ortho*-positions) are blocked by the neighbouring phenylenes (see *Figure 18*). As a consequence, the entire macrocycle is distorted to minimize this repulsion. Therefore, not a circular but rather an ellipsoidal structure is obtained. The tetraphenylbenzene and biphenyl moieties attached to the CPP ring exert additional strain, since they cannot rotate freely and experience mutual repulsion. Thus, the odd-number of phenylene rings and conjunction with sterical crowdedness induces a strong twist of phenylene units, which in turn, because of the twisting, does result in reduced flexibility.

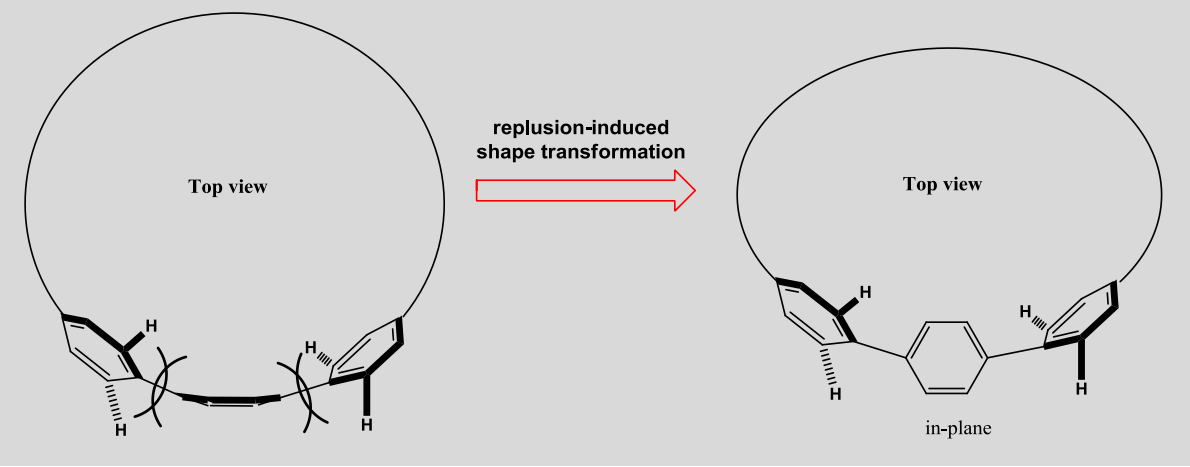

Figure 18: schematic explanation of the shape transformation. Phenylene unit aquires an in-plane arrangement (see crystal structure *vide supra*).

To highlight the twisting of phenylene units of the CPP core, the single crystal X-ray structure of the polyphenylene cylinder is also shown from a frontal view in *Figure 19*. The average dihedral angles vary between 42° and an astonishing 84°. These values are unprecedented, since the maximum dihedral angles for [9]CPP[20] and cHPB trimer **1** are 44° and 67°, respectively. These high dihedral angles either lead directly or in neighboring positions to strong twists of single phenyl units with a maximum internal dihedral angle (C_{ipso}-C_{ortho}-C_{orth}-C_{ipso}) of 8.2°. A quinoidal-type character of **38** (bond shortening), as reported for [9]CPP,[147] cannot be observed, owing to the previously described large dihedral angles between adjacent phenyl rings. Also, the extreme twisting of this macrocycle can be a reason for why macrocycle **38** decomposed at elevated temperatures (100 °C): an oxidation of phenylene units or a ring opening would result in a strong relief of strain energy, leading to a diminished or no pyramidalization angle.

Figure 19: single crystal X-ray structure of **38** wireframe model. Hydrogen atoms and solvent molecules are omitted for clarity. CPP ring labeled in red.

The ring strain can also be investigated by quantum mechanical calculations *via* homodesmic reactions. For such qualitative comparisons, the energy of the strained macrocycle vs. the linear oligomer is compared, encompassing the same number of atoms of each element. This approach could not be applied to structure **38** and its larger homologues,

which are presented in the following chapter, since the molecules are structurally too complex to achieve calculations in a reasonable amount of time with basis sets that are comparable to other molecules studied throughout the literature. Thus, we did not undertake such investigations.

3.2.1.4. Oxidative Dehydrogenation

To accomplish a successful bottom-up synthesis of CNTs, the remaining bonds between freely rotating arene rings, as indicated by the drawing, need to be fused by an intramolecular condensation. Such reactions can either be performed in solution or on surface.

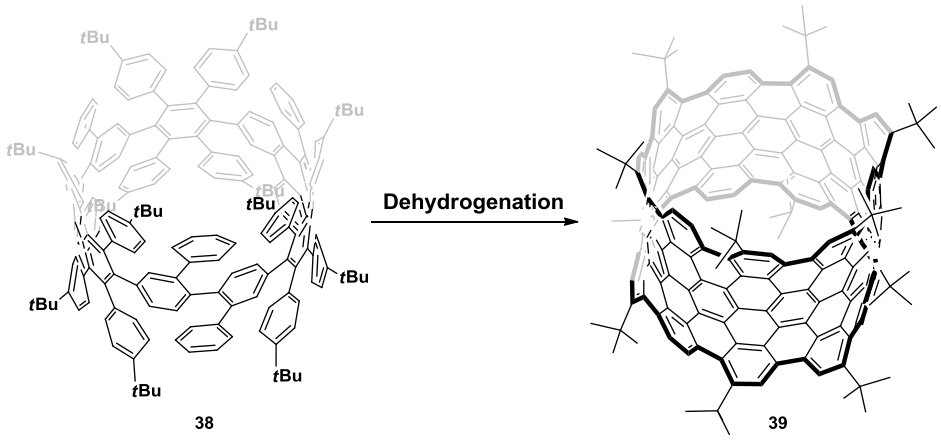

Scheme 12: proposed cyclodehydrogenation as a last step toward a bottom-up synthesis of **39**.

The oxidative cyclodehydrogenation, as the solution-based approach, is a well-known reaction to fuse C-C bonds of polyphenylens[123-124, 148-149] and has even shown promising results for several non-planar structures.[150-152] The surface based-approach is usually conducted for polyphenylene structures that yield planar products, which are otherwise difficult to access, as they do not contain solubilizing chains to prevent aggregation and, as a consequence, display poor or no solubility in solution. In comparison to the solution-based approach, which is conducted between r.t. and 100 °C, during surface-mediated intramolecular condensation dehydrogenation temperatures as high as 500 °C can be applied.[55, 153] Because of the different reactions conditions and scopes of these approaches, both methods were investigated and the results will be discussed in the following two sections.

3.2.1.4.1. Solution-based approach

The oxidative cyclodehydrogenation, as shown in *Scheme 13*, was first conducted using a standard reaction protocol: **38** was reacted with $FeCl_3$ at r.t. for 2 d. After work-up, an orange solution was obtained which showed a very broad mass distribution ("hill") between the starting mass of 2727 g/mol and title mass of **39** of 2653 g/mol (MALDI-TOF). The crude product was purified by preparative TLC and subsequently by preparative GPC which afforded several fractions, ranging from a yellow fluorescing solution (lowest molecular weight) to a red one (highest molecular weights).

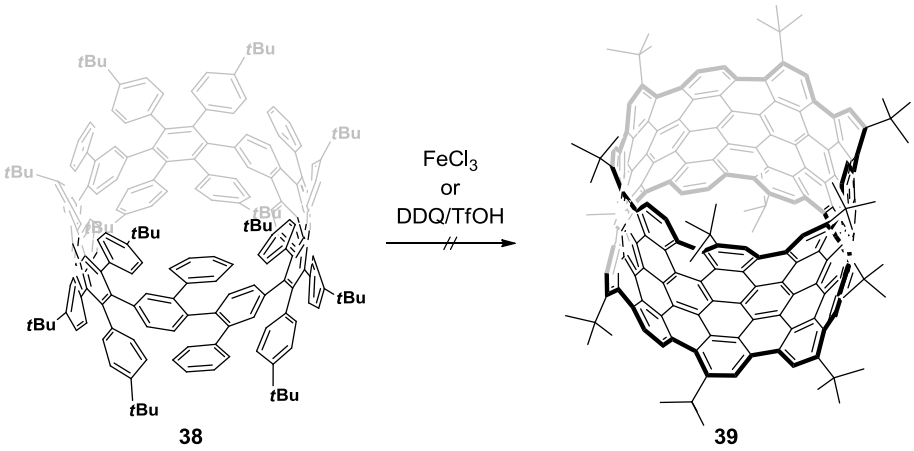

Scheme 13: Synthetic approaches toward a bottom-up synthesis of CNTs

The different fractions were analyzed by Wen Zhang in our group, using our new MALDI-TOF-MS spectrometer. His measurements showed that a separation by molecular weight, i.e., hydrodynamic radius was achieved. Unfortunately, each fraction contained several products apparently showing masses higher than that of the starting material (Ag^+ is the counter ion during these measurements). This finding is very surprising, since a clean starting material having a single mass was used. Disappointingly, the various peaks could not be assigned to intermediate products. Ion mobility measurements were not possible, due to the low S/N ratio.

The use of different oxidants, such as DDQ/TfOH at r.t. led to a decomposition of the macrocycle after several hours. The observed mass peaks could not be assigned to any fragments. Mass spectrometry measurements during the first hours showed a partial dehydrogenation (broadening of the peak) after which degradation took place. This ruled

out the use of DDQ/TfOH for a high temperature approach (up to 110 °C known in the literature).[149]

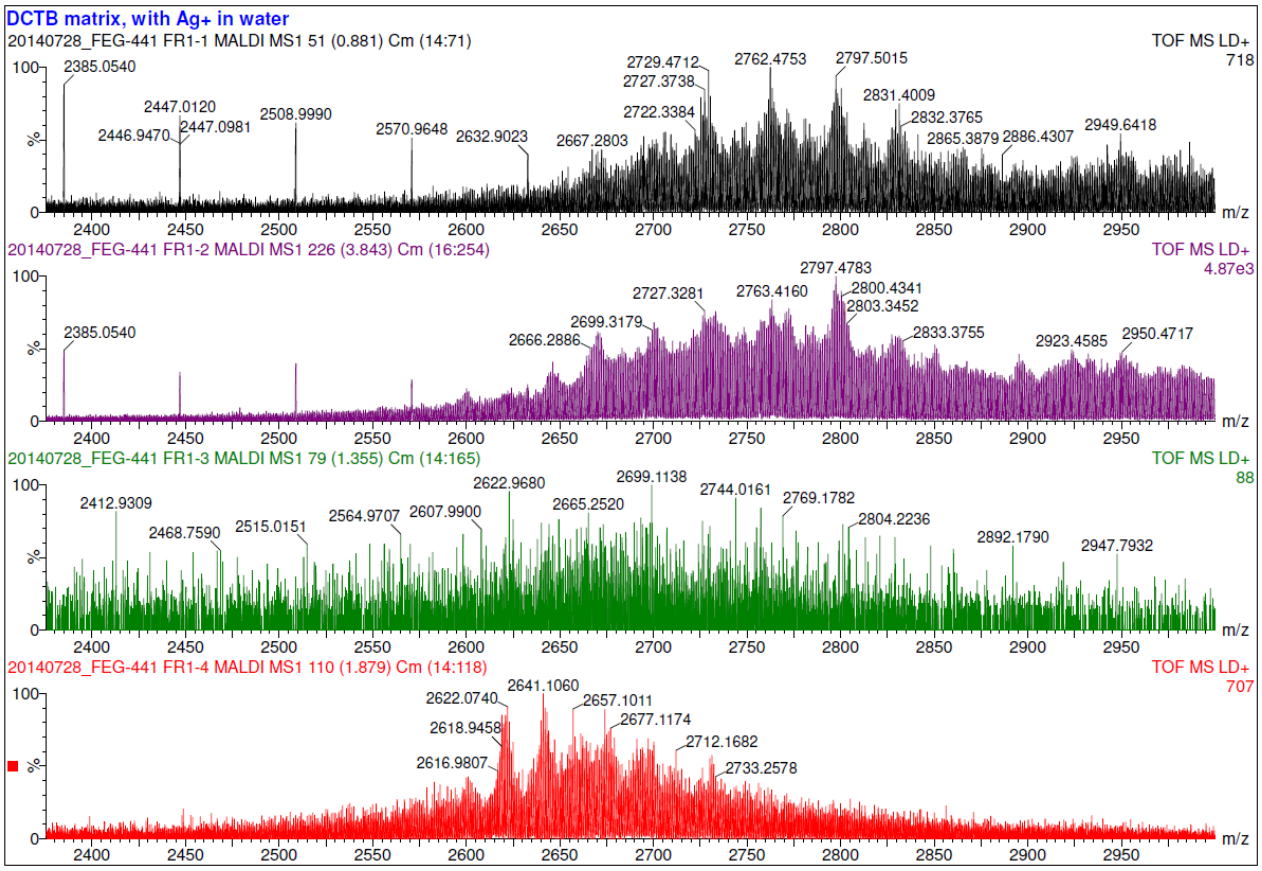

Figure 20: MALDI-TOF MS spectrum. DCTB matrix, with Ag^+ in water.

Based on the X-ray crystal structure analysis of the starting material **38** and our results with $FeCl_3$, a cyclodehydrogenation at elevated temperatures could have been favorable due to the high rigidity of the macrocycle and the thus reduced probability of electronic interaction between neighboring phenyl rings. As stated before, the decomposition made this approach not possible.

Hence, we opted for a surface mediated cyclodehydrogenation, which has been successfully applied for a number of precursors for the synthesis of conjugated polyaromatic structure and graphene nanoribbons.[54-55, 154-155]

3.2.1.4.2. Surface-mediated Oxidative Cyclodehydrogenation

In collaboration with the group of *Prof. Dr. R. Fasel*, *Eidgenössische Materialsprüfungs- und Forschungsanstalt* (EMPA), Switzerland, the oxidiative cyclodehdrogenation on metal surfaces was studied with STM. First, the sublimation and visualization on gold and platinum surfaces was conducted. Afterwards, the oxidative dehydrogenation could be studied on metal surfaces at different temperatures.

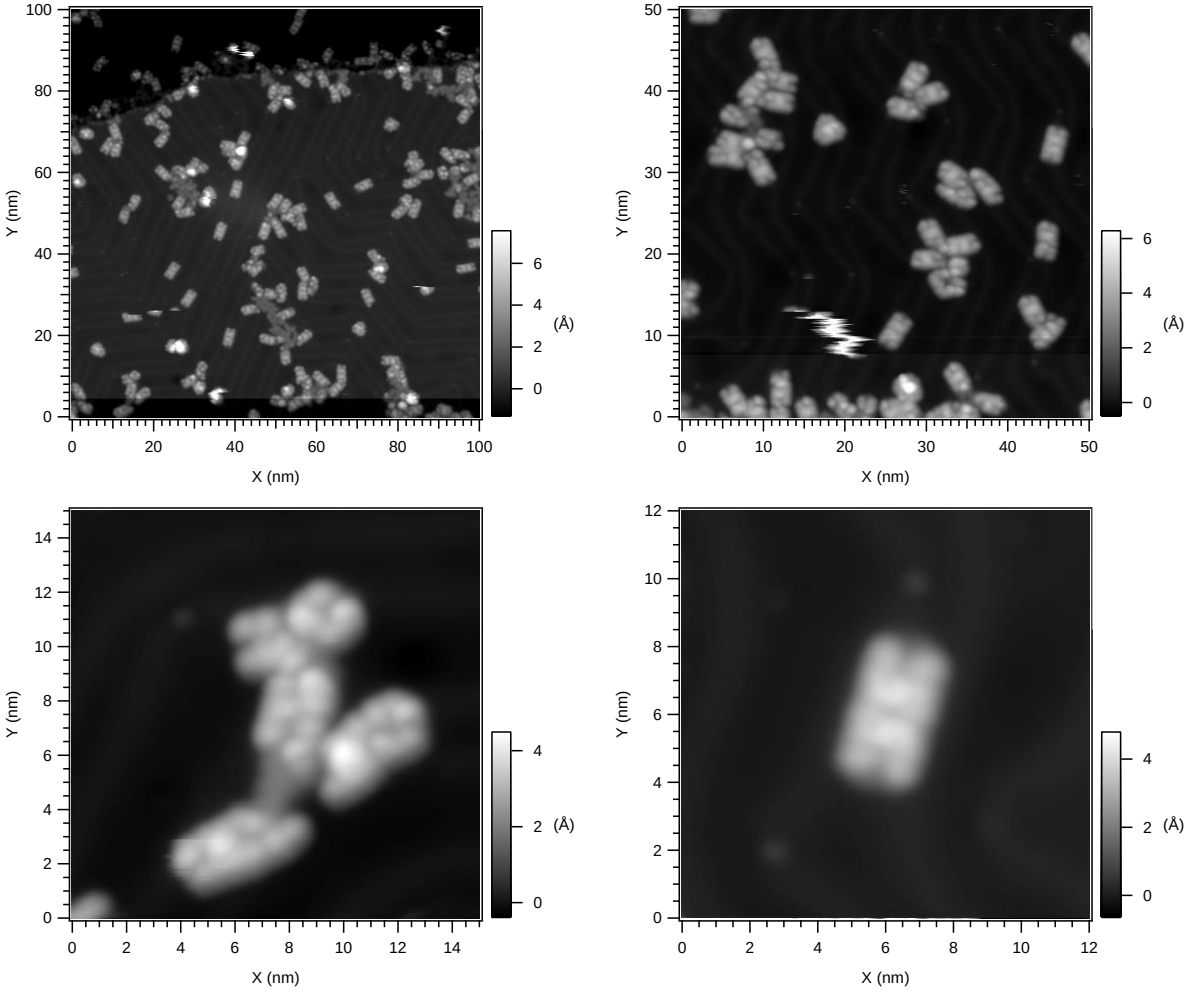

Figure 21: STM images recorded at 4 K on Au(111) surface of **38** at different resolutions showing objects with similar topology.

To our surprise, the polyphenylene cylinder [9]PPC **38** could be sublimed at 600 °C. At 77 K, no molecules were visible by STM on an Au(111) surface. However, the measurements indicated mobile objects, as faint streaks were recorded during the measurement. Thus, the temperature was decreased to 4 K. As a consequence, the mobility

of the molecules was reduced so much that rectangular objects were observed at the step edges of the gold surface. After annealing the sample at 300 °C, elongated structures were observed, as depicted in *Figure 21*. Most of these structures have rectangular topologies with two maximum heights at the long sides and a valley in the center (see *Figure 22*). At first glance, the observed structures seem surprising, since one would expect more square than rectangular objects based on the X-ray crystal structure dimensions (LWH: 1.30 nm x 1.18 nm x 1.60 nm). At the beginning we thought that these structures resemble opened-up PPCs, giving rise to GNR precursors with a theoretical length of 3.8 nm; the lateral extension could support this hypothesis. However, first, the apparent height of 0.4 nm is too large for a twisted polyphenylene. Second, a simple model of the molecule relaxed in vacuum is shown, which also depicts the "tight" belt of the central CPP ring and, to its left and right, the freely rotating phenyl or 4-*t*bu-phenyl substituents. Third, the apparent longitudinal extension of polyphenylene cylinders is assigned to the *t*-butyl groups which lead to an overestimation of size.

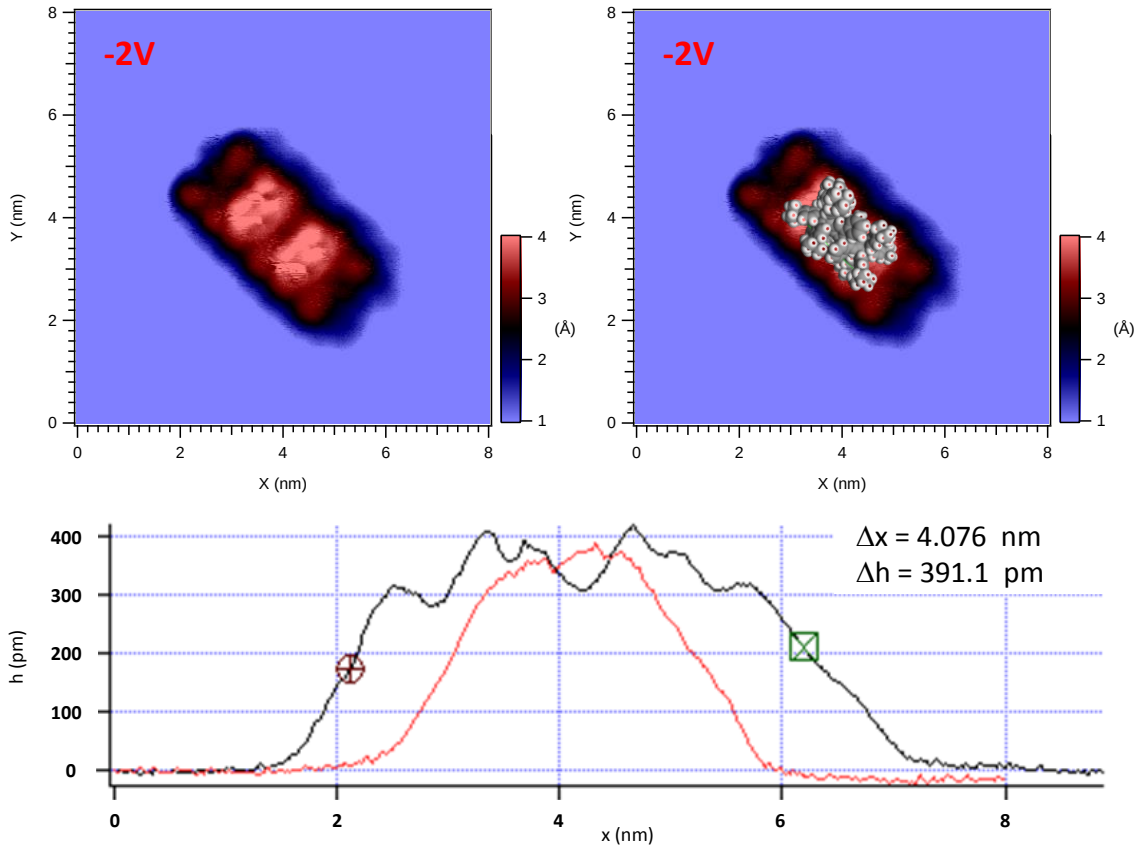

Figure 22: STM images with higher resolution. Extension of the polyphenylene cylinder on gold surface (111). Lower picture: size extension of the PCCs. Black line = width; red line = breadth.

After visualization of [9]PPC **38**, a possible intramolecular cyclodehydrogenation was investigated. Therefore, the sample was annealed at 325 °C for 60 min (see *Figure 23*). The experiments show an aggregation or even intermolecular coupling of single molecules, resembling oligomeric structures (see right). In addition, a flattening of the PPC was observed, which can be derived from the apparent height and the vanished hill-valley-hill that can be seen of the untreated [9]PPC structures on the left (see *Figure 23*). The use of a Pt(111) surface, which is reported to be more reactive to induce intramolecular dehydrogenation of single molecules than Au(111), did not produce any changes of the structures after subsequent annealing from 200 °C to 400 °C.

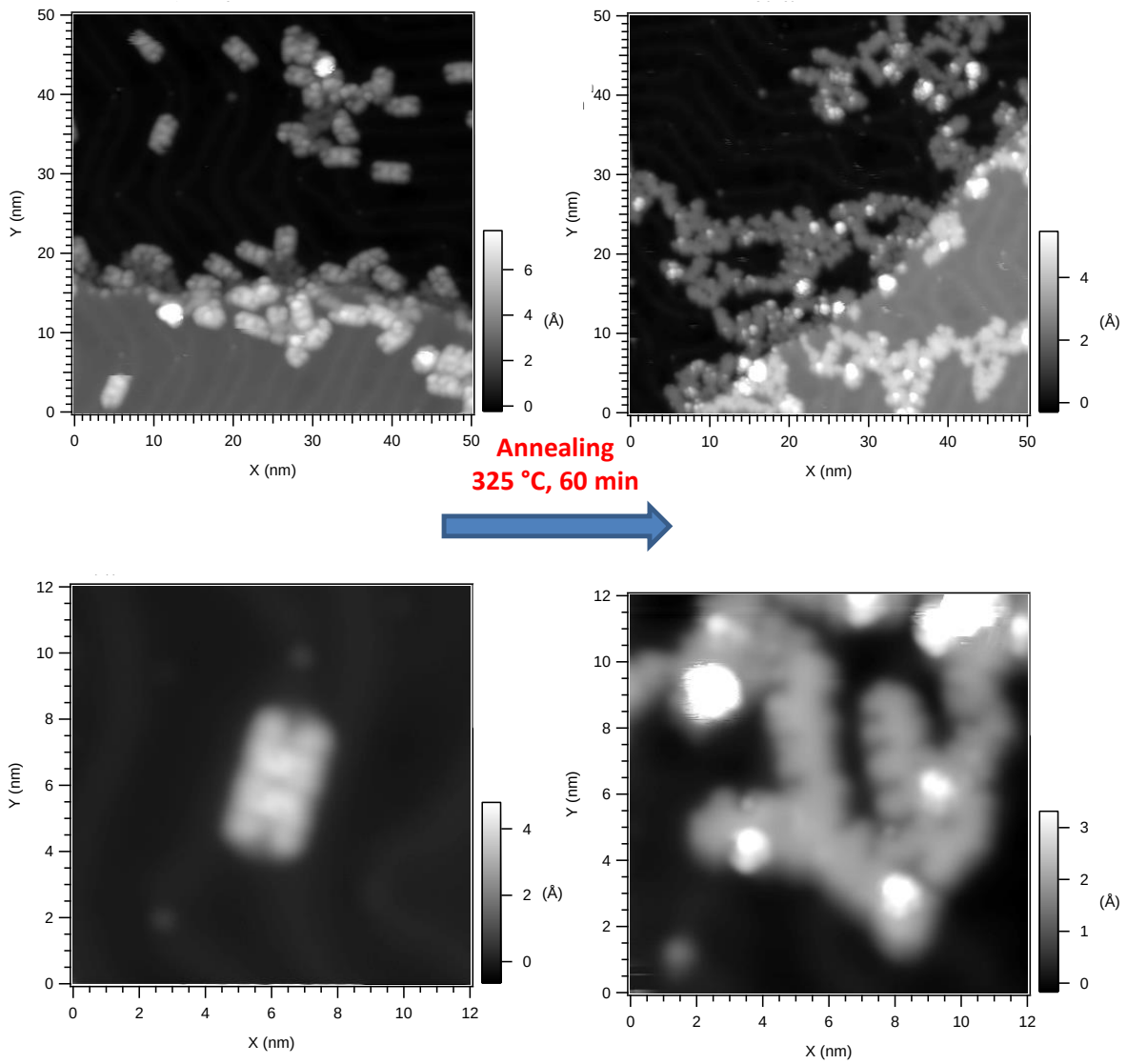

Figure 23: Annealing of **38** at 325 °C: intermolecular coupling and flattening of the structures was observed.

In conclusion, the solution-based oxidative cyclodehydrogenation and the surface-based thermally induced dehydrogenation did not afford the desired CNTs. In the first case, only a partial dehydrogenation was observed. Mass spectrometry analysis showed a very broad peak. Intermediate products, however, could not be assigned. With STM, the [9]PPC could be visualized. Subsequent dehydrogenation yielded flatted, oligomeric structures. The bottom-up synthesis of CNTs could not be achieved, independent of the pursued strategy.

3.2.1.5. Summary

In this chapter, the synthesis of a [9]CPP based polyphenylene cylinder **38** was described. To do so, a kinked precursor **34** was synthesized and converted into diiodide **35**. By means of a copper-mediated oxidative homocoupling, a trimerization of the precursor was achieved to give the kinked macrocycle **25**. After reductive aromatization, a strained [9]PPC **38** was obtained. As a final step toward a successful bottom-up synthesis, the oxidative cyclodehydrogenation was investigated. However, neither a solution-based nor a surface-mediated approach afforded the desired CNT – probably due to too high ring strain and geometric constraints.

3.2.2. [15]CPP containing PPC

In the previous chapter (*vide supra*), the synthesis of a [9]CPP containing PPC **38** was described and oxidative cyclodehydrogenation, as a final step toward a successful bottom-up synthesis of CNTs, was investigated. However, only a partial cyclodehydrogenation was observed. The dehydrogenation was supposedly hampered by high ring strain, which was deduced from the X-ray crystal structure. Here, an expansion of the PPC is described, increasing the number of phenylene rings by six; the new PPC **41** is thus based on a 15-membered CPP. We envisioned that a decrease in ring strain could afford smooth cyclodehydrogenations to give short CNT segments.

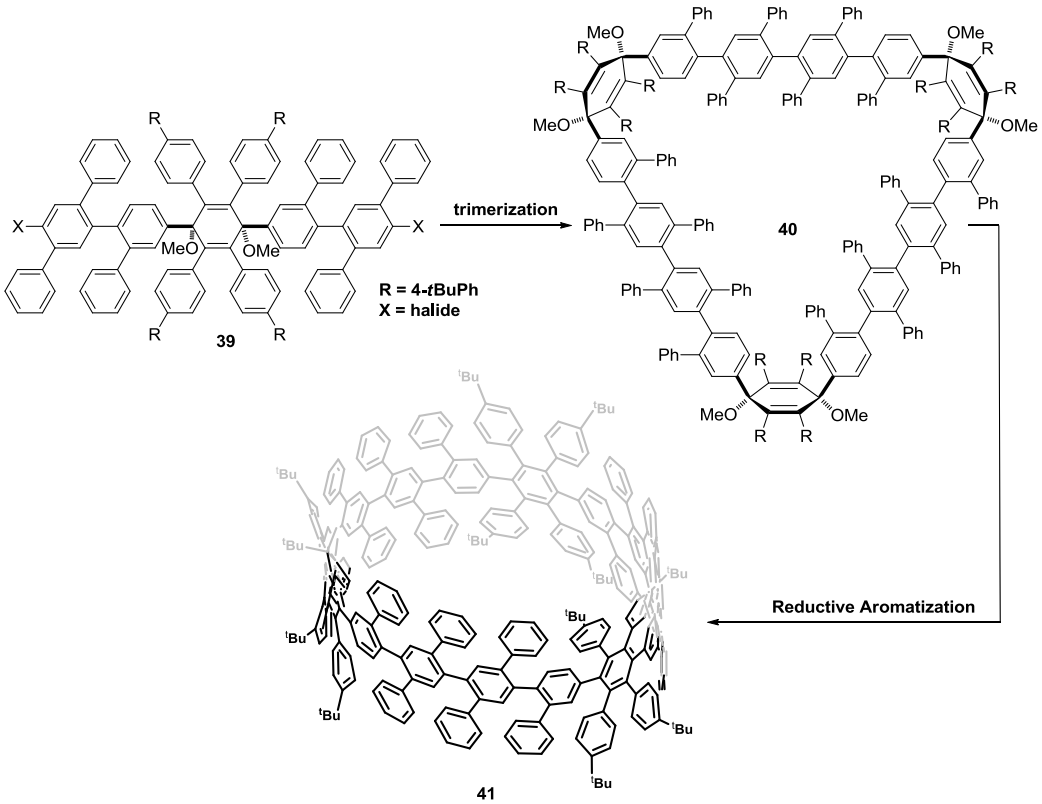

Scheme 14: Synthetic concept of a [15]CPP containing PPCs.

The general synthetic strategy for ring expansion by six phenylene units is shown in *Scheme 14*. The previously introduced kinked diiodide **35** is expanded by two terphenyl units to give **39**. This extended building block is designed in an analogous fashion, corresponding to its smaller congener, so that trimerization can be performed *via* the previously established oxidative homocoupling. Reductive aromatization is to give the expanded macrocycle **41**.

3.2.2.1. Extended Precursors

In this section, the synthesis of the extended precursor **39** is described (*vide supra*). A synthetic route was developed to couple the borlyated terphenyl **44** with a modified biphenyl by *Suzuki* coupling. Initially, the synthesis started off with the literature known *Suzuki* coupling of 1,4-dibromo-2,5-diiodobenzene with phenyl-boronic acid which afforded terphenyl **43** in good yields. Desymmetrization of **43** was achieved by monolithiation and subsequent borylation with *i*PrOBpin to give boronate **44** in satisfying yields (53%). For the synthesis of **46**, the previously prepared biphenyl **16** was subjected to *n*-BuLi and silylated at the 5-position, yielding **45**. Lithiation with *n*-BuLi and quenching with iodine afforded **46**. *Suzuki* coupling of **44** with **46** afforded **47** in good yields (73%). Iododesilylation with ICl resulted in the formation of **48**.

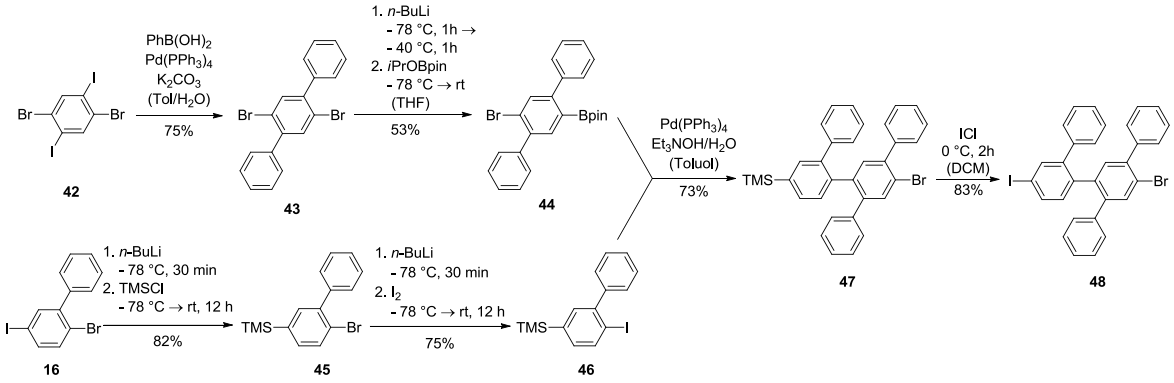

Scheme 6: Synthesis of **48**.

The successful synthesis of building block **48** was a proof of principle whether the coupling of sterically crowded Br-terphenyl **44** and, more importantly, its TMS-protected derivative **55** (*vide infra*) is feasible. At first, it was assumed that the *Suzuki* coupling might pose a challenge due to the high sterical demand exerted by the phenyl groups, which was not the case, as stated above.

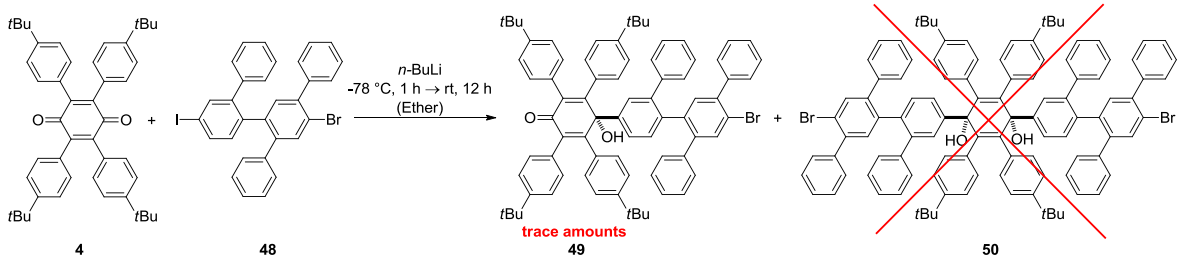

Scheme 15: Synthesis of terphenyl extended building block **50**.

With compound **48** in hand, the coupling with benzoquinone **4** was studied, expecting to afford a kinked diol, despite the likelihood of a partial debromination during lithiation of **48** – previously observed for **17** (see *Scheme 3, p. 21*) –, as this was an easy proof of principle whether these two substrates react with each other (see *Scheme 15*). Unfortunately, the MALDI-MS spectrum showed only a small amount of the monoaddition product **49**; deiodinated starting material was primarily obtained. This strategy failed and hence we did not opt for a substitution of bromine by a TMS group, as a general strategy to avoid dehalogenation during the reaction. More so, the approach was entirely given up, since it required 12 synthetic steps. In addition, compound **48** was used in excess, as two to three equivalents of the lithium organyle are generally required per carbonyl carbon to quantitatively afford the kinked cyclohexa-2,5-diene-1,4-diol from quinone **4**.

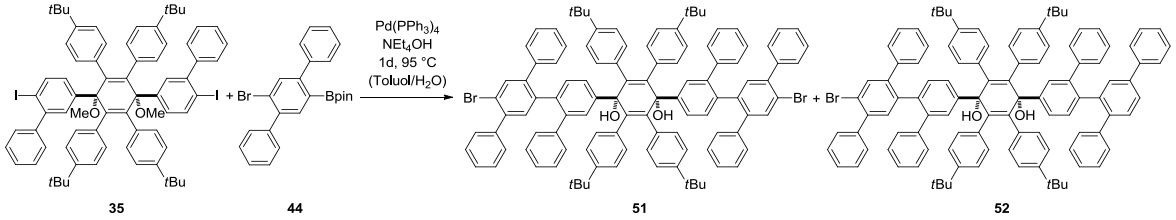

Scheme 16: Synthesis of **6**. Demethylation of methoxy groups due to the harsh *Suzuki* reaction conditions

To overcome these challanges, the kinked 1,4-dimethoxycyclohexa-2,5-diene **35** was terphenylated using *Suzuki* coupling (see *Scheme 16*). The reaction gave the demethylated products **51** and **52**, where demethylation was attributed to the harsh coupling conditions, induced by NEt_4OH (see *Figure 24*). This was a very promising result, as it proved the general feasibility of this coupling.

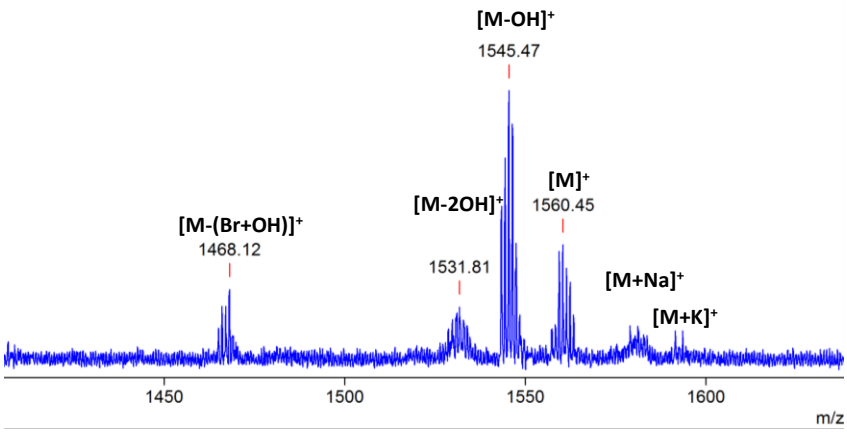

Figure 24: MALDI-TOF spectrum of **51** and **52**. The peaks of $[M]^+$, $[M\text{-}OH]^+$ and $[M\text{-}2OH]^+$ showed demethylation as a consequence of the very harsh Suzuki coupling conditions.

For an efficient and successful synthesis of an extended precursor, a TMS protected precursor **55** was developed and the reaction conditions for *Suzuki* coupling were optimized. Both proved to be much more challenging than initially expected.

The synthesis of the desymmetrized terphenyl will be described first. Two routes for **55** were initially investigated: in route a), dilithiation of a 1,4-diiodo *p*-terphenyl **53** and subsequent quenching with TMSCl and *i*PrOBpin was studied. This approach failed due to a too low solubility of the starting material. For b), desymmetric bromodesilylation of **54** with BBr_3, and subsequent hydrolysis to afford the boronic acid derivative was expected to give **55**. Surprisingly, this synthetic approach only afforded a naked terphenyl.

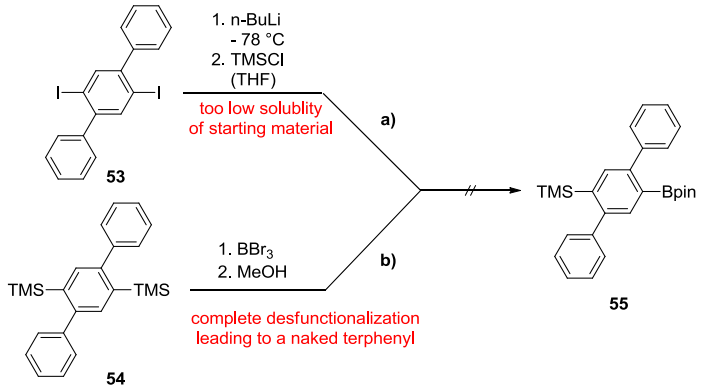

Scheme 17: unsuccessful studies toward terphenyl **55**

Route c) eventually yielded the desired terphenyl **55**. Following a literature procedure,[156] 1,4-diiodobenzene **56** was deprotonated with LDA and quenched with TMSCl to give **57** (74%). The *bis*(silane) was phenylated *via Suzuki* coupling to give terphenyl **54** in good yields (78%). To desymmetrize **54**, 0.5 equivalents of iodinemonochloride were used to give the desymmetrized *p*-terphenyl **58** and starting material **54** (see *Scheme 18*). Iodine monochloride was used in shortfall to avoid diiodination of **58**. For borylation, the mixture of **58**, **54** and **9** was used since they could not be separated by column chromatography or recrystallization, as polarity and structural differences are too marginal. This, fortunately, did not hamper borylation, since **8** is chemically inert in the presence of *n*-BuLi. The borylation of **58** yielded **55** in satisfying yields (37%); previous borylations of related terphenyls, having a comparable sterical demand, gave similar results.

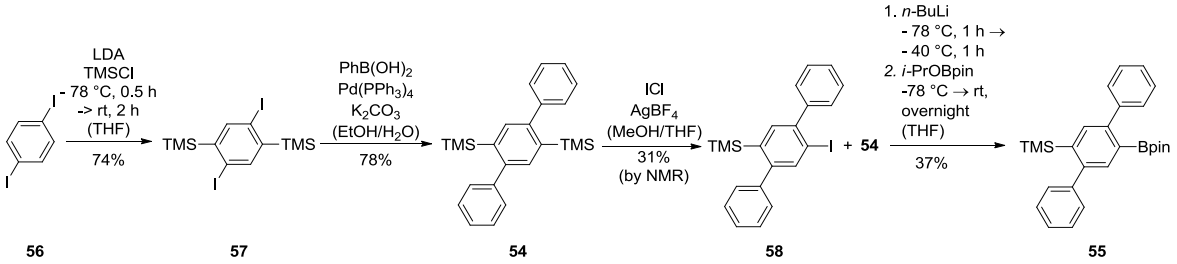

Scheme 18: Synthesis of the TMS-protected and desymmetrized terphenyl boronate **55**

In *Scheme 19*, the ^{1}H-NMR spectrum of the TMS-protected terphenyl boronate **54** is depicted. The integrals of the TMS and boronate group reveal a quantitative borylation. The singlets at 7.55 ppm and 7.63 ppm of the protons attached to the central phenylene reflect its asymmetric nature. This was supported by the ^{13}C-NMR spectrum (not shown), where a line splitting of the two phenyl groups is observed. All integrations are in agreement with expectations.

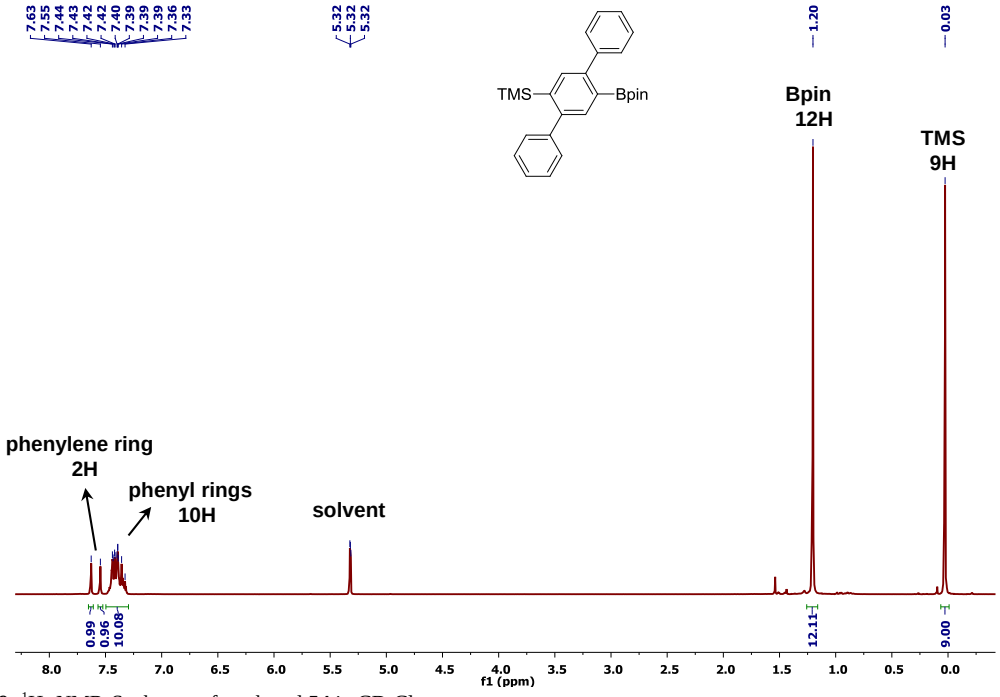

Scheme 19: ^{1}H- NMR-Spektrum of terphenyl **54** in CD_2Cl_2 at r.t..

With this building block in hand, the extended precursor was synthesized *via* coupling of the terphenyl boronate **54** with diiodide **35** using *Suzuki* coupling. The coupling was carefully optimized since the use of K_2CO_3 afforded a mixture (2:1) of the title compound **59** and monoterphenylated-deiodinated starting material; separation of this mixture was very tedious and therefore not feasible for a large scale approach. The use of *SPhos* as ligand, which it utilized for sterically demanding Suzuki couplings in combination

with K_3PO_4, gave a similar product distribution. The use of Cs_2CO_3 could suppress deiodination to give **59** in very good yields (81%). This may be explained by its higher solubility in organic solvents and its increased basicity. After iododesilylation in the presence of $AgBF_4$ (see *Scheme 20*) the desired expanded dihalide **60** was obtained.

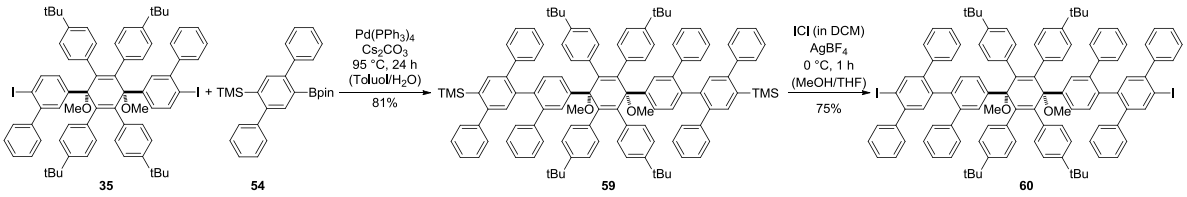

Scheme 20: Synthesis of extended building block **60**.

In *Figure 25*, the NMR spectrum of **59** is depicted. At 0.1 ppm, the signal of the TMS group is observed, whereas the signal of the *t*-butyl groups appears at 1.02 ppm. The integration of these two peaks reflects the theoretical ratios of 1:2. This is also well in line with the integral of the methoxy group (3.71 ppm). Furthermore, no peaks for a possible hydroxyl group at around 2.6 ppm were detected; demethylation of the methoxy groups could be avoided due to the presence of $AgBF_4$ (see also *Scheme 8, p. 26*). The number of the aromatic protons is also in agreement with expectations. Due to signal overlap in the aromatic region, it becomes very difficult to derive any additional information from these protons.

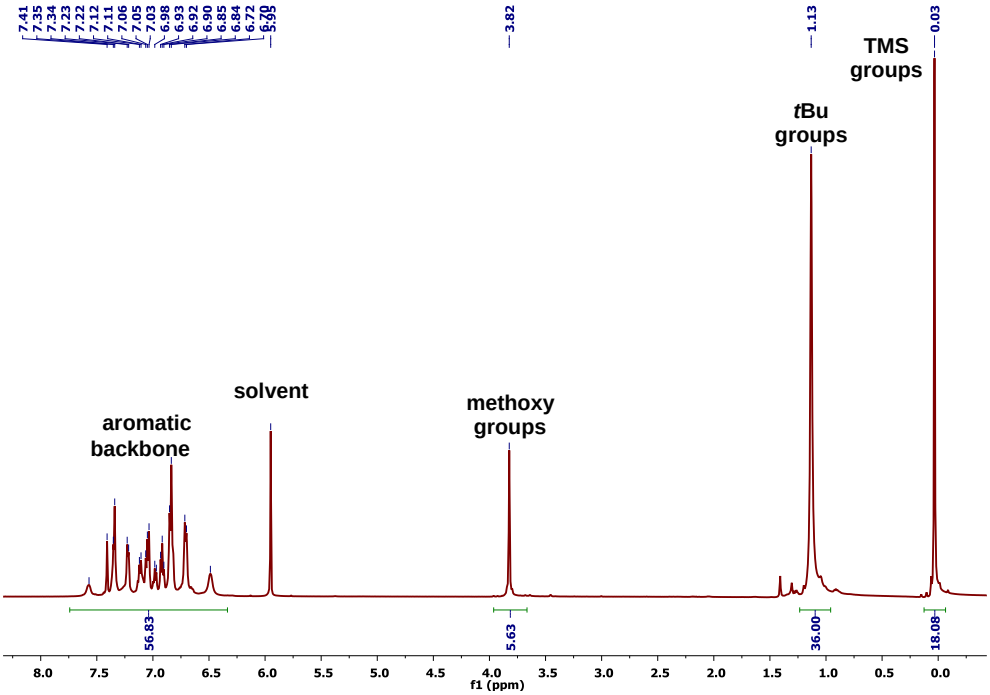

Figure 25: 1H-NMR spectrum of 12 measured in $C_2D_2Cl_4$ at 100 °C. The integration from left to write: 56:6:36:18.

The structure and the high symmetry of **59** are also supported by the ^{13}C-NMR-spectrum, shown in *Figure 26*. The non-aromatic carbon atoms are detected between 0 ppm and 85 ppm, and are in agreement with expectations and measurements of the starting materials. In the aromatic region, only 27 peaks out of the theoretically possible 29 peaks are observed. These missing peaks can be attributed to isochrony, as the spectrum was recorded at high concentration.

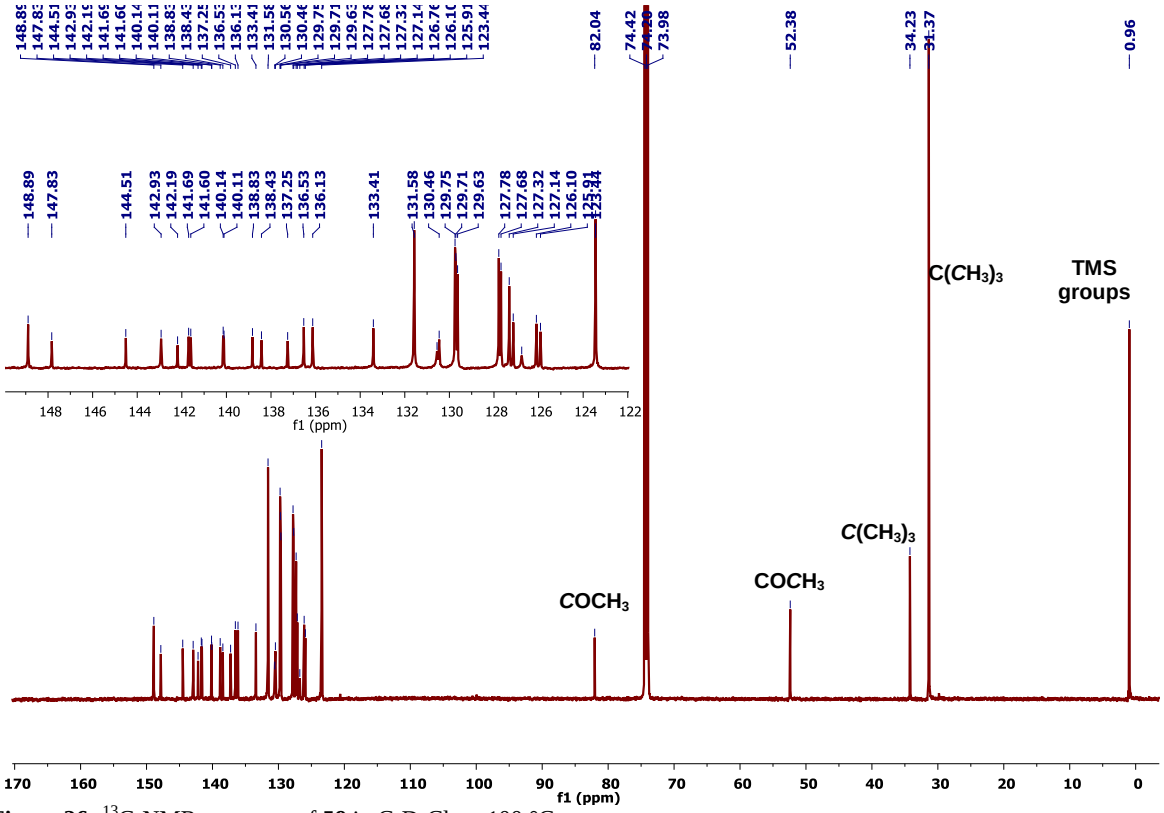

Figure 26: ^{13}C-NMR spectrum of **59** in $C_2D_2Cl_4$ at 100 °C.

As described for the ^{1}H-NMR spectrum, single peaks for carbon atoms of the *t*-butyl, TMS, methoxy groups, and quarternary carbon neighbouring (MeO*C*) are observed, whereas unsymmetric 1,4-dimethoxycyclohexa-2,5-dienes, such as monoterphenylated compounds, show a splitting of the peaks in the ^{1}H- as well as ^{13}C-NMR-spectrum (see *Figure 43, p. 78).* The high sensitivity and the thus straightforward structure elucidation render NMR a very helpful method to distinguish between symmetric and asymmetric structures. This becomes especially important during macrocycle synthesis, as these compounds are symmetric and should feature one singlet peak for the aforementioned non-aromatic protons and carbon atoms, respectively.

3.2.2.2. Synthesis

The synthesis of the [15]PPC was performed in an analogous fashion to the previously described [9]PPC: the extended precursor **60** was trimerized via an *Ullmann*-type homocoupling to give the macrocycle **61** in 10% yield (see *Scheme 21*).

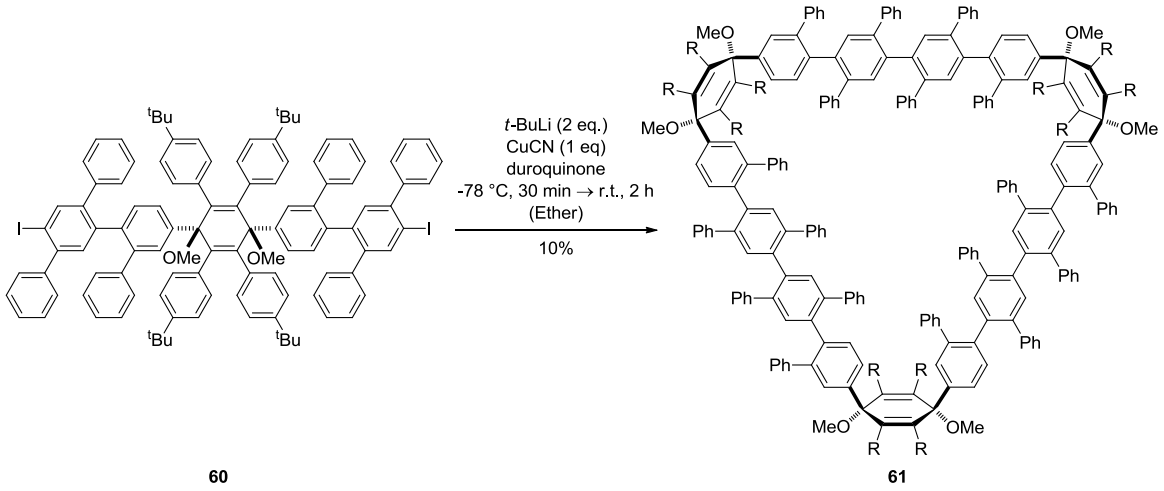

Scheme 21: Synthesis of macrocycle **61** *via* an oxidative homocoupling.

The purification of **61** was more tedious than for [9]PPC **35**, as the six terphenyl units provided additional solubility which rendered fractional precipitation impossible. Therefore, the macrocycle was roughly purified by column chromatography and fully purified by recycling GPC, taking advantage of the lower hydrodynamic radius of the cyclic precursor in comparison to its linear homologue. The observation of two peaks in the elugramm with nearly the same hydrodynamic radius provided first evidence for the macrocyclization. The findings were supported by HR-MS measurements. A mass of 4283.2796 m/z for the title compound **61** was detected, which matches with the theoretically calculated mass up to the fourth digit (4283.2796 m/z). In the isotopic pattern, peaks of linear homologues were not observed, supporting a successful purification. Third, macrocycle **61** exhibits a high symmetry, rendering the *t*-butyl and methoxy groups chemically and magnetically equivalent. This leads to *single* peaks for the *t*-butyl and the methoxy groups (1.17 ppm and 3.88 ppm, respectively), as shown in the ^{1}H-NMR spectrum in *Figure 27*. In contrast, the linear homologue shows a splitting of each signal, giving to separate singlets in a 2:1 ratio.

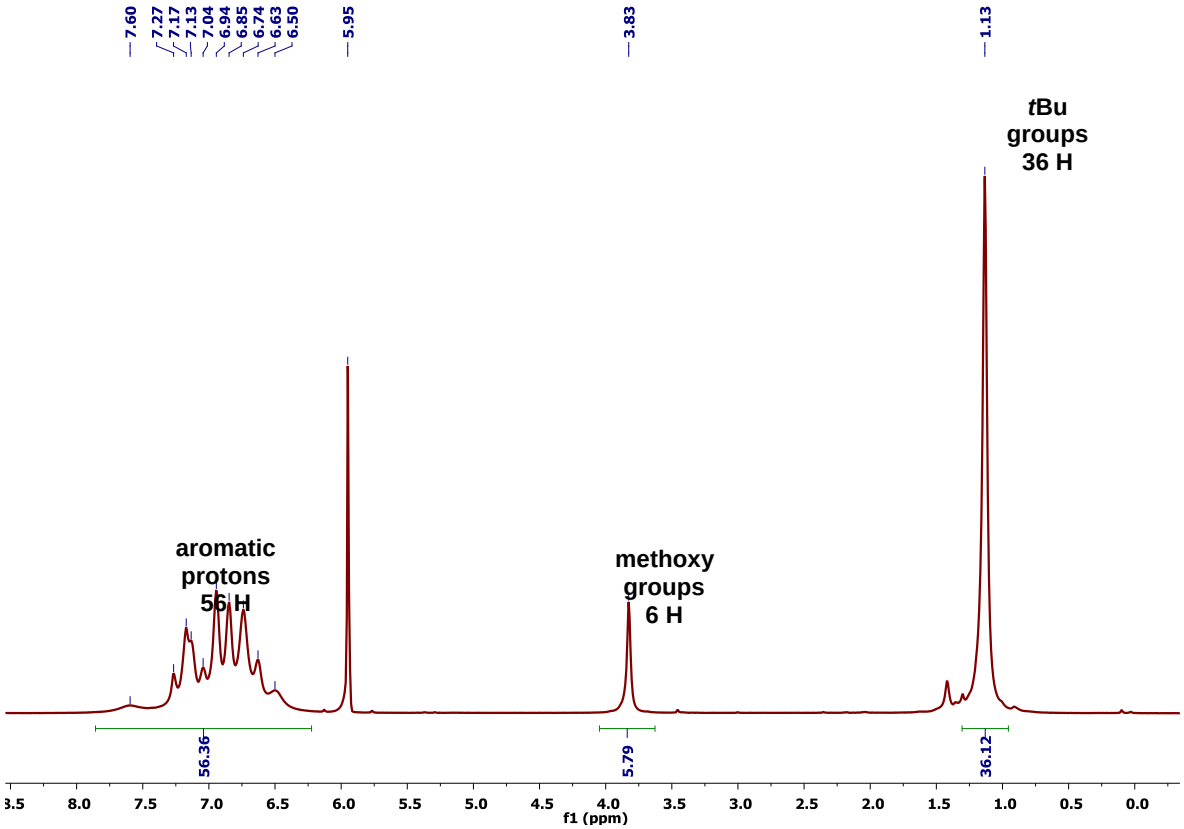

Figure 27: ^{1}H-NMR spectrum of macrocycle **61** in $C_2D_2Cl_4$ recorded at 100 °C.

In the last step, the pure kinked macrocycle **61** was reductively aromatized to give the [15]CPP polyphenylene cylinder **62** in 48% yield. The highly soluble product (unpolar solvents; THF) was characterized by HR-MS and ^{1}H- and ^{13}C-NMR spectroscopy.

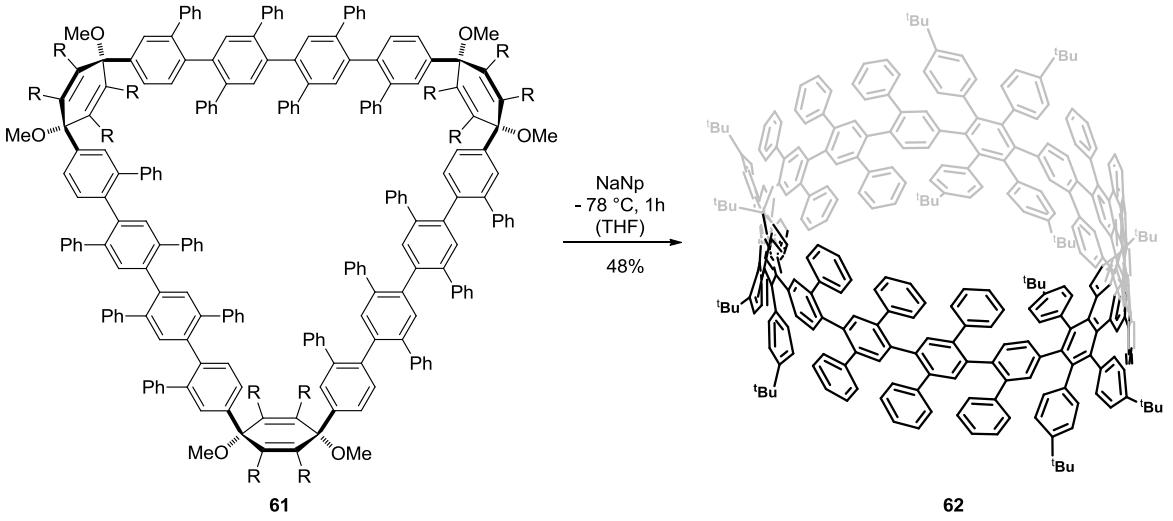

Scheme 22: Synthesis of 15[CPP] based polyphenylene cylinder **62**.

HR-MS reveals a mass of 4097.1693 m/z which is in agreement with the theoretical mass of 4097.1693 m/z up to the fourth digit. Furthermore, the isotopic pattern matches with the theoretical pattern, as depicted in *Figure 28*. If an intensity increase of the experimental isotopic pattern at 4099 m/z had been observed (mass of linear trimer), the sample would have been contaminated by its linear trimer, since it bears two additional hydrogen atoms. The analytical data does not support this viewpoint and hence renders the sample pure.

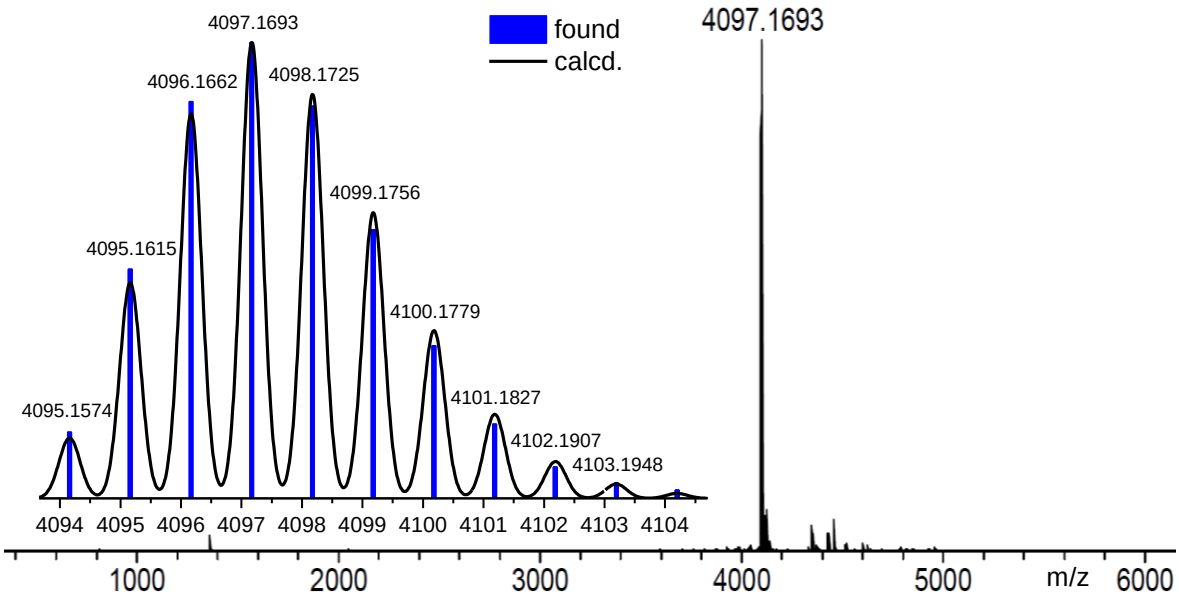

Figure 28: HR-MS-spectrum of 15[CPP] based polyphenyle cylinder

^{1}H-NMR sepctroscopy also provides clear evidence for macrocycle formation. Temperature-dependent measurements were conducted from 25 °C to 140 °C. With increasing temperatures, merging of the rotamers was observed, giving one singlet for the *t*-butyl groups due to symmetry considerations. Other structural features cannot be derived from the NMR spectrum, as the aromatic protons overlap too strongly.

In more detail, the measurements revealed that the *t*-butyl groups split into several peaks at room temperature, ranging from 0.5 ppm to 1.5 ppm. The sharp peaks hint at rotamers with low exchange rates. Upon heating to 60 °C, the peaks merge into a single broad one, reaching the coalescence point, where the signals of the slow and fast exchange overlap. With increasing temperature, the full width at half maximum decreased until a sharp singlet was observed at 140 °C which arises from the fast exchange in combination with a high rotational frequency of the molecule. Hence, NMR spectroscopy purports to the presence of

rotamers, which could hinder oxidative cyclodehydrogenation at r.t. due to interlocked structures (see *chapter 4.5*).

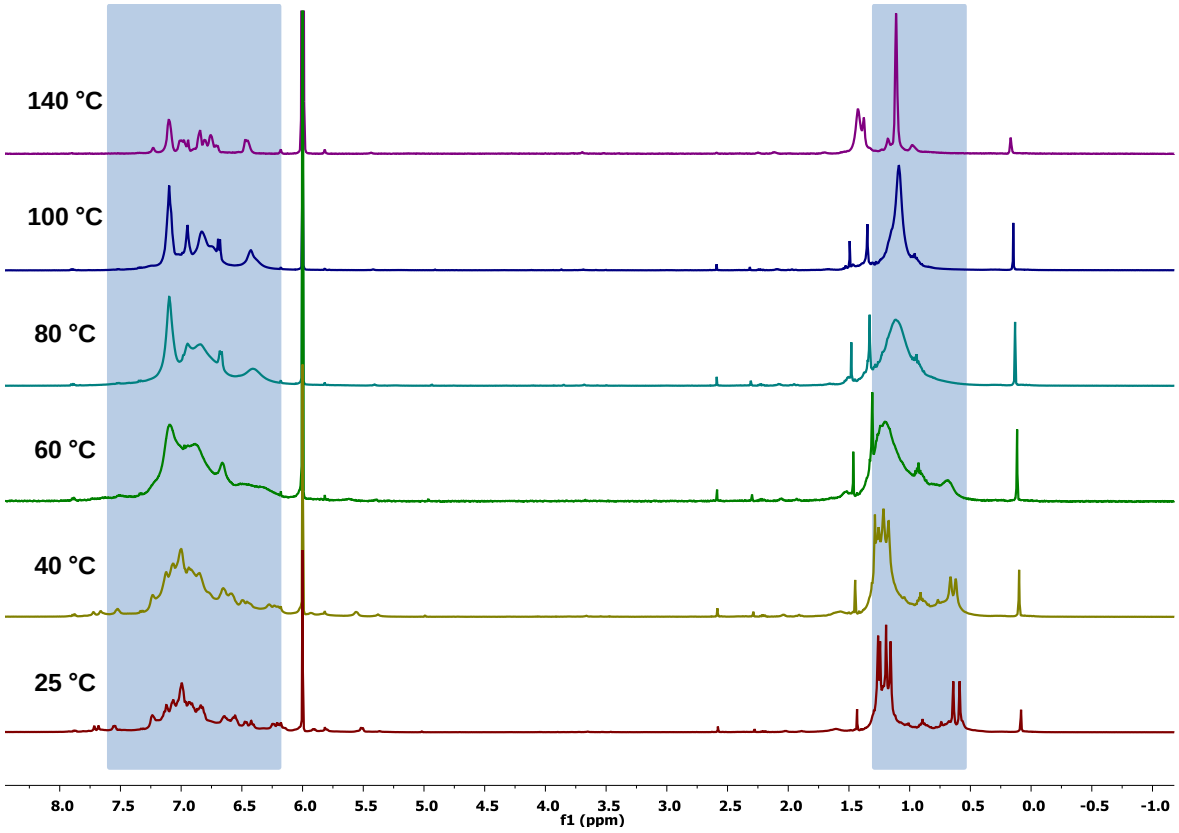

Figure 29: High temperature NMR spectra of **62** recorded in $C_2D_2Cl_4$ at various temperatures: r.t., 40 °C, 60 °C, 80 °C, 100 °C, and 140 °C.

To sum up, the synthesis of the extended precursor **60**, its trimeriziation and successful reductive aromatiziation were presented. The synthesis of **60** was achieved by a *Suzuki*-mediated terphenylation of the kinked diiodide **35**. The subsequent cyclization, to give the triangular macrcyle **62**, was performed analogously to its smaller congener **25**. Reductive aromatization with sodium napthalenide as reducing agent afforded the [15]CPP based PPC **62**. This macrocycle could be characterized by mass spectrometry and NMR spectroscopy. The latter showed that several rotamers are present at 25 °C (see *Figure 29*) derived from the splitted signal of the *t*-butyl groups. The presence of rotamers at 25 °C is unfavorable for the oxidative cyclodehydrogenation (see *next chapter*), since interlocked structures can hamper cyclodehydrogenation.

3.2.2.3. Oxidative Cyclodehydrogenation - Studies

After synthesis of [15]PPC **62**, the oxidative cyclodehydrogenation toward short CNT segments was studied. In order to achieve this goal, a loss of 120 hydrogen atoms is necessary to form the corresponding CNT **63**, as shown in *Scheme 23*. In the previous study (see *p. 32*), the cyclodehydrogenation of the [9]PPC was investigated: a decrease of mass was observed, however, showing a mixture several of compounds which could not be separated. The incomplete cyclodehydrogenation was assigned to a too small ring size. Therefore, the larger ring with six additional phenylenes in the CPP core was expected to overcome the ascribed drawbacks.

As before, the extended PPC **62** was subjected to different dehydrogenative conditions, such as DDQ/$Sc(OTf)_3$, and DDQ/TfOH and $FeCl_3$.[148-149, 157-160] The first two conditions led to decomposition of the cycle or the formation of degraded products that could not be assigned by mass spectrometry, whereas $FeCl_3$ at r.t. led to detectable products. The crude product was purified by preparative TLC and six different fractions could be obtained. The spectra resembled a broad mass either peaking or determinating at 4050 m/z. From these spectra, one could derive different dehydrogenated compounds that were formed during the reaction.

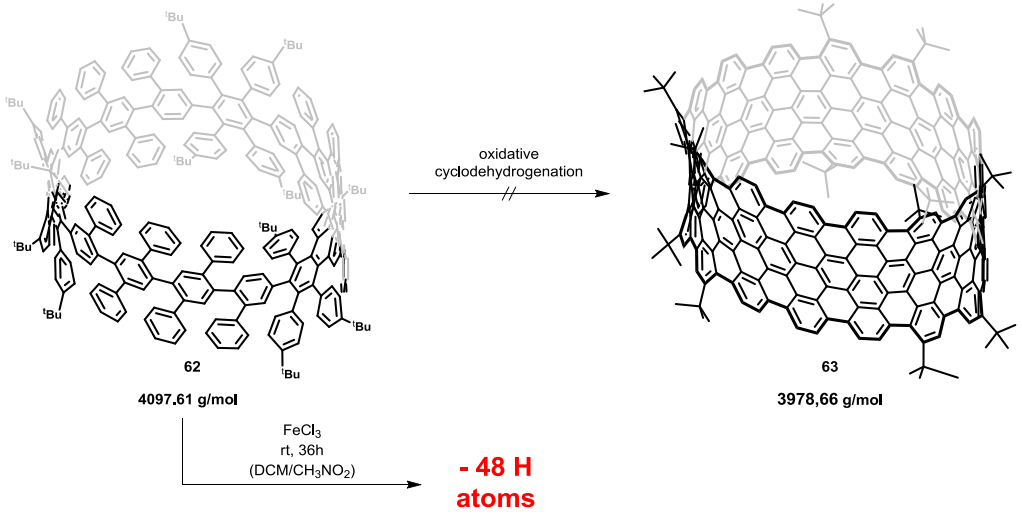

Scheme 23: oxidative cyclodehydrogenation of **62**. The mass is derived from MALDI-TOF measurements (see *Figure 30*).

Two representative spectra are shown in *Figure 30*. In the upper spectrum, a broadened peak at around 4050 *m/z* was observed, depicting a loss of 48 H atoms. This most promising fraction for structure elucidation was purified by HPLC, using a *Buckyprep* column. Despite

purification by prep TLC and HPLC chromotography, no improved MALDI spectra could be obtained.

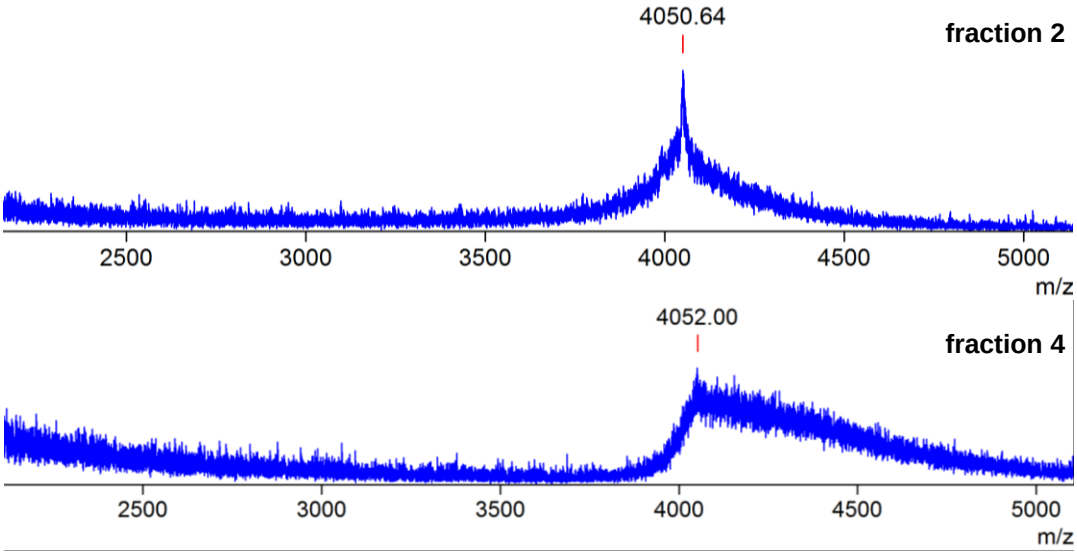

Figure 30: MALDI-MS after HPLC purification using a bucky prep column (faction 2 (upper), fraction 4 (lower).

As a consequence, the interpretation of the results is limited: it can be stated that an oxidative dehydrogenation took place, since a decrease of the monodisperse starting material **62** was observed. This is also in agreement with the orange fluoresecence after work-up. However, no solid information could be obtained regarding the structural composition of the product mixture.

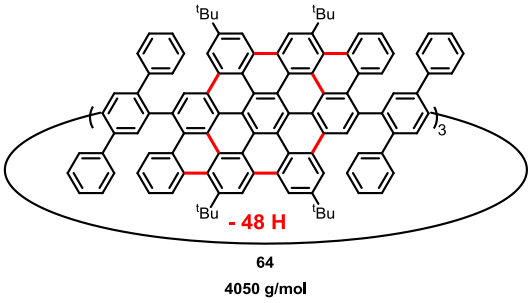

Scheme 24: hypothetical structure on the account of - 48 hydrogen atoms of a polydisperse MALDI-MS spectrum.

Nonetheless, based on the observed MALDI-TOF results (discussion: *vide supra*), a structure was drawn on the basis of 24 newly formed bonds, which equals a loss of 48 hydrogen atoms. Despite the poor data and missing structural information, a structure can be proposed: as shown in *Scheme 24*, the loss of 48 hydrogen atoms equals the formation of phenyl-extended HBCs.

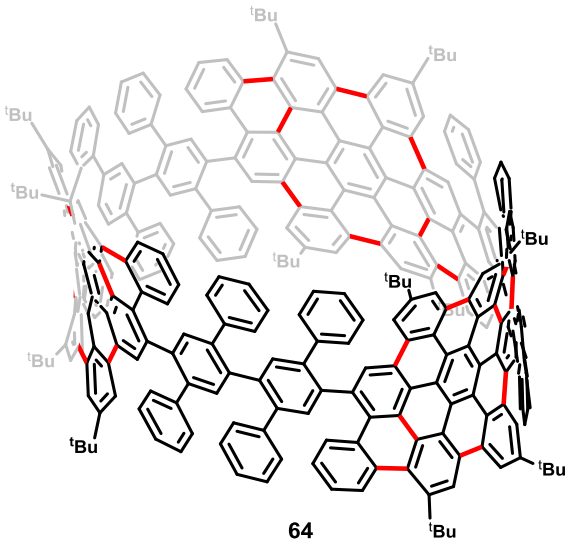

Scheme 25: proposed structure of **64** after loss of 48 hydrogen atoms due to bond C-C annulation.

In case of a cyclic structure, this could mean that a) the ring strain reaches a certain maximum at which no further dehydrogenation can occur; b) the increased strain in conjunction with the high rotational freedom of the terphenyl units leads to locked, rigid rotamers that cannot interact with neighbouring phenyls to form additional C-C bonds; c) structural defects (not drawn) could have occurred during the reaction that irreversibly terminated cyclodehydrogenation, which is supported by the broadened peaks. In case of an opened-up cylinder, the structural design could be the reason for an incomplete cyclodehydrogenation; our studies[161] with model systems, however, have never shown a ring opening.

In conclusion, the above described findings render the synthesis of a larger PPC and the preparation of structurally different precursors necessary. These approaches are discussed in the next chapter.

3.2.2.4. Summary

In this chapter, the successful synthesis of the [15]CPP based PPC **62** was described and its oxidative cyclodehydrogenation toward a bottom-up synthesis of ultrashort CNT was investigated.

To expand the [9]CPP based PPC **38** radially by six phenylenes, the kinked diiodide **35** had to be extended by two terphenyls. To do so, an efficient route for the preparation of an asymmetric, TMS-protected terphenyl **55** was developed, which bears a boronate in *para*-position to the TMS-group. After that, optimized reaction conditions for the *Suzuki* coupling with the kinked precursor **35** gave the bisterphenylated adduct **59** in good yields (81%). Macrocyclization *via* the previously applied oxidative *homo*coupling and reductive aromatization yielded the [15]PPC **63** in similar yields to [9]PPC.

As a last step toward ultrashort CNTs, the oxidative cyclodehydrogenation with $FeCl_3$ was investigated, which afforded a partially fused macrocyle showing a loss of 48 H atoms; for [9]PPC **38**, the loss of hydrogen atoms could not be accounted for due to a broad mass distribution and also higher masses. Satisfyingly, for the oxidatively cyclodehydrogenated [15]PPC **63**, a relatively sharp peak could be observed by MALDI-MS. Based on the loss of 48 hydrogen atoms, a partially fused cylinder structure was proposed, in which the hexaphenylbenzene and their *meta*-phenyl extended *para*-phenylenes were completely fused, i.e., all possible bonds of the macrocycle were fused except for the six terphenyls.

From these results, one can derive that it is necessary to synthesize larger cycles (see *chapter 3.2.3.*) as well as cycles with different connectivity patterns (see *chapter 3.4*).

3.2.3. Synthesis of [21]PPC

3.2.3.1. Synthesis

To reduce the ring strain of PPCs, enabling a smooth cyclodehydrogenation, an extension of six phenylene rings was performed to give a [21]CPP based polyphenylene cylinder. The strategy is performed analogously to the synthesis of the extended precursor **60** (see chapter *3.2.2.1. Extended Precursor, p.40).*

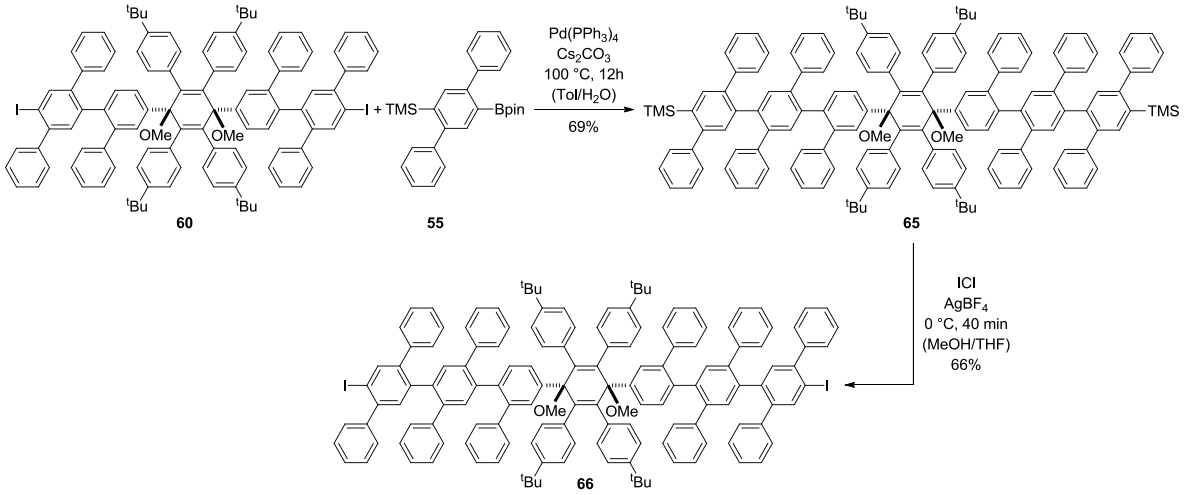

Scheme 26: Synthesis of doubly extended diiodide **66**.

To do so, **60** was extended by two terphenyls **55** to afford a doubly extended precursor (see *Scheme 26*). The yield of the *Suzuki* coupling dropped by 10% to 69% in comparison to its smaller homologue **59**, as the excess of boronate could not be fully removed by column chromatography. Thus, **65** was additionally purified by preparative GPC. The NMR spectrum is in agreement with expectations: the ratios of the TMS-, *t*-Butyl, methoxy groups (*18:36:6*) and aromatic protons (*80 H*) are in line with the theoretical number.

Subsequent iododesilylation of **65** with ICl gives **66** in good yields (75%). In *Figure 31*, the ^{1}H-NMR spectrum of the doubly extended diiodide **66** is shown. One singlet each was observed for the *t*-butyl (36 H) and methoxy groups (6 H). 78 of the 80 protons are detected as a multiplett from 6.5 ppm to 7.7 ppm. The remaining two protons are low field-shifted and can be assigned to protons in the *ortho*-position of the two outer terphenyls. These peaks have been observed for the desymmetrized terphenyl, too (see chapter *3.2.2.1.* Extended Precursor). These peaks additionally prove the quantitative terphenylation.

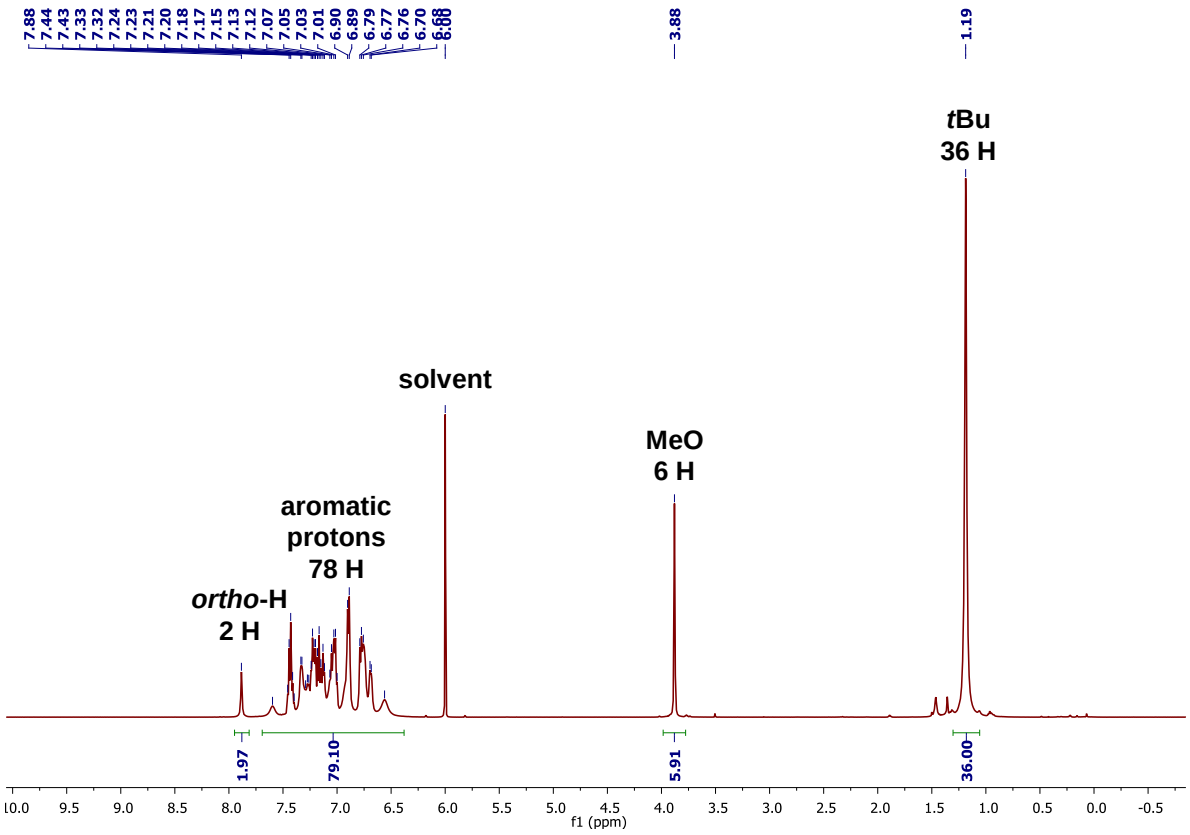

Figure 31: ^{1}H-NMR spectrum of the doubly extended terphenyl **66** recorded in $C_2D_2Cl_4$ at 100 °C.

The synthesis of **66** by the previously used *Ullmann*-type homocoupling led to the kinked 21-membered macrocycle **67** (*see Scheme 27*). The title compound was obtained in a disappointingly low yield (2.4%!) due to a very challenging purification which required a pre-purification by column chromatography, two recycling GPC runs and a final purification by preparative TLC.

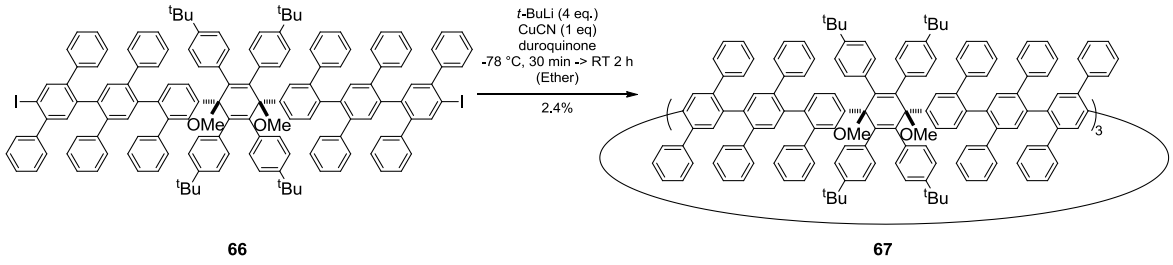

66 **67**

Scheme 28: Synthesis of the kinked macrocycle **67**.

67 was characterized by HR-MS and NMR spectroscopy. The detected mass of 5652.8643 m/z is in very good agreement with the theoretical mass of 5652.8464 m/z (see *Figure 73, p.174).* More importantly, the isotopic pattern does not contain any shifted or

underlying peaks from a possible linear homologue and thus HR-MS indicates a successful purification, as the observed and simulated isotopic pattern match.

In *Figure 32*, the ^{1}H-NMR spectrum of the kinked macrocycle **67** is shown. The integration of the signals of the *t*-butyl and methoxy groups as well as the aromatic protons (36:6:82) are in very good agreement with the theoretically expected number of 36:6:80. Furthermore, the sharp peaks of the *t*-butyl and the methoxy groups prove its cyclic nature (see discussion *Figure 13, p. 47*).

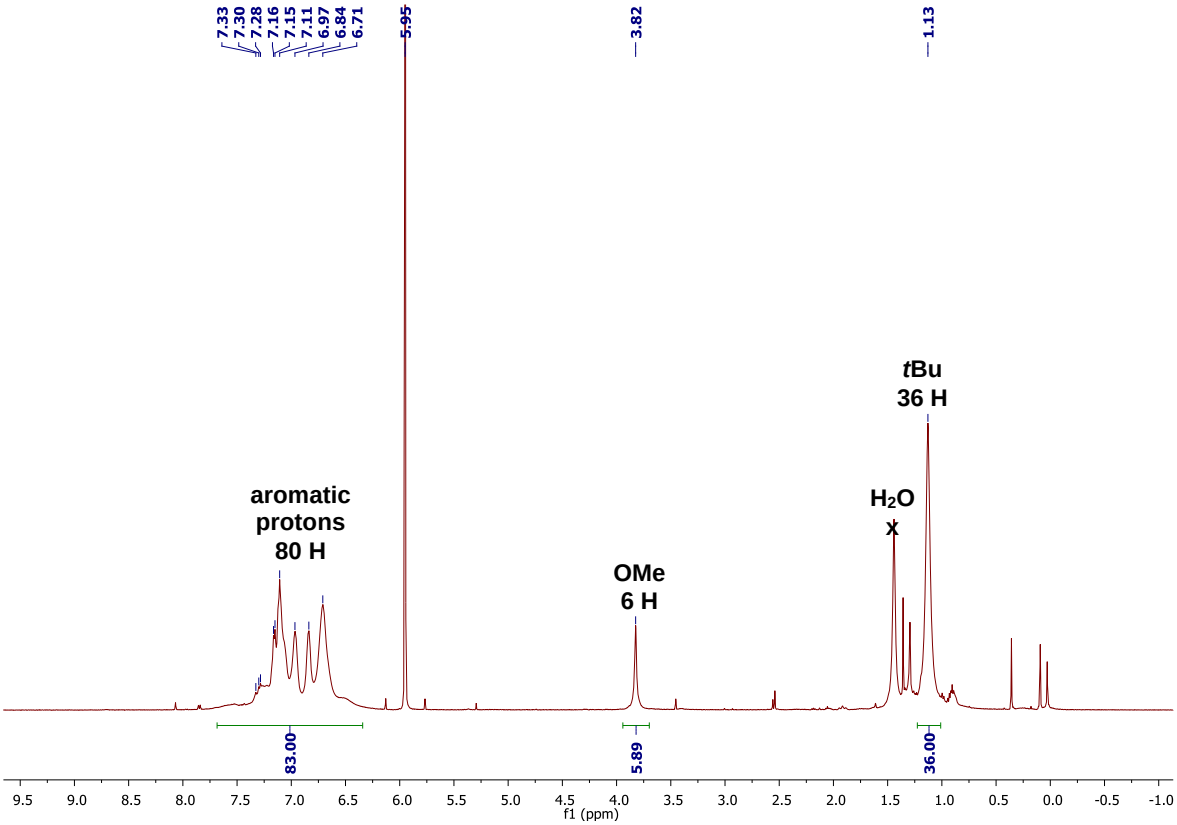

Figure 32: ^{1}H-NMR spectrum of macrocycle **67** recorded in $C_2D_2Cl_4$ at 100 °C.

The above shown ^{1}H-NMR spectrum contains various small peaks (0.0-0.5 ppm; 1.2-1.5 ppm = water, aliphatic impurities; 2.5-3.5 ppm; 5.4 ppm; and 7.8-8.2 ppm) that cannot be fully assigned. Despite enormous purification efforts (Silical gel & GPC), a removal of these impurities could not be achieved. No impurities, however, were detected by HR-MS measurements.

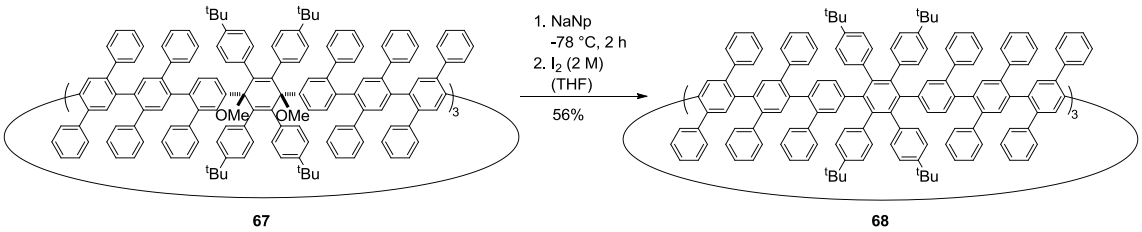

Scheme 29: Synthesis of the [21]CPP based PPC **68**.

Due to the low yield of the macrocyclization, a ^{13}C-NMR spectrum could not be recorded. Nonetheless, the synthesis was continued and the small amount was subjected to reductive aromatization conditions using NaNp (see *Scheme 29*). The HR-MS proved the formation of the doubly extended macrocycle [21]PPC.

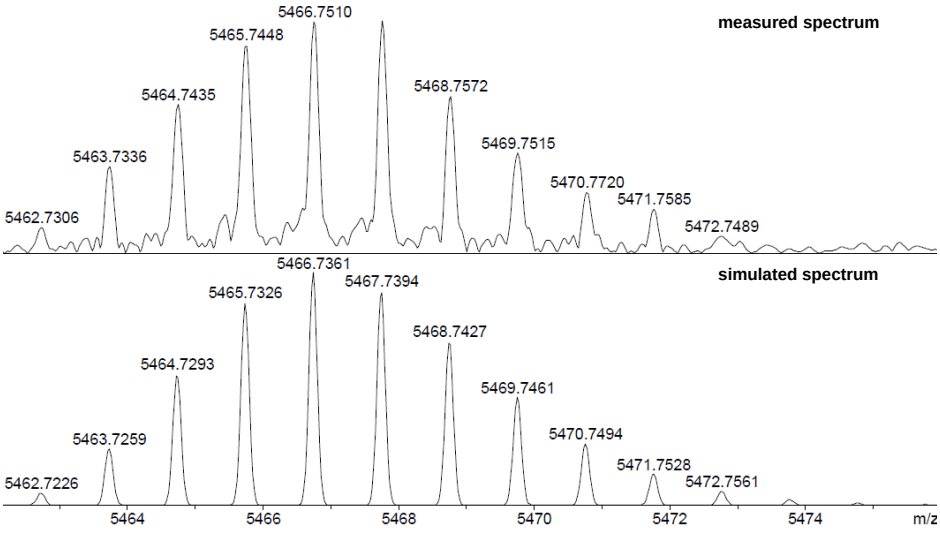

Figure 33: HR-MS spectrum of **68**

The ^{1}H-NMR spectrum, however, shows the presence of impurities in the aliphatic region similar to the mass spectrum of the starting material **67** that could not be separated despite preparative GPC purification. As a consequence, **68** contains impurities that cannot be assigned. Furthermore, no ^{13}C-NMR spectrum could be recorded due to too low quantities. The synthesis of the smaller cylinders showed that HR-MS is a very reliable method to characterize the here presented PPCs. Therefore, we can conclude that – despite impurities – we could obtain a [21]CPP. The oxidative cyclodehydrogenation (next chapter) was investigated as well as the optical properties of all PPCs are discussed (see *chapter 3.2.4*).

3.2.3.2. Oxidative Dehydrogenation - Studies

The oxidative cyclodehydrogenation of the [21]PPC **68** was studied to find out whether larger macrocycles enable smoother dehydrogenations. The sample was subjected to $FeCl_3$ and stirred for 1d at r.t. Disappointingly, no masses could be detected with our mass spectrometer. Despite, several attempts, the strain-dependent oxidative cyclodehydrogenation of even larger cycles could not be answered.

3.2.4. Optical Properties

In this chapter, the optical properties of the [9]PPC **38**, [15]PPC **62** and [21]PPC are discussed. In *Figure 34*, the absorption and emission spectra of **38**, **62** and **68** are depicted. The absorption maxima of **38**, **62** and **68** peak at around 260 nm. The cyclic hexaphenyl benzene trimer ([3]CHPB)[110] that contains six phenyl rings fewer than as its congener **38**, however, shows a 60 nm higher absorption maximum. The absorption properties of this structure show similar absorption maxima as for CPPs with n = 8-15 which lie between 337 nm and 340 nm.[125, 162]. The molar absorptivity for [9]CPP and [15]CPP is between 36000 $M^{-1}cm^{-1}$ and 32000 $M^{-1}cm^{-1}$, whereas [21]CPP has a distinctively lower absorptivity. This can be due to impurities that were observed in the ^{1}H-NMR spectrum that could not be removed despite intense purification. The actual concentration might thus be lower than used for the calculation of the molar absorptivity.

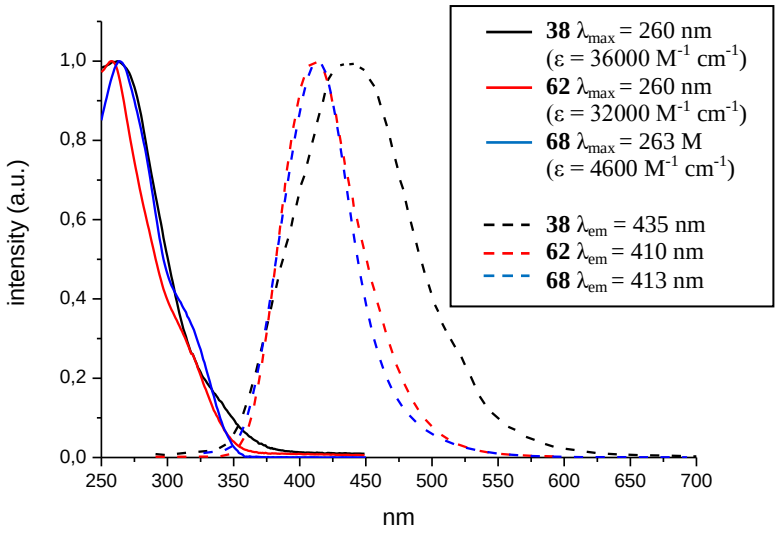

Figure 34: UV-Vis and Fluorescence spectra of **38** and **62** and **68** (hexane)

The impact of strain between the two macrocycles **38** to **62**, **68** is more pronounced for the emission spectra. The 9-membered ring **38** reaches its maximum at 435 nm, whereas the 15-membered **62** and the 21- ring **68** do so at 410 nm and 413 nm, respectively. The *Stokes* shift towards a longer wavelength can be explained by a planarization of the structure in the excited state, giving rise to a quinoid-like structure.[163] A planarization is usually to bring about a red-shift in the fluorescence peak. For CPPs, a red shift of emission is observed from 424 nm ([13]CPP) to 533 nm ([8]CPP) has been observed in the literature.[86] The differences in emission wavelength display an asymptotic behavior as they differ between [12]CPP and [13]CPP by 4 nm.[162] A similar behavior is found for the above described PPCs.

3.2.5. Summary

In this chapter, the synthesis of three different PPCs was presented, which contain 9-membered **38**, 15-membered **62** and 21-membered **68** central CPP rings. The synthesis is based on a kinked building block **35** with an instrinsic kinking angle of 70°. Due to this angle, an *Ullman*-type *homo*coupling of **35** affords cyclic trimers with a triangular structure. Upon reduction with low-valent titanium, the above stated PPCs can be obtained (see *Scheme 30*).

For the synthesis of its higher homologues, the kinked building unit **35** was bis- or tetrakisterphenylated. To do so, a concise synthesis of a TMS-protected terphenylboronate **54** was developed, which was then successfully employed for the extension of **35** by Suzuki coupling. By following this strategy, diiodide **35** can be extended *via* the introduction of two or four terphenyls, respectively, giving **59** and **65**. After iododesilylation, the diiodides **60** and **66** were obtained. Oxidative homocoupling afforded extended triangular macrocycles **61** and **67**. Analogously, reductive aromatization gaves cycles **62** and **68** (see *Scheme 30*).

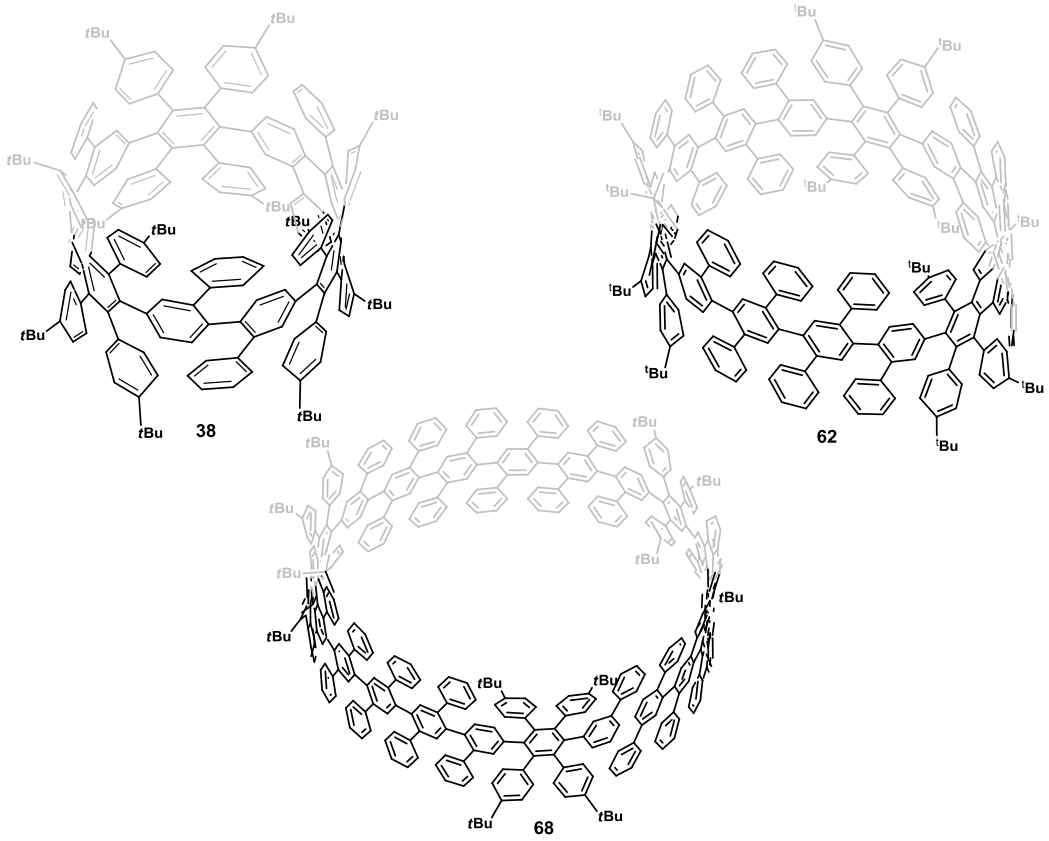

Scheme 30: successfully synthesized [9]PPC **38**, [15]PPC **62** and [21]PPC **68**.

For all three PPCs **38**, **62** and **68**, the oxidative cyclodehydrogenation was studied. For [9]PPC, the cyclodehydrogenation was also studied on Au and Pt surfaces, which was monitored by STM.

In solution, the [9]PPC and [15]PPC showed a partial cyclodehydrogenation, whereas no masses could be detected for the [21]PPC. In detail, the oxidative cyclodehydrogenation was studied in solution under different reaction conditions. With $FeCl_3$, a partial dehydrogenation with a broad mass distribution was observed for **38**. For **62**, fortunately, a maximum could be detected by MALDI-MS, showing a mass loss of 48 hydrogen atoms. This number of hydrogen atoms accounts for a complete cyclodehydrogenation of the three hexaphenylbenzene units and their neighboring biphenyls. This cyclodehydrogenation pattern is based on the assumptions of lowest rotational freedom: hexaphenylbenzene units consist of phenyl rings that twist along their bonding axis, whereas terphenyl units cannot only twist along this axis, but additionally along the *para*-phenylene-bonding axis. This can lead to an "out-of-plane" twisting of the terphenyls. As a consequence, they are too far away from neighbouring moieties to undergo cyclodehydrogenation. To overcome ring strain or interlocked intermediates, we planned to perform oxidative cyclodehydrogenation at higher temperatures. However, the use of DDQ with *Lewis*/*Brønsted* acids at r.t. led to the decomposition of the molecules.

To be able to use a catalytically active surface in conjunction with higher temperatures, surface-mediated cyclodehydrogenation was studied for the [9]PPC **38**. The structure could be evaporated and deposited on gold and platinum surfaces. Unfortunately, the dehydrogenation at 325 °C led to a flattening of the structure. Therefore, a successful bottom-up synthesis of **38** on surfaces cannot be reported either.

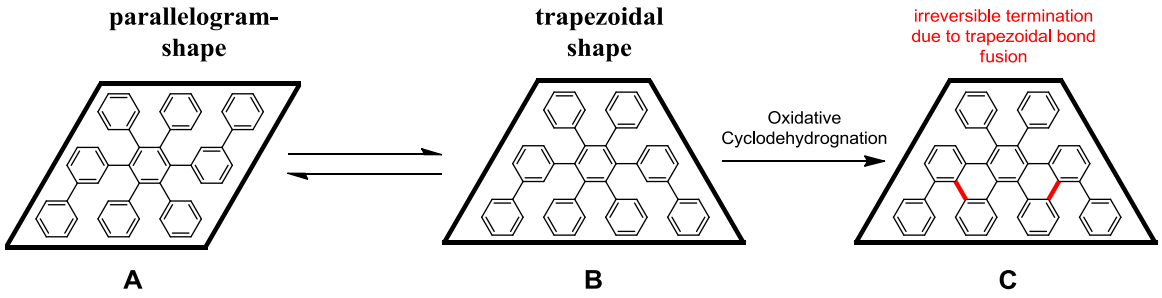

Scheme 31: Parallelogram-shape and trapezoidal shape. Cyclodehydrogenation from B to C leads irreversible termination due to trapezoidal bond fusion; rotation of trapez due to high ring string not possible.

So far, none of the above described approaches yielded a bottom-up synthesis of CNTs from PPC cylinders. One explanation could be that not only ring strain is crucial for achieving a bottom-up synthesis, but also the structural built-up. The presented structures contain freely rotating biphenyls and terphenyls. These moieties do not only form parallelogram-shaped structures (see *Scheme 31*) but can also result in trapezoidal structures that irreversibly terminate cyclodehydrogenation. Therefore, a prefusion of the biphenyl and terphenyl units to the kinked moiety was envisioned. The experimental results will be described in the next chapter.

3.3. Parallel-Fragment Approach – Prefused Cylinders

The ring expansion *via* the introduction of terphenyl units to reduce ring strain did not lead to a smooth cyclodehydrogenation, giving short CNT segments. Therefore, precursor **70** was envisioned to prefuse terphenyl units to obtain **72**. This macrocycle was foreseen to contain three hexaphenylbenzene units (see *Scheme 32*) that are interconnected by partially fused ribbon segments.

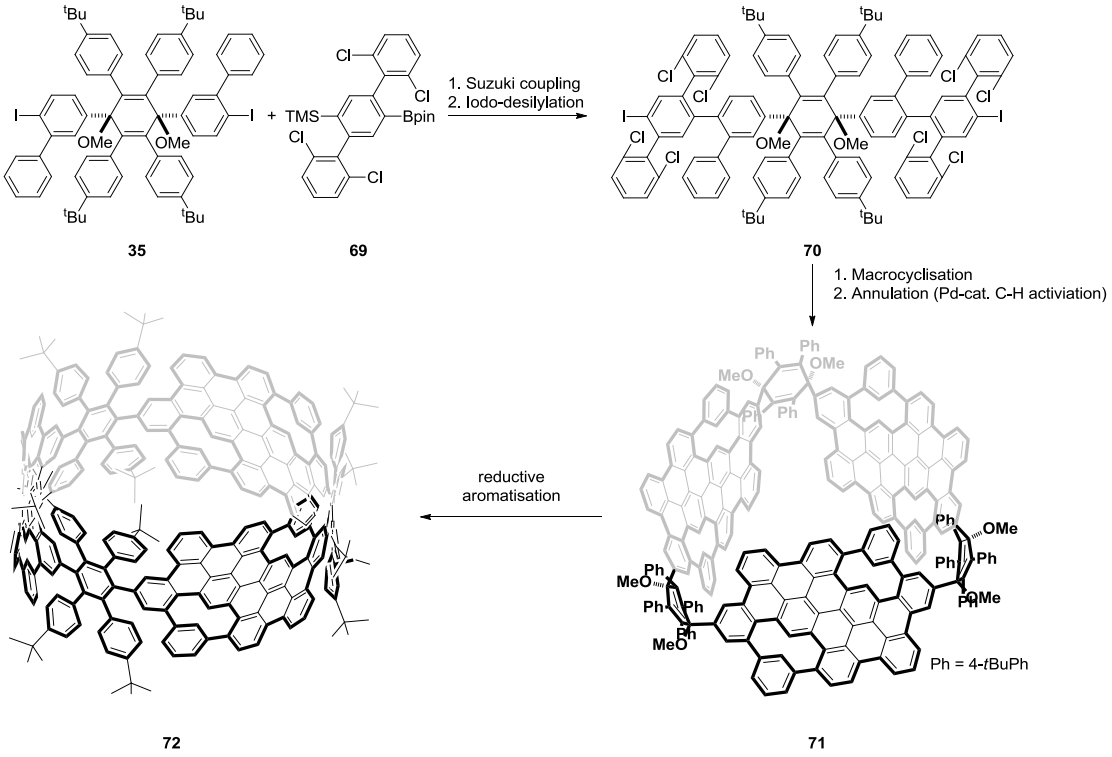

Scheme 32: synthetic strategy toward prefused macrocycle **72**.

This strategy could be advantageous because of several reasons: first, after macrocyclization of **70** and subsequent annulation (Pd-catalyzed *C-H* activation) of the strain-free macrocycle, the reaction is to give **71**. Most likely, not all bonds will be closed, however, still yielding three relatively rigid fragments. Second, the very powerful reductive aromatization would lead to a highly strained macrocyle **12** which would already contain three *pre*-bend segments. Thus, only the remaining more reactive "hexaphenylbenzene" units would have to undergo oxidative cyclodehydrogenation. Third, the *pre*-bend macrocycle would also contain fused terphenyl units. These terphenyl units usually pose a challenge for the oxidative cyclodehydrogenation, as they have a higher degree of rotational

freedom than the hexaphenylbenzene-type units of the macrocycle. Fourth, palladium-catalyzed *C-H*-activations,[164] as a different approach, can be performed in the presence of high sterical demand and ring strain; many successful examples[165] are known for the synthesis of geodesic molecules, such as corannulenes, sumanenes and structural congeners,[166-168] where also a high ring strain needs to be overcome. Fifth, this approach would also lead to the formation of the more strained nonlinear bonds of the CNT segments, after reductive aromatization.

3.3.1. Synthesis of Tetrachlorinated Terphenyls

For the synthesis of **69**, the commercially available boronic acid **73** was to be coupled with the diiodide **57** *via Suzuki* coupling. Different *Suzuki* conditions, $Pd(PPh_3)$ with Cs_2CO_3 or Et_4NOH and $Pd(OAc)_2$ with SPhos and K_2PO_4 as ligand and base, respectively, were studied to couple **73** with **57**. All attempts failed, as no product was observed; the starting materials could be recovered.

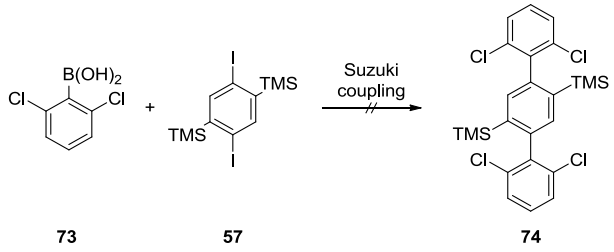

73 **57** **74**

Scheme 33: First synthetic approach toward tetrachlorinated terphenyl **74**.

From synthetic experiences in our group, sterically hindered boronic acids are known to hamper coupling more strongly than similarly crowded aryl halides. Therefore, the reactivities of the two substrates were switched. The diboronate **74** was synthesized via dilithiation of the dihalide **57** (*vide supra*). The *Suzuki* coupling using $Pd(PPh_3)_4$ and K_2CO_3 or Cs_2CO_3 (sample 1-3) resulted in the formation of mono- but also tri- and tetraphenylated products, which could be additionally confirmed by analysis of the isotopic pattern (FD-MS). These findings indicated that a coupling between the substrates had taken place. In addition, a partial desilylation was observed, hinting at a cleavage of the Si-C-bond. These findings are very surprising since *Hiyama* couplings only take place if the Si-C bond is polarized, usually achieved by fluorides. In the presence of S-Phos, the formation of small amounts of the title compound **74** was observed, but the reaction also gave rise to the above

mentioned side products. The best results were achieved with $Pd(PPh_3)_4$ and Et_4NOH as base. However, the title compound was only obtained in 15% yield after a very challenging purification (see *Scheme 34*).

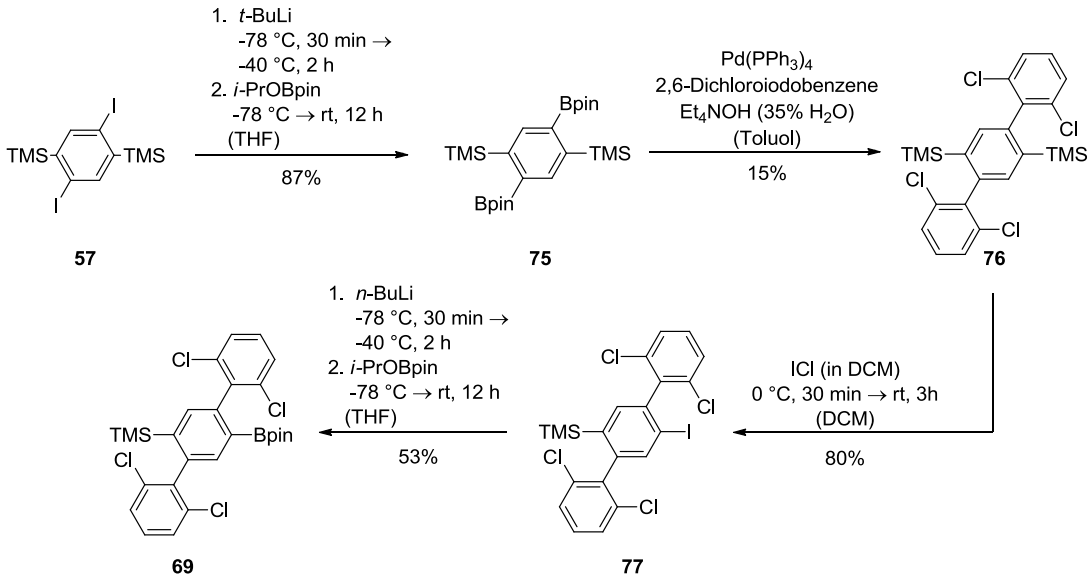

Scheme 34: Synthesis of terphenyl **69**.

Since the *Suzuki* coupling of **75** with 2,5-dichloroiodobenzene led to various side products, the structure of **76** was additionally verified by X-ray chrystallography (see *Figure 35*). The phenyl rings are twisted out of plane due to the sterical hindrance of the chlorine atoms and the TMS groups.

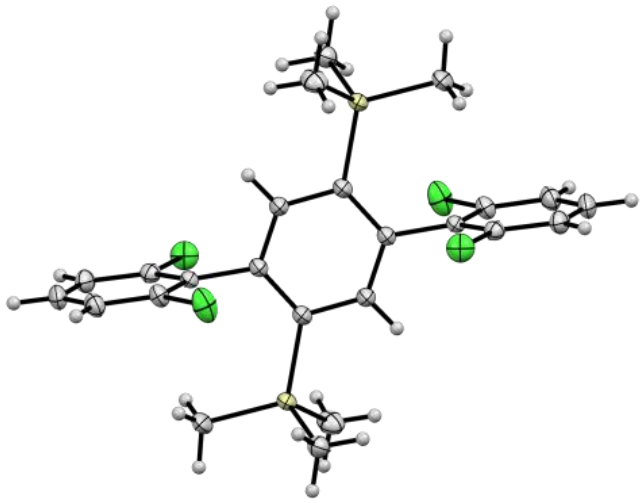

Figure 35: Single crystal X-ray structure of **77**. Chlorine atoms are labeled in green; silicon atoms labeled in yellow.

In the next step, the coupling of the borylated terphenyl **69** with the kinked diiodide **35** was investigated. As shown in *Table 1*, none of the reaction conditions screened for the *Suzuk*i coupling afforded the desired product **70** (*vide infra*) – not even a mono-terphenylation was observed. For conditions 1 to 3, only starting material or decomposed starting material **69** was obtained. The use of a harsher base (NEt_4OH) led to higher masses. However, none of obtained molecular weights could be assigned to any of the expected masses. The use of S-Phos as ligand failed either.

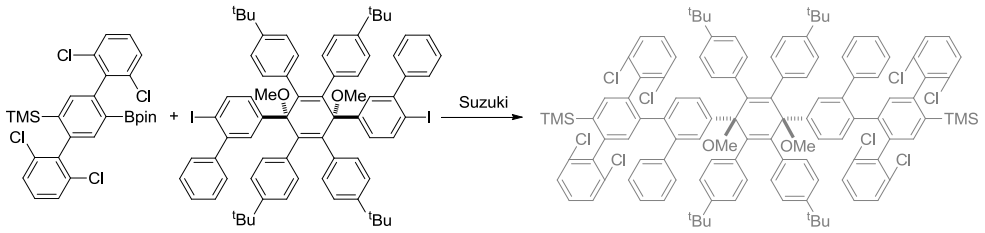

69 **35** **70**

Table 1: reactions conditions

sample	catalyst/ligand	base	temperature (°C)	reaction time h	yield
1	$Pd(PPh_3)_4$	Cs_2CO_3	90	12	*no product*
2	$Pd(PPh_3)_4$	Cs_2CO_3	110	12[1]	*no product*
3	$Pd(PPh_3)_4$	Cs_2CO_3	140	2[1]	*no product*
4	$Pd(PPh_3)_4$	Net_4OH	80	4	*no product*
5	$Pd_2(dba)_3$/S-Phos	Cs_2CO_3	110	2[1]	*no product*

[1] microwave reaction

The unsuccessful attempts might be due to the increasing sterical demand of the bis(dichlorophenyl)phenylene boronate **69**. As stated before, it is more favorable to have a higher sterical demand at the aryl halide than at the boronate. Therefore, the reactivities of the two building blocks were inverted (see *Scheme 35*).

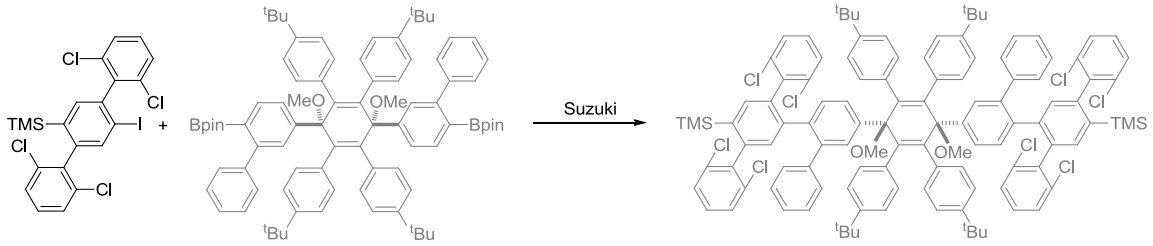

77 **78** **79**

Scheme 35: switiching of reactivites.

Several attempts were undertaken to synthesize diboronate **78** which surprisingly failed. This was probably due to the low lithiation rate of the biphenyls which require a low

reaction temperature (- 40 °C). Since the title compound **79** could not be synthesized, this approach was given up.

3.3.2. Summary

In this chapter, the synthesis of an *octa*chlorinated kinked precursor **70** was attempted. This building block was to be used for macrocylization and subsequent prefusion *via* C-H-activation to afford **71** (see *Scheme 34*). The ribbon containing macrocycle was to be dehydrogenated to give CNTs *via* a bottom-up synthesis.

To achieve the above proposed goal, a synthesis for the tetrachlorinated terphenyl **69** was developed, which was very challenging due to the increased sterical hindrance, induced by the four chlorine atoms. The preparation of **69** could be realized by reacting diboronate **75** with two equivalents of 1,3-dichloroiodobenzene. As shown in *Scheme 36*, **69** was to be coupled with **35**. However, under all tested reaction conditions, **70** could not be obtained. Therefore, the reactivities of the two building blocks should be inverted. Disappointingly, the borylation of **35** could not be achieved. Thus, the *Suzuki* coupling could not be studied under inverted reaction conditions.

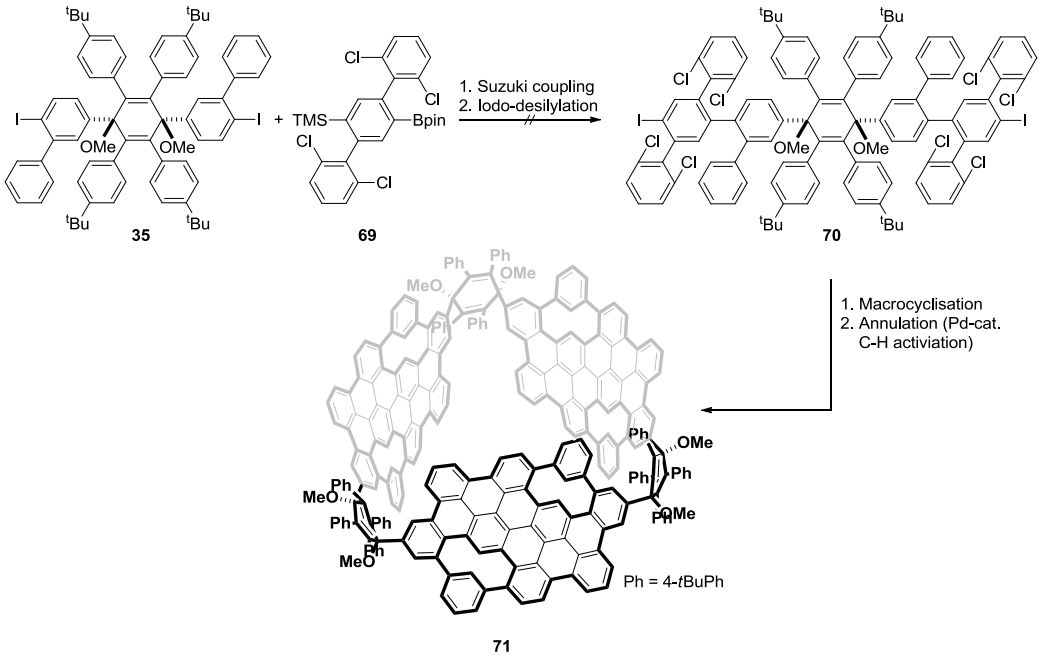

Scheme 36: synthestic approach toward perfused macrocycle **71**.

Despite the tedious synthesis of terphenyl **69**, the unsuccessfull *Suzuki* coupling between **35** and **71** forced us to give up this route.

3.4. Congested *cyclic*-Hexaphenylbenzene Hexamers

In this chapter, the congested *cyclic-hexaphenylbenzene* approach is described. As highlighted in the previous chapters, an incomplete oxidative cyclodehydrogenation was obtained during the final step for a solution-mediated bottom-up synthesis of ultrashort CNTs: the parallelogram-type connectivity pattern (see *route A, Scheme 37*), which was inherent for all the above described synthetic strategies, can lead to defect-structures during cyclodehydrogenation (see *chapter 3.2.5, Summary*), which renders the formation of CNTs impossible (*vide infra* for detailed discussion). Therefore, an alternative approach *via* congested HPB units (see route B, *Scheme 37*) is presented. This connectivity pattern is expected to be advantageous, as the phenyl rings attached to the central CPP ring have less rotational freedom than the phenyl rings of the biphenyls (see *parallelogram approach*).

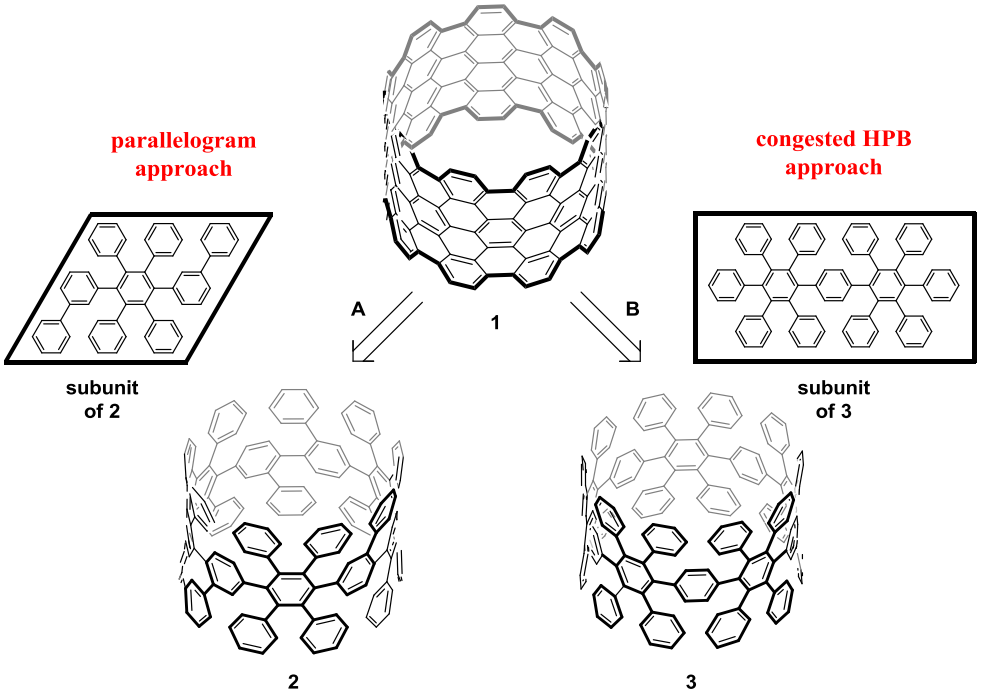

Scheme 37: parallelogram approach *via* route A toward **2** and congested HPB via route B to give **3** .

In *route B*, both macrocycles consist of congested hexaphenylbenzene units (see *Figure 36*), as highlighted by structure **82** in the black frame. They can be seen as structural congeners of cyclic-hexaphenylenzene trimers, with the exception that, in this case, two hexaphenylbenzene moieties share one phenylene ring to give a congested *cyclic*-hexaphenybenzene hexamer **84** which renders it a structural precursor of CNTs. To emphasize their differences, the shared phenylenes have been labeled in red. In addition, its

weakly strained C_2-symmetric congener **108** is depicted (see *Figure 36*), which can be obtained under milder reduction conditions.

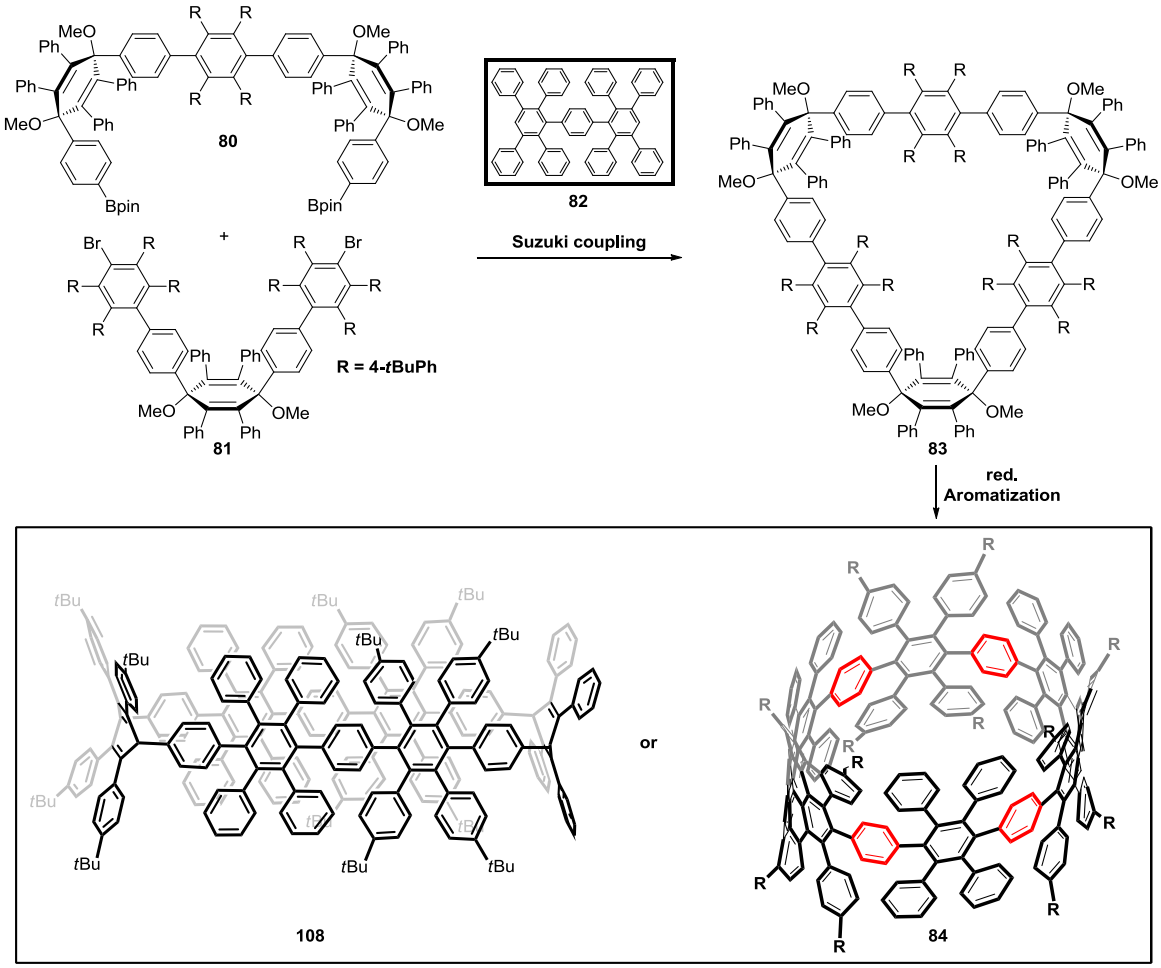

Figure 36: Synthesis of a congested cyclic HPB hexamers **84** and its serendipitously discovered C_2 congener **108**.

On the one side, the idea for this macrocyclic structure is based on the synthesis of oligophenylene structure **85** and the correspondingly cyclodehydrogenated planar PAH **2** (see *Figure 37*).[116, 169-171] On the other side, this approach is supported by the preparation of tetraphenylbenzene **12**[172-173] and the successful combination of both ideas for the synthesis of GNRs by *Yang* in our group (see *Figure 37*).[53, 174] He could show that his AA- and BB-type polycondensation approach, using a dihalide and diboronate, can afford linear polyphenylenes that can be dehydrogenated to give GNRs. These promising results hinted at the possibility to substitute the linear diboronate **89** by a kinked diboronate to form novel, even-numbered macrocycles.

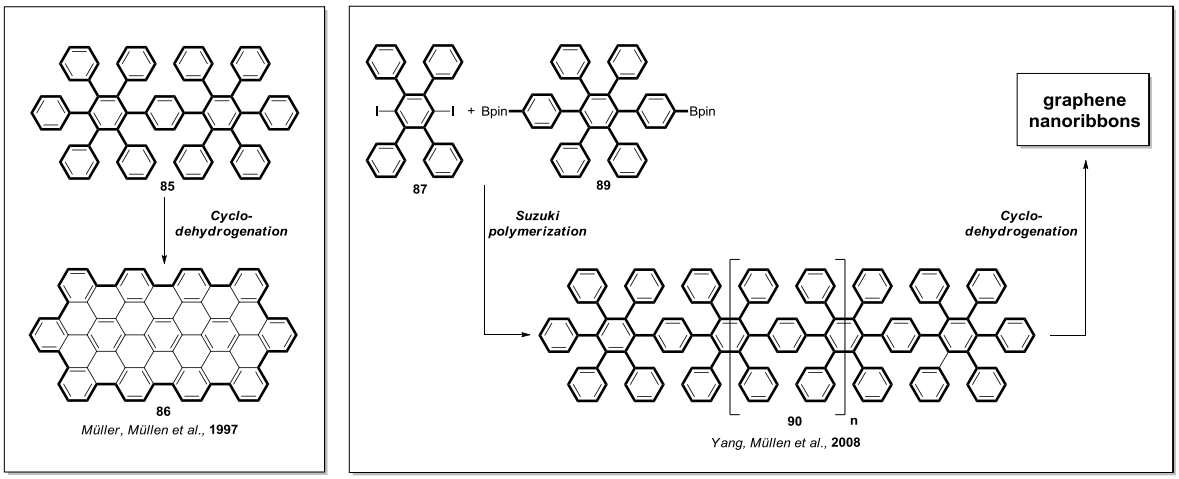

Figure 37: Synthesis of graphene nanoribbons by *Müller et al.* (left) and *Yang et al.* (right) in our group.

Based on the previously discussed results, the here presented approach has several advantages: first the outlined molecule **84** is rotationally restricted due to its constitution, possibly giving rise to a smooth cyclodehydrogenation which, in turn, can lead to the formation of defect-free bottom-up synthesized CNT segments – provided that no rearrangements, etc. occur. In contrast, parallelogram-type structures can principally lead to trapezoid-like structures (see *Figure 38*) that inadvertently rule out complete cyclodehydrogenations; second, even-numbered, naked CPP rings are slightly less strained than their odd-numbered counterparts,[175-176] since they are not pushed into ellipsoidal conformations by geometric constrains; third, the congested HPB approach results in a higher number of C-C bonds per average number of carbon atoms in comparison to the parallelogram approach.

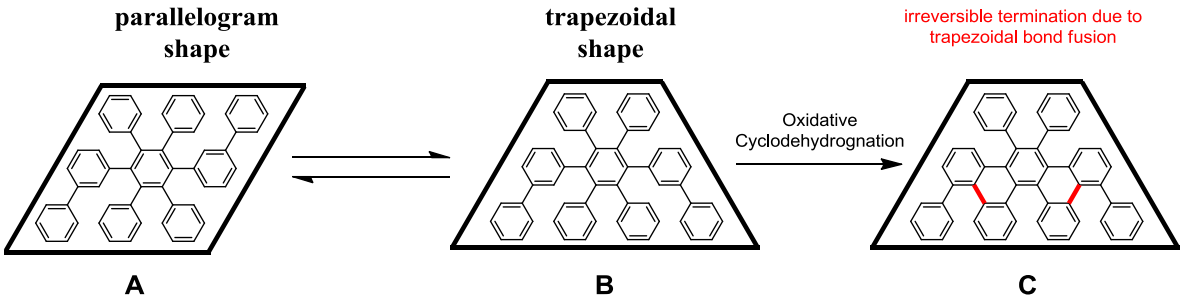

Figure 38: unwanted trapezoidal formation that can be irreversibly manifested by cyclodehydrogenation, terminating CNT formation.

The preparation follows a different synthetic route in comparison to the parallelogram approach, since two different precursors with a mono- and doubly kinked structure need to

be prepared instead of one. As a consequence, the cyclization cannot be performed *via* a homocoupling. Instead, the *Suzuki* coupling is used to react dibromide **94** and diboronate **95** with each other to give macrocycle **83**. As previous findings have shown, the kinking angle of 70° of the 3,6-dimethoxycyclohexadiene results in the formation of trimers. Therefore, we opted for the introduction of three kinked moieties into the two building blocks: one kinked moiety in **81** and two in **80**.

3.4.1. Synthetic considerations

The synthesis of the new congested HPB based macrocycles **84** and **108** was first investigated by using the available starting materials which had been synthesized for the previous macrocycles. Therefore, the *tetra*-(4-*t*Bu-phenyl)benzoquinone **4** was chosen as a starting material.

When developing a synthetic route, the precursor was designed to be best suited for an oxidative cyclodehydrogenation. Therefore, the molecular build-up was taken into consideration to minimize sterical repulsion and also simplify NMR characterization due to high symmetry. Hence, an alternating pattern of tetra-(4-*t*-butylphenyl)benzene and tetraphenylbenzene units within the macrocycle was employed (*vide supra*).

3.4.2. Synthesis of 12[CPP] based telescopic hexaphenylbenzene hexamer

3.4.2.1. Development of building blocks.

Diboronate **93** was synthesized following a general strategic outline developed in our group, however, adapted to the structural needs for macrocyclization (see *Scheme 38*).[110] To do so, quinone **4** was reacted with 4-iodophenyl lithium to give **91**, which almost exclusively afforded the drawn *cis*-diol. Quantiative methylation of **91** and subsequent borylation afforded **92**. The poor yield can be explained by extensive dehalogenation during borylation. Later on, iodine was substituted by bromine, resulting in an almost quantitative borylation. The catalytic borylation afforded **93** in poor yields (20%), since dehalogenation required purification by column chromatography. This led to high losses of the final product, since **93** shows strong tailing on silica.

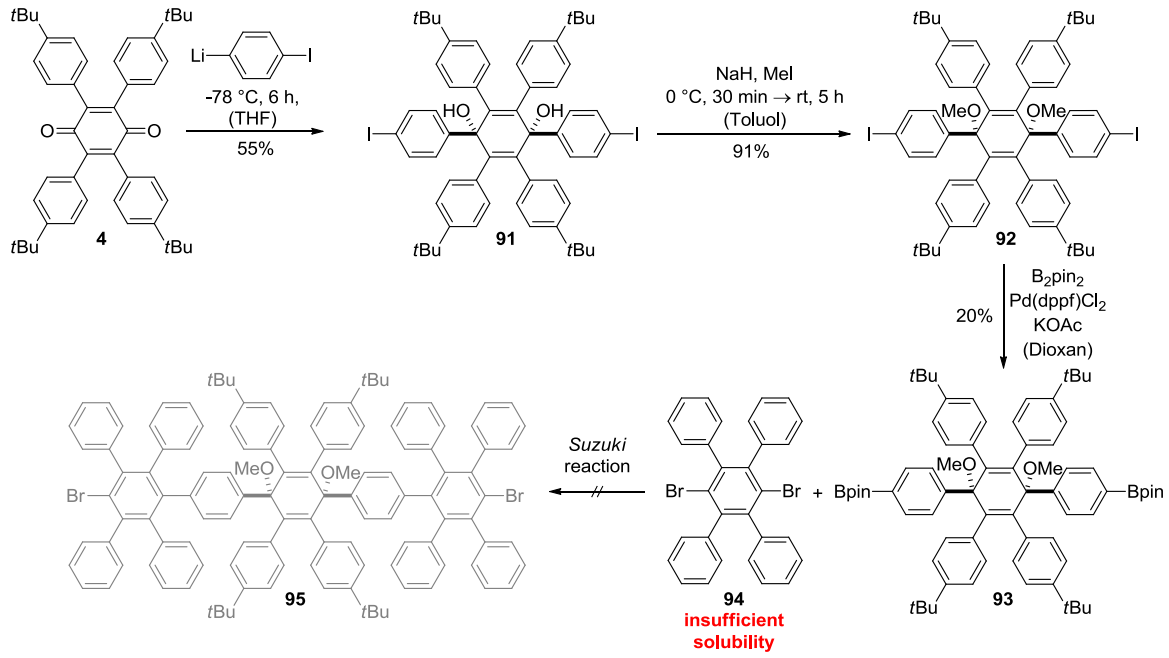

Scheme 38: First attempt to synthesize dibromide **95**.

With this novel kinked diboronate in hand, the 1,4-dibromotetraphenylbenzene was synthesized *via* the *Hart* reaction in typical yields (53%).[173] The compound was purified by recrystallization. Already then, the low solubility of this compound was apparent, especially in the context of further functionalization and preparation of the AA- and BB-type precursors, *i.e.*, monokinked dibromide **81** and dikinked diboronate **80**, respectively. Due to the low solubility of **94**, the synthesis of the unsymmetric dibromide **95**, where an excess of dibromide **94** is necessary, was not feasible, despite the high reaction temperature of 100 °C for *Suzuki* couplings. Therefore, this strategy was given up.

Instead, the *t*-butyl groups were shifted from the kinked 1,4-dimethoxycyclohexadiene to the tetraphenylbenzene derivative to increase its solubility. The synthesis of the *tetrakis*-(4-*t*-butylphenyl)benzene **97** proved to be unexpectedly challenging, since the presence of 4-*t*-butylphenyl *Grignards* led to the formation of side products. The synthesis of such *tetra*phenylbenzenes was pioneered by the *Hart* group.

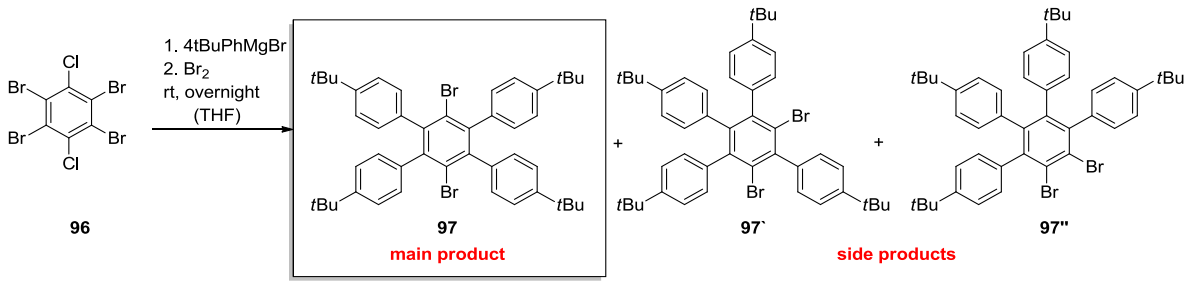

Scheme 39: Synthesis of **10** and its corresponding isomers.

From the literature, including our own group, several examples with *para*-alkyl substituted phenyl *Grignards* are known to give to tetraphenylaryl-1,4-dihalides.[172-173] However, the use of 4-*t*-BuPhMgBr afforded a mixture of constitutional isomers. By NMR, **97** was observed as the main product, but also **97**' (15% yield); the formation of **97**'' cannot be ruled out. Separation of isomers by column chromatography was not possible. To avoid isomer formation, the *Hart* reaction was performed at 0 °C. Still, a mixture of isomers was obtained in similar yields. Even lower temperatures reduced the reaction rate by so much that the desired product was not obtained in reasonable amounts.

In their seminal paper, *Hart* and coworkers reported also the use of hexabromobenzene **98** instead of tetrabromodichlorobenzene **96** for certain alkylated *Grignard* reagents. Thus, standard reaction conditions were employed, using **98** instead of **96** (see *Scheme 40*). Under these conditions, the reaction exclusively afforded the desired product, after purification. The moderate yield of 40% (literature 50%-60% for other derivatives) for this reaction is compensated by the easy purification, which is achieved by subsequent washing of the sample with water, methanol, toluene and hexane.

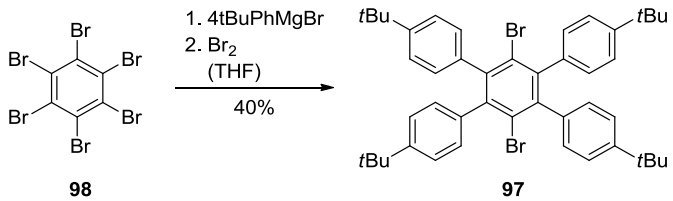

Scheme 40:Synthesis of 3',6'-dibromo-4,4"-di-tert-butyl-4',5'-bis(4-(tert-butyl)phenyl)-1,1':2',1"-terphenyl (**97**).

The difference between 4-*t*-butylphenyl and literature known *Grignard* reagents is their electron density: the here used 4-*t*-BuPh *Grignard* is the most electron-rich of the reagents studied in literature. Therefore, we expected that a lowering of the reaction temperature could reduce side product formation or even exclusively yield the target dihalide **97**, which, however, was proven otherwise by the experimental findings.

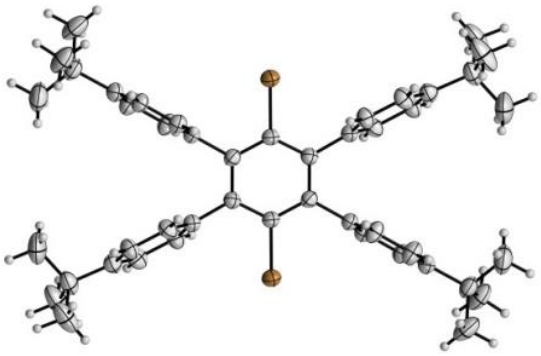

Figure 39: X-ray crystal structure of **97**; ORTEP drawing at a 50% probability level. Bromine atoms labeled in brown. Recrystallized from DCM/MeCN.

Mechanistic studies on this reaction were performed by the *Hart* group. Their proposed mechanism is described in *Scheme 41*. In previous studies with deuterated solvents, they found that *para*-metalations are favoured over *ortho*- and *meta*-metalation. By studying various chlorinated arynes, they proposed a stepwise mechanism. However, they do not provide an explanation for why the hexabromo- or the tetraobromodichlorobenzene worked better or not, depending on the kind of *Grignard* substrate they applied. Neither do I!

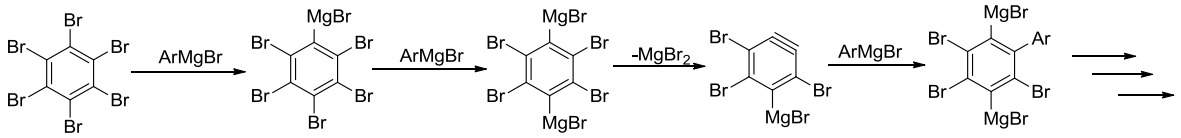

Scheme 41: reaction mechanism postulated by *Hart*.

To simplify the synthesis of the dikinked bisboronate **103** (see *p. 77*), dibromide **97** was was desymmetrized by monolithiation with *n*-BuLi and quenched with chlorotrimethylsilane to give the title compound **98** in 50% yield (see *Scheme 42*).

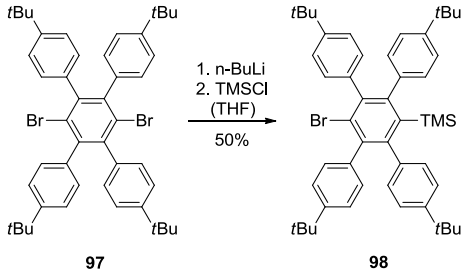

Scheme 42: Synthesis of desymmetrized tetraphenylbenzene **5**.

The structure of **98** can be proven by NMR spectroscopy (see *Figure 40*): its desymmetric nature can be derived from the splitting of the *t*-Bu group as well as the splitting of the aromatic protons, resembling two doublets and one pseudo triplet. An interesting observation is the upfield shift of the TMS group by 0.5 ppm. This is due to the aromatic

ring current induced by the neighboring phenyl ring. These subtleties are also reflected in the precursor **105** (see *p.77*).

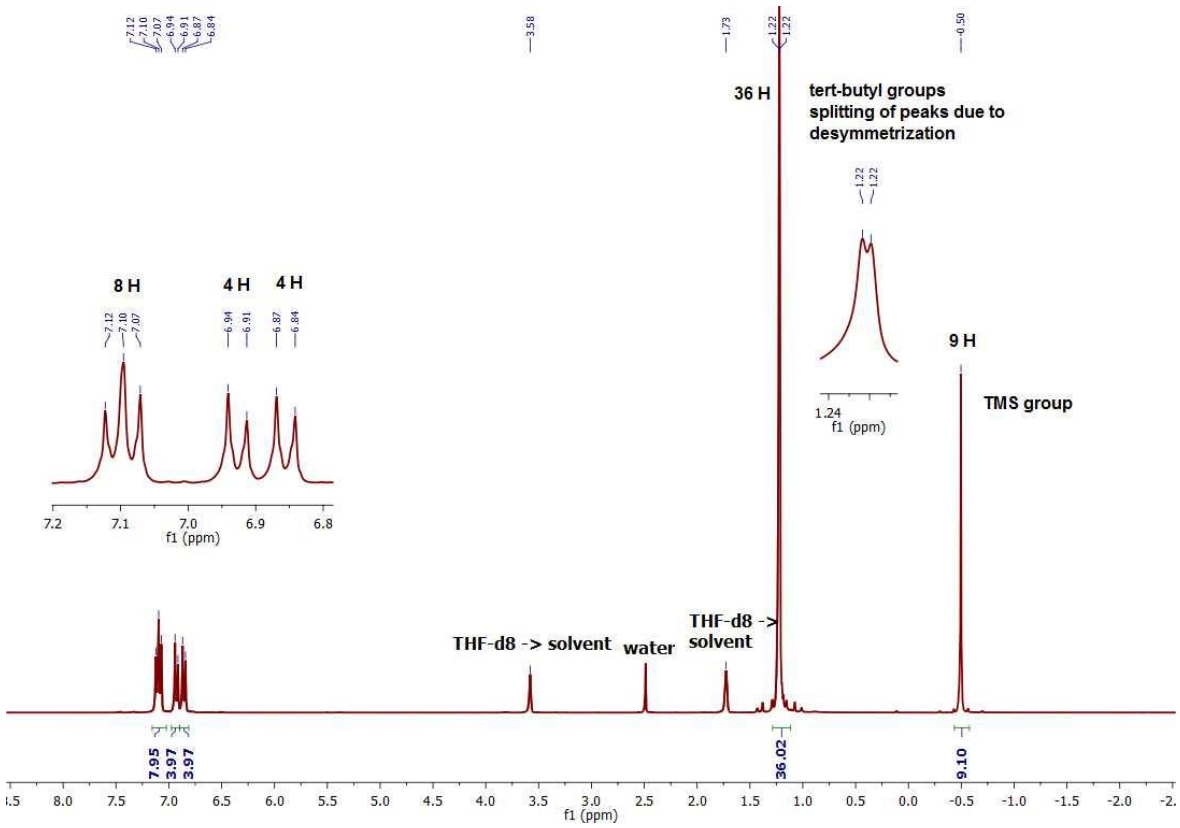

Figure 40: NMR spectrum of **98** measured in THF-d_8 at r.t..

The kinked diboronate **102** was synthesized (see *Scheme 43*) following a previously outlined route, except the fact that iodine was substituted by bromine, as aryl iodides gave poor yields due to dehalogenation during catalytic borylation. To do so, 1,4-dibromobenzene was lithiated with *n*-BuLi and reacted with quinone **99** to give **100** in 61% yield; here, only trace amounts of the *trans* product were obtained. Methylation of **100** afforded compound **101**. The dibromide **101** was catalytically borylated to give **102** in good yields (89%). As mentioned before (see *Scheme 38, p.72*), the borylation of its corresponding arly iodide gave poor yields (20%) due to deiodination which resulted in a tedious and messy purification by column chromatography. Switching to bromides afforded a clean reaction; the product was conveniently purified by recrystallization from hexane.

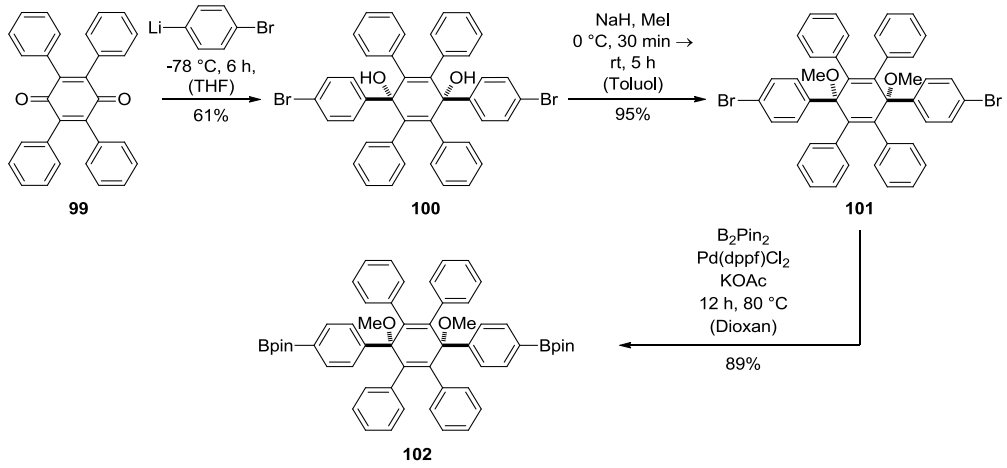

Scheme 43: Synthesis of **102**.

Since the biting angle of bisboronate **102** is important for the macrocyclization, especially regarding the dikinked building blocks, its crystal structure was investigated (see *Figure 41*). As expected, the biting angle for **102** is 70 ° and thus similar to diiodide **92**, previously used by T. Nishiuchi for *Yamamoto*-type macrocyclizations.[110]

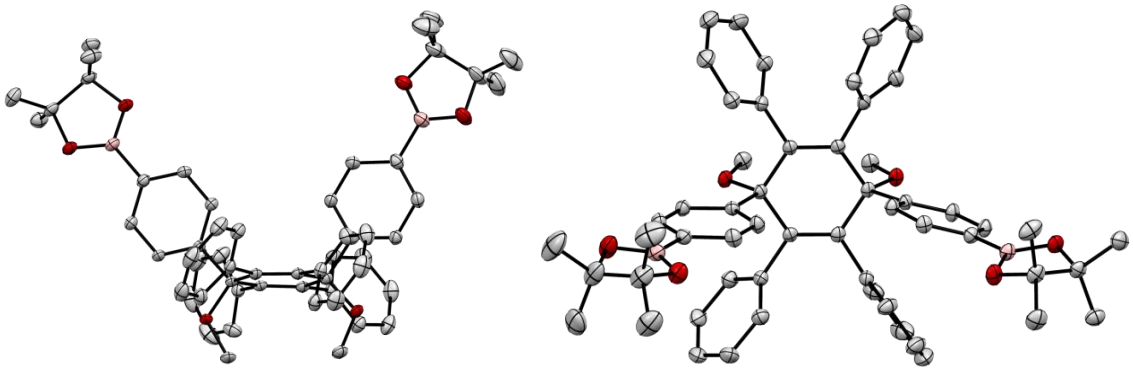

Figure 41: X-ray crystal structure of **102**.; ORTEP drawing at a 50% probability level; oxygen atoms are labeled in red, boron atoms are labeled in pink. Side view (left) and front view (right). The biting angle (left image) is 70.7 °. Hydrogen atoms are omitted for clarity.

With the three building blocks **97**, **98** and **102** in hand, the synthesis of the monokinked dihalide **103** and dikinked diboronate **104** was investigated.

3.4.2.2. Precursor Synthesis

The synthesis of the precursors **103** and **104** will be described in this section. To avoid polymerization and to achieve the synthesis of AA- and BB-type precursors, a 4-fold excess of one of the reagents was used.

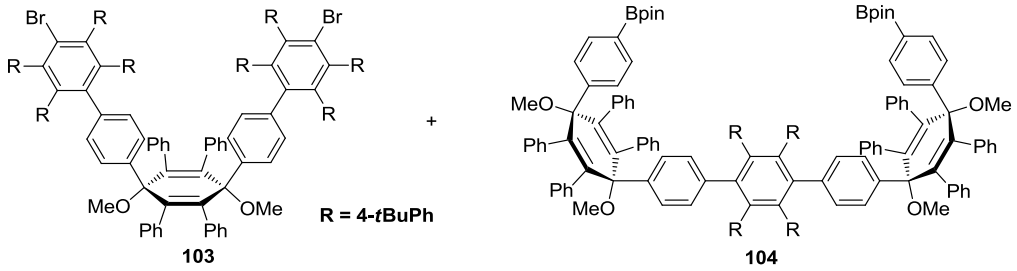

Scheme 44: Mono- and dikinked compounds **103** and **104**.

First, the synthesis of **106** was investigated. Therefore, the *cis*-3,6-dimethoxycyclohexadiene was coupled with the TMS-protected tetraphenylbenzene **98** (see *Scheme 45*). The reaction was performed using microwave-assisted *Suzuki* coupling to give **105** in 70% yield.

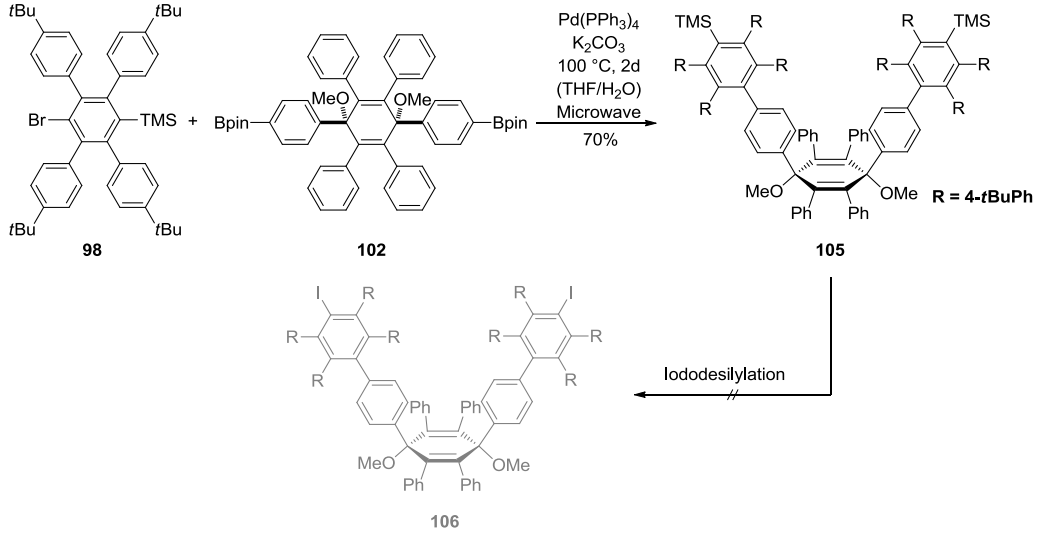

Scheme 45: Synthesis of **105**.

The structure of compound **105** could be elegantly proven by NMR spectroscopy (see *Figure 42*): the ^{1}H-NMR shows a more pronounced splitting (two singlets) of the *t*-butyl groups in comparison to the starting material **98** (see spectrum *Figure 40*). The singlets for the two methoxy groups prove the preserved symmetry of the kinked building block.

Iododesilylation of **105** was expected to smoothly give **106**. However, all attempts failed. Previous studies on 1,4-dimethoxycyclohexadienes have shown that the presence of iodine monochloride, as iododesilylation agent, can only be successfully conducted in the presence of $AgBF_4$. Without soluble silver salts, demethylation of the methoxy groups occurrs, leading to irreversible rearrangements. Apparently, the presence of silver salts reduces the reactivity of iodine monochloride by so much that no conversion of the starting material was obtained. Without silver salt, the iodosilylation runs smoothly, however, an irreversible demethylation of the methoxy groups takes place.

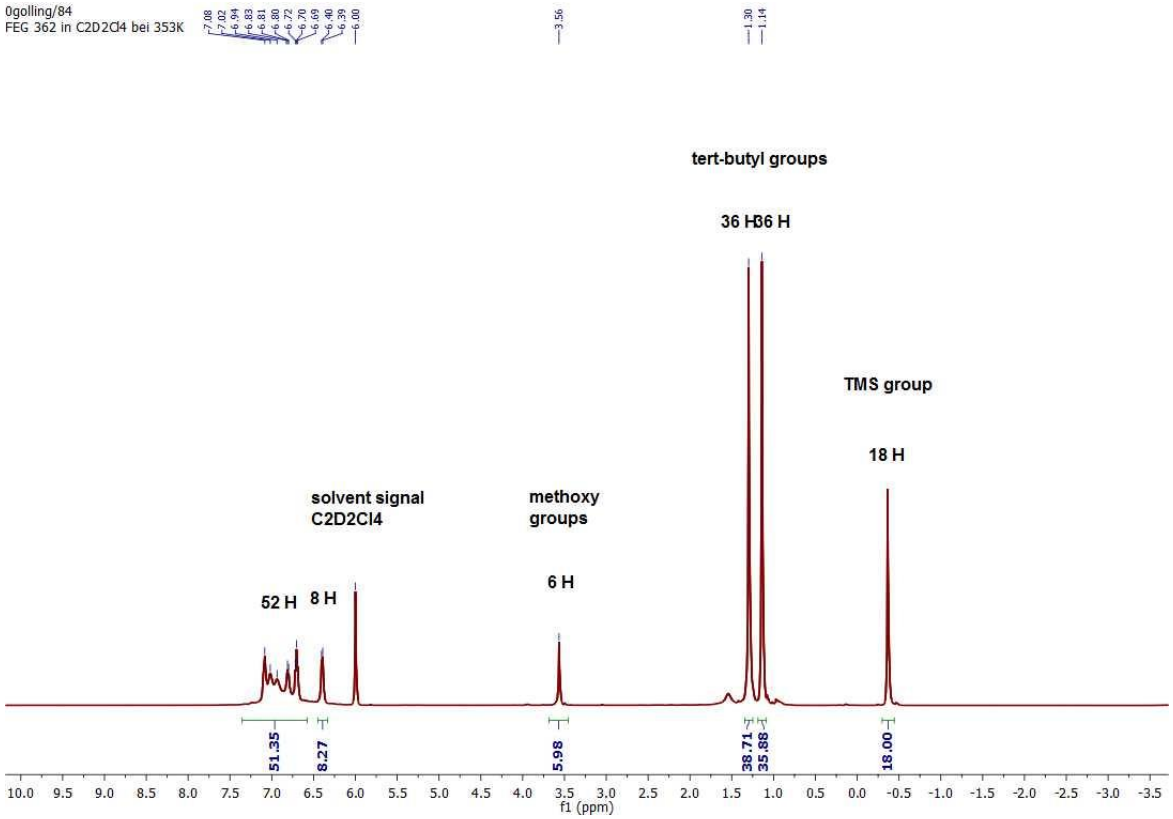

Figure 42: ^{1}H-NMR spectrum of **105** was measured in $C_2D_2Cl_4$ at 80 °C.

To overcome this problem, other solvents or solvent combinations were investigated, since this reaction requires a fine tuning between the solubility of the silver salt and the reactivity of iodine monochloride. The challenging aspect lies in the solubility of the two reagents: silver tetrafluoroborate is preferably dissolved in polar solvents, whereas iodine monochloride is known to react best in DCM or chloroform.[177-180]

No conversion was observed for reactions in THF and DMF. Under diluted reaction conditions, using DCM and $AgBF_4$, quantitative demethylation was observed, nonetheless.

Other reagents such as NIS, NBS and bromine were investigated under various conditions. Disappointingly, clean reaction conditions could not be developed. Therefore, this approach was given up.

As a consequence of the failed iododesilylation, another approach was pursued which was avoided in the first place because of possible dehalogenations during coupling. However, after careful optimization, a 4-fold excess of dibromide **97** in the presence of diboronate **101** led to the monokinked dibromide **103** in 35% yield (see *Scheme 46*). Due to the use of cesium carbonate as base during *Suzuki* coupling, debromination could be suppressed. ^{1}H-NMR spectroscopy confirmed the formation of **103**; mass spectrometry indicated a small amount of monodebrominated product, which is negligible for macrocyclization.

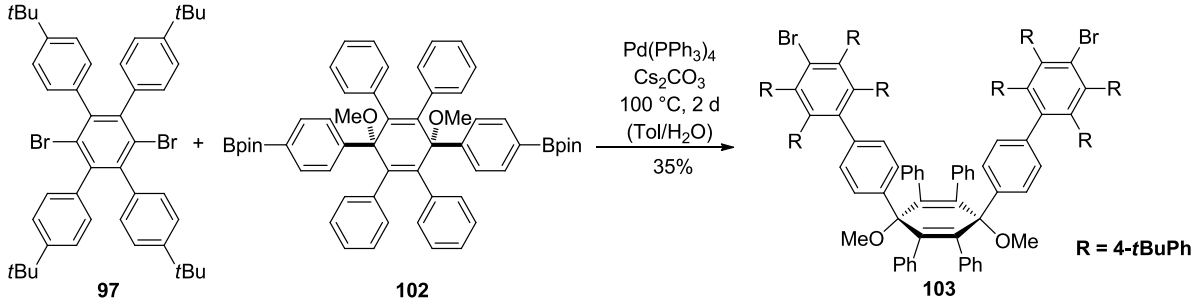

Scheme 46: synthesis of dibromide 1.

The corresponding dikinked bisboronate **104** was synthesized by inversed stoichometries of the starting material: a 4-fold excess of **97** was coupled with **101** to give the title compound **102** in comparable yields.

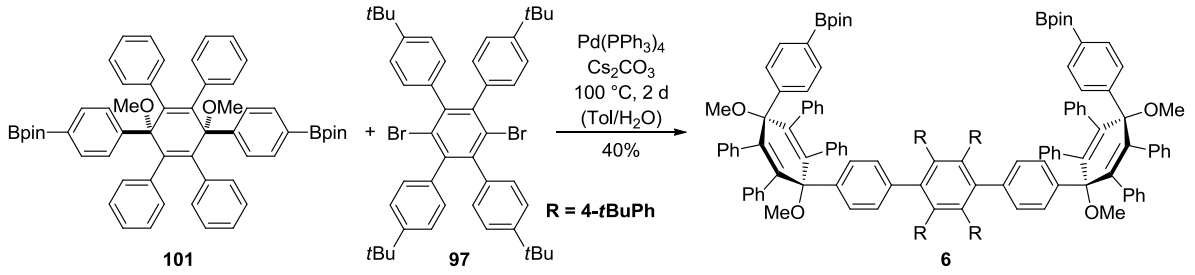

Scheme 47: Synthesis of diboronate **103**

The high symmetry of this building block is reflected by its ^{1}H-NMR spectrum, showing a singlet for the methyl groups of the boronate and the *t*-butyl groups of the central tetraphenylbenzene derivative, whereas the unsymmetric methoxy groups are splitted into two separate singlets.

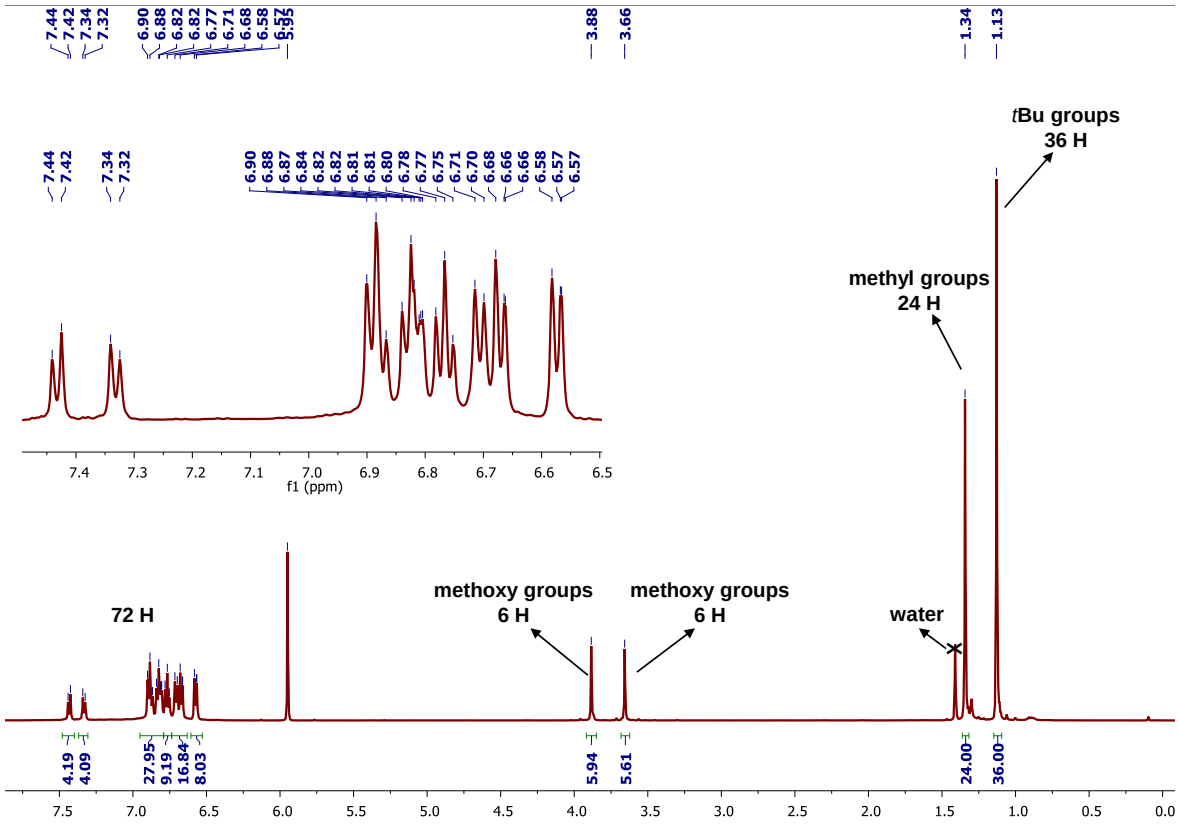

Figure 43: ^{1}H-NMR spectrum of compound **103**. The spectrum was recorded in $C_2D_2Cl_4$ at 93 °C

3.4.2.3. Macrocyclisation

To synthesize the kinked macrocycle **83** (see *Scheme 48*), dibromide **103** was coupled with bisboronate **104**. MS indicated that intramolecular cyclization is favored over polymerization under the described reaction protocol, since few peaks with low intensity were observed at around 5400 m/z, ascribed to the formation of a trimer. These positive findings were assigned to the diluted reaction solution: the confined geometry of the *in situ* formed dimers renders the intramolecular cyclization more favorable over polymerization. HR-MS, however, did not only reveal the formation of the cyclic product, but also of linear dimers which also became obvious during purification by recycling-GPC, as two peaks (linear and cyclic product) were observed. As expected, the structure with the lower hydrodynamic radius could be assigned to the macrocycle, whereas the compound with the higher hydrodynamic radius was still bearing an additional boronate (MS measurements) and was therefore linear. As macrocycle **83** is unstable on silica gel, purification was entirely conducted by recycling-GPC. Despite automatization, purification remained

tedious, as 25 cycles, equaling two days of continuous purification, were necessary to achieve a complete separation. In between, removal of side products was necessary to avoid outrunning of the main product by impurities.

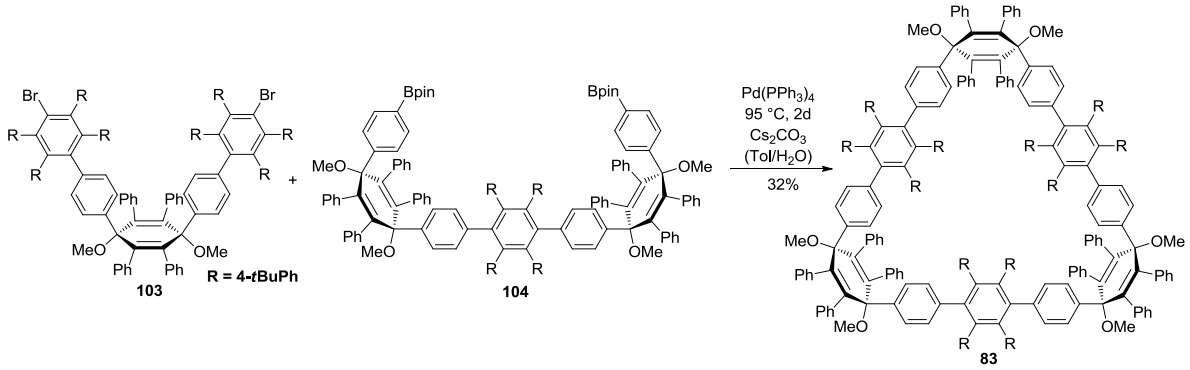

Scheme 48: macrocyclization of **102** and **103** to give **83**

During the synthetic studies toward compound **83**, also the dimer **106**, as shown in *Scheme 49*, was obtained. As a simpler building block, we asked ourselves, whether this building block could also be converted to macrocycle **83**. This approach was also feasible, however, giving drastically lower yields. This is due to the polycondensation-type reaction, which leads to dimerization, dimerization of the dimers, etc. Therefore, only a very small fraction of the title compound is obtained, whereas the rest affords tetramers and octamers.

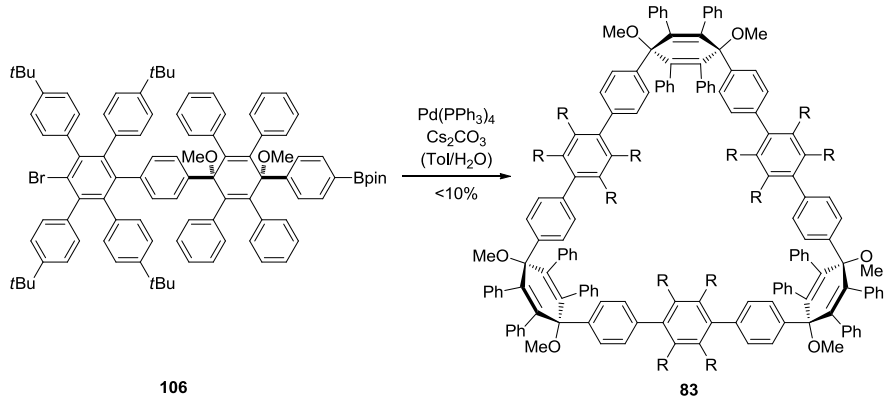

Scheme 49: Synthesis of **83** *via* trimerization of **106**.

The structure of **83** was also proven by NMR spectroscopy. The ^{1}H-NMR (see *Figure 44*) reveals the remarkable symmetry of **83**: sharp singlets are observed for the *t*-butyl group at 1.07 ppm and the methoxy group at 3.55 ppm, giving 36 H and 6 H, respectively. For the aromatic protons, nine independent signals are observed; the integration of these signal yields the theoretically expected number of protons. To assign these peaks to the

corresponding moieties and exact positions within the molecule, 2D-NMR experiments, such as NOESY and COSY, were performed (see *Figure 45* and *Figure 46*).

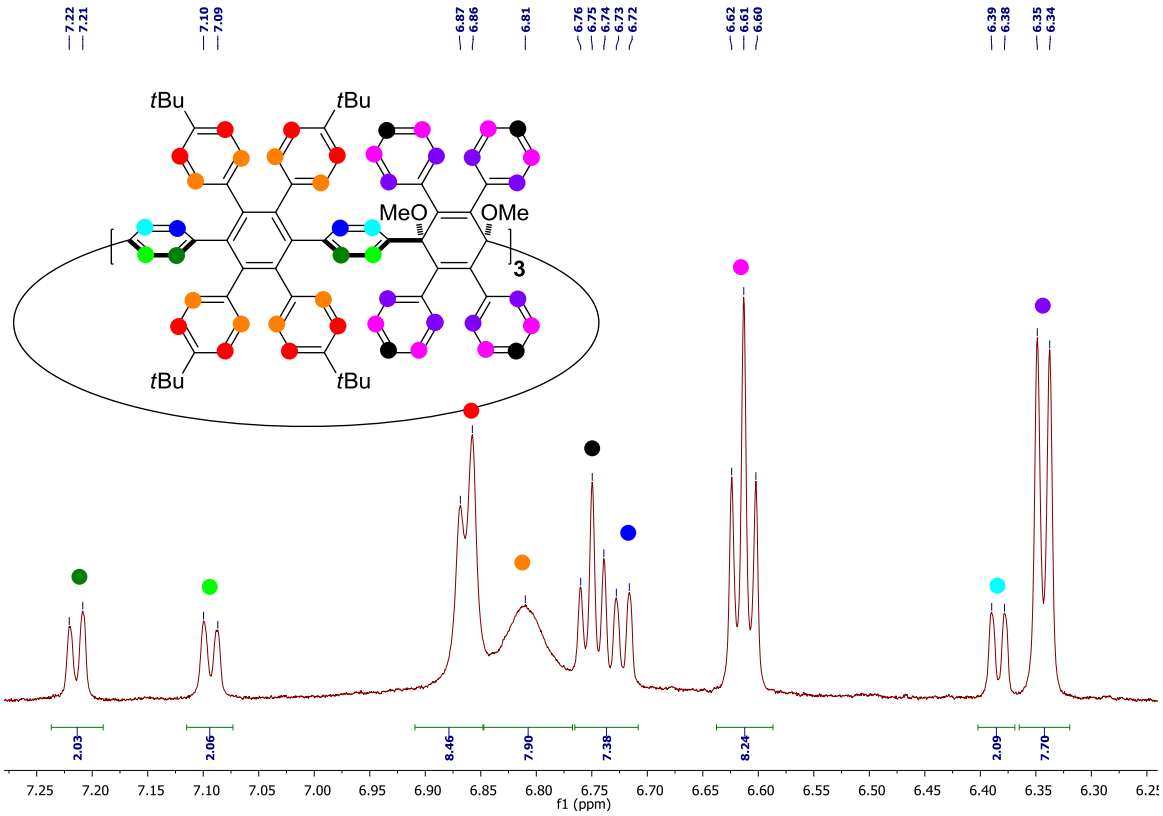

Figure 44: NMR-spectrum of **83** recorded at 80 °C in $C_2D_2Cl_4$

Based on the symmetry of macrocycle **83**, nine instead of seven signals were observed for the aromatic protons. To understand the occurrence of additional peaks and to be able to assign every single peak, NOESY and COSY spectra were recorded. In *Figure 45*, the NOESY spectrum of compound **83** is shown. In this spectrum, the through-space coupling between the protons of the methoxy group with its neighbouring groups is highlighted by colored rectangles. The methoxy group is suited best to explain the appearance of two additional aromatic signals, as the kinking angle of the cyclohexadiene reduces the "visibility" of neighbouring protons.

In the NOESY spectrum, a through-space coupling of several groups is recorded. However, only the through-space couplings of the methoxy group with four magnetically different protons are highlighted, since they provide the most value information for proton assignment. The purple and the pink rectangle can be addressed to the protons of the *ortho*- and *meta*-protons of the phenyl rings attached to the 3,6-dimethoxycyclohexa-1,4-diene.

This is also supported by the integration, multiplicity and coupling constants obtained from the ^{1}H-NMR spectrum (see *Figure 44*).

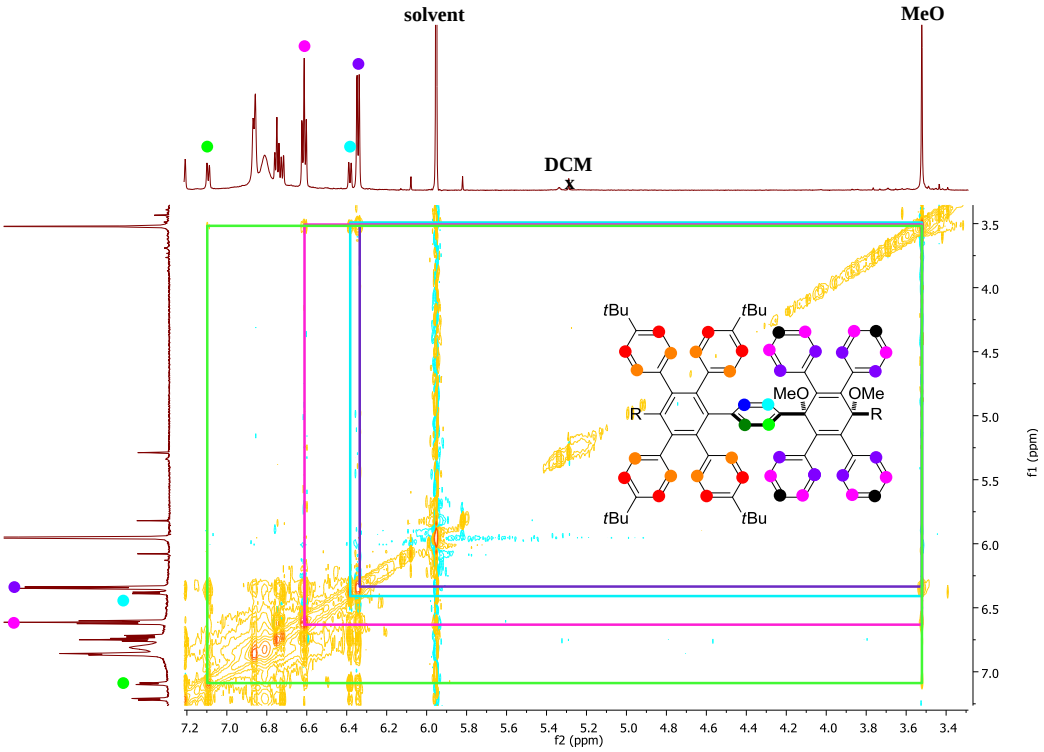

Figure 45: NOESY spectrum of compound **83** recorded at 60 °C in $C_2D_2Cl_4$ (700 MHz).

The light blue and light green rectangles (see *Figure 45*) belong to a split up A-B spin-system: by integration, multiplicity and integration (see *Figure 44*), these protons are attached to the phenylene ring, which bridges the cyclohexadiene and the *tetrakis*(4-*t*-butyl-phenyl)benzene moieties. However, instead of the expected two signals, the A-B spin-system is split up into a spin-system with four different signals. This splitting is due to the interlocking of the phenylene rings which renders all four protons magnetically different, as two of them point inwards, whereas the other two point outwards of the macrocycle and thus experience magnetically different surroundings.

Coming back to the NOESY-spectrum, a through-space coupling is observed for the two aforementioned signals. The light blue labeled protons show a higher coupling intensity than the more remote light green labled protons. This can be explained by the distant-dependent signal intensity inherent for NOE measurements, as the nuclear *Overhauser* effect (NOE) scales with $1/r^6$, with *r* being the distance between the interacting nuclei. In addition, a twisting of the phenylene is also necessary to give rise to through-space

coupling, since the proton nuclei is otherwise shielded by the phenylene ring to which it is attached. A question arises at this point for why one does not observe the other two protons (dark blue, dark green). This can be rationalized by two arguments: first, the phenylene ring bound to the kinked 3,6-dimethoxycyclohexa-1,4-diene points away from the methoxy group (for visualization see *Scheme 50*). Therefore, the lightly colored protons lie on the "visual axis" between the methoxy group and the dark colored protons. Second, the distance between these protons in comparison to the lightly colored protons is much larger, rendering the signal intensity smaller.

With this information and the clearly visible *roof effect* (see *Figure 44*), the remaining two dark labeled peaks can be assigned. To further support this finding, a COSY spectrum was recorded (see *Figure 46*). In this spectrum, only the ^{4}J-couplings are highlighted by two rectangles, whereas the intense ^{3}J-couplings are not shown. These weak signals denote the couplings between the two lightly labeled protons and the couplings between the darkly labeled protons. This unambiguously proves the last part the above described phenylene spin-system and its assignments.

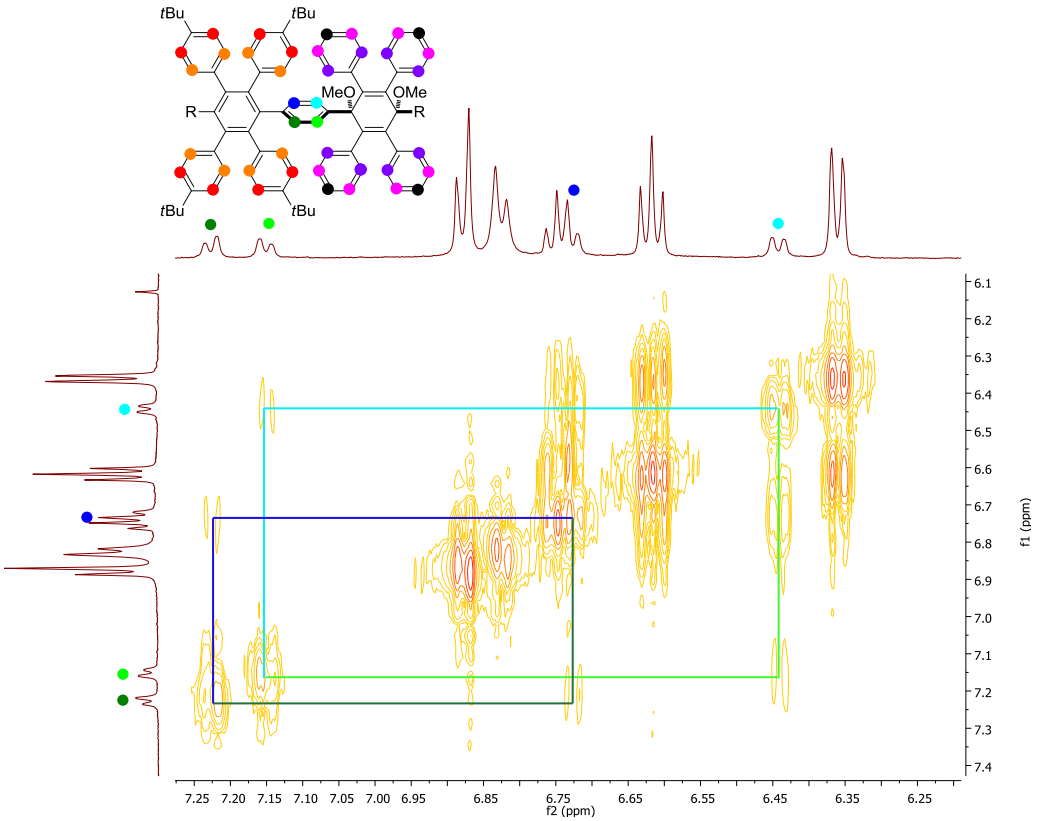

Figure 46: COSY (80°C, $C_2D_2Cl_4$, 500 MHz). The weak ^{4}J coupling is highlighted by the two rectangles.

In *Scheme 50*, a 3D representation of macrocyle **83** is shown to visualize the interlocked geometry of the phenylene rings, which therefore give rise to four different aromatic proton signals.

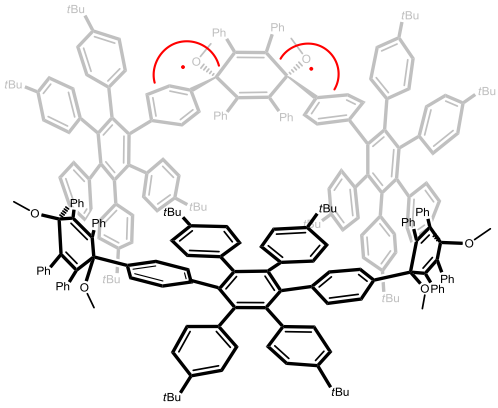

Scheme 50: 3D representation of macrocycle **83** based on 2D NMR spectra discussed above. The expected angle of ca. 90° between the phenylenes the cyclohexadiene unit is labeled in red.

To obtain the congested *cyclic*-hexaphenylbenzene hexamer, sodium napthalenide was used as a reducing agent. However, a color change of the reducing agent or the reaction solution, respectively, from green to purple was not observed. Instead, the solution turned blue, hinting at the formation of anionic species. The reaction was therefore quenched with methanol, giving rise to a product with an unusually weak fluorescence. Mass spectrometry proved the experimental assumptions, as the product mass was four hydrogen atoms higher than the one of the title product **16** (see *Scheme 51*).

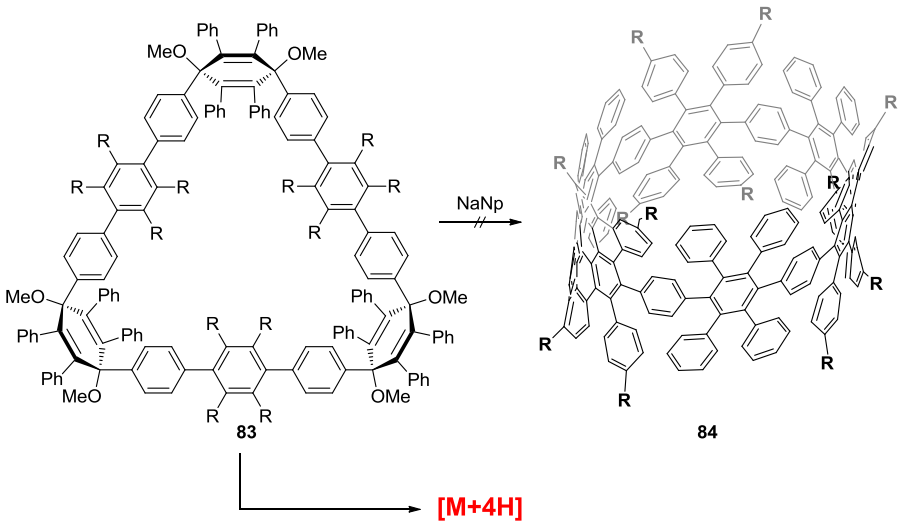

Scheme 51: Attempted synthesis of [12]CPP containing congested *cyclic*-hexaphenylbenzene hexamer **84**

A product with an additional four hydrogen atoms was expected to yield a molecule with two kinked units (see *Scheme 52*). However, not the proposed structure **107** was obtained but rather the C_2-symmetric compound **108** (see *X-ray crystal structure*, *Figure 47*).

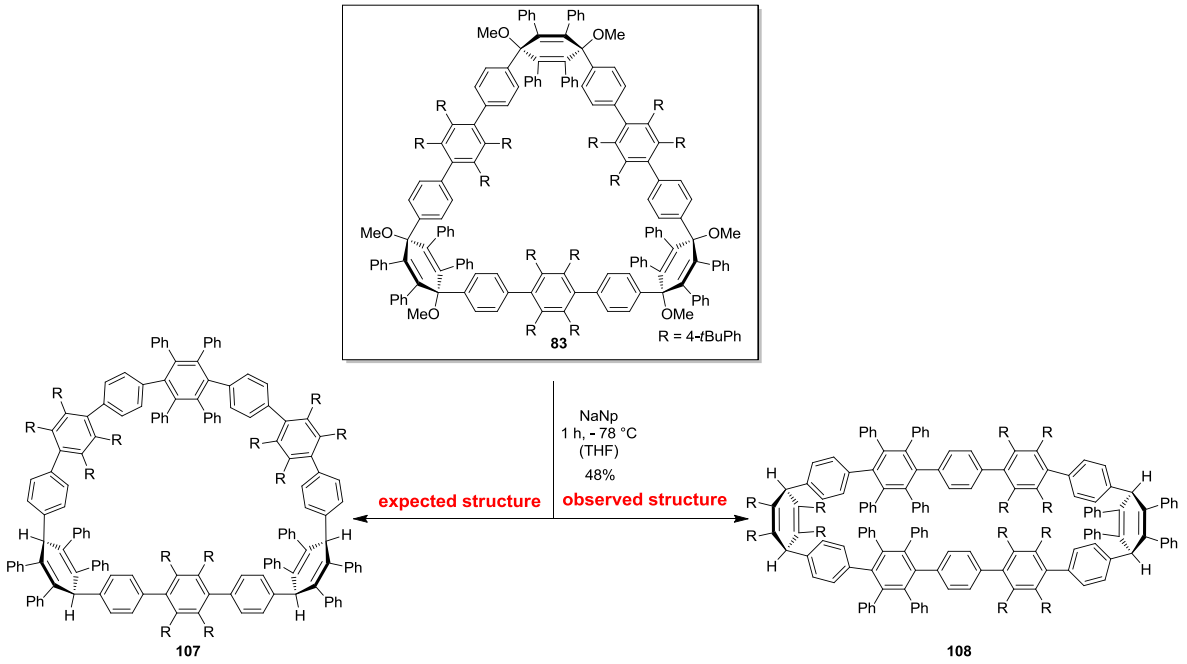

Scheme 52: Expected and observed structure after reductive aromatization of **83**

In *Scheme 52*, the expected (left) and the observed (right) structures are drawn. Compound **107** was expected on the basis of mechanistic considerations for a sodium napthalenide-mediated reductive aromatization. This reaction is to happen *via* a consecutive one-electron process.[20] The expulsion of the methoxy groups leads to a monoanion and then to a dianion which then transforms to the energetically more favorable arene. In this specific case, however, the reaction comes to a halt, leaving the dianion at its *in situ* generated positions of the molecular framework. Then, the intermediates converges to the thermodynamically most favorable tetraanion: thus, one kinked unit remains at its original position containing *tetra*phenyl substituents; the other kinked unit is shifted by two phenylenes to a *tetrakis*(4-*t*-butylphenyl) (see *Scheme 53*). In detail, the intermediately formed anion migrates to the neighbouring positions, eventually forming the thermodynamically most stable tetraanion (see **83a** and **83b**, *Scheme 53*). Its kinking angle is too large for rearomatization. Protonation preserved this unexpected structure, giving rise to **108**.

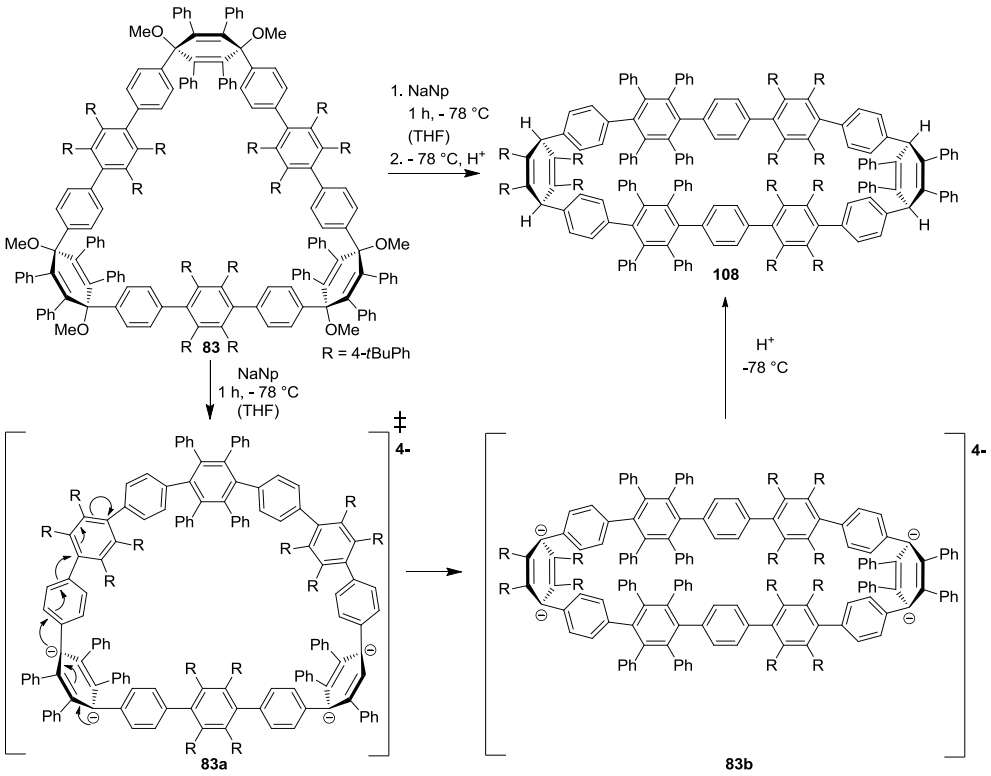

Scheme 53: proposed mechanism for the charge shift of **83a** to the thermodynamically more stable tetraanion **83b**.

Surprisingly, single crystals of structure **108** could be obtained after very slow (four weeks) vapor diffusion (MeCN) into DCM. The X-ray chrystallographic charcterization gave rise to the beautiful crystal structure shown below (see *Figure 47*).

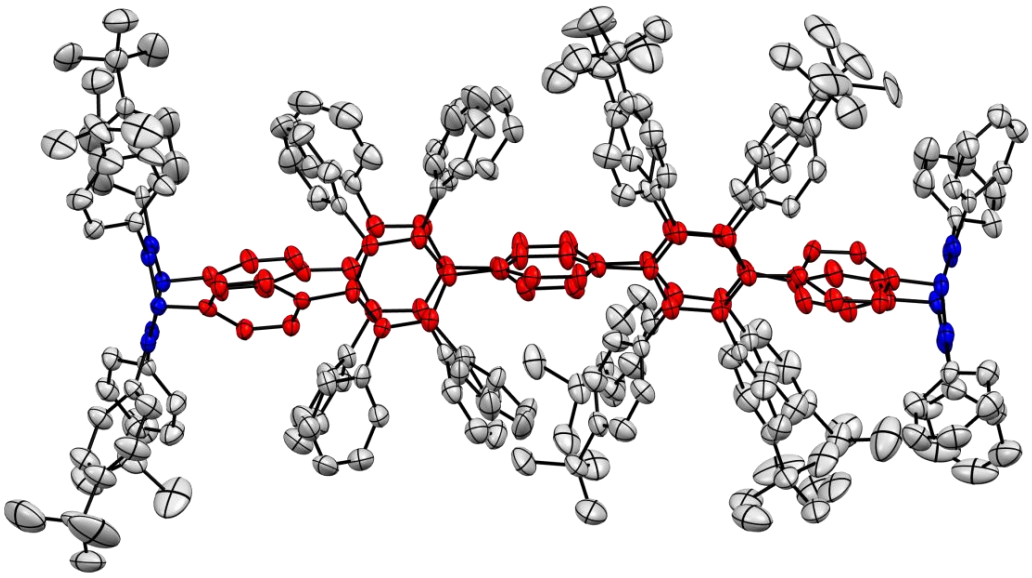

Figure 47: X-ray crystal structure. ORTEP drawing at a 50% probability level. All hydrogen atoms are omitted for clarity. Phenylene units are labeled in red. *para*-substituted 1,4-dimethoxycyclohexa-2,5-dienes are labeled in blue. Solvent molecules are omitted for the sake of clarity.

First of all, the crystal structure of **108** depicts a macrocycle that contains *tetrakis*(4-*t*BuPh) and *tetra*phenyl building blocks in the desired alternating pattern. The two pentaphenylene derivatives (labeled in red) are almost parallel to each other, containing the congestested hexaphenyl benzene motif which was foreseen as a precursor. The angles of the quaternary carbon atoms of the *cis*-1,4-cyclohexa-2,5-diene moieties are highly distorted, resulting in a weakly bent pentaphenylene structure, as shown in the wireframe model of the X-ray crystal structure of **108** (see *Figure 48*).

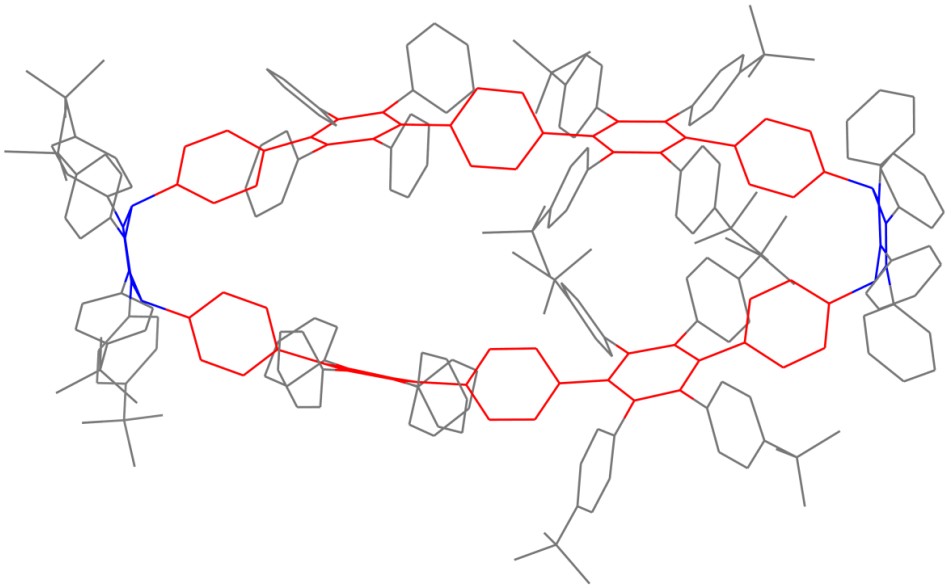

Figure 48: X-ray crystal structure of **108** from on top. The wireframe drawing is used for better visualization. All hydrogen atoms are omitted for clarity. Phenylene units are labeled in red. *para*-substituted 1,4-dimethoxycyclohexa-2,5-dienes are labeled in blue.

To obtain a fully aromatized CPP ring, **108** was subjected to DDQ at temperatures up to 100 °C. From the literature, it is known that *para*-substituted cyclohexa-1,4-dienes can be aromatized to give phenylenes. This has also been successfully shown for π-extended [9]CPPs.[83, 181] Here, however, the desired strained CPP ring (see *Scheme 51*) could not be obtained.

Therefore, we investigated whether harsher reaction conditions could afford the [12]PPC from the triangular macrocycle **83**. Instead of the relatively mild reducing conditions with NaNp (- 78 °C), we applied low valent titanium, which had been used for the parallelogram approach of the [9]PPC. In comparison to the above described reductive aromatization, the reaction is performed at 80 °C. The difference of reaction temperature between the two

approaches is 160 °C. This more powerful method furnished the congested cyclic-hexaphenylbenzene hexamer [12]PPC **84** (see *Scheme 54*).

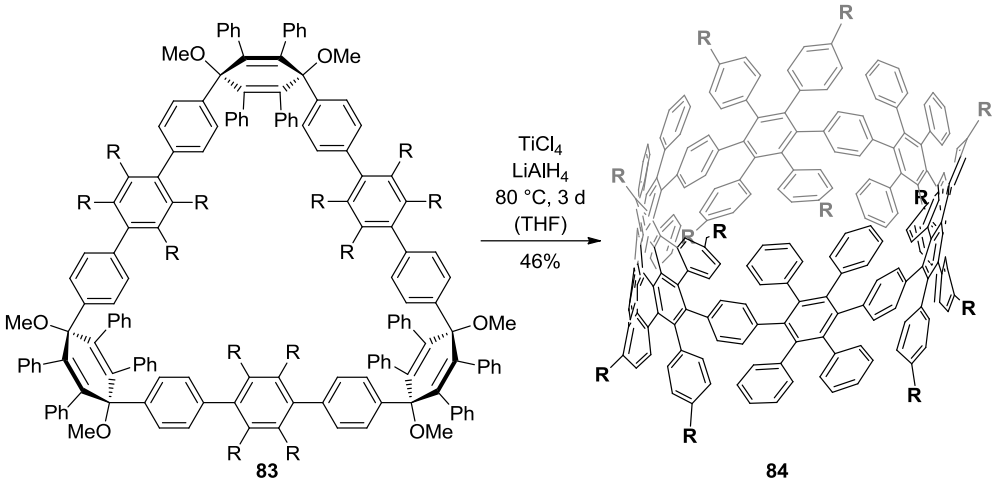

Scheme 54: Synthesis of the congested *cyclic*-hexaphenylbenzene hexamer ([12]PPC)

The macrocycle has been characterized by HR-MS spectrometry and NMR spectroscopy. The MS results are in agreement with the theoretically calculated mass (see *Experimental Part: Figure 77*). X-ray crystallographic analysis could not be performed since the obtained single crystals were too small. As a consequence, an insufficient number of uniqe reflexes was observed to resolve the structure. Therefore, 2D-NMR spectra were recorded to characterize **84**.

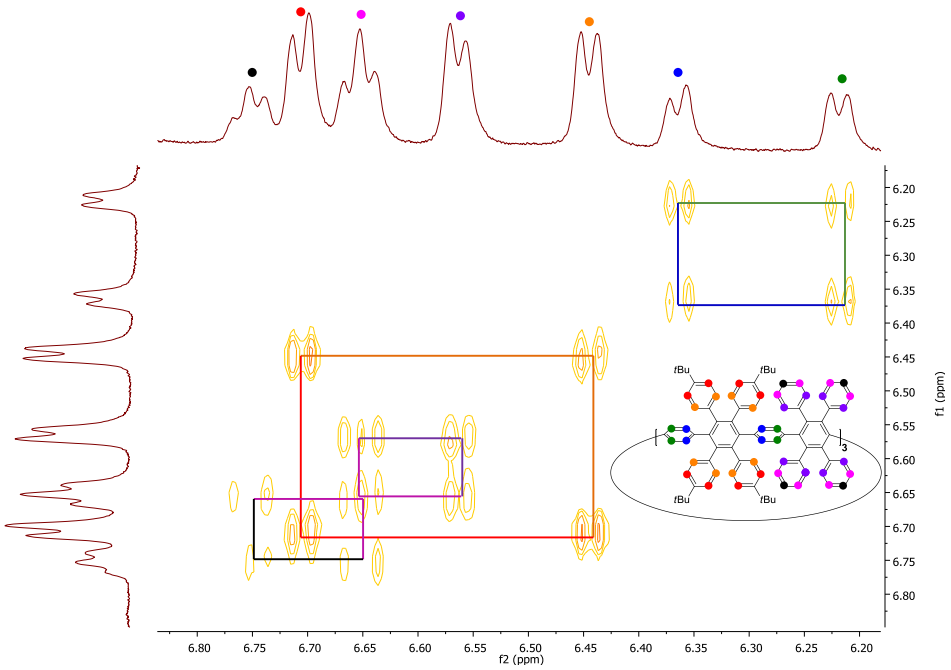

Figure 49: ^{1}H-^{1}H-COSY (500 MHz) of **84** recorded at 298 K in $C_2D_2Cl_4$.

In *Figure 49*, the ^{1}H-^{1}H-COSY of **84** is shown. The high symmetry of macrocycle **84** reduces the number of different spin-systems to three. These systems are labeled by colored rectangles. The observed couplings within the corresponding moieties are well in line with integration and mulitiplicity. With this knowledge in hand, all protons could be unambgiously assigned, except for the phenylene ring which is labeled with blue and green dots. Therefore, a NOESY spectrum was recorded to assign these protons.

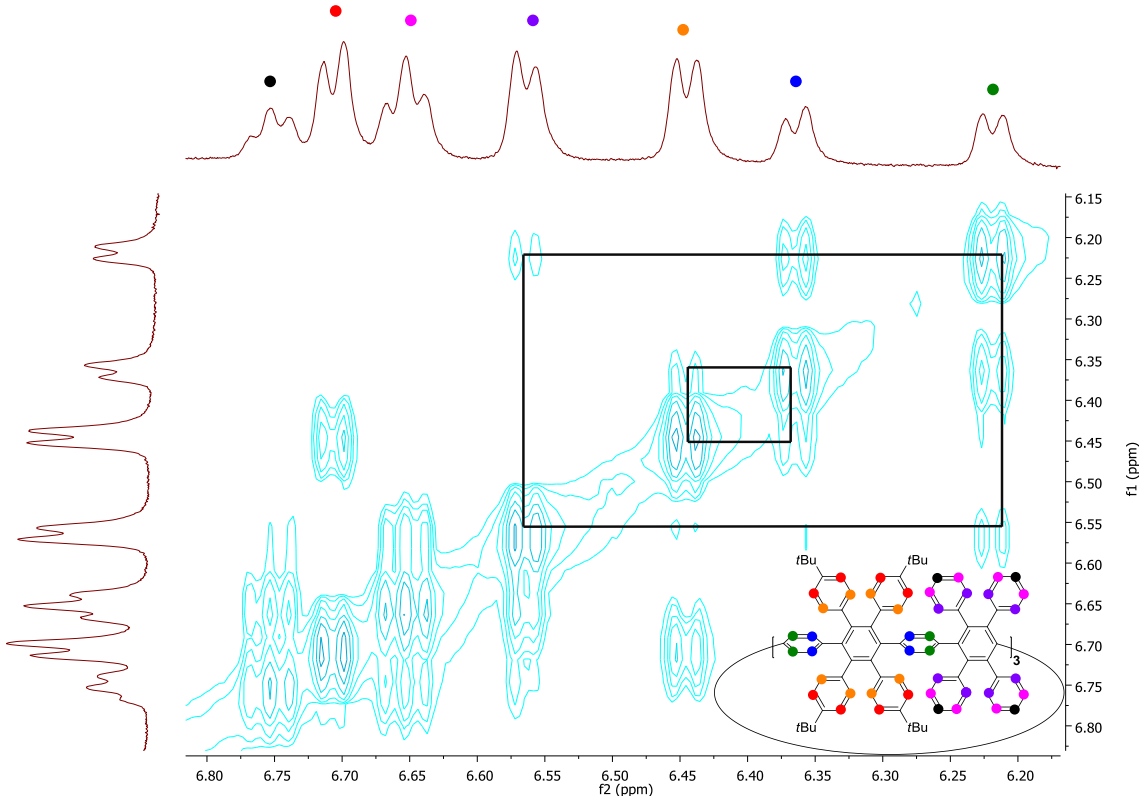

Figure 50: NOESY-spectrum of **84** recorded at 298 K in $C_2D_2Cl_4$. Intense through-space coupling between protons of the bridging phenylene with its neighboring 4-*t*BuPh and phenyl ring highlighted in black frames.

In *Figure 50*, the NOESY spectrum of compound **84** is shown. The two black rectangles depict the through-space coupling between the blue and green labeled protons of the phenylene unit with its closest neighbors. For the green labeled protons, a through-space coupling with the purple labeled protons is observed, whereas the blue labeled protons couple with the organe labeled protons. From these findings, one obtains a full assignment of all protons of **84**. Thus, NMR experiments confirm the HR-MS results.

3.4.3. Oxidative Cyclodehydrogenation

After the successful preparation of [12]PPC **84** and its C_2-symmetric congener **108**, the oxidative cyclodehydrogenation was investigated. Therefore, both compounds were subjected to $FeCl_3$.

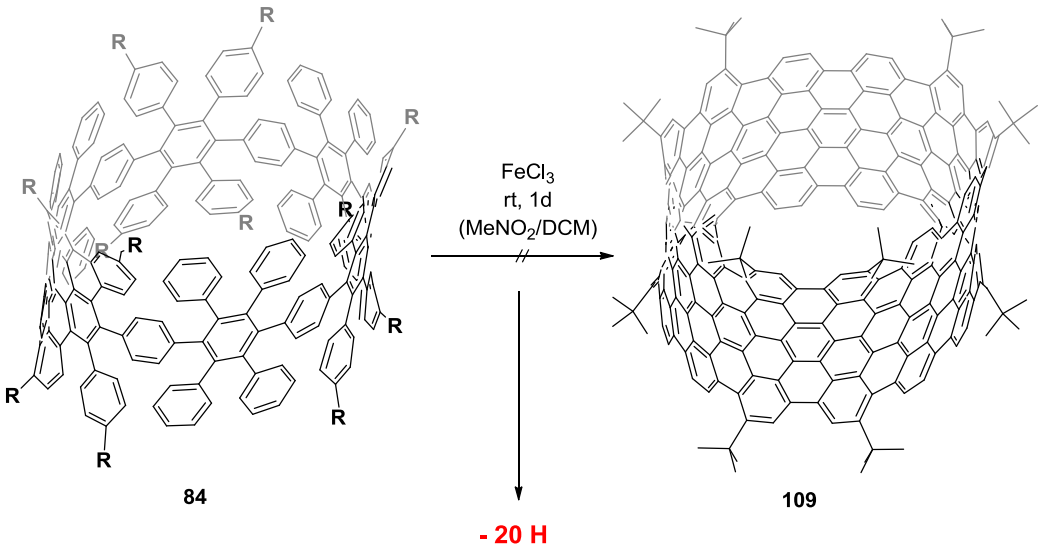

Scheme 55: oxidative cyclodehydrogenation of **84**

The oxidative cyclodehydrogenation of **84** yielded a mixture of products. Thus, the crude product was separated by preparative TLC to investigate the product distribution further. In *Figure 51*, the mass spectra of compound **84** are shown. The separation afforded various products ranging from 3389 m/z as the most unpolar product, to 3408 m/z, as the most polar product. The lightest fraction was subjected to $FeCl_3$ again. Disappointingly, no further decrease in mass could be observed. Room temperature and high temperature approaches for cyclodehydrogenation with other oxidizing agents, such as DDQ, $Sc(OTf)_3$ and/or TfOH, led to decomposition of the starting material and gave product mixtures that did not yield masses in the expected product range. As a consequence, this approach was given up and the final goal still remains elusive.

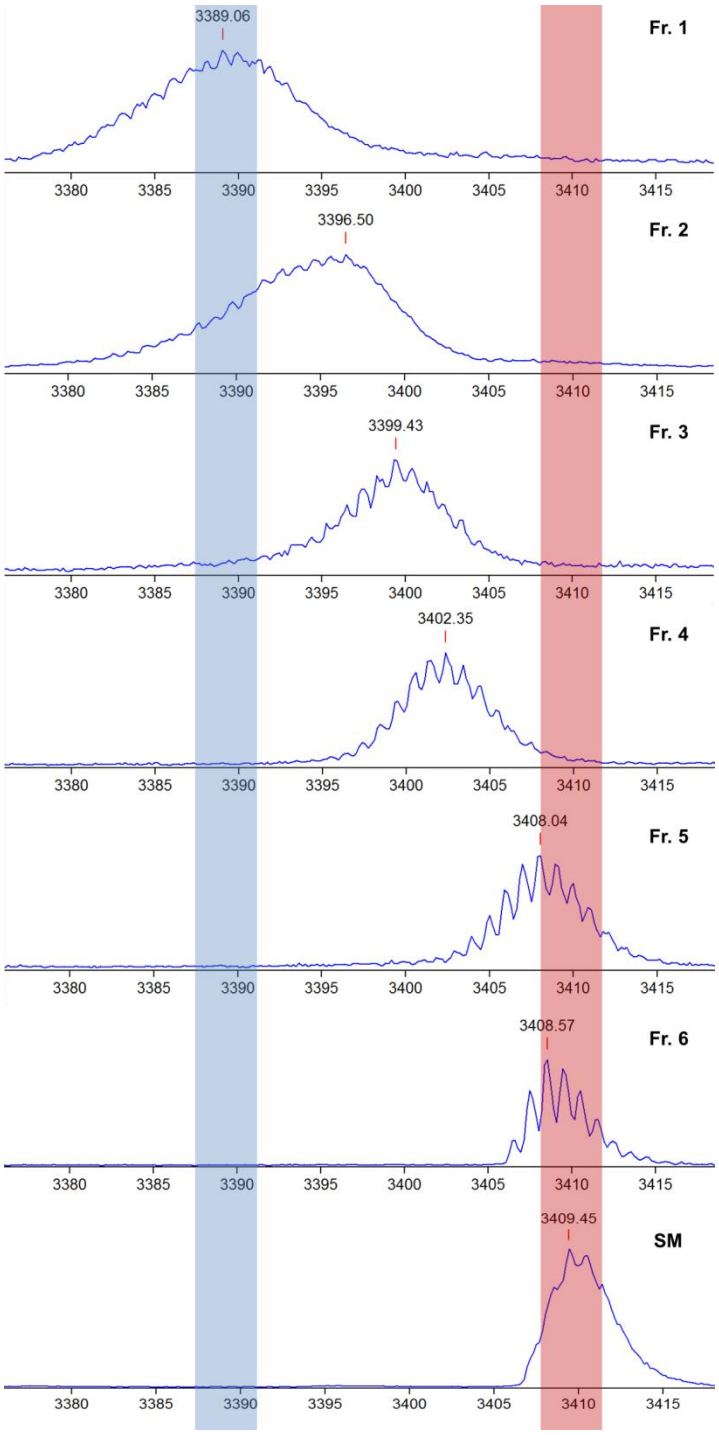

Figure 51: oxidative cyclodehydrogenation of **84**. Upper left (Fr.1) first fraction. Bottom: starting material

As the previous attempt failed (see *Scheme 55*), the C_2-symmetric compound **108** was also investigated. As can be seen from the X-ray crystal structure, (see *Figure 48*) the two pentaphenylenes, being bridged by two cyclohexa-2,5-dienes, are only slightly bent. Thus,

compound **108** is expected to undergo oxidative cyclodehydrogenation. In addition, cyclohexadienes are known to form phenylenes in the presence of oxidizing agents.[83] This renders a bottom-up synthesis of a CNT possible.

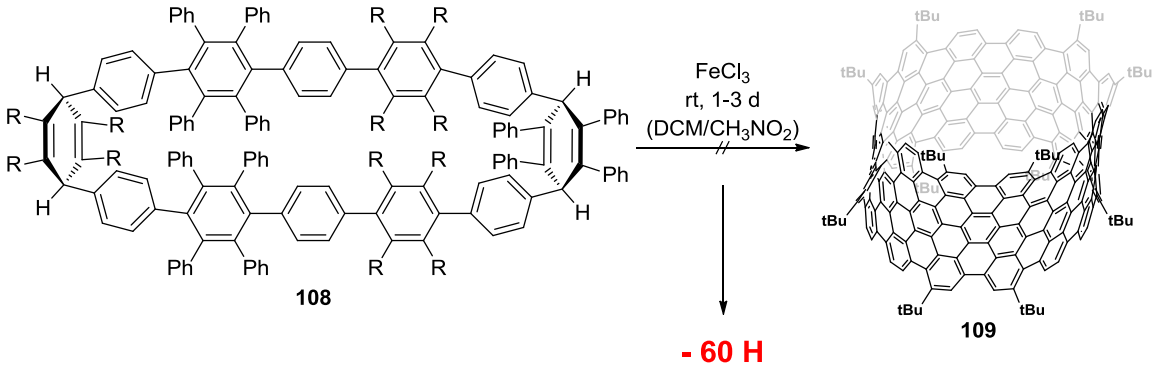

Scheme 56: Oxidative cyclodehydrogenation of **108**.

The C_2-symmetric compound **108** was subjected to $FeCl_3$. The reaction progress was monitored by MS. Spectra were recorded after 1d and 3d. In *Figure 52*, the mass spectrum of **108** after cyclodehydrogenation for 1d is shown. Four peaks are observed at 3370 m/z, 3355 m/z, 3317 m/z and 3299 m/z. The mass of the starting material is 3415 m/z.

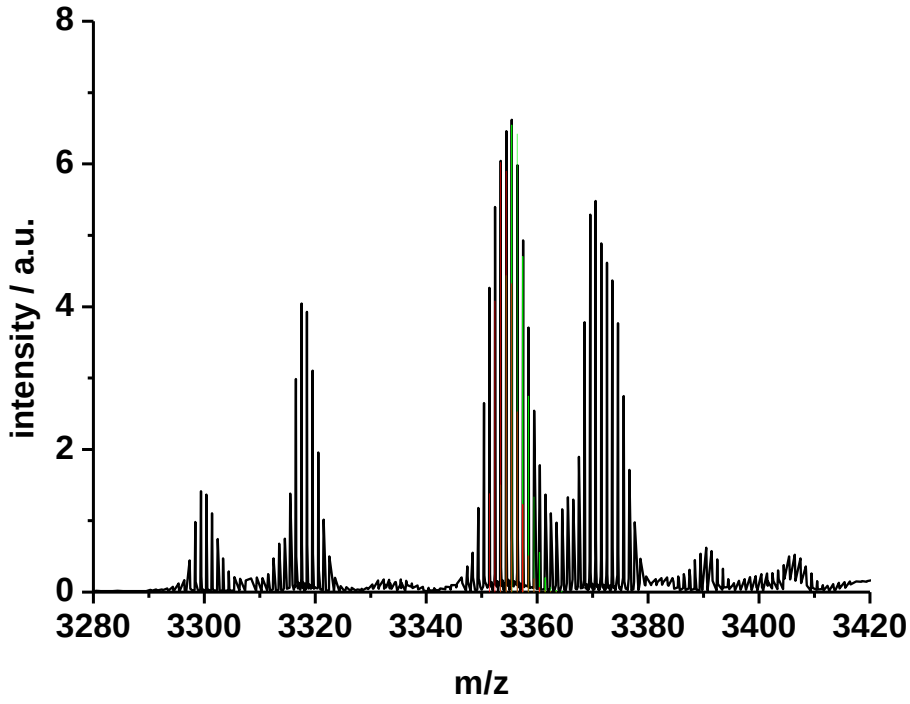

Figure 52: HR-MS (MALDI) spectrum of compound **108** after cyclohydrogenation (1d). Red isotopic pattern for a cyclodehydrogenated compound with a sum formula of $C_{264}H_{182}$ and its two hydrogen atoms heavier congener: $C_{264}H_{184}$. Reaction conditions: $FeCl_3$ r.t., 24 h, filtration through a short bad of silica with DCM/THF and subsequent separation by preparative GPC column.

To understand the observed masses, initially, a closer look was taken at the intermediate mass of 3355 m/z. The lower masses will be discussed in the following spectra (*vide infra*). The mass of 3370 m/z cannot be convincingly explained by a structural intermediate and is thus not further discussed.

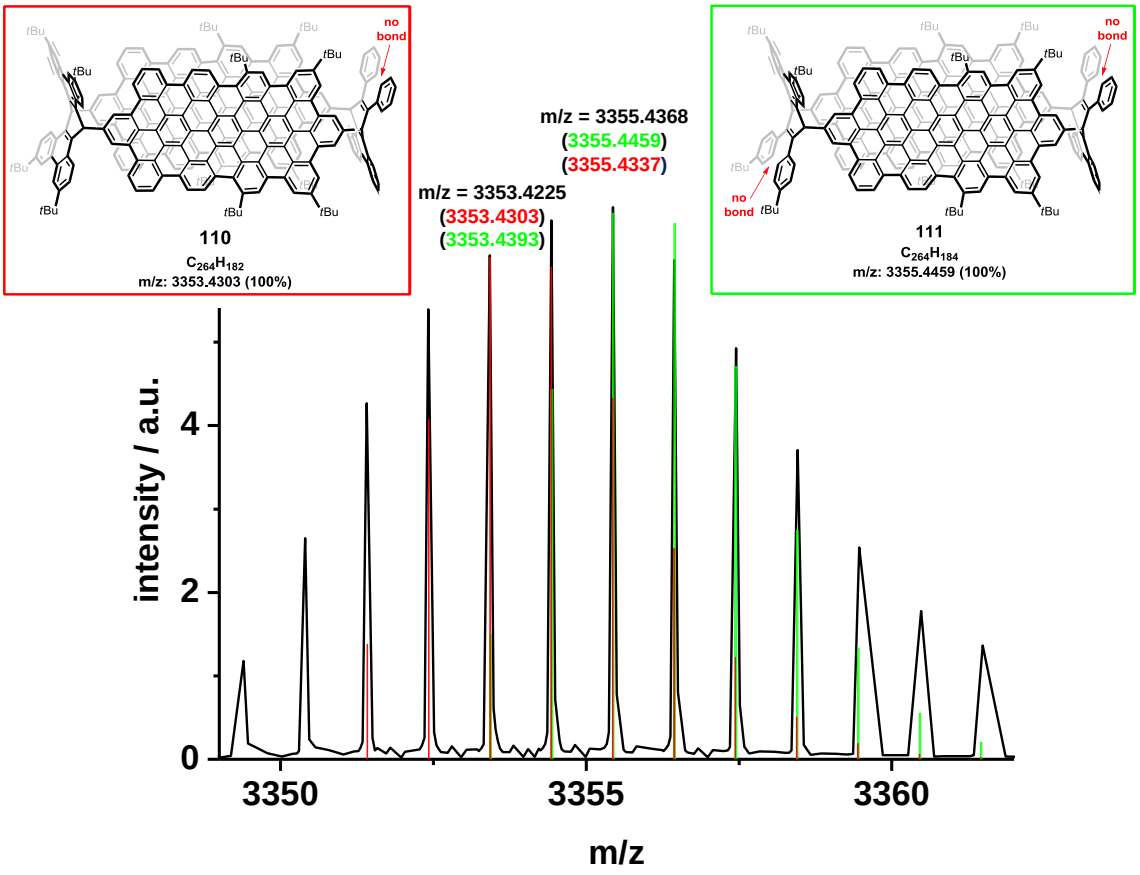

Figure 53: section of the mass spectrum of compound **108** after cyclodehydrogenation for 1d with $FeCl_3$ at r.t.. Red spectrum: one bond missing; green spectrum two bonds missing.

In *Figure 53*, a small section of the mass spectrum between 3350 m/z and 3360 m/z is shown. The sum formulas for two interemediates (red, left; green, right) are shown. These structures can be hyposized on the structure of the starting material, as the crystal structure hinted at a bent pentaphenylene unit that should smoothly undergo cyclodehydrogenation to give a short nanoribbon segments. The sum formula of the theoretically calculated mass (green) deviate by 0.01 g/mol; such an error range has been observed for molecules with similar molecular weight, of which the structure had been confirmed by X-ray crystallography before MS measurements. Therefore, the experimental findings may very well be in agreement with the outlined sum formula. Partially cyclodehydrogenated ribbons

in conjunction with chloro-de-*t*-butylation were to give a mass of 3356.5180 m/z, which is of by 1.1 m/z. In addition, such a partial cyclodehydrogenation is not expected on the basis off experimental experiences; however, it cannot be ruled out. Partial dehydrogenation with chlorination gives a mass of 3355.8215 m/z, which is unlikely because only two bonds of the starting material have been fused. One can conclude that the above given sum formula matches with the experimental findings.

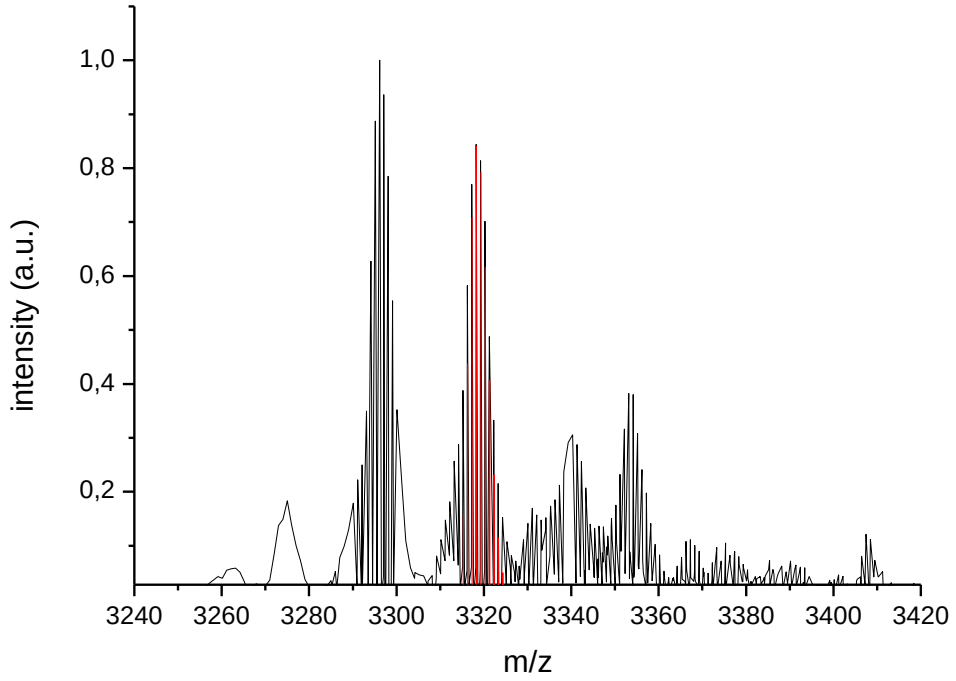

Figure 54: mass spectrum of comound **108** after cyclodehydrogenation for 3d at r.t..

After 3d, the spectrum shows an increase in intensity for the signals at 3318 m/z and 3396 m/z, whereas the peaks around 3353 m/, which are assigned to the cyclodehydrogenated dicyclohexadiene-bridged bisribbon **110**, decreased in intensity and were additionally shifted by 2 m/z to lower masses; the peaks at 3370 m/z disappeared. In the range from 3340 m/z to 3260 m/z five different peaks can be observed. The mass difference between each of them equals 22 m/z. These findings are a first indicator that a side reaction has occurred, namely a chloro-*de*-t-butylation, as the mass difference between a chlorine atom and a *t*-butyl group equals 22.1 m/z. With this having said, the peaks around 3318 m/z were more closely investigated (see *Figure 55*), as this mass could have also hinted at a bottom-up synthesis of an ultrashort CNT:

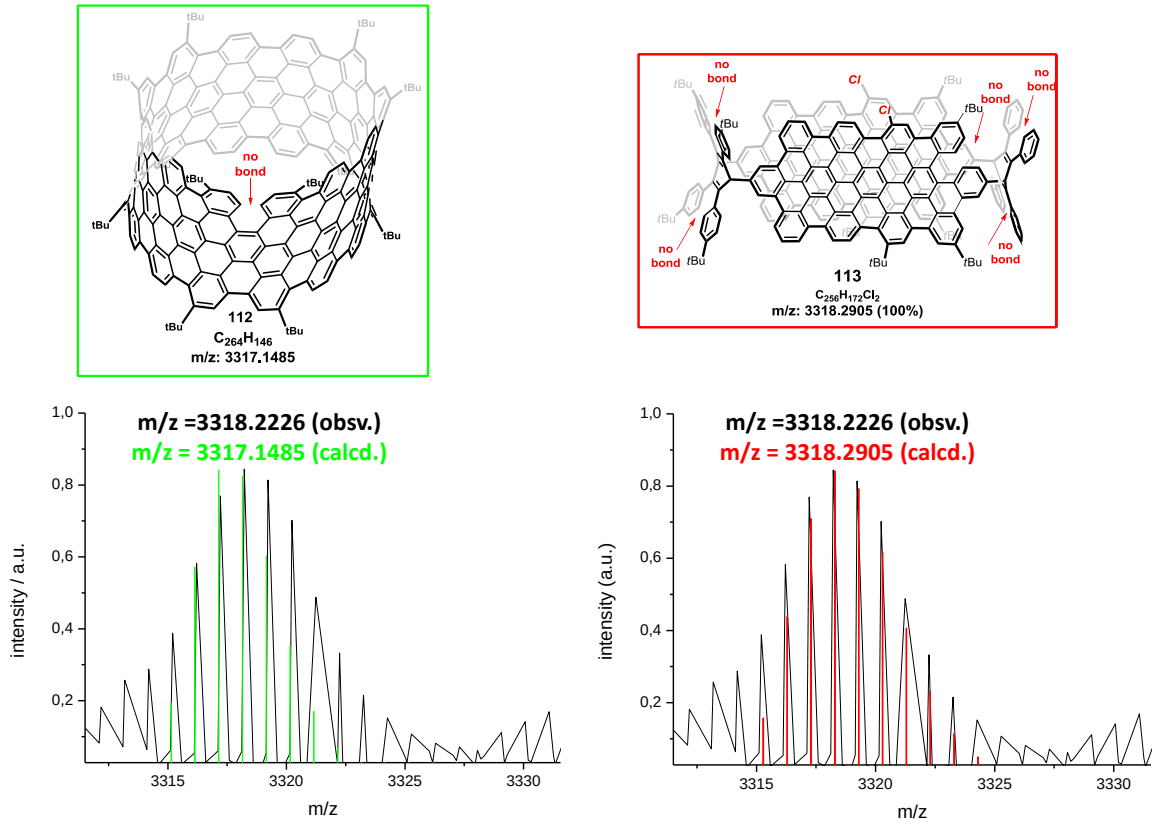

Figure 55: HR-MS (MALDI) spectrum of **108** after cyclodehydrogenation for 3d with $FeCl_3$.

In *Figure 55*, two sections of the mass spectrum of **108** are shown after cyclodehydrogenation for 3d at r.t. In the left spectrum, the hypothetical structure of an almost fully fused CNT is depicted. The calculated mass spectrum of this structure is shown in green. The difference between the observed and calculated mass is 1 m/z; the deviation is thus beyond the error limit. From these and the above described findings, one can conclude that oxidative cyclodehydrogenation did not lead to CNT **112**. The mass spectrum for the simulated structure of **113** hints strongly at the formation of a bis(de-*t*butylated) and concomittantly dichlorinated compound, as the mass and the corresponding isotopic patterns are in good agreement. One has to state, however, that only the sum formula can be concluded and a structural hypothesis, as shown here, is entirely based on chemical intuition. To get further inside, the *pre*-purified samples were separated by reversed-phase HPLC column to enrich one of the fractions. Higher molecular weight fractions (3370 m/z) could be separated of. However, the other fraction contained a mixture of 3355 m/z, 3317 m/z and 3296 m/z.

To elucidate the structure of this intermediate, several attempts were undertaken to grow single crystals from the crude solution. Disappointingly, single crystals could not be obtained.

3.4.4. Summary

In this chapter, the synthesis of a congested *cyclic*-hexaphenylbenzene hexamer, [6]CCHPB, **84** and its unexpected C_2-symmetric congener **108** is presented. The precursor structures for these two macrocyles were obtained *via* dimerization of the monokinked dibromide **102** and the dikinked bisboronate **103** which furnished a triangular macrocycle **83** under *Suzuki* conditions. To obtain [6]CCHPB, the triangular macrocyle **83** was subjected to low-valent titanium. Oxidative cyclodehydrogenation of this macrocycle led to a loss of 20 hydrogen atoms, at which the reaction came to a halt. Other oxidizing agents such as DDQ/TfOH/$Sc(OTf)_3$ were also investigated. However, they led to a decomposition of the macrocycle and afforded fragments that could not be assigned my mass spectrometry.

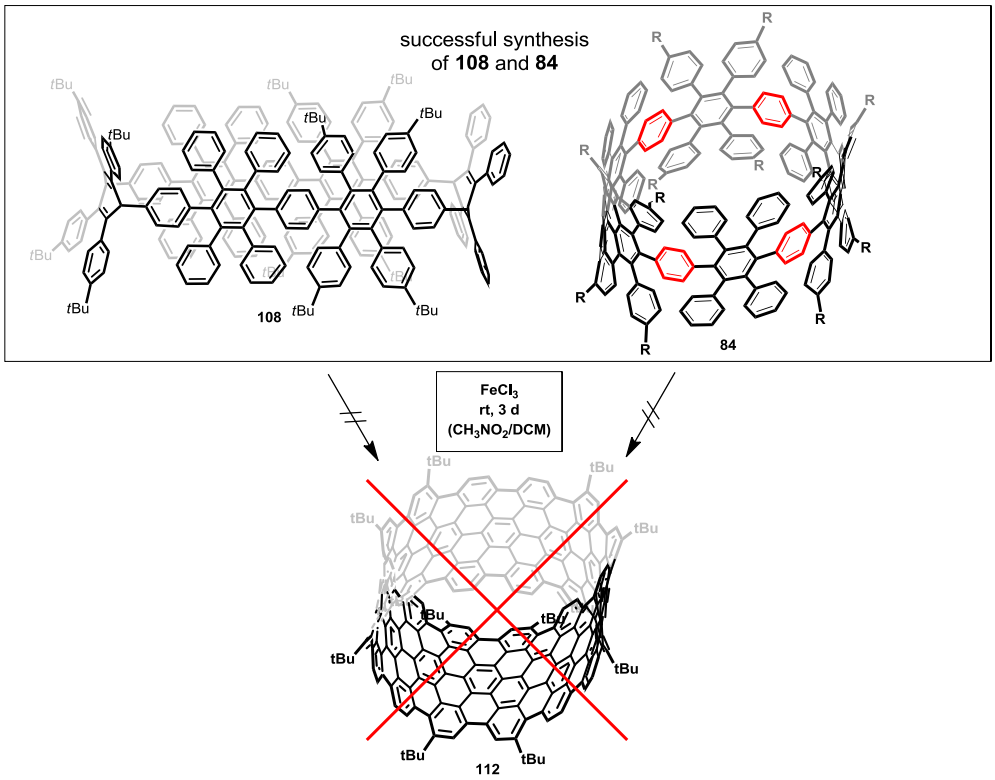

Scheme 57: successful synthesis of **108** and **84** as possible precursors to **112**.

For the synthesis of the C_2-symmetric congener **108**, the reductive aromatization was performed with NaNp. Under these milder reductive reaction conditions, only one of the

three cyclohexa-1,4-dienes was aromatized. The other cyclohexa-1,4-diene moieties were not aromatized, giving rise to a beautiful C_2-symmetric macrocycle. Astonishingly, one of the four *in situ* generated electron pairs of the intermediate tetranion migrated to give a thermodynamically more favorable macrocycle. The structure could be elucidated by single crystal X-ray crystallography. As this structure contains two pentaphenylenes that are bridged by 3,6-connected cyclohexa-1,4-dienes, a smooth condensation of this ribbon-like structure was expected. Oxidative cyclodehydrogenation with $FeCl_3$ fullfilled the high hopes of these serendipitously discovered structure, as mass spectrometry showed a loss of 60 hydrogen atoms, which has hitherto between the highest degree of cyclodehydrogenation. However, chloro-*de*-*t*butylation set in during the reaction. As mass spectrometry can only reveal the sum formula of the obtained molecular structure, several attempts were made to grow single crystals to get structural insights. Disappointingly, all attempts failed.

3.5. New Soluble Polyphenylene Precursors: Structural Studies by DFT and DLS

In this chapter, a new approach for the synthesis of linear polyphenylene derivatives is presented, using *oligo-trans*-3,6-dimethoxycyclohexa-1,4-dienes. To do so, monomeric units were coupled *via* a previously described oxidative homocoupling to give kinked oligomers. Their structure was investigtead by DFT and dynamic light scattering (DLS). It was investigated whether these structures can be reductively aromatized and converted to linear polyphenylenes.

3.5.1. Introduction

The synthesis and application of rigid oligomers has garnered a great interest in organic electronics[182-183] and directed self-organization,[184] since they serve as well-defined molecular species between small molecules and polymers. They combine the synthesis, ease of purification and molecular characterization of small molecules[2] and correlation of their physical properties to defect-free polymers. In addition, oligomers can also display distinct properties on their own right. In this regard, *oligo*(paraphenylenes) (OPP)s play an important role as low band gap materials[185-187] and chromophores[188-189]. For liquid-phase syntheses, various strategies have been developed to overcome diminishing solubility of OPPs with increasing number of repeating units. The attachment of alkyl chain to the monomeric units improves solubility so much that higher oligomers obtained.[190-192] However, solubility increasing groups reduce conjugation due to chain twisting. This drawback was circumvented by bridging *p*-biphenyl units with five membered rings to give ladder polymers.[193-195] For the synthesis of "naked" OPPs, transition-metal-catalyzed polymerization of cyclohexa-1,3-dienes[196] or oligomeric dihydro precursors from cyclic diketons can be used.[197-198] Both approaches, however, require a two-step procedure to reach OPPs. The development of new methods for the preparation of highly soluble and stiff precursors that can deposited and converted[155, 199] on surfaces to defined polyphenylenes is of great interest, as their fundamental properties could be studied.

3.5.2. Synthesis & Oligomerization

During the synthesis of the *cis*-kinked 3,6-dimethoxycyclohexa-1,4-diene **33**, which was described earlier, also the formation of its corresponding *trans*-product was observed. The *cis*- and *trans*-product can be easily separated by column chromatography. The *trans*-product was collected as an intersting "side product" and then treated in the same manner as before (see *Scheme 58*): diol **108** was methylated using MeI. Subsequent iododesilylation furnished the desired *trans*-diiodide **110** in excellent yields (90%).

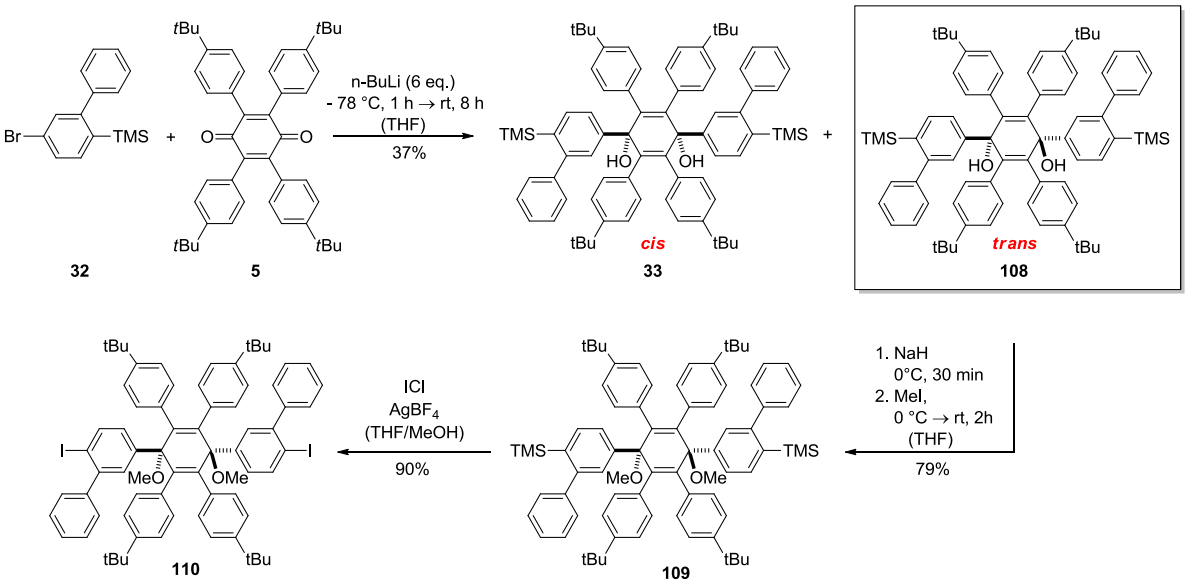

Scheme 58: Synthesis of *trans*-3,6-dimethoxycyclohexa-1,4-diene **110**.

The oligomerization of **110** was achieved *via* an oxidative homocoupling. By mass spectrometry, up to 12 repeating units were observed, using the linear mode of the spectrometer, which gives a better S/N ratio. Separation by fractionate precipitation, subsequent preparative GPC and finally exhaustive recycling-GPC afforded pure oligomers up to 9 repeating units.

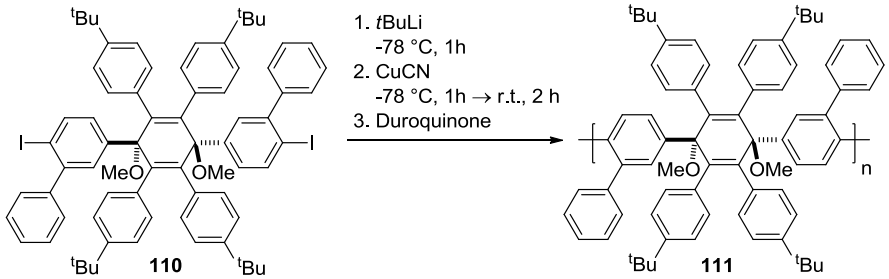

Scheme 59: polymerization of *trans*-3,6-dimethoxycyclohexa-1,4-diene giving oligomers of **111**.

In *Figure 56*, the MALDI-TOF measurements of compounds **111-1**, and **111-2** and **111-3** are shown. Several peaks of each individual compound are observed, which is due to demethoxylation during ionization of 3,6-dimethoxycyclohexa-1,4-dienes moieties.

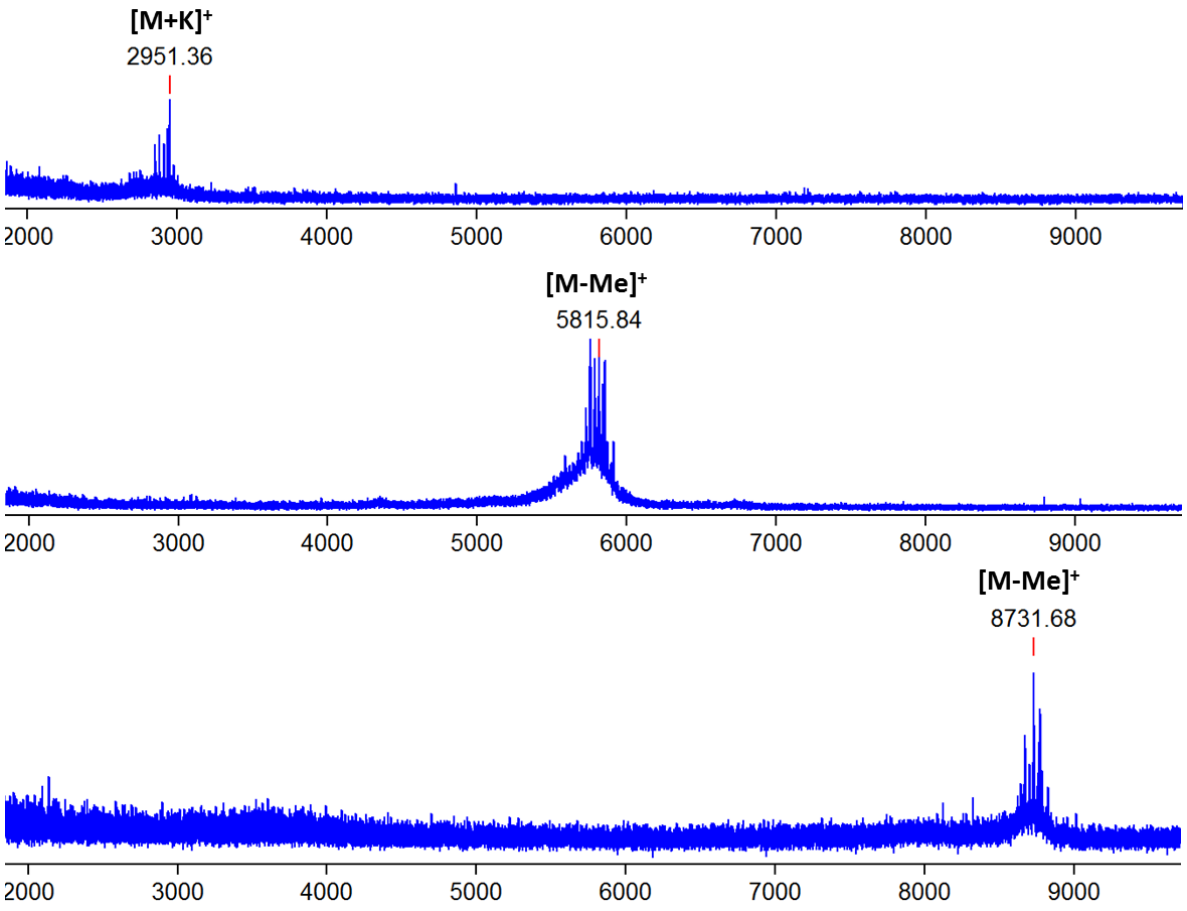

Figure 56: mass spectrum of the purified nonamer **111-1**, **111-2** and **111-3**. The spectra show the typical demethoxylation pattern for 3,6-dimethoxy-cyclohexa-1,4-dienes.

Each individual oligomer was also investigated by NMR spectroscopy. For trimer **111-1**, a symmetry-dependent signal splitting for the *t*-butyl and methoxy group was observed, which gave rise to an expected number of three individual singlets. For the corresponding trimeric macrocycle **38** (see *p. 29*), in contrast, only one singlet for the *t*-butyl and methoxy group is observed. Such structural subtleties could not be derived for the higher oligomers **111-2** and **111-3**, since lower diffusion coefficients led to peak-broadening.

Based on the *trans*-3,6-dimethoxycyclohexadiene moiety, we expected the formation of linear oligomers, independent of the torsion of each moiety. Therefore, DFT calculations were performed.

3.5.3. DFT studies

Geometry optimizations, using DFT calculations at the B3LYP/6-31G(d) level of theory, were conducted for trimer **111-1** (see *Figure 57*). The calculations confirmed the expected linear structure. The *trans*-configuration imposes this geometry upon the trimer. In the left image, **111-1** is depicted from a frontal view. The calculations show that the methoxy groups are within a certain radius, independent of which moiety they belong to. This confirms the linear structure on a theoretical level.

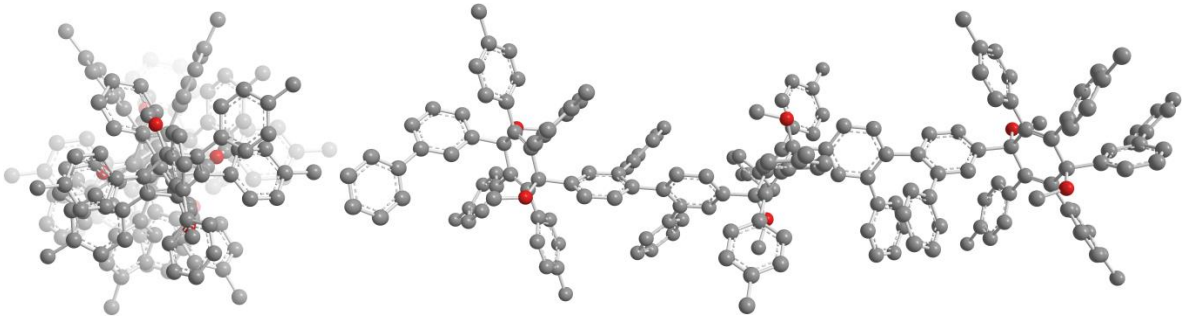

Figure 57: geometry optimization (DFT) of **111-1** calculated at the B3LYP/6-31G(d) level of theory. Frontal view (left) and side view (right). *T*-butyl groups were substituted by methyl to reduce computing time.

Based on this positive result, the structure of **111-1** was also investigated experimentally. Therefore, dynamic light scattering (DLS) studies of each indidivudal monomer were conducted to confirm their rigidity.

3.5.4. DLS studies

DLS measurements were performed in collaboration with Amelie Koch and Prof. Fytas to investigate the rigidity of oligomers **111-1**, **111-2** and **111-3**. Therefore, the trimer, hexamer and nonamer were dissolved in Et_2O and investigated by dynamic light scattering.

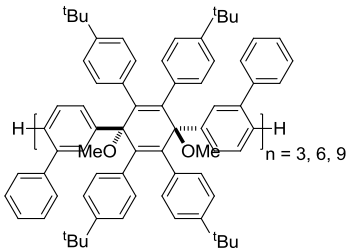

Scheme 60: oligomers **111-1**, **111-2**, and **111-3** were investigated with DLS.

Et_2O was chosen as a solvent because of its low refractive index which increases the contrast between solute and solvent. In *Figure 58*, the translational diffusion coefficients for

rods (D_{rod}, green) and prolate ellipsoids ($D_{prolate}$, brown) vs. the aspect ratio *L/d* of the structures are depicted. The theoretical values are calculated for an oligomer diameter *d* of 1.3 nm (left) and 1.5 nm (right), which is the range of the calculated width of the oligomers. The horizontal shaded regions denote the range of experimental *D* for the three oligomers **111-1**, **111-2**, and **111-3**. For d = 1.3 nm, the computed values for both rods and prolate ellipsoids are similar, and the assumed lengths of the molecules are 3.2 nm ± 0.1 nm, 6.0 ± 0.5 nm and 9.3 ± 2.5 nm for trimer ,hexamer and nonamer, respectively. These L values confirm to the ratio 1:2:3 of the three oligomers and are in agreement with theoretical calculations.

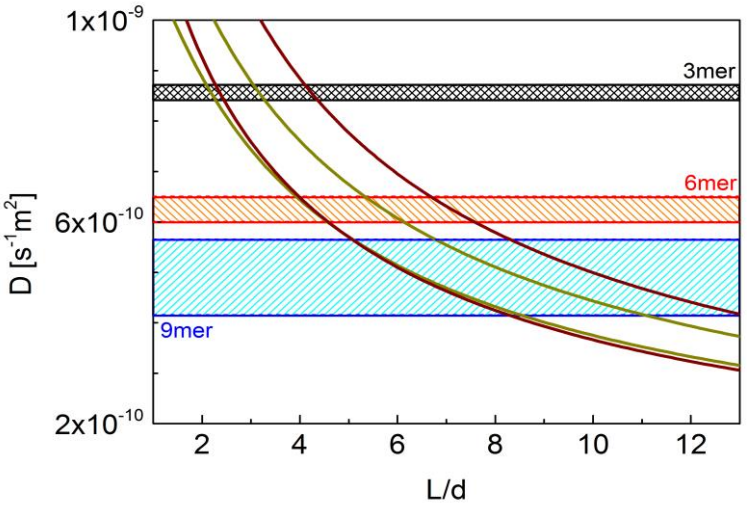

Figure 58: Translational diffusion *D* vs. aspect ratio *L/d* for cylinder with length *L* and diameter *d*. The two solid lines are theoretical predictions for d=1.3 nm (upper line) and d = 1.1 nm , whereas the horizontal shaded regions denote the range of experimental D for the oligomer solutions. For d=1.3 nm, the length assumes 3.3±0.1nm, 6.4±0.5nm and 10±2.5nm for trimer, hexamer and nonamer respectively. These L values confirm to the ratio 1:2:3.

Thus, the DLS measurements confirm the linearity of the three different oligomers, since a proportional increase in length for rod-like structures would not have been observed otherwise. Since we opted for a new synthetic approach for linear poly-*p*-phenylenes, the reductive aromatization is discussed next.

3.5.5. Linear Polyphenylenes

To develop a route for the synthesis of linear polyphenylenes, we investigated the reductive aromatization of cyclohexadiene-based oligomers (*vide supra*). The reductive aromatization had been previously employed for the preparation of various PPCs, such as **38** or **84**, by using NaNp or low valent titanium.

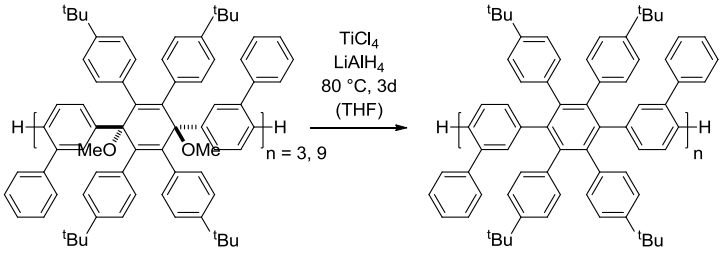

Scheme 61: reductive aromatization and expected product

Therefore, **111-1** was subjected to NaNp at – 78 °C, which gave a mixture of partially reduced cyclohexadienes moieties, which could not be separated by column chromatography or preparative TLC. Longer reaction times did not alter the product distribution. As a consequence, **111-1** was subjected to low valent titanium to yield a polyphenylene derivative of **112-1**. Surprisingly, the observed mass was 4 hydrogen atoms lower than the title mass. For the reductive aromatization of macrocycles, a lighter mass had never been observed. These unexpected findings might be due to a reductively induced dehydrogenation[201] that took place within the *in situ* formed polyphenylene **112-1**.

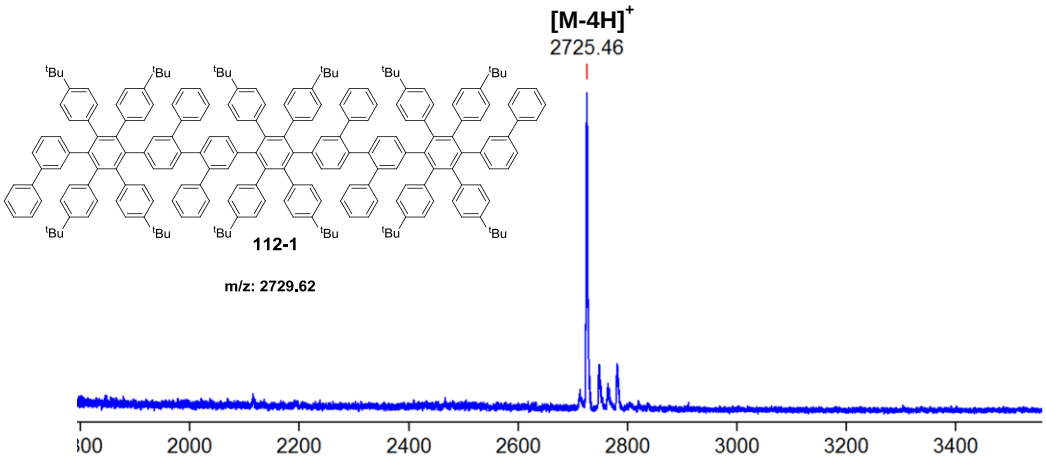

Figure 59: MALDI-MS spectrum of compound **112-1** after reductive aromatization. Besides the - 4H main product, also the corresponding $[M-4H+Na]^+$ and $[M-4H+K]^+$ are observed. In addition, minor traces of an oligomer which still contains one cyclohexadiene moiety is observed.

Similar results were obtained after reductive aromatization of nonamer **111-3**. The molecular weight of the observed structure was 10 hydrogen atoms lower than the title mass of **112-3**. The structure of the reductively aromatized polyphenylene derivative could not be elucidated.

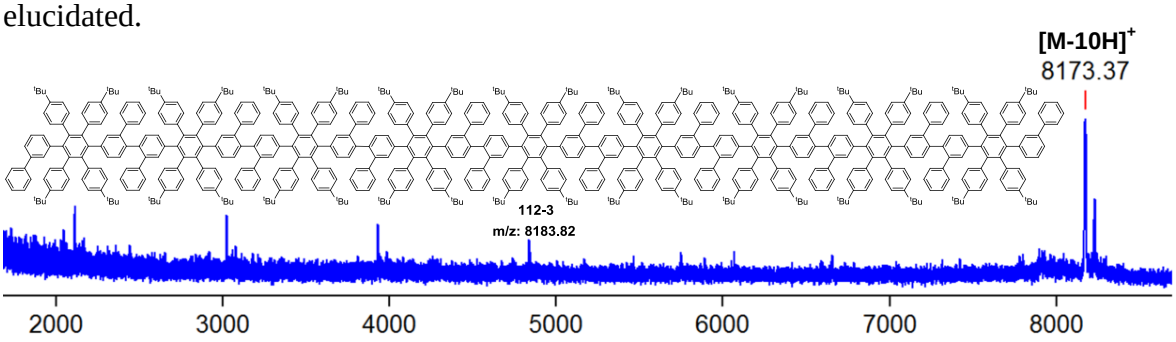

Figure 60: reductive aromatization of **111-3**. $[M-10H]^+$ its derivative with one cyclohexadiene unit is observed.

As the polyphenylenes could not be unambigiously characterized, we did not performed DLS measurements to investigate the rigidity of these structures.

3.5.6. Summary

Oligo-trans-cyclohexa-1,4-diene were synthesized to investiage their rigidity as possible precursors for polyphenylene structures. The monomer **110** was polymerized *via* an oxidative coupling to yield oligomers with up to 12 repeating units. Successful separation could be achieved up to nonamers. To investigate the stiffness of these oligomers, DLS studies were conducted in collaboration with Amelie Koch and Prof. G. Fytas at MPIP. Their measurments confirmed the ratio of 1:2:3 from trimer to nonamer, which proved their inherent linear structures. The conversion of these oligomers to polyphenylenes was not successful, as the title mass of the trimer was 4 hydrogen atoms and for the nonamer 10 hydrogen atoms lower. The structure of these polyphenylene derivatives could not be elucidated.

In summary, such cyclohexadiene precursors or possible corresponding derivatives could be of interest for self-organization on surfaces and subsequent thermal or chemical aromatization.

IV. Summary

In this work, the bottom-up synthesis of polyphenylene cylinders (PPC)s and derived congeners (see *Figure 61*) with different radial extension and connectivity patterns was investigated. Their structural motifs render them precursors of CNTs. After the successful synthesis of different PPCs, the oxidative cyclodehydrogenation was studied to give CNTs. This resulted in the formation of partially fused macrocycles. For a concise bottom-up synthesis of CNTs, however, an annulation between all phenyl and phenylene rings would have been necessary. Furthermore, the synthesis of *trans*-3,6-dimethoxy-cyclohexa-1,4-diene oligomers was achieved as precursors for the synthesis of linear poly-*p*-phenylenes. Theoretical calculations and DLS measurements confirmed the formation of stiff cyclohexadiene oligomers.

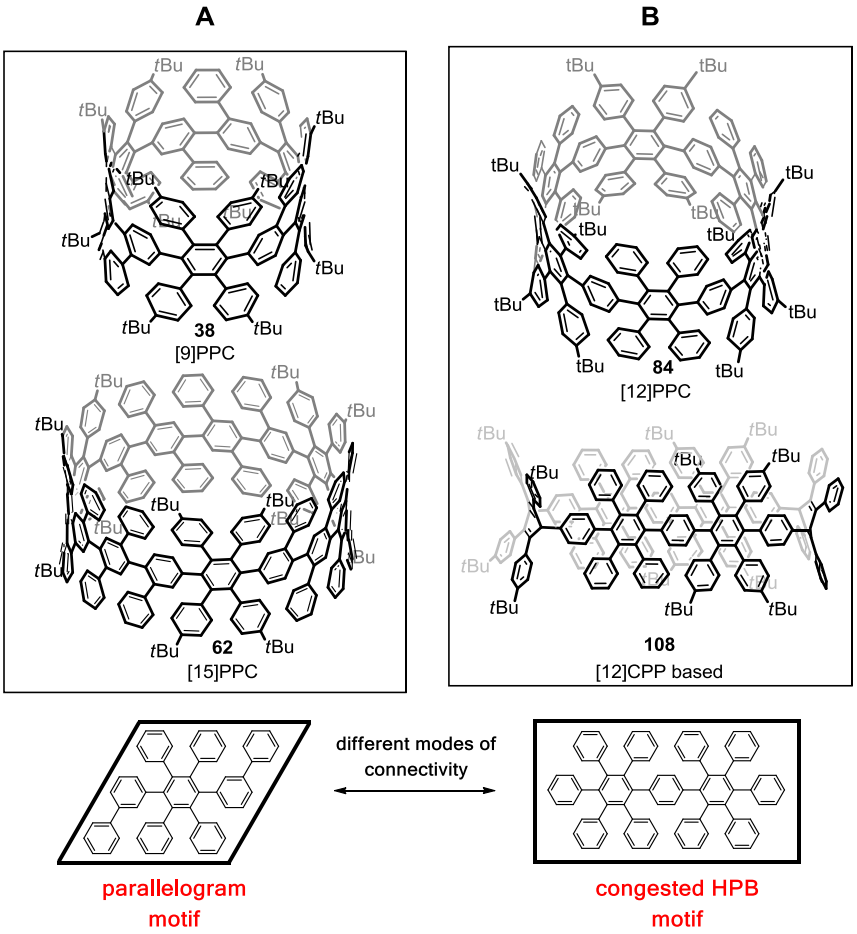

Figure 61: synthesized PPCs and their modes of connectivity.

In the first chapter, the synthesis of PPCs is presented, which are based on parallelogram-shaped subunits (see *Figure 61, left*). These compounds are structural congeners of HPBs, however, being extended by two phenyls rings each. Three different PPCs, bearing this structural motif, were synthesized: [9]PPC **38**, [15]PPC **62** und [21]PPC **68**. These CPP-derived structures were prepared from triangular macrocycles that contained 3,6-connected cyclohexadienes (see *Scheme 62*).

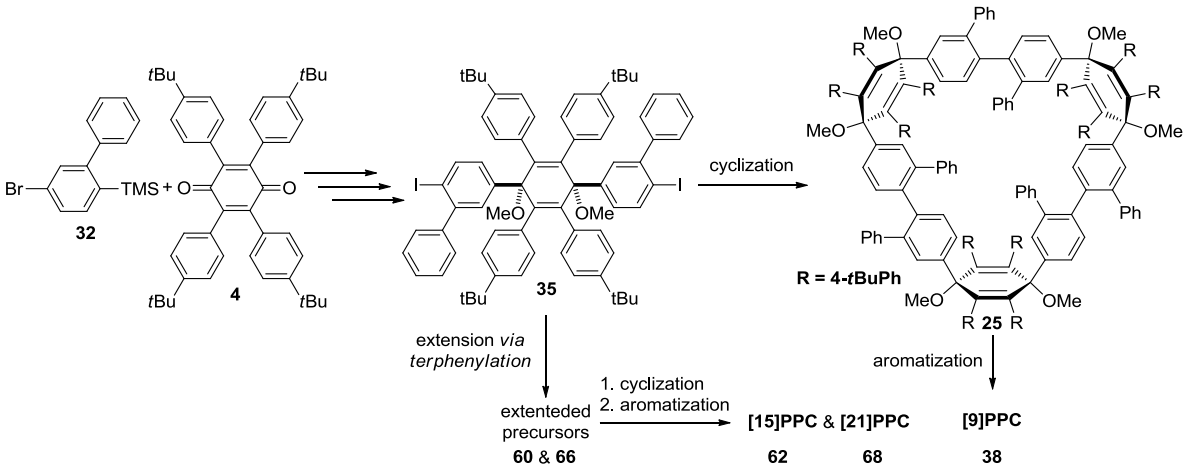

Scheme 62: Synthetic strategy for parallelogram-type PPCs.

To convert these precursors into CNTs, we investigated an intramolecular annulation *via* an oxidative cyclodehydrogenation. For [9]CPP, mass spectrometry indicated incomplete dehydrogenation, which was ascribed to the high ring strain. This was derived from the single crystal X-ray structure, where neighboring phenylene moieties exhibited dihedral angles up to 86°. Cyclodehydrogenation at elevated temperatures led to decomposition of the starting material. Therefore, we opted for a surface-mediated cyclodehydrogenation at temperature beyond 300 °C, which was conducted in collaboration with the group of Prof. Fasel at EMPA, Switzerland. The reaction progress and conversion to give the desired CNTs was followed by STM. The PPC **38** could be successfully sublimed at 600 °C and visualized by STM; at 365 °C, an intramolecular dehydrogenation on Au(111) and Pt(111) surface, however, could not be observed. The results rather hinted at an intermolecular coupling.

Larger PPCs ([15] and [21] PPC) with hence reduced ring strain were prepared to enable a smooth dehydrogenation. In order to do so, two and four terphenyl units, respectively, were coupled to the kinked building blocks. After trimerization, [15]PPC **62** and [21]PPC **68**

were obtained *via* a reductive aromatization, which was previously applied for the [9]PPC **38**. Despite radial expansion, an incomplete cyclodehydrogenation was observed for [15]PPC, pointing at an exclusive dehydrogenation of the hexaphenylbenzene cores of the macrocycles (see *Figure 62*). For **68**, no results could be obtained after cyclodehydrogenation, since MS measurements failed.

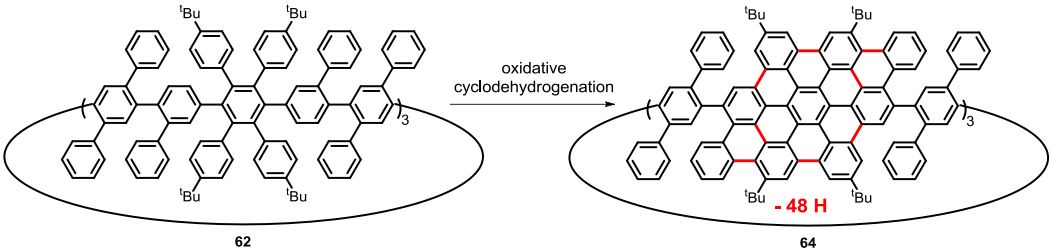

Figure 62: oxidative cyclodehydrogenation of **62** and its proposed product **64**

In the second chapter (see *Scheme 63*), we aimed at reducing the rotational freedom of the biphenyl and terphenyl moieties. Therefore, we opted for a prefusion of biphenyl and terphenyl units to give linearly fused ribbon segments. To do so, tetrachlorinated terphenyl units should be coupled with the kinked building block **35**. After cyclization, the freely rotating fragments were to be fused *via* a palladium-catalyzed *C-H* activation. The tetrachlorinated precursor **69** could be successfully synthesized. However, a coupling between these sterically demanding substrates (**35** and **69**) was not achieved, despite intense efforts. Thus, this approach was given up.

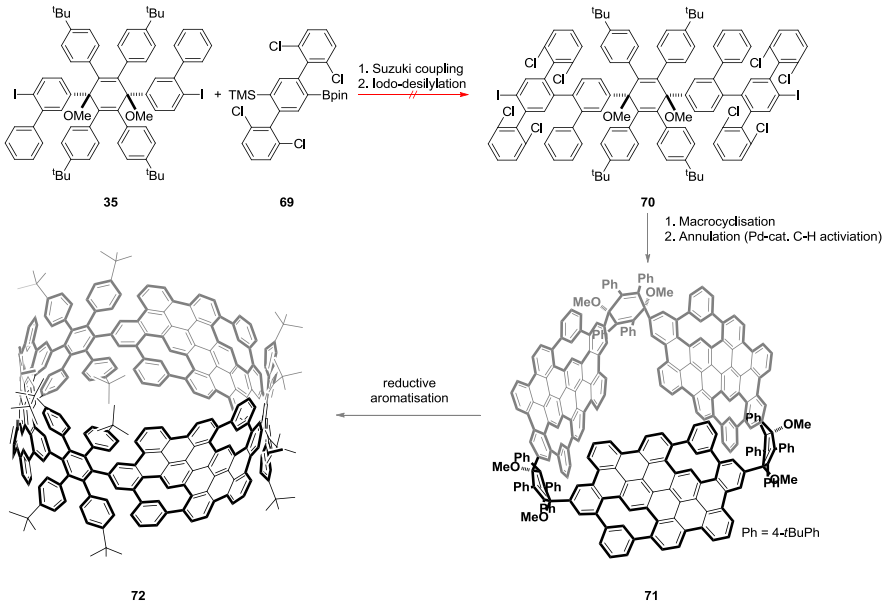

Scheme 63: synthetic approach toward perfused macrocycles which could not be realized since *Suzuki* coupling failed.

In the third chapter (see *Figure 61, route B*), a different retrosynthetic approach was pursued to avoid freely rotating biphenyls and terphenyls, reducing the overall rotational freedom. This strategy was expected to suppress the formation of defect structures during cyclodehydrogenation, giving rise to a clean CNT formation.

These macrocyclic structures are based on congested hexaphenylbenzenes, i.e., two HPBs share one phenylene moiety. A closely related structural motif was developed in our group for the synthesis of extended hexa-*peri*-benzocoronenes and linear graphene nanoribbons in 1998 and 2008.[53, 170] The difference between the previous and the here presented approach is that three kinked units need to be introduced into the precursor to enable macrocyclization. The desired [12]PPC **84** was successfully synthesized, containing the congested HPB connectivity pattern. Toward the synthesis of [12]PPC **84**, it was serendiptiously discovered that milder reductive reaction conditions lead to a beautiful C_2-symmetric macrocycle **108** that contains two kinked 3-6-connected cyclohexa-1,4-dienes (see *Scheme 64*), which was confirmed by X-ray analysis. Oxidative cyclodehydrogenation led to an unprecedented degree of bond formation, proving this structural design to be superior. Nonetheless, a concise bottom-up synthesis of CNTs could not achieved with the congested HPB approach either.

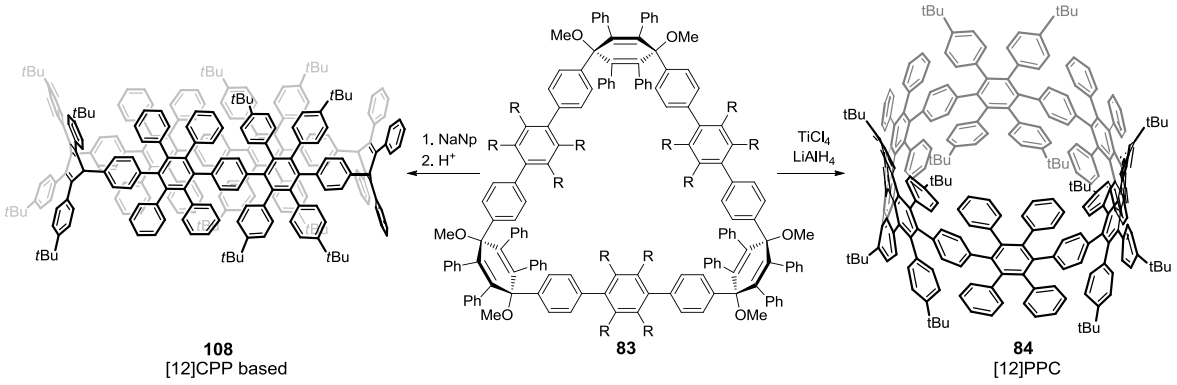

Scheme 64: Syntehsis of [12]PPC **84** and its C_2-symmetric congener **108**.

In the fourth chapter, a side product of the kinked precusor for the synthesis of **38** was used to study a new route for the preparation of linear polyphenylenes from highly soluble *trans*-kinked precursors. For the macrocycle synthesis, we exclusively opted for the *cis*-kinked 3,6-dimethoxycyclohexa-1,4-dienes. However, the synthesis of the *cis*-product also afforded its *trans*-analogon. This compound was used for an oxidative coupling to give linear oligomers (see *Scheme 65*). Their rigidity was investigated by dynamic light scattering

(DLS) and the results were supported by DFT calculations, confirming the formation of linear structures. After reductive aromatization, unexpectedly, only linear polyphenylene derivatives were obtained, as additional bond fusion occurred within the polyphenylene structure which rendered it obsolete to study their behavior in solution, since a precise structural elucidation could not be achieved.

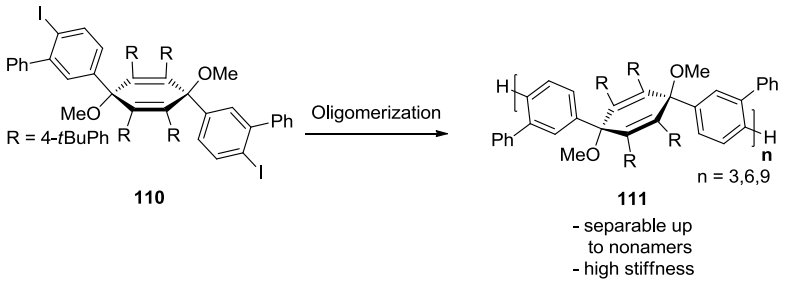

110 **111**

- separable up to nonamers
- high stiffness

Scheme 65: Preparation of 3,6-oligomerized cyclohexa-1,4-dienes.

In conclusion, we could successfully synthesize different PPCs that function as direct precursors of CNTs. However, neither the bottom-up synthesis in solution nor an on-surface approach afforded monodisperse and soluble CNT fragments. Nonetheless, the congested HPB approach proved to be superior in comparison to the parallelogram approach in terms of degree of cyclodehydrogenation. These findings can open up new ways for feature studies on concise solution-mediated syntheses of CNTs. Furthermore, we developed a new route for the synthesis of poly-*p*-phenylene precursors and confirmed their linear structurs with DLS.

V. Outlook

The "holy grail"[102, 146, 202] - a bottom-up synthesis of CNTs - still remains elusive, as it has not yet been realized, despite several attempts that have been reported in the literature. The groups of *Jasti*, *Itami*, *Isobe*, *Yamag*o and *Müllen* have developed different strategies to achieve this goal: naphthalene[111], pyrene,[106-107] chrysene[101], hexaphenylbenzene[161] and other fragments[97-100] have been embedded into CPPs. However, all of these approaches have in common, that the CPP rings are connected at more than one point by a single bond. This is due to the very high ring strain that is exerted on the fragments, making it difficult to synthesize such rings or fuse the remaining bonds.

Prompted by the synthesis of a cyclic hexpahenylbenzene trimer in our group, we tried to overcome this challenge by introducing new precursor designs and phenylene-extended macrocycles (up to [21]central rings) that resemble a CNT precursor structure. Despite our intense efforts toward this goal, a successful bottom-up synthesis was not realized.

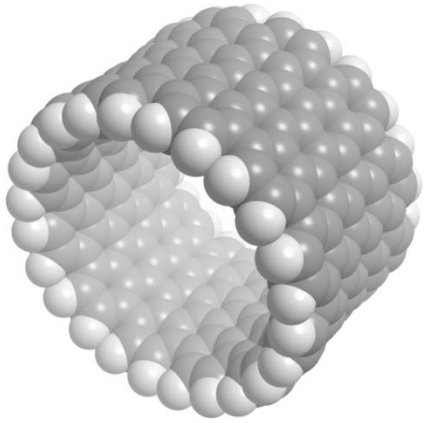

Figure 63: space-filling model of a [12,12]CNT segment. Height of the CNT equals a tetracene.

Based on the above described results, one can envision approaches with even larger macrocycles that do not exhibit such a high ring strain and thus enable smoother dehydrogynations. However, an increase of ring size makes synthesis and – especially – purification very demanding and time consuming. A possible strategy is shown in *Scheme 66* which can pave the way for a [24]PPC. The synthetic feasibility for the synthesis of a bisboronate has already been proven.

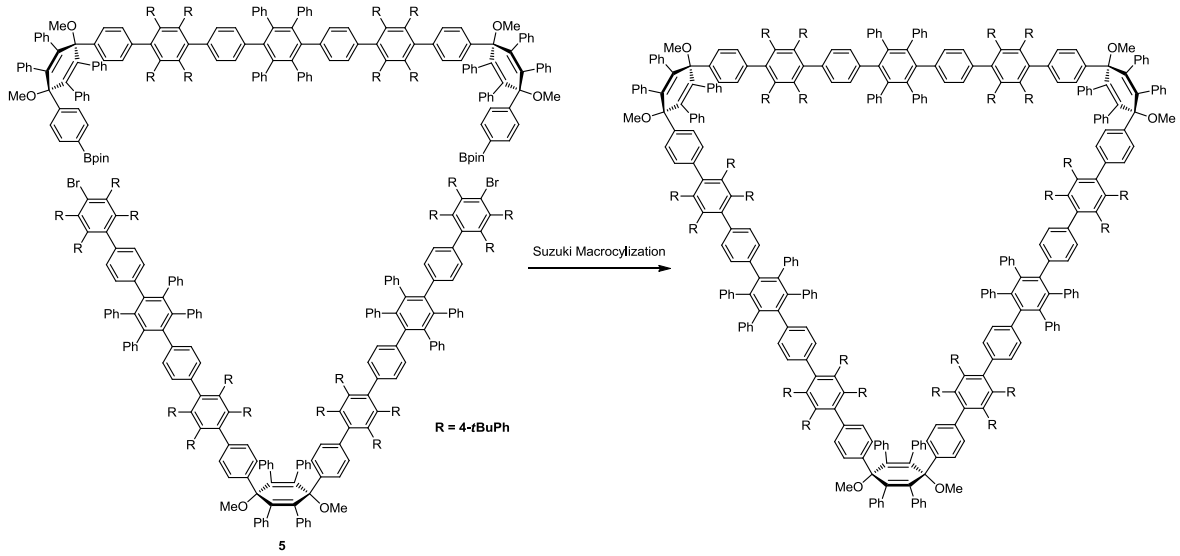

Scheme 66: a strategy to extend the [12]CPP based PPZ toward a [24]PPZ. The diboronate has been synthesized.

Another approach could be to completely redesign the molecule. In order to do so, a new retrosynthetic concept needs to be developed that takes the experiences from this project and of competing groups into consideration: *via* the oxidative cyclodehydrogenation bonds can be fused to a certain degree. However, at some point, the reaction comes to a halt and can also lead to strain induced rearrangements.[109-110] On the basis of these experimental findings, more strain needs to be exerted on the CNT precursor, in the first place, to possibly afford smooth cyclodehydrogenations. This seems to be of paramount importance. Moreover, restricted rotational freedom diminishes or can even completely suppress strain induced rearrangements. This could possibly afford cyclodehydrogenation under high ring strain, since *para*-connected phenylenes cannot be twisted out of the plane, as expected for the presented PPCs. Besides, the interconnection of CPP rings, as shown in *Figure 64*, could also enable high temperature oxidative cyclodehydrogenation using DDQ in conjunction with strong *Brønsted* and *Lewis* acids at 100 °C or even higher temperatures. In our case, DDQ led to the decomposition of the precursors, which could be due to oxidative ring opening.

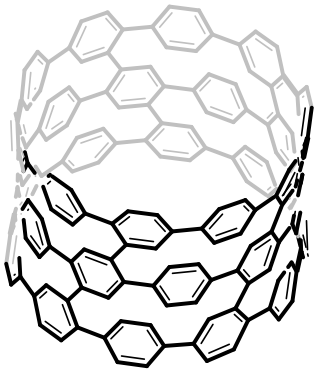

Figure 64: a possible precursor that contains three CPP rings that are interconntected by briding terphenyl units.

In *Figure 64*, a precursor structure is drawn that follows the outlined synthetic guidelines *(vide supra*): three CPP rings are interconnected by bridging terphenyl units. In this case, three strained CPP rings are present. Hence, cyclodehydrogenation would not have to overcome possible kinetic barriers, stemming from ring strain to enable C-C bond condensation. Furthermore, the restricted rotational freedom should increase the likelihood of interaction between phenyl moieties.

VI. Experimental Part

6.1 General Information

Unless otherwise stated, the commercially available reagents and dry solvents were used without further purification. The reactions were performed using standard vacuum-line and Schlenk techniques, work-up and purification of all compounds was performed under air and with reagent-grade solvents. Column chromatography was done with silica gel (particle size 0.063-0.200 mm from Macherey-Nagel) and silica coated aluminum sheets with fluorescence indicator from Macherey-Nagel were used for thin layer chromatography. Preparative thin layer chromatography was done with PLC silica gel 60, F254, 2 mm sheets on glass from Merck. Melting points were determined on a Büchi hot stage apparatus. The 1H-NMR and 13C-NMR spectra were recorded on a Bruker AVANCE 250, Bruker AVANCE 300, Bruker AVANCE 500 and Bruker AVANCE 700 spectrometer in the listed deuterated solvents. Trimethylsilane (δ 0.00 ppm) or the deuterated solvent was used as an internal standard. Solution UV-Vis absorption and emission spectra were recorded at room temperature on a Perkin-Elmer Lambda 900 spectrophotometer and J&M TIDAS spectrofluorometer. Field desorption (FD) mass spectra were obtained on a VG Instruments ZAB 2 SE-FPD. MALDITOF mass spectra were recorded on a Bruker Reflex II-TOF spectrometer using trans-2-[3-(4-tert-butylphenyl)-2-methyl-2-propenylidene]-malononitrile (DCTB; Aldrich, >99%) as matrix. High resolution MALDI mass spectrometry measurements were performed on a Solarix ESI-/MALDI-ICR (9.4T) system (Bruker Daltonics, Germany), with a SmartBeam laser II. The system was internally calibrated in positive mode using sodium trifluoroacetate (Fluka, >99%) or sodium perfluoroheptanoate (Fluka, >99%) on quadratic calibration mode. A total of 10-400 shots were accumulated for each mass spectrum. The results were calculated using Data Analysis software (Bruker Daltonics, Germany). High-performance liquid chromatography (HPLC) was performed on a HPLC facility from Agilent, pump series 1100, with a photo detector series 1200 (wavelength of 380 nm) using a column from Macherey-Nagel (MN HD18 125/4 mm; 5 μm grain-size).

6.1.1. 2D NMR experiments

^{1}H-NMR (700 MHz) and ^{13}C-NMR (176 MHz) measurements were executed on Bruker Avance III 700 NMR spectrometers with a 5 mm QXI probe endowed with a z-gradient. The spectra were received with π/2-pulse lengths of 13.8 μs (^{1}H) and 16 μs (^{13}C) and a sweep width of 10500 Hz (15 ppm) for ^{1}H and 35000 Hz (200 ppm) for ^{13}C. A relaxation delay of 2s was used for both nuclei. The temperature was held at 298.3 K and calibrated with a standard ^{1}H methanol NMR sample. The control of the temperature was realized with a VTU (variable temperature unit) and an accuracy of +/- 0.1K, which was checked with the standard Bruker Topspin 3.2 software. A standard proton spectrum was recorded with 1024 transients. The 2D ^{1}H,^{13}C-HSQC (heteronuclear single quantum correlations via double inept transfer and phase sensitive using Echo/Antiecho-TPPI gradient selection with decoupling during acquisition) experiment was run with 4096 points in f2 and 512 points in f1 dimension and an averaged ^{1}J-CH coupling constant of 145Hz. Before Fourier transformation, the data were zero filled to 1024 points in f1 and multiplied by a window function (q-sine bell or sine bell) in both dimensions. The assignment of the protons was realized with a 2D-^{1}H,^{1}H NOESY (nuclear overhauser enhancement spectroscopy) and 2D-^{1}H,^{1}H COSY. The used mixing time in this experiment was kept at 250 ms. The spectroscopic widths of the homo-nuclear 2D COSY and NOESY experiments were typically 10000 Hz in both dimensions (f1 and f2) and the relaxation delay was 1.3s.

6.2 Synthesis

6.2.1. 4,4''-di-tert-butyl-4',5'-bis(4-(tert-butyl)phenyl)-[1,1':2',1''-terphenyl]-3',6'-dione (**4**)[135]

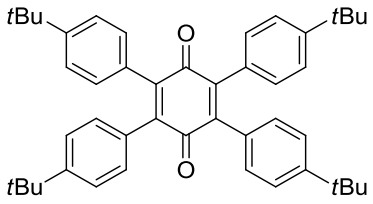

4

$C_{46}H_{52}O_2$
m.w.: 636.90 g/mol

p-bromanil (10 g, 23.6 mmol, 1 eq.) und 4-*t*butylphenylboronic acid (25.2 g, 141.6 mmol, 6 eq.) and $Pd(PPh_3)_4$ (2.7 g, 2.36 mmol, 0.1 eq.) were dissolved in THF (250 mL). After addition of aq. K_2CO_3 (130 g, 944 mmol, 40 eq.) (8 M), the reaction mixture was degassed (3x) and refluxed for 36 h. The reaction mixture was extracted with Et_2O (3x) and washed with water (3x) and brine (3x). The combined fractions were dried over Na_2SO_4 and the solvent was removed until complete dryness. The crude product was purified by column chromatography (Hex/DCM 8:2 →7:3 Hex/DCM) to give the title compound **4** (6.65 g, 10.4 mmol, 44%).

^{1}H NMR (300 MHz, CD_2Cl_2): δ [ppm] = 7.26 (d, ^3J = 8.6 Hz, 8H), 7.02 (d, J = 8.6 Hz, 8H), 1.29 (d, ^3J = 5.4 Hz, 36H).

^{13}C NMR (75.5 MHz, CD_2Cl_2): δ [ppm] = δ 187.64, 151.67, 143.50, 130.89, 124.80, 34.89 (CCH$_3$), 31.33 (CH$_3$).*

*one peak missing due to isochrony.

MS (FD, 8 kV) (m/z): obsvd. for $[M]^+$: 636.2. (calcd. 636.4).

Analytical Data in accordance with literature.[135]

6.2.2. Synthesis of 4-bromo-3-iodobenzoic acid (**12**)[203]

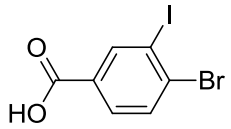

12

$C_7H_4BrIO_2$
m.w.: 326.91 g/mol

I_2 (5.52 g, 21.7 mmol) and then $NaIO_4$ (1.55g, 7.23 mmol) were added portionwise to H_2SO_2 (140 mL, 95%) under stirring. After 30 min at r.t. a dark brown iodinating solution was obtained containing ca. 49 mmol (1.1 equiv) of the I^+-intermediate. 4-bromobenzoic acid (10 g, 50 mmol, 1 equiv) was added in one portion to the iodinating solution containing the I^+-intermediate and the resulting solution was stirred for 1 h at 25–30 °C. Then the reaction mixture was slowly poured into stirred ice water (300 g). The crude products were collected by filtration, washed with cold water, dried preliminarily on a the sintered-glass filter by suction, then air-dried in the dark, and recrystallized from DCM (150 mL) to give **12** (11.4 g, 35.0 mmol, 70%).

^{1}H NMR (300 MHz, DMSO): δ [ppm] = 8.36 (d, *J* = 1.6 Hz, 1H), 7.83 (s, 1H), 7.82 (d, *J* = 1.8 Hz, 1H).

^{13}C NMR (75 MHz, DMSO): δ [ppm] = 165.48, 140.47, 133.97, 132.91, 131.79, 130.38, 102.21.

MS (FD, 8 kV) (m/z): obsvd. for $[M]^+$: 327.1. (calcd. 325.8).

Elemental Analysis for $C_7H_4BrIO_2$: meas. C, 25.23 (calcd. C, 25.72), H, 0.28 (H, 1.23).

Mp: 225 °C.

6.2.3. 4-bromo-3-iodoaniline (**14**)

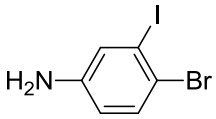

14

C_6H_5BrIN
MW: 297,92 g/mol

4-Bromo-3-iodobenzoic acid (1.20 g, 3.67 mmol, 1 eq.) (**12**), diphenylphosphoryl azide (1.21 g, 4.40 mmol, 1.2 eq.) and dry triethylamine (0.82 g, 1.13 mL, 8.07 mmol, 2.2 eq.) are dissolved in dry *t*-BuOH (60 mL) under argon and the reaction mixture is refluxed for 5 h. After that, the solvent is removed until complete dryness and the reaction mixture is purified by column chromatrography (hexane/DCM → 4:1) to give 1.35 (92%) of the crude carbamate. Without, further chracterisation, the crude product is dissolved in 25 mL of DCM and a mixture of TFA/DCM (7.5 mL/25 mL) is dropwise added and stirred overnight. The reaction mixture is washed with 1 M HCl (3x). Then, NaOH is added to the aq. phase until pH 9 is reached. The aq. phase is extracted with DCM (3x) and the combined fractions were dried over $MgSO_4$. The solvent is removed *in vacuo* to give **14** (0.91 g, 90%).

^{1}H NMR (300 MHz, $CDCl_3$): δ [ppm] 7.32 (d, *J* = 8.6 Hz, 1H), 7.20 (d, *J* = 2.7 Hz, 1H), 6.52 (dd, *J* = 8.5, 2.7 Hz, 1H), 3.67 (s, 2H).

^{13}C NMR (75 MHz, $CDCl_3$): δ [ppm] 146.41, 132.77, 126.22, 117.31, 116.63, 101.50.

MS (FD, 8 kV) (m/z): obsvd. for [M^+]: 296.6 (calcd. 296.9).

Elemental Analysis for $C_{12}H_{10}BrN$: meas. C, 24.32% (calcd. C, 24.19); H, 1.51 (H, 1.69), N, 4.89 (N, 4.70).

Mp: 32 °C.

6.2.4. Synthesis of 6-bromo-[1,1'-biphenyl]-3-amine (**15**)

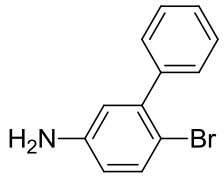

15

$C_{12}H_{10}BrN$
m.w.: 248.12 g/mol

14 (3.66 g, 12.3 mmol, 1 eq.), phenylboronic acid (2.24 g, 18.4 mmol, 1.5 eq.) and $Pd(PPh_3)_4$ (0.28 g, 0.25 mmol, 2 mol%) were dissolved in toluene. After addition of 2M K_2CO_3 in EtOH (32 mL), the reaction was degassed and heated to 80 °C for 2d. The reaction mixture was extracted with DCM (3x) and washed with Brine (3x). The combined

fractions were dried over $MgSO_4$ and purified by column chromatography (Hex/DCM 7:3) to afford **15** (2.38 g, 9.60 mmol, 78%).

^{1}H NMR (300 MHz, CD_2Cl_2): δ [ppm] = 7.40 (m, 6H), 6.66 (d, J= 2.7 Hz, 1H), 6.55 (dd, 2.7,8.7 Hz, 1H), 3.71 (s, 2H).

MS (FD, 8 kV) (m/z): obsvd. for [M^+]: 247.1.(calcd. 247.0).

Elemental Analysis for $C_{12}H_{10}BrN$: meas. C, 58.15% (calcd. C, 58.09%); H, 4.09% (H, 4.06%). N, 5.45% (N, 5.65%).

Mp: 51 °C.

6.2.5. Synthesis of 2-bromo-5-iodo-1,1'-biphenyl (**16**)[138-139]

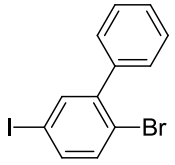

16

$C_{12}H_8BrI$

m.w.: 359.00 g/mol

p-TsOH·H_2O (4.19 g, 22.0 mmol, 3 eq.) is dissolved in MeCN (30 mL). After addition of the amine **15** (1.82 g, 7.34 mmol, 1 eq.), the solution was cooled to 10 °C and a mixture of KI (3.05 g, 18.4 mmol, 2.5 eq.) and $NaNO_2$ (1.01 g, 14.7 mmol, 2 eq.) in water (6 mL) was added dropwise. The reaction mixture was neutralized with an aq. $NaHCO_3$. The crude product was then washed with $Na_2S_2O_3$ and brine (3x). The combined organic fraction were dried over $MgSO_4$ and dried *in vacuo*. The crude product was purified by column chromatography (hexane) to give **16** (2.35 g, 89%) as a white solid.

^{1}H NMR (300 MHz, CD_2Cl_2): δ [ppm] = 7.68 (d, *J* = 2.2 Hz, 1H), 7.55 – 7.35 (m, 7H).

^{13}C NMR (75 MHz, $CDCl_3$) δ [ppm] = 144.74, 139.94, 139.78, 137.70, 134.76, 129.30, 128.23, 128.18, 122.68, 92.47.

MS (FD, 8 kV) (m/z): obsvd. for [M^+]: 357.4, (calcd. 357.9).

Elemental Analysis for $C_{12}H_8BrI$: meas. C, 40.27 (calcd. C, 40.95); H, 1.25 (H, 2.25).

Mp: 48 °C.

6.2.6. Synthesis of 3-bromo-4-chloroaniline (**20**)

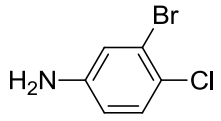

20

C_6H_5BrClN
m.w.: 206.47 g/mol

3-Bromo-4-chlorbenzoic acid (4.00 g, 17.0 mmol, 1. eq.) (**19**), diphenylphosphoryl azide (5.61 g, 20.4 mmol, 1.2 eq.) and dry triethylamine (5.2 mL, 37.4 mmol, 2.2 eq.) wis dissolved in dry *t*-BuOH (200 mL) under argon and the reaction mixture is refluxed for 5 h. After that, the solvent is removed until complete dryness and the reaction mixture is purified by column chromatrography (hexane/DCM 8:2 → hexane/DCM 5:5) 4.57 g (87%) of the crude carbamate. Without, further chracterization, the crude product is dissolved in 80 mL of DCM and a mixture of TFA/DCM (25 mL/80 mL) is dropwise added and stirred overnight. The reaction mixture is washed with 1 M HCl (3x). Then, NaOH is added to the aq. phase until pH 9 is reached. The aq. phase was extracted with DCM (3x) and the combined fractions were dried over $MgSO_4$. The solvent is removed *in vacuo* to give **20** (2.74 g, 89%).

^{1}H NMR (300 MHz, CD_2Cl_2) δ [ppm] = 7.18 (d, *J* = 8.6 Hz, 1H), 6.95 (d, *J* = 2.7 Hz, 1H), 6.58 (dd, *J* = 8.6, 2.7 Hz, 1H), 3.81 (s, 2H).

^{13}C NMR (75 MHz, CD_2Cl_2) δ [ppm] = 147.13, 131.01, 122.81, 122.74, 119.81, 115.75.

MS (FD, 8 kV) (m/z): obsvd. for C_6H_5BrClN [M^+]: 207.1 (calcd. 206.9).

Elemental Analysis for $C_{12}H_{10}BrN$: meas. C, 35.23(calcd. C, 34.90), H, 2.24 (H, 2.44), N, 6.65 (N, 6.78).

Mp: liquid at r.t.

6.2.7. Synthesis of 6-chloro-[1,1'-biphenyl]-3-amine (**21**)

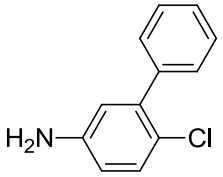

21
$C_{12}H_{10}ClN$
m.w.: 203,67 g/mol

3-Bromo-4-chloroaniline (**20**) (1.55 g, 7.5mmol, 1 eq), phenylboronic acid (1.37 g, 11.3 mmol, 1,5 eq.), $Pd(PPh_3)_4$ (0.17 g, 0.15 mmol, 2 mol%) and a solution of K_2CO_3 (11.3 mL, 2 M) in EtOH were put into a Schlenk flask. After addition of toluene (22.5 mL) and degassing, the reaction is heated to 80 °C for 2 d. The crude product is exctracted with DCM (3x) and the combined fraction were dried over $MgSO_4$. Column chromatography (hexane/DCM 1:1) afforded **21** as a white solid (1.25 g, 6.2 mmol, 82%).

^{1}H NMR (300 MHz, CD_2Cl_2) δ [ppm] = 7.75 – 7.19 (m, 3H), 7.21 (d, *J* = 8.4 Hz, 1H), 6.63 (dt, *J* = 8.4, 2.7 Hz, 1H), 3.78 (s, 1H).

^{13}C NMR (75 MHz, CD_2Cl_2) δ [ppm] = 146.09, 141.36, 140.16, 130.75, 129.70, 128.35, 127.87, 121.29, 117.93, 115.51.

MS (FD, 8 kV) (m/z): obsvd. for [M^+]: 202.1 (calcd. 203.1).

Elemental Analysis for $C_{12}H_{10}BrN$: meas. C, 71.43 (calcd. C, 70.77); H, 5.11 (H 4.95), N 6.49 (N, 6.88).

6.2.8. Synthesis of 2-chloro-5-iodo-1,1'-biphenyl (**22**)

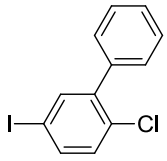

22
$C_{12}H_8ClI$
m.w.: 314.55 g/mol

p-TsOH·H_2O (3.55 g, 18.7 mmol, 3 eq.) was dissolved and MeCN (20 mL). After addition of amine **21**(1.26 g, 6.22 mmol, 1 eq.), the solution was cooled to 10 °C and a mixture of KI

(2.58 g, 15.6 mmol, 2.5 eq.) and $NaNO_2$ (0.86 g, 12.4 mmol, 2 eq.) in water (4 mL) was added dropwise. The reaction mixture was neutralized with an aq. $NaHCO_3$. The crude product was then washed with $Na_2S_2O_3$ and brine (3x). The combined organic fractions were drived over $MgSO_4$ and the solvent was removed until complete dryness. The crude product was purified by column chromatography (hexane) to give **22** (1.58 g, 5.02 mmol,81%) as a white solid

^{1}H NMR (300 MHz, CD_2Cl_2) δ [ppm] = 7.71 (d, *J* = 2.2 Hz, 1H), 7.62 (dd, *J* = 8.4, 2.2 Hz, 1H), 7.42 (qd, *J* = 4.6, 2.9 Hz, 5H), 7.22 (d, *J* = 8.4 Hz, 1H).

^{13}C NMR (75 MHz, CD_2Cl_2) δ [ppm] = ^{1}H NMR (300 MHz, $CDCl_3$) δ 142.9, 140.4, 138.4, 137.9, 132.9, 131.9, 129.7, 128.6, 128.5, 91.8.

MS (FD, 8 kV) (m/z): obsvd. for [M^+]: 314.3 (calcd. 313.9).

Elemental Analysis for $C_{12}H_{10}BrN$: meas. C, 46.42 (calcd. C, 45.82); H, 2.37 (H, 2.56%).

Mp: 42 °C.

6.2.9. Synthesis of (1''s,4''s)-2'',3'',5'',6''-tetrakis(4-(tert-butyl)phenyl)-4''',6'-dichloro-1'',4''-dihydro-[1,1':3',1'':4'',1''':3''',1''''-quinquephenyl]-1'',4''-diol (**23**)

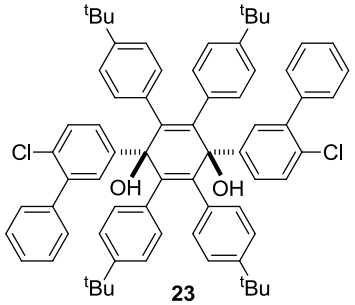

23

$C_{70}H_{70}Cl_2O_2$
m.w.: 1014.21 g/mol

2-chloro-5-iodo-1,1'-biphenyl (**22**) (5.35 g, 16.9 mmol, 4.9 eq.) was dissolved in Et_2O (200 mL) and cooled down to – 78 °C. After addition of *n*-BuLi, the reaction mixture was stirred for 30 min. Then a precooled solution of 2,3,5,6-*tetrakis*(4-*t*butylphenyl)benzodiquinon **4** (2.2 g, 3.5 mmol, 1 eq.) in Et_2O (250 mL) was slowly added. The reaction was stirred for 1 h, warmed to r.t. and stirred overnight. The crude product was purified by column chromatography (6:4 dichloromethane/hexane → dichloromethane) to give **23** (1.5 g, 14.8 mmol, 42%) as a white solid.

^{1}H NMR (300 MHz, CD_2Cl_2): δ [ppm] = 7.45 (d, *J* = 6.6 Hz, 2H), 7.30 – 7.20 (m, 8H), 7.05 (dd, *J* = 6.7, 2.9 Hz, 6H), 6.89 (d, *J* = 8.5 Hz, 8H), 6.67 (d, *J* = 8.3 Hz, 8H), 2.45 (s, 2H), 1.05 (s, 36H).
^{13}C NMR (75 MHz, CD_2Cl_2) δ [ppm] = 149.68, 142.21, 141.02, 135.64, 134.66, 131.73, 131.65, 129.66, 128.24, 127.93, 127.81, 124.13, 118.14, 100.43, 75.41, 34.52, 31.26.*
*two peaks not detected due to isochrony.

MS (FD,8 kV) (m/z): obsvd. for $C_{70}H_{70}Cl_2O$ [M^+]: 1012.7 (calcd.1012.5).

Elemental Analysis for $C_{70}H_{70}Cl_2O_2$: could not be measured due to instability of the compound

Mp: not determined due to decomposition of the compound above 40 °C.

6.2.10. Synthesis of (1''s,4''s)-2'',3'',5'',6''-tetrakis(4-(tert-butyl)phenyl)-4''',6'-dichloro-1'',4''-dimethoxy-1'',4''-dihydro-1,1':3',1'':4'',1''':3''',1''''-quinquephenyl (**23**)

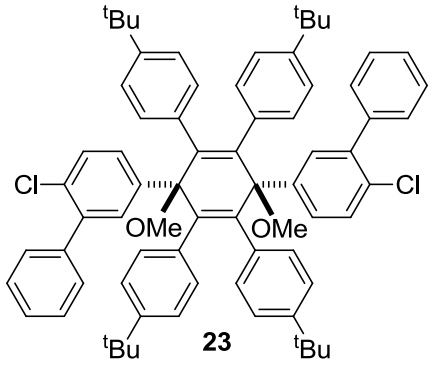

23

$C_{72}H_{74}Cl_2O_2$
m.w.: 1042.26 g/mol

23 (1.5 g, 1.48 mmol, 1 eq.) was dissolved in THF (8 mL) and cooled to 0 °C. After 30 min, NaH (60% mineral oil) (0. 27 g, 4.43 mmol, 3 eq.) was added and the solution was stirred for another 30 min until MeI (0.55 mL, 8.87 mmol, 6 eq.) was added. After 2 h, first methanol and then water was added and the reaction mixture was extracted with Et_2O (3x). The combined organic fractions were dried over $MgSO_4$. The crude product was purified by column chromatography to give **19** (1.25 g, 1.20 mmol, 81%) as a white solid.

^{1}H NMR (300 MHz, CD_2Cl_2): δ [ppm] 7.31 (s, 1H), 6.92 (d, *J* = 8.5 Hz, 1H), 6.68 (d, *J* = 6.9 Hz, 1H), 3.87 (s, 1H), 1.14 (s, 36 H).

^{13}C NMR (75 MHz, CD_2Cl_2) δ [ppm] = 149.63, 143.21, 142.32, 135.95, 131.37, 131.11, 129.76, 128.21, 127.90, 124.06, 81.48, 34.49, 31.27.

MS (MALDI) (m/z): obsvd. for [M^+]: 1040.9 (calcd. 1040.5).

Elemental Analysis for $C_{12}H_{10}BrN$: meas. C, 82.53 (calcd. C, 82.97), H, 7.51 (H, 7.16).

Mp: 245 °C.

6.2.11. Synthesis of 5-bromo-[1,1'-biphenyl]-2-amine (**30**)[204]

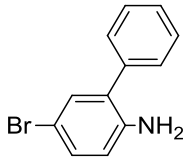

30

$C_{12}H_{10}BrN$
m.w.: 248.12 g/mol

2-Aminobiphenyl (**29**) (20 g, 118 mmol, 1 eq.), ammonium bromide (12.7 g, 130 mmol, 1.1 eq.) and glacial acetic acid (240 mL) were put into a Schlenk flask and H_2O_2 (35 wt%) (4.42 g, 11.2 mL) was slowly added. The reaction was stirred overnight at r.t. and then cooled down to 0 °C. The reaction mixture was slowly neutralized with a saturated solution of NaOH. The reaction mixture was extracted with Et_2O (3 x, 150 mL) and the combined organic fractions were dried over $MgSO_4$. After evaporation, the crude mixture was purified by column chromatography (hexane → hexane/DCM 6:4), yielding **30** (19.6 g, 67%) as a brownish solid.

^{1}H NMR (300 MHz, CD_2Cl_2): δ [ppm] = 7.51 – 7.34 (m, 5H), 7.28 – 7.17 (m, 2H), 6.71 – 6.62 (m, 1H), 3.83 (s, 2H) ppm.

^{13}C NMR (75.5 MHz, CD_2Cl_2): δ 143.43, 138.64, 133.04, 131.35, 129.69, 129.35, 129.24, 128.04, 117.37, 110.07 ppm.

MS (MALDI) (m/z): obsvd. for $C_{12}G_{10}BrN$ [M^+]: 246.6 (calcd. 247.0).

Elemental Analysis for $C_{12}H_{10}BrN$: meas. C, 58.15% (calcd. C, 58.09); H, 4.09 (H, 4.06); N 5.45 (N, 5.65).

Mp: 55 °C.

6.2.12. Synthesis of 2-bromo-5-iodo-1,1'-biphenyl (**31**)

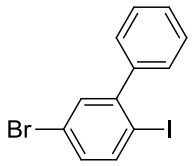

31

$C_{12}H_8BrI$
m.w.: 359.00 g/mol

p-TsOH·H_2O (4.19 g, 22.02 mmol, 3 eq.) was dissolved in MeCN (30 mL), using a large stirring bar. After addition of **30** (1.82 g, 7.34 mmol, 1 eq.), the reaction mixture was cooled down to 10 °C and an aq. solution (6 mL) of $NaNO_2$ (1.01 g, 14.7 mmol, 2 eq.) and KI (3.05 g, 18.4 mmol, 2.5 eq.) was added over 30 min. After 30 min, the reaction was warmed to r.t. and stirred for another 1 h. The reaction solution was extracted with dichloromethane (3 x 10 mL), washed with $NaHCO_3$ (3x), $Na_2S_2O_3$, and then with brine. The reaction mixture was dried over $MgSO_4$ and the solvent was removed *in vacuo*. The crude product was purified by column chromatography (hexane) to give **31** (2.35 g, 89%) as a white solid.

^{1}H NMR (300 MHz, CD_2Cl_2): δ [ppm]: 7.82 (dd, *J* = 8.4, 1.1 Hz, 1H), 7.55 – 7.39 (m, 4H), 7.38 – 7.28 (m, 2H), 7.20 (d, *J* = 8.4 Hz, 1H).

^{13}C NMR (75.5 MHz, CD_2Cl_2): δ [ppm]: 148.90, 143.38, 141.19, 133.26, 132.22, 129.49, 128.50, 122.74, 96.96.

Elemental Analysis for $C_{12}H_8BrI$: meas. C, 39.91 (calcd. C, 40.15), H, 2.32 (H, 2.25).

MS (FD, 8 kV) (*m/z*): obsvd. for $C_{12}H_8BrI$ [M^+]: 357.5 (calcd. 357.9).

Mp: 50 °C.

6.2.13. Synthesis of (5-bromo-[1,1'-biphenyl]-2-yl)trimethylsilane (**32**)

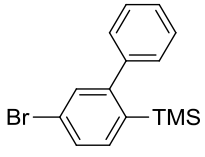

32

$C_{15}H_{17}BrSi$
m.w.: 305.28 g/mol

31 (10 g, 27.9 mmol, 1 eq.) was dissolved in THF (300 mL) and the solution was cooled down to -78 °C. After addition of *n*-BuLi (17.4 mL, 27.8 mmol, 1 eq.), the reaction was stirred for 30 min, quenched with TMSCl (3.5 mL, 27.8 mmol, 1 eq.) and stirred overnight at r.t.. The reaction mixture was extracted with Et_2O (3x), washed with water, brine and dried over $MgSO_4$. The crude product was purified by column chromatography (hexane) to give **32** (7.8 g, 25.5 mmol,92%) as a white solid.

^{1}H NMR (300 MHz, CD_2Cl_2) δ [ppm] = 7.49 (d, *J* = 1.2 Hz, 2H), 7.43 – 7.34 (m, 4H), 7.30 – 7.22 (m, 2H), -0.02 (s, 9H).

^{13}C NMR (75.5 MHz, CD_2Cl_2) δ [ppm] = 151.62, 143.50, 138.06, 136.72, 132.63, 129.67, 129.61, 128.25, 127.94, 123.26, 0.54.

MS (FD, 8 kV) (*m/z*): obsvd. for $C_{15}H_{17}BrSi$ [M^+] = 306.2 (calcd. 306.0).

Elemental analysis for $C_{15}H_{17}BrSi$: meas. C, 58.37% (calcd. C, 59.01%); H, 6.04 (H, 5.61).

Mp: 47 °C.

6.2.14. Synthesis of (1''s,4''s)-2'',3'',5'',6''-tetrakis(4-(tert-butyl)phenyl)-4''',6'-bis(trimethylsilyl)-1'',4''-dihydro-[1,1':3',1'':4'',1''':3''',1''''-quinquephenyl]-1'',4''-diol (**33**)

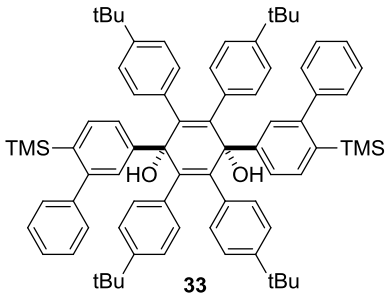

33

$C_{76}H_{88}O_2Si_2$
m.w.: 1089.68 g/mol

32 (3.4 g, 11.1 mmol, 4.8 eq.) was dissolved in THF (50 mL) and cooled down to – 78 °C. After addition of *n*-BuLi, the reaction mixture was stirred for 30 min. Then a precooled solution of 2,3,5,6-*Tetrakis*(4-*t*butylphenyl)benzodiquinone[3] (**4**) (1.5 g, 2.30 mmol, 1 eq.) in THF (9 mL) was slowly added. The reaction was stirred for 1 h, warmed to r.t. and stirred overnight. The crude product was purified by column chromatography (6:4 dichloromethane/hexane → dichloromethane) to give **33** (1.1 g, 1.01 mmol, 44%) as a white solid.

^{1}H NMR (300 MHz, CD_2Cl_2) δ [ppm] = 7.57 (d, *J* = 7.3 Hz, 2H), 7.47 (d, 2H), 7.33 – 7.24 (m, 6H), 7.11 – 6.97 (m, 6H), 6.92 (d, *J* = 8.5 Hz, 8H), 6.70 (d, *J* = 8.4 Hz, 8H), 2.60 (s, 1H), 1.12 (s, 36H), 0.00 (s, 18H)

^{13}C NMR (75.5 MHz, CD_2Cl_2) δ [ppm]: 149.26, 148.95, 144.94, 143.45, 141.04, 137.39, 135.23, 134.26, 131.76, 129.71, 129.26, 127.85, 127.25, 125.53, 123.84, 75.73, 34.46, 31.27, 0.76.

HR-MS (MALDI) (*m/z*): obsd. for $C_{78}H_{88}O_2Si_2$ [M^+]: found 1088.6323 (calcd. 1088.6317)

Elemental Analysis for $C_{78}H_{88}O_2Si_2$: compound not stable.

Mp: > 40 °C (decomposition).

6.2.15. Synthesis of ((1''s,4''s)-2'',3'',5'',6''-tetrakis(4-(tert-butyl)phenyl)-1'',4''-dimethoxy-1'',4''-dihydro-[1,1':3',1'':4'',1''':3''',1''''-quinquephenyl]-4''',6'-diyl)bis(trimethylsilane) (**34**)

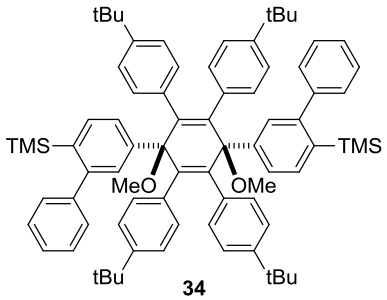

34

$C_{78}H_{92}O_2Si_2$
m.w.: 1117.73 g/mol

33 (1.1 g, 1.01 mmol, 1 eq.) was dissolved in THF (10 mL) and cooled to 0 °C. After 30 min, NaH (60% mineral oil) (0.18 g, 3.03 mmol, 3 eq.) was added and the solution was stirred for another 30 min until MeI (0.38 mL, 6.06 mmol, 6 eq.) was added. After 2 h, first methanol and then water was added and the reaction mixture was extracted with Et_2O (3 x). The combined organic fractions were dried over $MgSO_4$. The crude product was purified by column chromatography to give **34** (1.08 g, 0.97 mmol, 95%) as a white solid.

^{1}H NMR (500 MHz, $C_2D_2Cl_4$, 373 K) δ [ppm] = 7.68 (s, 2H), 7.46 – 7.25 (m, 10H), 7.07 (s, 4H), 6.87 (d, *J*=8.5, 8H), 6.71 (d, *J*=8.4, 8H), 3.92 (s, 6H), 1.18 (s, 36H), 0.03 (s, 18H).

^{13}C NMR (126 MHz, $C_2D_2Cl_4$) δ [ppm] =148.40, 147.95, 144.81, 143.13, 142.54, 136.00, 135.89, 133.13, 131.00, 129.35, 127.12, 126.51, 125.45, 122.94, 81.55, 73.80, 52.01, 33.82, 30.97, 0.57.

HR-MS (MALDI) (*m/z*) = obsvd. for $C_{78}H_{92}O_2Si_2$[M^+]: 1116.6628 (calcd. 1116.6630).

Elemental Analysis for $C_{78}H_{92}O_2Si_2$: meas. C, 70.49 (calcd. C, 70.58); H, 6.02 (H, 6.09).

Mp: 95 °C.

6.2.16. Synthesis of (1''s,4''s)-2'',3'',5'',6''-tetrakis(4-(tert-butyl)phenyl)-4''',6'-diiodo-1'',4''-dimethoxy-1'',4''-dihydro-1,1':3',1'':4'',1''':3''',1''''-quinquephenyl (**35**)

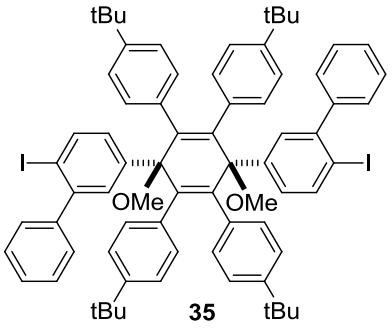

35

$C_{72}H_{74}I_2O_2$
m.w.: 1225.17 g/mol

34 (760 mg, 0.70 mmol, 1 eq.) and $AgBF_4$ (409 mg, 2.10 mmol, 3 eq.) were dissolved in a 2:1 mixture of THF (8 mL) and MeOH (4 mL). The solution was cooled to 0 °C and ICl (1 M in DCM) (2.10 mL, 2.10 mmol, 3 eq.) was dropwise added. After 40 min, the reaction was quenched with an aq. $Na_2S_2O_3$ solution, extracted with Et_2O (3x) and dried over $MgSO_4$. The solvent was removed *in vacuo* and the crude product was purified by column chromatography (6:4 hexane/dichloromethane) to give **35** (765 mg, 0.62 mmol, 89%) as a white solid.

^{1}H NMR (500 MHz, $C_2D_2Cl_4$, 373 K) δ [ppm] = 7.74 (s, 2H), 7.36 (s, 10H), 7.08 (s, 40H), 6.92 (d, *J*=8.4, 8H), 6.71 (d, *J*=8.3, 8H), 5.91 (s, 6H), 1.19 (s, 1H).

^{13}C NMR (126 MHz, $C_2D_2Cl_4$, 373 K) δ [ppm]: 148.92, 145.36, 144.08, 143.37, 142.54, 138.01, 135.31, 130.93, 130.46, 129.09, 127.86, 127.45, 127.20, 123.25, 95.89, 81.29, 52.01, 33.88, 30.95.

HR-MS (MALDI) (*m/z*): obsvd. for $C_{72}H_{74}I_2O_2[M^+]$: 1224.3758 (calcd. 1224.3773).

Elemental Analysis for $C_{72}H_{74}I_2O_2$: meas. C, 70.52 (calcd. C, 70.58%); H, 6.01 (H, 6.09).

Mp: 277°C.

6.2.17. Synthesis of triangular macrocycle **25**

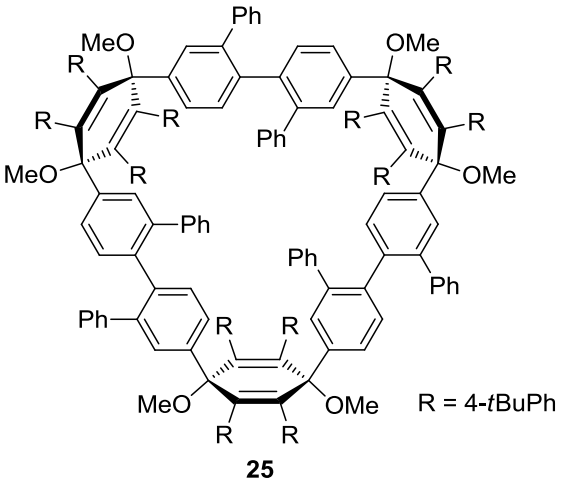

25

$C_{216}H_{222}O_6$
m.w.: 2914,07 g/mol

35 (875 mg, 0.52 mmol, 1 eq) was dissolved in Et_2O (260 mL) and cooled to – 78 °C. After addition of *t*-BuLi (1.7 M in pentane) (0.67 mL, 2.2 mmol, 4.2 eq.), the reaction solution was stirred for 40 min. Then, CuCN (46.6 mg, 0.52 mmol, 1 eq.) was added and the reaction was stirred for 2.5 h until it was warmed to r.t.. After another 3 h, duroquinone (256 mg, 1.56 mmol, 3 eq.) was added. The solvent was removed *in vacuo*, dissolved in 2 mL dichloromethane and precipitated from MeOH. The crude product was purified by column chromatography (6:4 hexane/dichloromethane) to give **25** (45.4 mg, 15.6 µmol, 9%) as a white solid.

^{1}H NMR (500 MHz, $C_2D_2Cl_4$, 403 K) δ [ppm] = 7.79 (s, 2H), 7.44 (d, J = 7.1 Hz, 2H), 7.2 (s, 2H), 7.05-6.88 (m, 22H), 3.89 (s, 6H), 1.13 (s, 36H).

^{13}C NMR: could not be recorded due to decomposition at elevated temperature.

HR-MS (MALDI) (*m/z*): obsd. for $C_{216}H_{222}O_6$ [M^+]: 2913.6848 (calcd. 2913.7127).

Mp: > 300 °C

X-ray chrystallographic structure: CCDC *966738*. These data can be obtained from The Cambridge Crystallographic Data Cente *via* http://www.vddc.cam.ac.uk/data_request/cif.

6.2.18. Synthesis of [9]CPP-based polyphenylene cylinder **38**

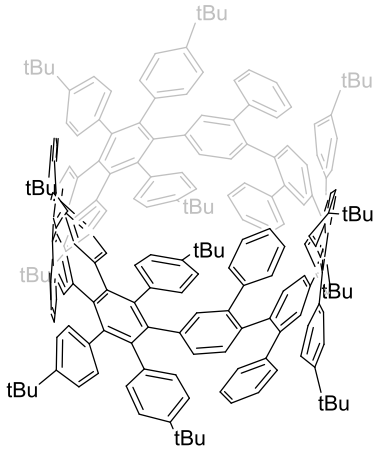

38
$C_{210}H_{204}$
m.w.: 2727.87 g/mol

25 (20 mg, 6.9 µmol) was dissolved in 5 mL THF and cooled down to – 78 °C. After addition of NaNp (1 M) (0.35 mL, 0.35 mmol), the reaction mixture was stirred for 3 h, quenched with $Na_2S_2O_3$ (2 M), and extracted with dichloromethane (3x). The combined organic fractions were dried over $MgSO_4$ and the solvent was removed in vacuo. The crude mixture was subjected to column chromatography to afford **38** (10.3 mg, 3.8 µmol, 55%) as a white solid.

^{1}H NMR (500 MHz, $C_2D_2Cl_4$, 413 K) δ [ppm] = 6.98 (pt, *J*=30.4, 28H), 6.70 (pd, *J*=7.7, 4H), 1.22 (s, 36H).

^{13}C NMR: could not be recorded due to decomposition at elevated temperature.

HR-MS (MALDI) (*m/z*): obsvd. for $C_{210}H_{204}$ [M^+] = 2727.5986 (calcd. 2727.6024).

Mp: > 300 °C.

X-ray crystal structure: CCDC 966737. These data can be obtained from The Cambridge Crystallographic Data Cente via www.vddc.cam.ac.uk/data_request/cif.

6.2.19. Synthesis of (6-bromo-[1,1'-biphenyl]-3-yl)trimethylsilane (**45**)

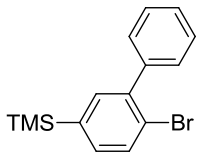

45
$C_{15}H_{17}BrSi$
m.w.: 305.28 g/mol

16 (2 g, 5.57 mmol, 1 eq.) was given into a Schlenk flask and dissolved in THF (100 mL). The reaction solution was cooled to – 78 °C. After addition of *n*-BuLi (3.48 mL, 5.57 mmol, 1 eq.) the reaction was stirred for 30 min and TMSCl (0.73 g, 0.85 mL, 5.57 mmol, 1.2 eq.) was added. The reaction was warmed to r.t. and stirred overnight. After column chromatography (hexanes) **45** (1.41 g, 4.62 mmol, 83%) was obtained as a white solid.

^{1}H NMR (500 MHz, $C_2D_2Cl_4$, 373 K) δ [ppm] = 7.65 (d, *J* = 7.9 Hz, 1H), 7.40 (m, *J* = 14.0, 9.6, 5.9, 1.7 Hz, 7H), 0.27 (s, 9H).

^{13}C NMR (126 MHz, $C_2D_2Cl_4$, 373 K) δ [ppm] = 142.16, 141.80, 140.62, 136.58, 134.11, 132.71, 129.86, 128.36, 127.94, 123.84, -1.15.

MS (MALDI) (*m/z*): obsvd. for C15H17BrSi [M+] = 306.2 (calcd. 306.0).

Elemental Analysis for $C_{15}H_{17}BrSi$: meas. C, 59.13 (calcd. C, 59.01C); H, 1.07 (H, 5.61).

Mp: 36 °C.

6.2.20. Synthesis of (6-iodo-[1,1'-biphenyl]-3-yl)trimethylsilane (**46**)

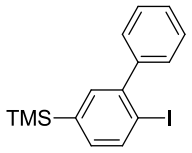

46
$C_{15}H_{17}ISi$
m.w.: 352.29 g/mol

45 (1.25 g, 3.48 mmol, 1 eq.) was given into a Schlenk flask and dissolved in THF (35 mL). The reaction solution was cooled down to – 78 °C. After addition of *n*-BuLi (2.82 mL, 4.42 mmol, 1.3 eq.) the reaction was stirred for 30 min and the *in situ* generated lithium organyle was quenched with I_2 (1.59 g, 6.26 mmol, 1.8 eq.). The reaction was warmed to r.t. and the

excess of I_2 was treated with $Na_2S_2O_3$. After column chromatography (hexanes) **46** (1.04 g, 2.95 mmol, 85%) was obtained as a white solid.

^{1}H NMR (500 MHz, $C_2D_2Cl_4$, 373 K) δ [ppm] = 7.94 (d, *J* = 7.8 Hz, 1H), 7.54 – 7.29 (m, 7H), 7.17 (dd, *J* = 7.8, 1.6 Hz, 1H), 0.27 (s, 11H).

^{13}C NMR (126 MHz, $C_2D_2Cl_4$, 373 K) δ [ppm] = 146.22, 144.87, 141.32, 139.18, 135.25, 134.05, 129.77, 128.33, 127.96, 99.93, -1.20.

MS (MALDI) (*m/z*): obsd. for $C_{15}H_{17}BrSi$ [M^+]: 352.2; (calcd 352.0).

Elemental Analysis for $C_{15}H_{17}BrSi$: meas. C, 51.67 (calcd. C, 51.14), H, 5.22 (H, 4.86).

Mp: 28°C.

6.2.21. Synthesis of 2-(5'-bromo-[1,1':4',1''-terphenyl]-2'-yl)-4,4,5,5-tetramethyl-1,3,2-dioxaborolane (**44**)

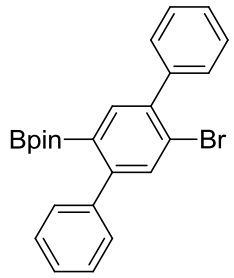

44

$C_{24}H_{24}BBrO_2$
m.w.: 435.16 g/mol

2',5'-dibromo-1,1':4',1''-terphenyl (**43**)[156] (2.53 g, 6.52 mmol; 1 eq) was dissolved in THF (150 mL), cooled down to – 78 °C and subjected to *n*-BuLi (1.6 M) (4,01 mL, 6.52 mmol, 1 eq.). The reaction mixture was warmed to – 40 °C and stirred for 2 h. Again, the solution was cooled down to – 78 °C and *i*-PrOBpin (1.21 g, 1.33 mL, 6.52 mmol, 1 eq.) was added. The reaction was warmed to r.t. and stirred overnight. After addition of water, the solution was extracted with Et_2O (3x) and dried over $MgSO_4$. The solvent was removed *in vacuo* and the crude product was subjected to flash chromatography (hexane/dichloromethane 1:1) to give **44** (1.50 g, 3.45 mmol, 53%) as a white solid.

^{1}H NMR (500 MHz, $C_2D_2Cl_4$, 373 K): δ [ppm] = 7.70 (d, *J* = 14.3 Hz, 2H), 7.52 – 7.32 (m, 10H), 1.20 (s, 12H).

^{13}C NMR (126 MHz, $C_2D_2Cl_4$, 373 K): δ [ppm] = 148.44, 141.65, 141.21, 140.83, 137.83, 133.82, 129.88, 129.43, 128.40, 128.03, 127.95, 125.03, 84.45, 24.79.

MS (MALDI) (*m/z*): obsvd. for $C_{24}H_{24}BBrO_2$ [M^+]: 435.5 ; (calcd. 434.1).

Elemental Analysis for $C_{24}H_{24}BBrO_2$: meas. C, 66.52 (calcd. C, 66.24); H, 5.66 (H, 5.56).

Mp: 143 °C.

6.2.22. Synthesis of (5'-bromo-4'-phenyl-[1,1':2',1'':2'',1'''-quaterphenyl]-4''-yl)trimethyl-silane (**47**)

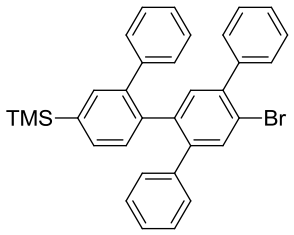

47

$C_{33}H_{29}BrSi$
m.w.: 533.57 g/mol

Terphenylboronic ester **44** (1.23 g, 2.83, 1 eq.), silane **46** (1.00 g, 2.83 g, 1 eq.) and $Pd(PPh_3)_4$ (0.33 g, 0.28 mmol, 10 mol%) were dissolved in toluene (25 mL). After addition of Et_4NOH (35% in H_2O) (14.1 mL, 34.0 mmol, 12 eq.), the reaction solution was heated to 90% and stirred overnight. The reaction mixture was extracted with DCM (3x) and washed with water (3x). The combined organic fractions were stirred over $MgSO_4$ and the solvent was removed until complete dryness. After column chromatography (hexane/toluene 9:1), the title compound **47** (1.95 g, 2.24, 79%) was obtained.

^{1}H NMR (500 MHz, $C_2D_2Cl_4$, 373 K) δ [ppm] = 7.52 (s, 1H), 7.50 – 7.29 (m, 11H), 7.23 – 7.03 (m, 7H), 6.75 (ddd, *J* = 5.3, 3.0, 1.5 Hz, 5H), 0.28 (s, 11H).

^{13}C NMR (126 MHz, $C_2D_2Cl_4$, 373 K) δ [ppm]: 143.04, 142.65, 142.32, 141.92, 141.70, 141.58, 140.79, 140.36, 136.56, 136.13, 135.72, 133.52, 132.20, 130.90, 130.79, 130.53, 129.36, 129.14, 129.06, 128.06, 127.58, 122.43, -0.03.

FD (FD, 8 kV) (*m/z*): obsvd. for [M^+]: 533.5 (calcd. 534.1).

Elemental Analysis for $C_{33}H_{29}BrSi$: meas. C, 74.58 (calcd. C, 74.28); H, 5.23 (H, 5.48) .

Mp: 183°C.

6.2.23. Synthesis of 5'-bromo-4''-iodo-4'-phenyl-1,1':2',1'':2'',1'''-quaterphenyl (**48**)

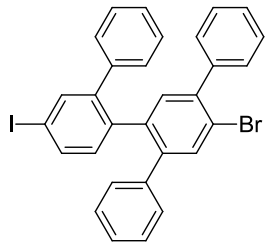

48
$C_{30}H_{20}BrI$
m.w.: 587.29 g/mol

BrTMS **47** (935 mg, 1.75 mmol, 1 eq.) was dissolved in DCM and cooled down to 0 °C. ICl (1 M in DCM) (1.93 mL, 1.93 mmol, 1.1 eq.) was slowly added and the reaction was stirred for 2 h at 0 °C. The reaction was quenched with an aq. NaOH solution. After addition of $Na_2S_2O_3$, the crude product was extracted with DCM (3x) and dried over $MgSO_4$ and the solvent was removed *in vacuo*. Column chromatography (Hex/Tol 9.5:0.5) afforded the title compound **48** (875 mg, 1.49 mmol, 85%) as colorless solid.

^{1}H NMR (500 MHz, $C_2D_2Cl_4$, 373 K) δ [ppm] = 7.65 (dd, *J* = 8.1, 1.8 Hz, 1H), 7.57 (d, *J* = 1.8 Hz, 1H), 7.52 (s, 1H), 7.40 (tdd, *J* = 7.4, 3.1, 1.3 Hz, 5H), 7.28 (s, 1H), 7.24 – 7.05 (m, 7H), 6.71 (ddd, *J* = 6.7, 5.1, 1.5 Hz, 4H).

^{13}C NMR (126 MHz, $C_2D_2Cl_4$, 373 K) δ [ppm] = δ 143.53, 141.91, 141.47, 140.72, 139.74, 139.40, 139.21, 138.64, 136.49, 134.78, 133.63, 129.82, 129.49, 129.43, 128.36, 128.25, 128.11, 127.20, 127.15, 121.81, 93.60.

MS (FD, 8 kV) (*m/z*): obsd. for $C_{30}H_{20}BrI$ [M^+] = 585.8 (calcd. 586.0).

Elemental Analysis for $C_{30}H_{20}BrI$: found. C, 61.29 (calcd. C, 61.35); H, 2.45 (H, 3.43).

Mp: 200 °C.

6.2.24. Trimethyl(5'-(4,4,5,5-tetramethyl-1,3,2-dioxaborolan-2-yl)-[1,1':4',1''-terphenyl]-2'-yl)silane (**58**)

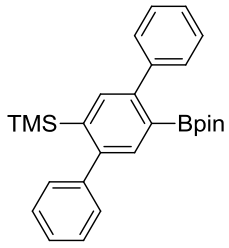

58

$C_{27}H_{33}BO_2Si$
m.w.: 428.45 g/mol

Terphenyl **54** was synthesized according to literature.[156] **54** (12.2 g, 32.6 mmol, 1 eq.) and $AgBF_4$ (6.02 g, 30.9 mmol, 0.95 eq.) were dissolved in a 2:1 mixture of THF (240 mL) and MeOH (120 mL) and the reaction solution was cooled down to 0 °C. After addition of ICl (1 M in dichloromethane) (30.9 mL, 30.9 mmol, 0.95 rq.), the solution was stirred for 1 h and quenched with an aq. solution of $Na_2S_2O_3$ (2 M). The crude product was extracted with Et_2O (3x) and dried over $MgSO_4$ The crude product was filtered through a pad of silica and was used without further purification. 9.1 g of the crude mixture (5.1 g, 11.9 mmol, 1 eq.) monoiodinated terphenyl; NMR yield) was dissolved in THF (380 mL), cooled down to – 78 °C and subjected to *n*-BuLi (19 mL, 11.9 mmol, 1 eq.). The reaction mixture was warmed to – 40 °C and stirred for 2 h. Again, the solution was cooled down to – 78 °C and *i*-PrOBpin was added. The reaction was warmed to r.t. and stirred overnight. After addition of water, the solution was extracted with Et_2O (3x) and dried over $MgSO_4$. The solvent was removed *in vacuo* and the crude product was subjected to flash chromatography (6:4 hexan/dichloromethane) to give **58** (3.3 g, 7.70 mmol, 24%) as a white solid.

^{1}H NMR (300 MHz, CD_2Cl_2) δ [ppm] = 7.63 (s, 1H), 7.55 (s, 1H), 7.48 – 7.29 (m, 10H), 1.20 (s, 12H), 0.03 (d, 9H).

^{13}C NMR (75.5 MHz, CD_2Cl_2) δ [ppm] = 147.57, 145.30, 144.67, 143.56, 141.29, 135.81, 135.65, 129.95, 129.56, 128.32, 128.10, 27.47, 127.34, 84.23, 24.81, 0.59.

MS (FD, 8 kV) (*m/z*): obsd. for $C_{27}H_{33}BO_2Si$ [M^+] = 428.0 (calcd. 428.2).

Elemental Analysis for $C_{27}H_{33}BO_2Si$: found C, 75.71 (calcd. C, 75.6); H, 7.53 (H, 7.76).

Mp: 187 °C.

6.2.25. Synthesis terphenyl-extended disilane **59**

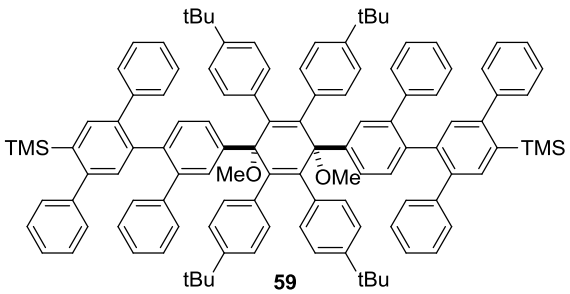

59

$C_{114}H_{116}O_2Si_2$
m.w.: 1574.31 g/mol

58 (861 mg, 2.01 mmol, 3 eq.), **35** (821 mg, 0.67 mmol, 1 eq.), $Pd(PPh_3)_4$ (77 mg, 67.0 µmol, 10 mol%) were added to a Schlenk flask. After addition of toluene (14 mL), a degassed aq. solution of cesium carbonate (3 M) (13 mL) was added and the reaction was heated to 95 °C. After 12 h, the reaction mixture was extracted with Et_2O (3x), dried over $MgSO_4$ and the solvent was removed *in vacuo*. The crude mixture was subjected to column chromatography (hexane/dichloromethane = 7/3) to afford **59** (854 mg, 0.54 mmol, 81%) as a white solid.

^{1}H NMR (500 MHz, $C_2D_2Cl_4$, 373 K) δ [ppm] = 7.77-6.22 (m, 56H), 3.87 (s, 6), 1.02 (s, 36H), 0.08 (s, 18).

^{13}C NMR (126 MHz, $C_2D_2Cl_4$, 373 K) δ [ppm] = 148.89, 147.83, 144.51, 142.93, 142.19, 141.69, 141.60 , 140.14, 140.11, 138.83, 138.43, 137.25, 136.53, 136.13, 133.41, 131.58, 130.56, 130.46, 129.75, 129.71, 129.63, 127.78, 127.68, 127.32, 127.14, 126.76, 126.10, 125.91, 123.44, 82.04, 52.38, 34.23, 31.37, 0.96.

HR-MS (MALDI) (*m/z*): obsvd. for $C_{114}H_{116}O_2Si_2$ [M^+]; 1573.8514 (calcd. 1573.8539).

Elemental analysis for $C_{114}H_{116}O_2Si_2$: found C, 85.56 (calcd. C, 86.97); H, 7.48 (H, 7.43).

Mp: 206 °C.

6.2.26. Synthesis terphenyl-extended diiodide **60**

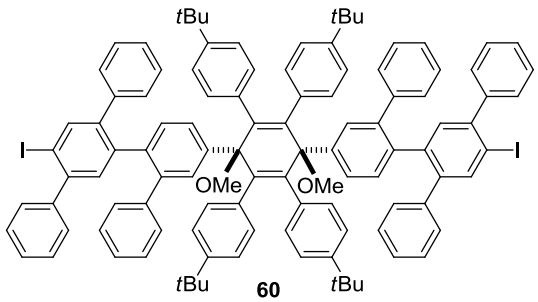

60

$C_{108}H_{98}I_2O_2$
m.w.: 1681.74 g/mol

59 (1.51 g, 0.96 mmol, 1 eq.) and $AgBF_4$ (0.75 g, 3.80 mmol, 4 eq.) were dissolved in a 2:1 mixture of THF (15 mL) and MeOH (7.5 mL) cooled down to 0 °C. After addition of ICl (1 M in DCM) (3.8 mL, 3.80 mmol, 4. Eq.), the reaction was stirred for 1 h and then quenched with an aqueous $Na_2S_2O_3$ (2 M). The mixture was extracted with Et_2O (3x), dried over $MgSO_4$ and the solvent was removed *in vacuo*. The crude mixture was first purified by column chromatography (7:3 hexane/dichloro-methane) and then recrystallized from hexane to give **60** (1.21 g, 75%, 0.72 mmol) as a white solid.

^{1}H NMR (500 MHz, $C_2D_2Cl_4$, 403 K) δ [ppm] = 7.87 (s, 2H), 7.61 (d, *J*=7.5, 2H), 7.49 – 7.29 (m, 12H), 7.21 (t, *J*=7.3, 2H), 7.16 – 7.00 (m, 14H), 6.89 (d, *J*=8.1, 12H), 6.75 (d, *J*=8.2, 8H), 6.61 (d, *J*=6.9, 4H), 3.90 (s, 6H), 1.19 (s, 36H).

^{13}C NMR (126 MHz, $C_2D_2Cl_4$, 403 K) δ [ppm] = 148.65, 144.82, 143.56, 142.55, 142.37, 141.45, 141.20, 140.49, 139.97, 139.76, 139.27, 136.93, 135.71, 133.36, 131.13, 130.41, 129.87, 129.20, 129.15, 129.13, 127.60, 127.40, 127.30, 127.15, 126.44, 126.32, 125.75, 122.96, 96.14, 81.68, 74.02, 73.80, 73.58, 51.90, 33.80, 30.91.

MS (MALDI) (*m/z*): calcd for $C_{108}H_{98}I_2O_2$ [M^+] = 1681.57, found 1681.95.

Elemental Analysis for $C_{56}H_{58}BO$: found C, 78.54 (C, 77.13); H, 5.23 (H, 5.87).

Mp: > 300 °C.

6.2.27. Synthesis of the hexakis(terphenyl)-extended triangular macrocycle **61**

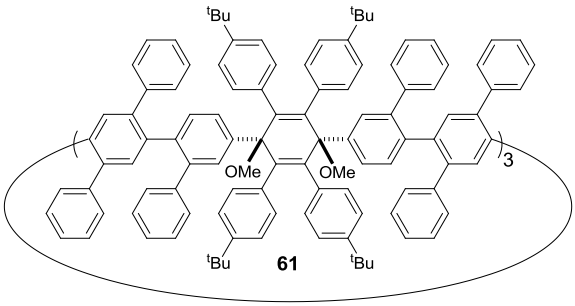

$C_{324}H_{294}O_6$
m.w.: 4283.81 g/mol

60 (1 g, 0.595 mmol, 1 eq.) was dissolved in Et_2O (300 mL) and cooled to – 78 °C. After addition of *t*-BuLi (1.7 M) (0.7 mL, 1.19 mmol, 2 eq.), the reaction was stirred for 40 min. Then, CuCN (53 mg, 595 µmol, 1 eq.) was added and the reaction was stirred for 1.5 h. The reaction was warmed to r.t. and stirred for another 2.5 h until duroquinone (0.29 g, 1.78 mmol, 3 mmol) was added. After 3 h, the reaction mixture was poured into MeOH and the precipitate was collected. The crude mixture was roughly purified by column chromatography (6:4 hexane/dichloromethane) and further purified by recycling-GPC (eluent: chloroform) to give **61** (80 mg, 1.87 µmol, 9.4%) as a white solid.

^{1}H NMR (500 MHz, $C_2D_2Cl_4$, 373 K) δ [ppm] = 7.92 – 6.25 (m, 56H), 3.88 (s, 6H), 1.18 (s, 36H).

^{13}C NMR (126 MHz, $C_2D_2Cl_4$, 373K) δ [ppm] = 148.95, 142.47, 141.66, 141.15, 140.91, 140.15, 139.94, 139.43, 138.70, 138.27, 136.16, 133.79, 133.43, 131.62, 130.62, 129.55, 128.63, 127.69, 127.58, 127.34, 127.22, 126.23, 126.13, 125.94, 123.41, 82.10, 52.33, 34.24, 31.38.

HR-MS (MALDI) (*m/z*): obsd. for $C_{324}H_{294}O_6$ [M^+]: 4283.2796 (calcd. 4283.2796).

Mp: > 300 °C.

6.2.28. Synthesis of the [15]CPP-based Polyphenylene Cylinder **62**

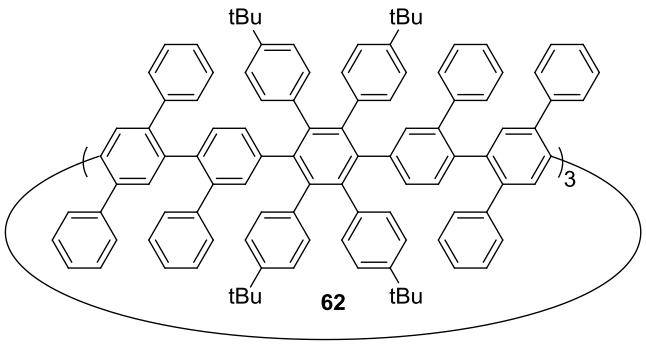

62

$C_{318}H_{276}$
m.w.: 4097.59 g/mol

1 (50 mg, 11.6 µmol, 1 eq.) was dissolved in 10 mL THF and cooled down to – 78 °C. After addition of NaNp (0.58 mL, 0.58 mmol, 25 eq.), the reaction mixture was stirred for 3 h, quenched with $Na_2S_2O_3$ (2 M), and extracted with DCM (3x). The combined organic fractions were dried over $MgSO_4$ and the solvent was removed in vacuo. The crude mixture was subjected to column chromatography (hexanes/DCM = 1:1) to afford **62** (23 mg, 5.61 µmol, 48%) as a white solid.

^{1}H NMR (500 MHz, $C_2D_2Cl_4$, 373 K) δ [ppm] = 7.30-6.67 (m, 48 H), 6.42 (s, 8H), 1.09 (s, 36 H).

^{13}C NMR (126 MHz, $C_2D_2Cl_4$, 373 K) δ [ppm] = 147.74, 141.47, 140.66, 140.42, 140.13, 140.04, 139.74, 139.51, 137.57, 131.17, 129.43, 129.24, 129.04, 127.42, 127.35, 127.22, 127.05, 126.08, 125.83, 125.73, 122.79, 120.23, 73.80, 33.70, 31.04.

HR-MS (MALDI) (*m/z*): obsvd. for $C_{318}H_{276}$ [M^+] = 4097.1693 (calcd. 4097.1693).

Mp: > 300 °C.

6.2.29. Synthesis of doubly extended kinked disilane (**65**)

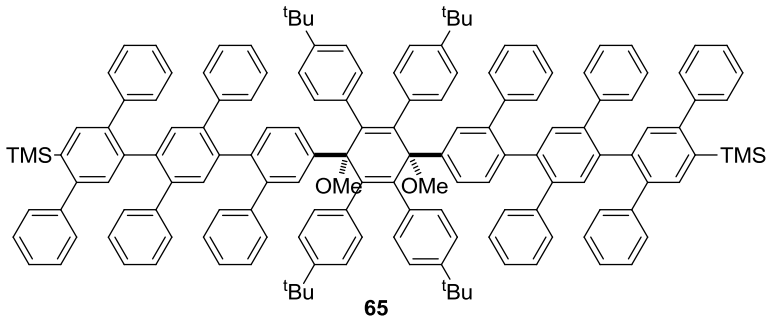

65

$C_{150}H_{140}O_2Si_2$
m.w.: 2030,89 g/mol

60 (770 mg, 0.46 mmol, 1 eq.), **58** (587 mg, 1.37 mmol, 3 eq.), $Pd(PPh_3)_4$ (53 mg, 46.0 µmol, 10 mol%) were added to a Schlenk flask. After addition of toluene (2.7 mL), a degassed aq. solution of cesium carbonate (3 M) (6.1 mL) was added and the reaction was heated to 95 °C. After 12 h, the reaction mixture was extracted with Et_2O (3x), dried over $MgSO_4$ and the solvent was removed *in vacuo*. The crude mixture was subjected to column chromatography (7:3 hexane/dichloromethane) and subsequent preparative GPC in THF to afford **65** (645 mg, 0.32 mmol, 69%) as a white solid.

^{1}H NMR (500 MHz, $C_2D_2Cl_4$) δ [ppm] = 7.71 – 6.38 (m, 40H), 3.89 (s, 3H), 1.20 (s, 18H), 0.10 (s, 9H).

^{13}C NMR (126 MHz, $C_2D_2Cl_4$) δ [ppm] = 149.48, 148.69, 145.00, 143.52, 142.80, 142.31, 141.63, 141.54, 140.68, 140.41, 140.26, 139.75, 139.59, 139.18, 138.79, 138.18, 137.27, 136.72, 134.56, 134.23, 133.68, 132.16, 131.27, 130.35, 130.19, 128.42, 128.39, 128.26, 128.20, 128.06, 127.75, 127.41, 126.82, 126.76, 126.59, 124.03, 82.60, 52.98, 34.83, 31.97, 1.53.

HR-MS (MALDI) (*m/z*): obsvd. for $C_{150}H_{140}O_2Si_2$ $[M]^+$: 2030.0430 (calcd. 2030.0418).

Elemental Analysis for $C_{150}H_{140}O_2Si_2$: meas. C, 86.63 (calcd. C, 88.87); H, 6.38 (H, 6.95%).

Mp: 245 °C.

6.2.30. Synthesis of doubly-extended kinked diiodide (**66**)

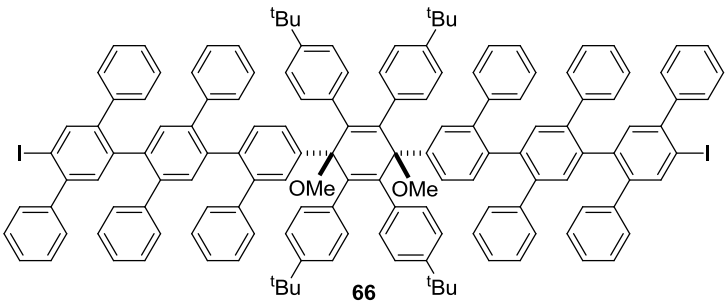

66

$C_{144}H_{122}I_2O_2$
m.w.: 2138,32 g/mol

65 (315 mg, 0.16 mmol) and $AgBF_4$ (121 mg, 0.62 mmol) were dissolved in a 2:1 mixture of THF (3 mL) and MeOH (1.5 mL) cooled down to 0 °C. After addition of ICl (1 M in DCM) (0.62 mL, 0.62 mmol), the reaction was stirred for 1 h and then quenched with an aq. $Na_2S_2O_3$ (2 M). The mixture was extracted with Et_2O (3x), dried over $MgSO_4$ and the solvent was removed *in vacuo.* The crude mixture was first purified by column chromatography (6:4 hexane/dichloro-methane) and then recrystallized from hexane to give **66** (220 g, 66%, 0.103 mmol) as a white solid.

^{1}H NMR (500 MHz, $C_2D_2Cl_4$, 373 K) δ [ppm] = 7.88 (s, 2H), 7.69 – 6.44 (m, 80H), 3.88 (s, 6H), 1.19 (s, 36H).

^{13}C NMR (126 MHz, $C_2D_2Cl_4$, 373 K) δ [ppm] = 149.13, 145.62, 144.00, 143.13, 142.55, 142.17, 141.87, 141.25, 141.03, 140.96, 140.29, 140.18, 140.09, 139.84, 138.20, 137.65, 136.30, 134.37, 133.74, 132.05, 131.76, 131.46, 130.81, 130.05, 129.82, 129.78, 129.51, 129.30, 128.27, 128.22, 128.16, 128.00, 127.86, 127.67, 127.05, 126.68, 126.48, 126.23, 123.85, 123.65, 123.43, 97.21, 82.20, 52.60, 34.44, 31.58.

HR-MS (MALDI) (*m/z*): obsvd. for $C_{144}H_{122}I_2O_2$ $[M]^+$: 2137.7557 (calcd. 2137.7562).

Elemental Analysis for $C_{144}H_{122}I_2O_2$: found C, 79.52 (C, 80.88), H, 6.25 (H, 5.75).

Mp: > 300 °C.

6.2.31. Synthesis of doubly extended triangular macrocycle **67**

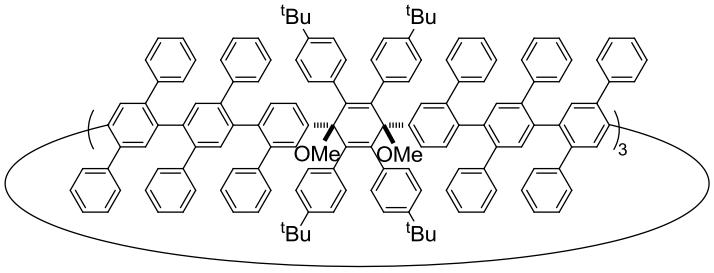

67

$C_{432}H_{366}O_6$
m.w.: 5653.52 g/mol

66 (201 g, 0.094 mmol, 1 eq.) was dissolved in Et_2O (300 mL) and cooled to – 78 °C. After addition of *t*-BuLi (1.7 M) (0.11 mL, 0.19 mmol, 2.1 eq.), the reaction was stirred for 1h. Then, CuCN (8.4 mg, 94 µmol, 1 eq.) was added and the reaction was stirred for 1.5 h. The reaction was warmed to r.t. and stirred for another 2 h until duroquinone (46.3 g, 0.28 mmol, 3 eq.) was added. After 3 h, the reaction mixture was poured into MeOH and the precipitate was collected. The crude mixture was roughly purified by TLC (4:6 hexane/dichloromethane) and further purified by gel permeation chromatography (eluent: chloroform) to give **67** (1.3 mg, 0.23 µmol, 2.4%) as a white solid.

^{1}H NMR (500 MHz, $C_2D_2Cl_4$, 373 K) δ [ppm] = 7.33-6.71 (m, 80 H), 3.82 (s, 6 H), 1.13 (s, 36 H).

^{13}C NMR too small amount for measurement.

HR-MS (MALDI) (*m/z*): obsvd. for C_{432} $H4_{66}$ O_6 $[M]^+$: 5652.8643 (calcd. 5651.8464).

6.2.32. Synthesis of a [21]CPP-based Polyphenylene Cylinder **68**

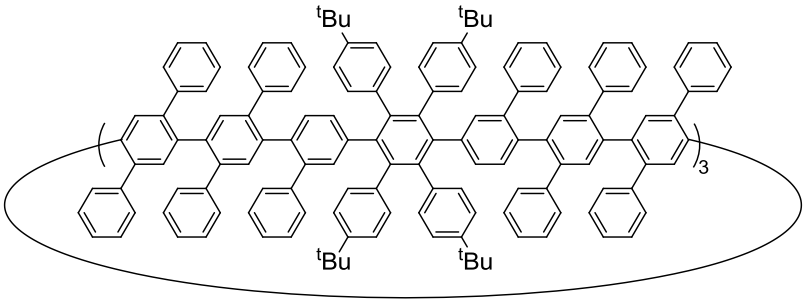

68

$C_{426}H_{348}$
m.w. 5467.32 g/mol

67 (7 mg, 1.24 µmol, 1 eq.) was dissolved in 4 mL THF and cooled down to – 78 °C. After addition of NaNp (0.06 mL, 61.9 µmol, 50 eq), the reaction mixture was stirred for 3 h, quenched with I_2 (2 M), and extracted with DCM (3x). The combined organic fractions were dried over $MgSO_4$ and the solvent was removed *in vacuo.* The crude mixture was subjected to column chromatography (hexanes/DCM = 1:1) to afford **68** (3.4 mg, 0.62 µmol, 50%) as a white solid.

^{1}H NMR line broadening, no interpretation possible.
HR-MS (MALDI) (*m/z*): obsvd. for $C_{426}H_{348}$ $[M]^+$: 5466.7510 (calcd. 5466.7361).
UV-VIS: 263 nm.
Emission: 413 nm.

6.2.33. Synthesis of (2,2'',6,6''-tetrachloro-[1,1':4',1''-terphenyl]-2',5'-diyl)bis(trimethylsilane) (**76**)

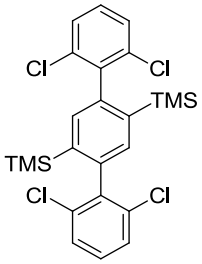

76

$C_{24}H_{26}Cl_4Si_2$
m.w.: 512.45 g/mol

75 (13 g, 27.4 mmol, 1 eq.), 1,3-dichloro-2-iodobenzene (37 g, 137 mmol, 5 eq.), and $Pd(PPh_3)_4$ (3.16 g, 2.74 mmol, 10 mol%) were put into a Schlenk flask and dissolved in toluene (270 mL). After addition of Et_4NOH (230 mL, 548 mmol, 20 eq.) (34% H_2O), the reaction was warmed to 100 °C and stirred for 24 h. The crude product was extracted with DCM (3x) and the combined fractions were dried over $MgSO_4$. Column chromatography (hexane) afforded **76** (2.1 g, 4.10, 15%) as a white solid.

^{1}H NMR (300 MHz, CD_2Cl_2) δ [ppm] = 7.43 (m, *J* = 8.0, 0.7 Hz, 4H), 7.36 – 7.25 (m, 4H), -0.00 (s, 18H).

^{13}C NMR (75 MHz, CD_2Cl_2) δ [ppm] = 142.00, 141.92, 140.07, 136.16, 135.84, 129.67, 128.21, -0.26.

MS (FD, 8 kV) (*m/z*): obsvd. for $C_{24}H_{26}Cl_4Si_2$ $[M]^+$ = 514.1 (calcd. 512.0).

Elemental Analysis for $C_{24}H_{26}Cl_4Si_2$: found C, 56.50 (calcd. C, 56.25); H, 5.11 (H, 5.11).

Mp: 203 °C.

X-ray Crystal Structure: CCDC 1028674. These data can be obtained from The Cambridge Crystallographic Data Cente via www.vddc.cam.ac.uk/data_request/cif.

6.2.34. Synthesis of trimethyl(2,2'',6,6''-tetrachloro-5'-iodo-[1,1':4',1''-terphenyl]-2'-yl)silane (**77**)

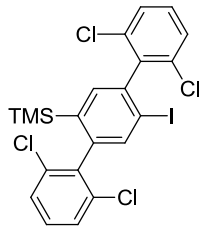

77

$C_{21}H_{17}Cl_4ISi$
m.w.: 566.16 g/mol

76 (1 g, 1.95 mmol, 1 eq.) was dissolved in dry DCM (10 mL) under argon and the reaction solution was cooled down to 0 °C. ICl (1.85 mL, 1.85 mmol, 0.95 eq) (1 M in DCM) and stirred for 30 min. Then, the reaction solution was warmed to r.t. and stirred for another 3 h. The reaction was quenched with an aq. solution of $N_2S_2O_3$. The crude product was extracted with DCM (3x) and the combined organic fractions were dried over $MgSO_4$. After column chromatography (hexane) **77** (720 mg, 12.7 mmol, 80%) was obtained as a white solid; 70 mg of the starting material **76** were recovered.

^{1}H NMR (300 MHz, CD_2Cl_2) δ [ppm] = 7.66 (s, 1H), 7.52 – 7.40 (m, 1H), 7.39 – 7.25 (m, 1H), 0.00 (s, 2H).

^{13}C NMR (75 MHz, CD_2Cl_2) δ [ppm] = 144.27, 141.96, 141.66, 140.38, 139.95, 139.48, 136.59, 135.91, 135.50, 1k30.28, 130.24, 128.42, 128.31, 100.16, -0.35.

MS (FD, 8 kV) (*m/z*): obsvd. for $C_{21}H_{17}Cl_4ISi$ $[M]^+$ = 566.1 (calcd. 565.9).

Elemental Analysis for $C_{21}H_{17}C_{l4}ISi$: found C, 44.91 (calcd. C, 44.55); H, 3.05 (H, 4.02).

Mp: 180 °C.

6.2.35. Synthesis of trimethyl(2,2'',6,6''-tetrachloro-5'-(4,4,5,5-tetramethyl-1,3,2-dioxaborolan-2-yl)-[1,1':4',1''-terphenyl]-2'-yl)silane (**69**)

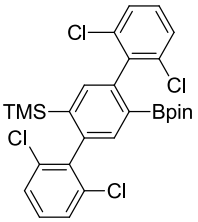

69

$C_{27}H_{29}BCl_4O_2Si$

m.w.: 566,23 g/mol

77 (790 mg, 1.40 mmol, 1 eq.) was dissolved in 12 mL THF and cooled to – 78 °C. After addition of *n*-BuLi and stirring for 30 min, the reaction was warmed to – 40 °C and stirred for 2 h. After cooling to – 78 °C, isopropoxyboronic acid pinacol ester (0.29 mL, 1.40 mmol, 1 eq.) was added, stirred for 30 min and the reaction was warmed to r.t.. After quenching with water, the reaction mixture was extracted with Et_2O (3x) and the combined fractions were dried over $MgSO_4$. After column chromatography (6:4 hexane/DCM), **69** (355 mg, 0.63 mmol, 45%). was obtained as a white solid.

^{1}H NMR (300 MHz, CD_2Cl_2) δ [ppm] = 7.51 – 7.36 (m, 6H), 7.33 – 7.19 (m, 2H), 1.13 (s, 12H), 0.02 (s, 9H).

^{13}C NMR (75 MHz, CD_2Cl_2) δ [ppm] = 142.45, 142.12, 141.91, 141.58, 141.35, 136.28, 136.07, 135.62, 135.43, 129.78, 129.00, 128.20, 127.85, 83.94, 24.80, -0.29.

MS (FD, 8 kV) (*m/z*): obsvd. for $C_{27}H_{29}BCl_4O_2Si$ $[M]^+$: 566.8 (calcd. 566.1).

Elemental Analysis for $C_{27}H_{29}BCl_4O_2Si$: found C, 56.42 (calcd.C, 57.27); H.4.49 (H 5.16).

Mp: 245-250 °C.

6.2.36. Synthesis of 3',6'-dibromo-4,4''-di-tert-butyl-4',5'-bis(4-(tert-butyl)phenyl)-1,1':2',1''-terphenyl (**97**)

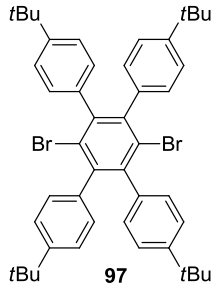

97

$C_{46}H_{52}Br_2$
MW: 764.71 g/mol

Hexabromobenzene (8.27 g, 15 mmol, 1 eq) was placed into a Schlenk flask and 5-tert-butylphenylmagnesium bromide (300 mL, 150 mmol, 10 eq.) was added and the reaction was stirred for 12 h. Then, the reaction was cooled down to 0 °C and slowly quenched with bromine. After quenching an excess amount of bromine with aq. $Na_2S_2O_3$, the crude product was extracted with Et_2O and the combined fractions were filtered through a fritted funnel. The filter cake was washed with water, EtOH, Hexan and Toluene to give the title compound **97**. The solvent of the filtrate was removed under *vacuo*. The solid residue was washed analogously to the filter cake. The reaction afforded **97** (5.1 g, 6.68 mmol 37%) as a white solid.

^{1}H NMR (300 MHz, THF) δ [ppm] = 7.14 (d, *J*=8.3, 8H), 6.94 (d, *J*=8.3, 8H), 1.21 (s, 36H).

^{13}C NMR (75 MHz, THF) δ [ppm] = 149.9, 144.5, 139.2, 130.5, 125.4, 124.6, 34.8, 31.4.

MS (FD, 8 kV) (*m/z*): obsvd. for $C_{46}H_{52}Br_2$ [M^+] = found 763.9.(calcd. 764.2)

Elemental Analysis for $C_{46}H_{52}Br_2$: found C, 71.46 (calcd. C, 72.25); H 6.46 (H, 6.85).

Melting Point: > 300 °C.

X-ray crystal structure: CCDC 1033268. These data can be obtained from The Cambridge Crystallographic Data Cente via www.vddc.cam.ac.uk/data_request/cif.

6.2.37. Synthesis of (6'-bromo-4,4''-di-tert-butyl-4',5'-bis(4-(tert-butyl)phenyl)-[1,1':2',1''-terphenyl]-3'-yl)trimethylsilane (**98**)

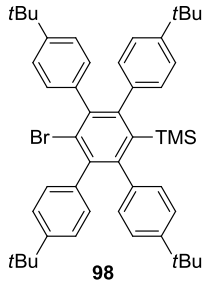

98

$C_{49}H_{61}BrSi$
m.w.: 758.00 g/mol

97 (0.40 g, 0.52 mmol, 1 eq.) was dissolved in THF (60 mL) and cooled down to – 78 °C. After drop-wise addition of *n*-BuLi (0.33 mL, 0.52 mmol, 1 eq.), the reation was stirred for 40 min and then quenchend with TMSCl (0.26 mg, 2.04 mmol, 4 eq.). The reaction was quickly warmed to r.t. and stirred for another 1h. After addition of water, the reaction mixture was extracted with DCM (3x) and dried over $MgSO_4$. Column chromatography (9.5/0.5 → Hex/Tol) gave **98** a white solid (193 mg, 49 %, 0.26mmol).

^{1}H NMR (300 MHz, THF) δ [ppm] = 7.16 – 7.02 (m, 8H), 6.93 (d, *J* = 8.3 Hz, 4H), 6.86 (d, *J* = 8.3 Hz, 4H), 1.22 (pd, 36 H), -0.50 (s, 9H).

^{13}C NMR (75 MHz, THF) δ [ppm] = 150.52, 150.12, 149.22, 142.78, 140.68, 139.84, 137.47, 131.96, 130.86, 127.47, 124.40, 124.04, 34.79, 34.77, 31.50, 31.48, 3.26.

MS (FD, 8 kV) *m/z* obsvd for $C_{49}H_{61}BrSi$ [M^+]: 757.8. (calcd. 758.4).

Elemental Analysis for $C_{49}H_{61}BrSi$: found C, 77.82% (calcd. C, 77.64); H, 8.11 (H, 8.32).

Mp: > 300 °C.

6.2.38. Synthesis of (1's,4's)-4-bromo-4'-(4-bromophenyl)-3',5',6'-triphenyl-1',4'-dihydro-[1,1':2',1''-terphenyl]-1',4'-diol (**100**)

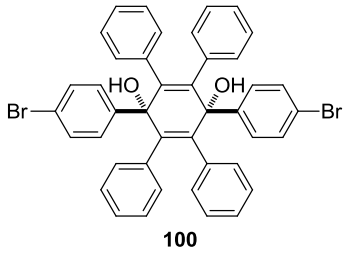

100

$C_{42}H_{30}Br_2O_2$
m.w.: 726,49 g/mol

1,4-dibromobenzene (9.26 g, 39.3 mmol, 1 eq.) was dissolved in THF (200 mL) and cooled down to –78 °C. After addition of *n*-BuLi (25.6 mL, 39.3 mmol, 1 eq.), the reaction mixture was stirred for 30 min. Then, a suspension of 2,3,5,6-*Tetrakis*(phenyl)benzodiquinone[135] (2.70 g, 6.54 mmol, 6 eq.) in THF (30 mL) was slowly added. The reaction was stirred for 2h, warmed to r.t. and stirred overnight. The crude product was purified by column chromatography (6:4 dichloromethane/hexane → dichloromethane → 8:2 Hex/EtOAc) to give **100** (2.9 g, 3.99 mmol, 61%) as a white solid.

^{1}H NMR (300 MHz, CD_2Cl_2) ^{1}H NMR (300 MHz, CD_2Cl_2) δ [ppm] =7.41 (d, *J* = 8.8 Hz, 4H), 7.29 (d, *J* = 8.5 Hz, 4H), 7.01 – 6.86 (m, 12H), 6.87 – 6.75 (m, 8H), 2.66 (s, 2H).

^{13}C NMR (75 MHz, CD_2Cl_2) δ [ppm] = 142.06, 141.05, 137.47, 131.85, 131.19, 129.42, 127.26, 126.82, 121.67, 75.26.

MS (FD, 8 kV) (*m/z*): obsvd. for $C_{42}H_{30}Br_2O_2$ $[M]^+$: 725.4 (calcd. 726.1).

Elemental Analysis: not measured due rapid decomposition of the sample.

Mp: decomposition > 40 °C.

6.2.39. Synthesis of (1's,4's)-4-bromo-4'-(4-bromophenyl)-1',4'-dimethoxy-3',5',6'-triphenyl-1',4'-dihydro-1,1':2',1''-terphenyl (**101**)

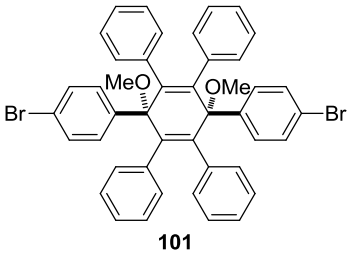

101

$C_{44}H_{34}Br_2O_2$
m.w.: 754,55 g/mol

100 (2.9 g, 3.99 mmol) was dissolved in 30 mL THF and cooled to 0 °C. After 30 min, NaH (0.48 mg, 12.0 mmol) (60% mineral oil) was added and the solution was stirred for another 30 min until MeI (3.4 g, 24.0 mmol) were added. The reaction was stirred at 0 °C for 2 h, then warmed to r.t. and stirred overnight. After quenching with methanol, water was added and the reaction mixture was extracted with Et_2O (3 x) and the combined organic fractions were dried over $MgSO_4$. The crude product was filtered through a short pad of silica (6:4 → Hexan/DCME) to give **101** (2.85 g, 3.78 mmol) as a white solid (95%).

^{1}H NMR (500 MHz, $C_2D_2Cl_4$, 373 K) δ [ppm] = 7.44 (d, *J* = 8.5 Hz, 4H), 7.35 (d, *J* = 8.7 Hz, 4H), 6.91 – 6.80 (m, 12H), 6.72 (dd, *J* = 8.1, 1.4 Hz, 8H), 3.89 (s, 6H).

^{13}C NMR (126 MHz, $C_2D_2Cl_4$,) δ [ppm] = 143.15, 142.55, 138.67, 131.64, 130.87, 130.18, 127.17, 126.71, 121.38, 81.77, 52.70.

MS (FD, 8 kV) (*m/z*): obsd. for $C_{44}H_{34}Br_2O_2$ $[M]^+$: 755.4 (calcd. 754.1).

Elemental Analysis for $C_{44}H_{34}Br_2O_2$: found C, 70.47 (calcd. C, 70.04); H, 4.54 (H, 4.30).

Mp: 292 °C.

6.2.40. Synthesis of 2,2'-((1's,4's)-1',4'-dimethoxy-2',3',5',6'-tetraphenyl-1',4'-dihydro-[1,1':4',1''-terphenyl]-4,4''-diyl)bis(4,4,5,5-tetramethyl-1,3,2-dioxaborolane) (**102**)

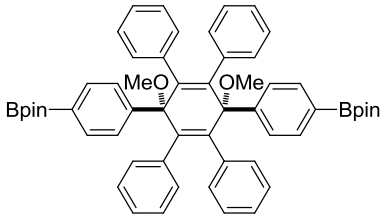

102

$C_{56}H_{58}B_2O_6$
m.w.: 848.68 g/mol

101 (1.3 g, 1.72 mmol, 1 eq.), B_2Pin_2 (3.78 g, 5.17 mmol, 3 eq.), KOAc (3.38 g, 34.4 mmol, 20 eq.), and $Pd(dppf)Cl_2$ (76 mg, 0.10 mmol, 10mol%) were dissolved in dioxane (15 mL). The reaction was heated to 80 °C and stirred for 24 h. After completion, the crude product was extracted with Et_2O (3x) and the combined organic fractions were dried over $MgSO_4$. After removal of solvent until complete dryness, the crude product was recrystallized from hexane/MeOH to give **102** (1.30 g, 1.53 mmol, 89%) as a white solid.

^{1}H NMR (500 MHz, $C_2D_2Cl_4$, 373 K) δ[ppm] = 7.63 (s, 1H), 6.90 – 6.77 (m, 1H), 6.72 (d, *J* = 6.9 Hz, 1H), 3.91 (s, 1H), 1.36 (s, 1H).

^{13}C NMR (126 MHz, $C_2D_2Cl_4$, 373 K) δ [ppm] = 145.66, 142.59, 138.55, 133.56, 131.22, 127.20, 126.35, 125.79, 83.50, 81.70, 52.01, 24.77.

MS (FD, 8 kV) (*m/z*): obsvd. for $C_{56}H_{58}B_2O_6$ $[M]^+$ = 848.0 (calcd. 848.4).

Elemental Analysis for $C_{56}H_{58}B_2O_6$: found C, 80.31 (calcd. C, 79.25); H, 6.89 (H, 7.35).

Mp: 300 °C.

X-ray crystal structure: CCDC *1028408*. These data can be obtained from The Cambridge Crystallographic Data Cente via www.vddc.cam.ac.uk/data_request/cif.

6.2.41. Synthesis of **105**

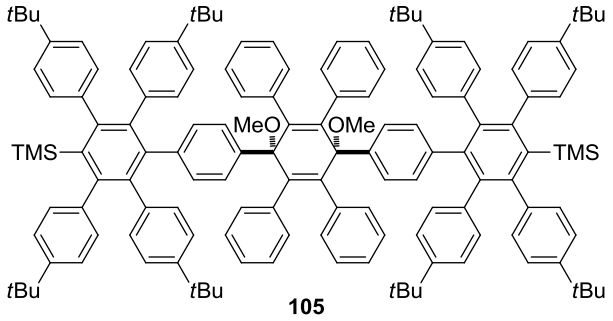

105

$C_{142}H_{156}O_2Si_2$
m.w.: 1950.93 g/mol

98 (200 mg, 0.26 mmol, 1 eq.), diboronate **102** (90 mg, 0.11 mmol, 2.5 eq.) and K_2CO_3 (608 mg, 4.40 mmol, 20 eq.) (3 M) were added to a 25 mL microwave tube. After addition of THF (2 mL), the reaction mixture was heated to 100 °C for 2d under microwave irradiation. The crude product was extracted with DCM (3x) and the combined fractions were dried over $MgSO_4$. The crude product was filtered through a short pad of silica and washed with DCM. The crude product was fully purified by prep. GPC (eluent THF) to give **105** (170 mg, 87.1 µmol, 61%).

^{1}H NMR (500 MHz, $C_2D_2Cl_4$, 373 K) δ [ppm] = 7.26 – 6.62 (m, 50H), 6.40 (d, *J* = 7.1 Hz, 8H), 3.56 (s, 6H), 1.30 (s, 39H), 1.14 (s, 36H), -0.36 (s, 18H).

^{13}C NMR (126 MHz, $C_2D_2Cl_4$, 373 K) δ [ppm] = 148.77, 148.31, 147.21, 141.60, 140.27, 140.10, 139.54, 138.34, 137.97, 137.95, 137.74, 136.16, 131.48, 131.41, 131.33, 130.07, 126.05, 125.32, 122.86, 122.61, 120.23, 81.59, 51.78, 34.01, 33.83, 31.24, 31.18, 3.27.

HR-MS (MALDI) (*m/z*): obsvd. for $C_{142}H_{156}Si_2$ $[M]^+$: 1950.1684 (calcd. 1950.1670).

Mp: > 300 °C.

6.2.42. Synthesis of monokinked dibromide **103**

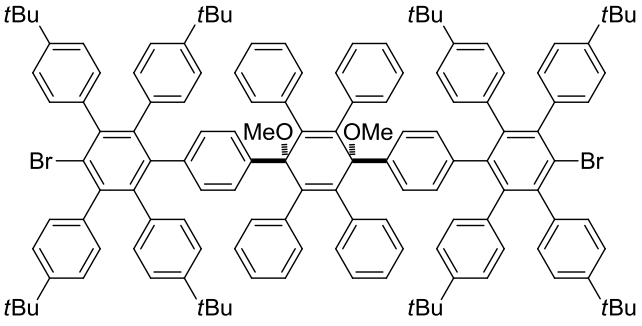

103

$C_{136}H_{138}Br_2O_2$
m.w.: 1964.36 g/mol

97 (100 mg, 0.14 mmol, 4 eq.), **102** (28 mg, 0.033 mmol, 1 eq.) and Cs_2CO_3 (215 mg, 0.66 mmol, 20 eq.) (3 M) were added to a 25 mL Schlenk tube. After addition of toluene (8 mL), the reaction mixture was heated to 95 °C and stirred for 2 d. The crude product was extracted with DCM (3x) and the combined fractions were dried over $MgSO_4$. The crude product was filtered through a short pad of celite and washed with DCM. The crude product was fully purified by preparative GPC (eluent THF) to give **103** (42 mg, 21.4 µmol, 65%).

^{1}H NMR (500 MHz, $C_2D_2Cl_4$, 373 K) δ [ppm] = 7.16 (d, *J* = 8.6 Hz, 8H), 7.01 (d, *J* = 8.4 Hz, 8H), 6.90 (d, *J* = 8.6 Hz, 8H), 6.85 (t, *J* = 7.4 Hz, 4H), 6.76 (t, *J* = 7.7 Hz, 8H), 6.72 (d, *J* = 7.2 Hz, 8H), 6.59 (m, *J* = 11.2, 8.8 Hz, 8H), 6.47 (d, *J* = 7.4 Hz, 8H).

^{13}C NMR (126 MHz, $C_2D_2Cl_4$, 373 K) δ [ppm] = 149.53, 148.61, 142.90, 142.61, 142.40, 139.81, 139.51, 139.42, 138.89, 138.69, 137.88, 132.03, 131.52, 130.90, 130.76, 127.03, 126.60, 126.14, 125.05, 124.08, 123.50, 82.16, 52.37, 34.68, 34.47, 31.77, 31.65.

HR-MS (MALDI) (*m/z*) = obsvd. for $C_{136}H_{138}Br_2O_2$ [M^+]: 1963.9097 (calcd. 1963.9086).

Mp: > 300 °C.

6.2.43. Synthesis of dikinked diboronate **104**

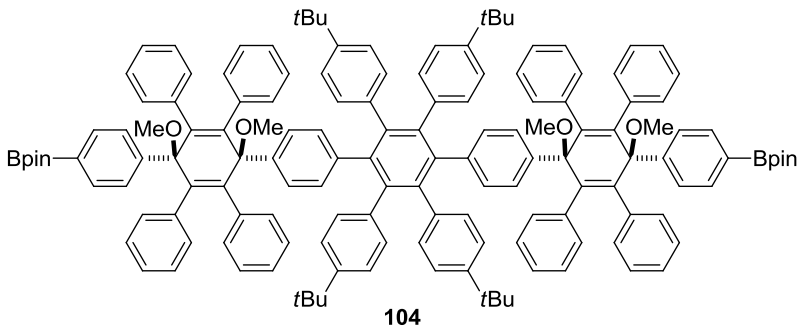

104

$C_{146}H_{144}B_2O_8$

m.w.: 2048.32 g/mol

97 (110 mg, 0.14 mmol, 1 eq.), **102** (732 mg, 0.86 mmol, 6 eq.) and Cs_2 CO_3 (5.63g, 17.3 mmol, 20 eq.) (3 M) were added to a 25 mL Schlenk tube. After addition of toluene (6 mL), the reaction mixture was heated to 95 °C and stirred for 2 d. The crude product was extracted with DCM (3x) and the combined fractions were dried over $MgSO_4$. The crude product was filtered through a short pad of celite and washed with DCM. The crude product was fully purified by preparative GPC (eluent THF) to give **104** (114 mg, 56.0 µmol, 40%).

^{1}H NMR (500 MHz, $C_2D_2Cl_4$) δ [ppm] = 7.43 (d, *J* = 8.0 Hz, 4H), 7.33 (d, *J* = 7.9 Hz, 4H), 6.88 (t, *J* = 8.2 Hz, 14H), 6.82 (dd, *J* = 9.5, 6.8 Hz, 14H), 6.79 – 6.74 (m, 10H), 6.69 (dd, *J* = 17.2, 7.6 Hz, 16H), 6.57 (d, *J* = 7.4 Hz, 8H), 3.88 (s, 6H), 3.66 (s, 6H), 1.34 (s, 24H), 1.13 (s, 36H).

^{13}C NMR (126 MHz, $C_2D_2Cl_4$) δ [ppm] = 148.10, 146.12, 143.39, 142.20, 141.25, 140.36, 139.45, 139.36, 139.20, 138.90, 138.68, 134.07, 132.13, 131.78, 131.35, 127.51, 126.86, 126.73, 126.23, 126.16, 123.46, 84.02, 82.20, 82.15, 74.62, 74.40, 74.18, 52.52, 52.46, 34.43, 31.77, 25.37.*

**C-13 shits for the unsymmetric 1,4-dimethoxycyclohexadiene not strong, thus isochromy of peaks can occur: 19-20 (theoretically). Detected 21.*

HR-MS (MALDI) *m/z* obsvd. for $C_{146}H_{144}B_2O_8$ = 2048.1080 (calcd. 2048.1098).

Elemental Analysis for $C_{146}H_{144}B_2O_8$ found C, 84.9 (calcd. C, 85.61); H, 8.49 (H, 7.09).

Mp: 290 °C.

6.2.44. Synthesis of triangular macrocycle **83**

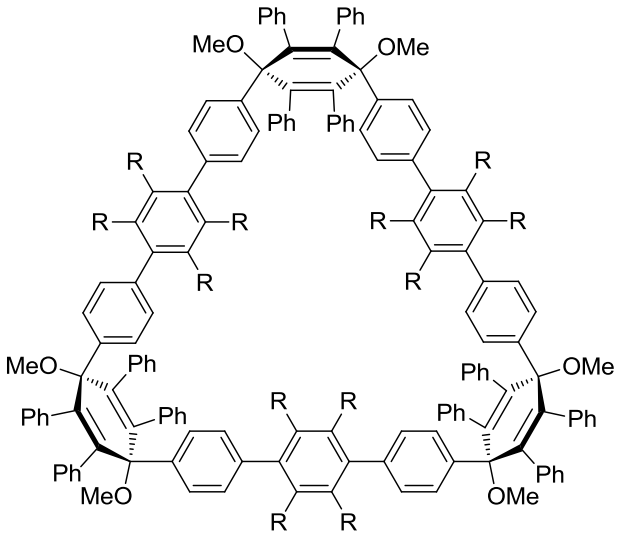

83

$C_{270}H_{258}O_6$

m.w.: 3598.93 g/mol

Dikinked diboronate **103** (18.2 mg, 8.9 µmol, 1 eq.), monokinded dibromide (17.5 mg, 8.9 µmol, 1 eq.) and Cs_2CO_3 (116 mg, 0.36 mmol, 40 eq.) (3 M) were added to a 25 mL Schlenk tube. After addition of toluene (5 mL, 2 mM), the reaction mixture was heated to 95 °C and stirred for 2 d. The crude product was extracted with DCM (3x) and the combined fractions were dried over $MgSO_4$. The crude product was filtered through a short pad of celite and washed with DCM. The crude product was fully purified by recycling GPC (eluent chloroforom) to give **83** (10.2 mg, 2.85 µmol, 32%).

^{1}H NMR (700 MHz, $C_2D_2Cl_4$, 333 K) δ [ppm] = 7.21 (d, *J* = 8.6 Hz, 6H), 7.09 (d, *J* = 9.0 Hz, 6H), 6.86 (d, *J* = 7.6 Hz, 24H), 6.81 (s, 24H), 6.75 (t, *J* = 7.3 Hz, 14H), 6.72 (d, *J* = 8.2 Hz, 6H), 6.61 (t, *J* = 7.6 Hz, 24H), 6.38 (d, *J* = 8.1 Hz, 6H), 6.34 (d, *J* = 7.8 Hz, 24H), 3.52 (s, 28H), 1.04 (s, 108H).

^{13}C NMR (176 MHz, $C_2D_2Cl_4$, 333 K) δ [ppm] = 147.68, 142.26, 141.34, 138.48, 138.40, 132.03, 131.67, 126.84, 123.41, 31.91.

HR-MS (MALDI) (*m/z*) = obsvd. for $C_{270}H_{258}O_6$ [M^+]: 3598.0038 (calcd. 3598.9946).

Mp: > 300 °C.

COSY (500 MHz, $C_2D_2Cl_4$, 353 K):

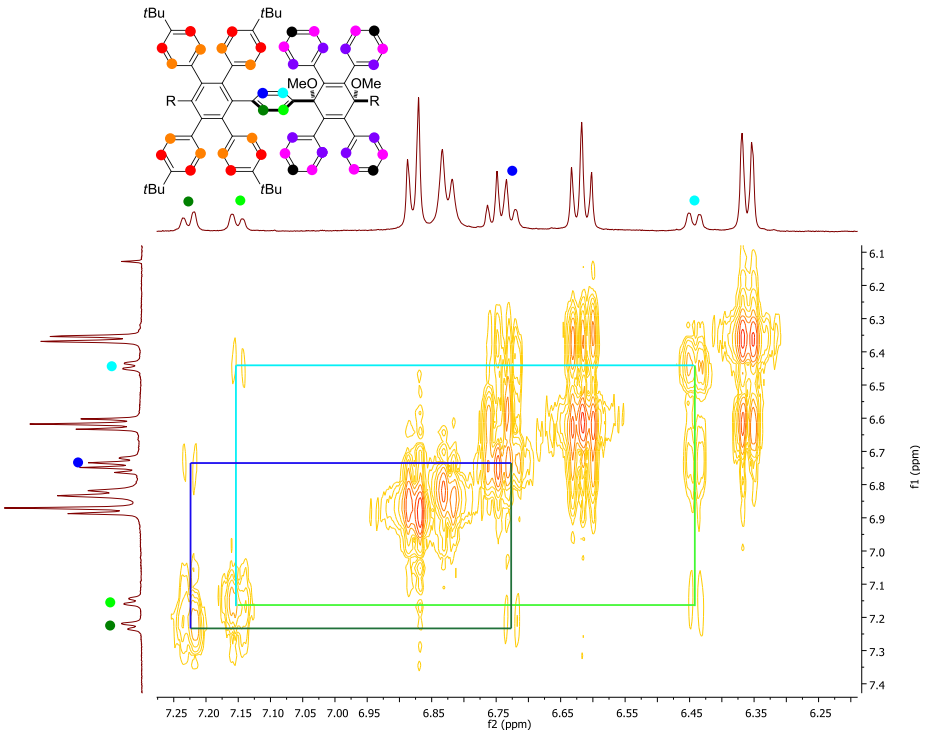

NOESY (500 MHz, $C_2D_2Cl_4$, 353 K)

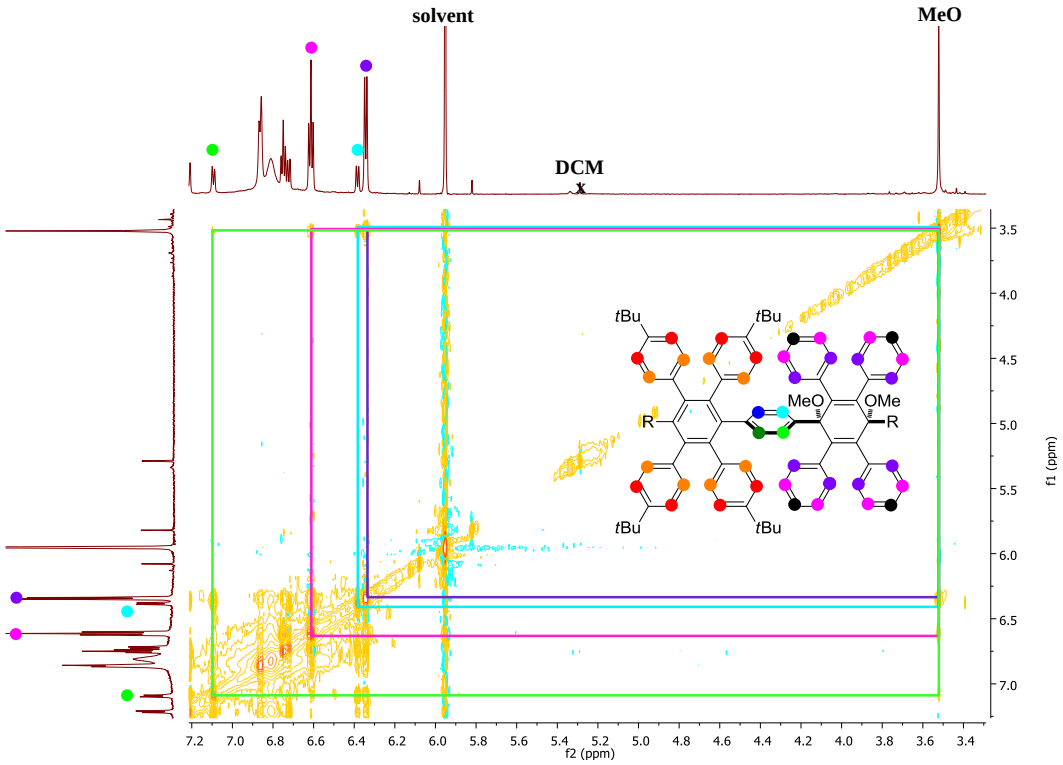

6.2.45. Synthesis of a C_2 symmetric cyclohexadiene macrocycle **108**

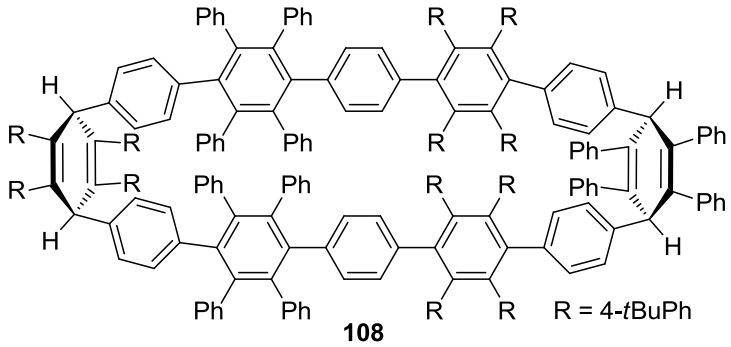

108

$C_{264}H_{244}$
m.w.: 3416.76 g/mol

83 (4 mg, 1.1 µmol, 1 eq.) were dissolved in THF (2 mL) and cooled to – 78 °C. Sodium napthalide (0.06 mL, 55.0 µmol, 50 eq.) in THF (1 M) was slowly added. Upon addition, the reaction color turned blue. The reaction solution was stirred at – 78 °C for 1 h and MeOH (0.5 mL) was added. The colorless reaction solution was warmed to r.t.. After addition of water, the crude product was extracted with DCM (3x) and the combined fraction were dried over Na_2SO_4. The solvent was removed under *vacuo* and the product was purified by preparative GPC (THF). **108** (1.8 mg, 0.53 µmol,48%) was obtained as a white solid.

HR-MS (MALDI) (*m/z*) = obsv. for $C_{264}H_{244}$ [M^+]: 3415.9072 (calcd. 3415.9154).

X-ray CCDC *1033267*. These data can be obtained from The Cambridge Crystallographic Data Centre via www.vddc.cam.ac.uk/data_request/cif.

Mp: > 300 °C.

6.2.46. Congested Cyclic Hexaphenylbenzene Hexamer **84**

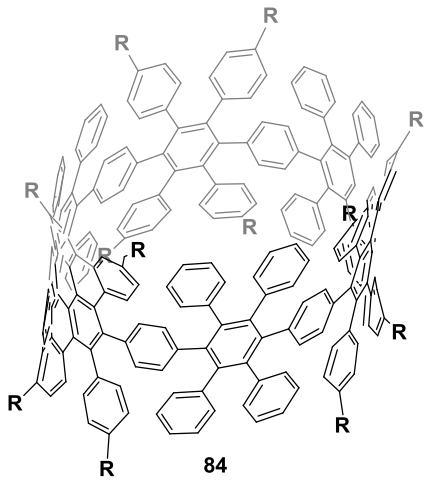

To $TiCl_4$ (0.054 ml, 0.50 mmol, 600 eq.) was added THF (10 mL) at 0 °C under argon atmosphere and stirred for 30 min at ambient temperature. After cooling to 0 °C again, a solution of $LiAlH_4$ in THF (1.00 ml, 2.0 M, 2.00 mmol, 2400 eq.) was added and stirred for 1h at 80 °C to generate low-valent titanium. A solution of **83** (3 mg, 0.83 µmol, 1 eq.) in THF (3 ml) was added and stirred for 3d at same temperature under absence of light. After cooling to 0 °C, the reaction was quenched by water and 2 M hydrochloric acid (Caution! Excess amount of unreacted $LiAlH_4$ explosively generate hydrogen gas by addition of water. Therefore, at first, a large glass adaptor or glass trap should be equipped with top of the reactor and several drops of water were slowly added to the reaction and extracted with dichloromethane. After filtration over celite, the organic layer was washed with water and brine, and dried over Na_2SO_4. After removing solvent in *vacuo*, the crude product was subjected to preparative GPC (THF) to give **84** (1.3 mg, 38.1 µmol, 46%)

^{1}H NMR (500 MHz, C2D2Cl4) δ [ppm] = 6.75 (t, 4H), 6.71 (d, J = 7.2 Hz, 8H), 6.65 (t, J = 6.7 Hz, 8H), 6.56 (d, J = 7.1 Hz, 8H), 6.44 (d, J = 7.3 Hz, 8H), 6.36 (d, J = 7.3 Hz, 4H), 6.22 (d, J = 7.2 Hz,
4H), 1.11 (s, 36H).

^{13}C NMR (126 MHz, C2D2Cl4) δ [ppm] = 131.75, 131.29, 130.22, 126.41, 123.06, 31.40.

HR-MS (MALDI) (*m/z*) = obsvd. for $C_{264}H_{240}$ [M^+]: 3411.8819 (calcd. 3411.8842).

Mp: > 300 °C.

6.2.47. Synthesis of **Ex1**

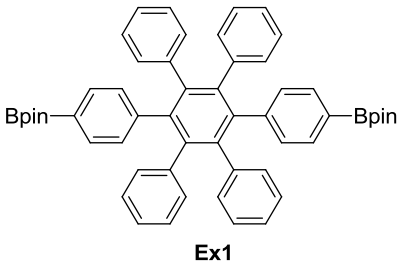

Ex1

$C_{54}H_{52}B_2O_4$
m.w.: 786,61 g/mol

„1,4"-dibromohexaphenylbenzene (1.00 g, 1.44 mmol, 1 eq.), B_2Pin_2 (0.88 mg, 3.46 mmol, 2.4 eq.), KOAc (2.83g, 28.8 mmol, 20 eq.), and Pd(dppf)Cl_2 (0.021 mg, 0.03 mmol, 10mol%) were dissolved in dioxane. The reaction was heated to 80 °C and stirred for 24 h. After completion, the crude product was extracted with Et_2O (3x) and the combined organic fractions were dried over $MgSO_4$. After removal of solvent until complete dryness, the crude product was recrystallized from hexane/MeOH to give **Ex1** (900 mg, 1.14 mmol, 79%) as a white solid.

^{1}H NMR (500 MHz, $C_2D_2Cl_4$, 373 K) δ [ppm] = 7.44 (d, *J* = 8.5 Hz, 4H), 7.35 (d, *J* = 8.7 Hz, 4H), 6.91 – 6.80 (m, 12H), 6.72 (dd, *J* = 8.1, 1.4 Hz, 8H), 3.89 (s, 6H).

^{13}C NMR (126 MHz, $C_2D_2Cl_4$) δ [ppm] = 143.15, 142.55, 138.67, 131.64, 130.87, 130.18, 127.17, 126.71, 121.38, 81.77, 52.70.

MS (FD, 8 kV) *m/z* obsvd. for $C_{54}H_{52}B_2O_4$ $[M]^+$ = 786.8 (calcd. 786.4).

6.2.48. Synthesis of **Ex1**

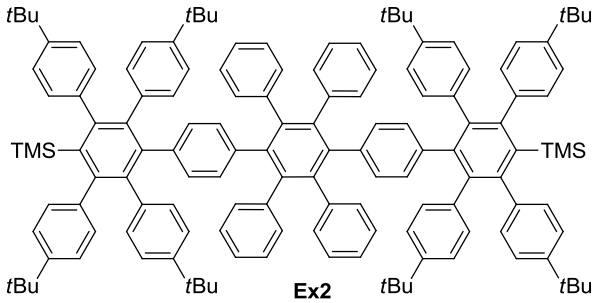

Ex2

$C_{140}H_{150}Si_2$
m.w.: 1888,86 g/mol

1-bromo-4-Tms -(tetraphenyl)benzene **92** (380 mg, 0.5 mmol, 2.2 eq), 1,4-bisboronate **Ex1** (180 mg, 0.23 mmol, 1 eq.), $Pd(PPh_3)_4$ (58 mg, 3.8 µmol, 10 mol%), aq. K_2CO_3 (650 mg, 4.60 mmol, 20 eq.) (3 M) were given in a flask and toluene (3 mL) was added. The reaction mixture was heated to 95 °C and stirred for 3 d. The crude product was extracted with DCM (3x) and the combined organic fractions were dried over $MgSO_4$. The crude product was purified by column chromatography (6:4 hex/dcM) to give 102 (65 mg, 0.034 mmol, 65%) as a white solid

^{1}H NMR (300 MHz, THF) δ [ppm] = 7.02 (d, *J* = 8.4 Hz, 8H), 6.94 – 6.85 (m, 16H), 6.80 – 6.66 (m, 12H), 6.53 (d, *J* = 8.3 Hz, 8H), 6.36 (dd, *J* = 7.8, 1.4 Hz, 8H), 6.26 (d, *J* = 8.4 Hz, 4H), 5.97 (d, *J* = 8.4 Hz, 4H), 1.18 (d, *J* = 3.2 Hz, 72H), -0.53 (s, 18H).

^{13}C NMR (75 MHz, THF) δ [ppm] = 149.70, 149.33, 148.02, 141.84, 141.41, 141.31, 141.24, 141.16, 140.55, 139.07, 137.74, 137.65, 136.85, 132.56, 132.50, 132.41, 130.95, 130.73, 127.36, 125.36, 123.92, 123.60, 34.89, 34.76, 31.75, 31.66, 3.69.

MS (FD, 8 kV) *m/z* obsvd. for $C_{140}H_{150}Si_2$ $[M]^+$ = 1888.2 (calcd. 1888.1).

Elemental Analysis for $C_{140}H_{150}Si_2$: meas. C, 88.26% (calcd. C, 89.02%); H, 8.19% (H, 8.00%).

Melting Point: > 300 °C.

6.2.49. Synthesis of **Ex3**

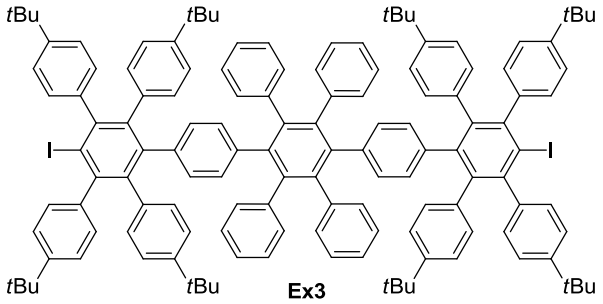

Ex3

$C_{134}H_{132}I_2$

m.w.: 1996,29 g/mol

BisTMS-Trimer **Ex2** (55 mg, 29.1 µmol, 1 eq.) was dissolved in DCM (7 mL) and cooled down to 0 °C. Fresh ICl (0.12 mL, 116 µmol, 4 eq.) (1 M) was added dropwise and the reaction mixture was stirred for 2 h at 0 °C. Then, the reaction was quenched with an aq. $Na_2S_2O_3$ solution and the crude product was extracted with DCM (3x) and the combined

fractions were dried over $MgSO_4$. Column chromatography (hexane/DCM -> 7:3) gave **Ex3** (50 mg, 25.0 µmol 86%) as a white solid.

^{1}H NMR (300 MHz, THF) δ [ppm] = 7.09 (d, *J* = 8.4 Hz, 8H), 6.94 – 6.78 (m, 28H), 6.54 – 6.41 (m, 16H), 6.18 (d, *J* = 8.4 Hz, 4H), 6.03 (d, *J* = 8.4 Hz, 4H), 1.20 (s, 36H), 1.18 (s, 36H).

^{13}C NMR (75 MHz, THF) δ [ppm] =149.45, 148.41, 147.22, 143.79, 141.88, 141.67, 141.09, 140.57, 140.30, 138.84, 137.79, 136.74, 132.41, 131.74, 131.01, 130.93, 130.75, 127.20, 125.45, 124.28, 123.72, 106.85, 34.77, 34.60, 31.51, 31.46.

MS (FD, 8 kV) *m/z* meas. for$C_{134}H_{132}I_2$ $[M]^+$ = 1995.1 (calcd. 1995.9).

Mp: > 300 °C.

6.2.50. Synthesis of **108**

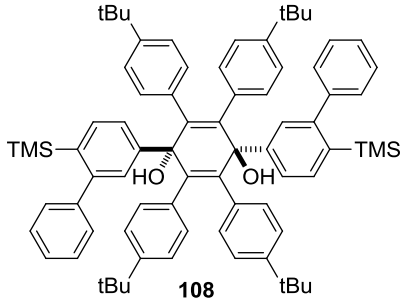

108

$C_{76}H_{88}O_2Si_2$
m.w.: 1089.68 g/mol

15 (5.99 g, 19.6 mmol, 4 eq.) was dissolved in THF (80 mL) and cooled down to – 78 °C. After addition of *n*-BuLi (12.3 mL, 19.6 mmol, 4 eq.), the reaction mixture was stirred for 30 min. Then a precooled solution of 2,3,5,6-Tetrakis(4-tertbutylphenyl)benzodiquinone[3] (2.5 g, 3.93 mmol, 1 eq.) in THF (13 mL) was slowly added. The reaction was stirred for 1 h, warmed to r.t. and stirred overnight. The crude product was purified by column chromatography (6:4 dichloromethane/hexane → 9:1 dichloromethane/hexane) to give **108** (1.93 g, 1.77 mmol, 45%) as a white solid.

^{1}H NMR (300 MHz, CD_2Cl_2) δ [ppm] = 7.59 (s, 2H), 7.50 (d, *J* = 7.8 Hz, 2H), 7.36 – 7.26 (m, 6H), 7.08 (d, *J* = 3.3 Hz, 6H), 6.95 (d, *J* = 8.6 Hz, 8H), 6.73 (d, *J* = 8.3 Hz, 8H), 2.68 (s, 2H), 1.14 (s, 37H), 0.03 (s, 18H).

^{13}C NMR (75.5 MHz, CD_2Cl_2) δ [ppm]: 149.22, 148.98, 144.96, 143.47, 141.05, 137.41, 135.25, 134.29, 131.77, 129.73, 129.28, 127.87, 127.27, 125.55, 123.86, 75.76, 34.48, 31.29, 0.78.

HR-MS (MALDI) (*m/z*): obsvd. for $C_{78}H_{88}O_2Si_2$ [M^+]: 1088.6323 (calcd. 1088.6317).

Elemental Analysis due to decomposition.

Mp: decomposition at 40 °C.

6.2.52. Synthesis of **109**

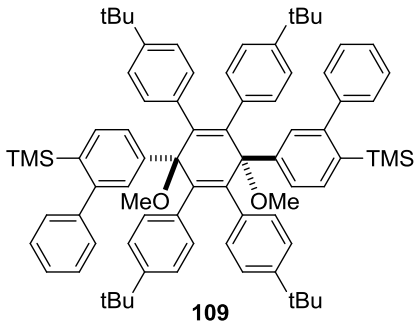

109

$C_{78}H_{92}O_2Si_2$
m.w.: 1117.73 g/mol

108 (2.7 g, 2.47 mmol, 1 eq.) was dissolved in THF (10 mL) and cooled to 0 °C. After 30 min, NaH (60% mineral oil) (173 mg, 7.23 mmol, 3 eq,) was added and the solution was stirred for another 30 min until MeI (2.06 g, 14.5 mmol, 6 eq.) was added. After 2 h, first methanol and then water was added and the reaction mixture was extracted with Et_2O (3 x). The combined organic fractions were dried over $MgSO_4$. The crude product was purified by column chromatography to give **109** (2.2 g, 1.97 mmol, 79%) as a white solid.

^{1}H NMR (500 MHz, $C_2D_2Cl_4$, 373 K) δ [ppm] = 7.63 (s, 2H), 7.32 (d, *J* = 7.7 Hz, 4H), 7.27 (s, 6H), 7.02 (s, 4H), 6.82 (d, *J* = 8.3 Hz, 8H), 6.66 (d, *J* = 8.3 Hz, 8H), 3.87 (s, 6H), 1.13 (s, 36H), -0.02 (s, 18H).

^{13}C NMR (126 MHz, $C_2D_2Cl_4$, 373 K) δ [ppm] = 149.02, 148.54, 145.43, 143.75, 143.14, 136.59, 136.50, 133.72, 131.60, 129.96, 127.71, 127.09, 126.07, 123.52, 82.17, 52.59, 34.41, 31.55, 1.15.

HR-MS (MALDI) (*m/z*) = obsv. for $C_{78}H_{92}O_2Si_2$[M^+]: 1116.6628 (calcd. 1116.6630).

Elemental Analysis for $C_{78}H_{92}O_2Si_2$: meas. C, 83.23% (calcd. C, 83.82%), H, 8.49% (H, 8.30%).

Mp: 108 °C.

6.2.53. Synthesis of **110**

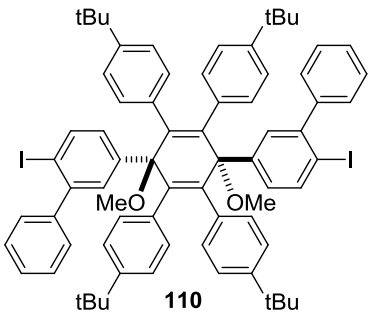

110

$C_{72}H_{74}I_2O_2$
m.w.: 1225.17 g/mol

109 (2 g, 1.63 mmol, 1 eq) and $AgBF_4$ (0.95 g, 4.90 mmol, 3 eq.) were dissolved in a 2:1 mixture of THF mL and methanol (4 mL). The solution was then cooled to 0 °C and ICl (1 M in DCM) (4.9 mL, 4.90 mmol, 3 eq.) was dropwise added. After 40 min, the reaction was quenched with an aq. $Na_2S_2O_3$ solution, extracted with Et_2O (3x) and dried over $MgSO_4$. The solvent was removed *in vacuo* and the crude product was purified by column chromatography (6:4 hexan/dichloromethane) to give **110** (1.70 g, 1.39 mmol, 85%) as a white solid.

^{1}H NMR (500 MHz, $C_2D_2Cl_4$, 373 K) δ [ppm] = 7.70 (d, *J* = 7.2 Hz, 2H), 7.34 (d, *J* = 25.4 Hz, 10H), 7.04 (s, 4H), 6.87 (d, *J* = 8.4 Hz, 8H), 6.67 (d, *J* = 8.4 Hz, 8H), 3.83 (s, 6H), 1.15 (s, 36H).

^{13}C NMR (126 MHz, $C_2D_2Cl_4$, 373 K) δ [ppm]: 149.53, 145.98, 144.70, 143.98, 143.15, 138.60, 135.93, 131.53, 131.06, 129.68, 128.47, 128.04, 127.79, 123.83, 96.47, 81.91, 52.60, 34.48, 31.55.

HR-MS (MALDI) (*m/z*): obsd. for $C_{72}H_{74}I_2O_2[M^+]$: 1224.7 (calcd. 1224.5).

Elemental Analysis for $C_{72}H_{74}I_2O_2$: meas. C 70.87 (calcd. 70.58%), H 6.32% (H 6.09).

Mp: 285 °C.

6.2.54. Synthesis of **111-1**

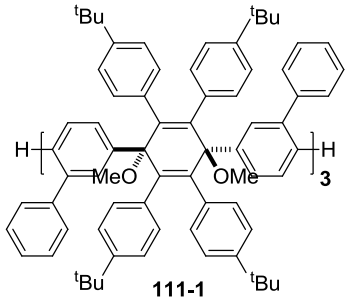

111-1

$C_{216}H_{224}O_6$

m.w.: 2916,09 g/mol

60 (1.6 g, 1.31 mmol, 1 eq.) was dissolved in Et_2O (150 mL) and cooled to – 78 °C. After addition of *t*BuLi (1.7 M) (3.24 mL, 5.50 mmol, 4.2 eq.), the reaction was stirred for 40 min. Then, CuCN (117 mg, 1.31 mmol, 1 eq.) was added and the reaction was stirred for 1.5 h. The reaction was warmed to r.t. and stirred for another 2.5 h until duroquinone (0.64 g, 3.9 mmol, 3 eq.) was added. After 3 h, the reaction mixture was poured into MeOH and the precipitate was collected. The crude mixture was roughly purified by column chromatography (6:4 hexane/dichloromethane) and further purified by precipitation, preparative GPC, and recycling-GPC (eluent: chloroform).

^{1}H NMR (500 MHz, $C_2D_2Cl_4$, 393 K) δ [ppm] = 7.62 – 7.44 (m, 3H), 7.33 – 6.85 (m, 14H), 6.76 (ddd, *J* = 21.5, 15.7, 6.1 Hz, 16H), 6.67 – 6.50 (m, 12H), 6.50 – 6.32 (m, 4H), 3.81 (s, 2H), 3.77 (s, 2H), 3.74 (s, 3H), 1.01 (d, *J* = 8.2 Hz, 36H).*

* the mehtoxy group shows three peaks which is due to unsymmetric nature.

^{13}C NMR (126 MHz, $C_2D_2Cl_4$, 39k3 K) δ [ppm]: ^{13}C NMR (126 MHz, $C_2D_2Cl_4$) δ 149.08, 143.86, 142.34, 142.02, 141.89, 141.77, 140.40, 140.22, 140.18, 138.97, 138.82, 136.37, 131.80, 131.69, 129.75, 128.81, 127.53, 127.36, 126.13, 125.69, 123.69, 82.20, 82.17, 82.08, 74.66, 74.62, 74.40, 74.18, 52.69, 52.66, 52.64, 34.48, 34.43, 33.16, 32.30, 31.64, 31.62, 31.57, 30.07, 29.69.

* three carbon peaks for methoxy group was observed, indicating the trimeric nature of this oligomer.

HR-MS (MALDI) (*m/z*): obsvd. for $C_{216}H_{224}O_6$ $[M+K]^+$: 2951.4 (calcd. 2954.7)

Mp: > 300 °C

6.2.55. Synthesis of **111-2**

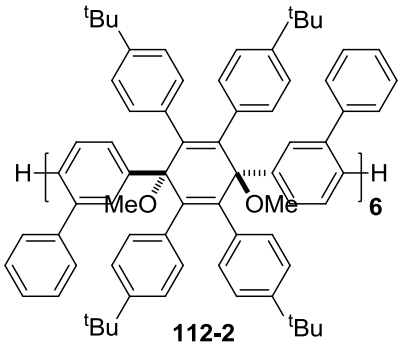

112-2

$C_{432}H_{446}O_{12}$
m.w.: 5830,16 g/mol

Synthesis: see above

^{1}H NMR (500 MHz, $C_2D_2Cl_4$, 353 K) δ [ppm] = ^{1}H NMR (500 MHz, $C_2D_2Cl_4$) δ 7.47 (dd, *J* = 37.7, 8.5 Hz, 1H), 7.10 (m, 2H), 7.25– 6.67 (m, 20H), 6.60 (m, 8H), 6.38 (m, 4H), 3.76 (s, 6H), 1.02 (m, 36H).*
*strong line broadening

^{13}C NMR (126 MHz, $C_2D_2Cl_4$, 353 K) δ [ppm] = 148.67, 139.81, 135.97, 131.37, 129.81, 129.30, 128.37, 127.11, 125.68, 124.58, 123.26, 81.64, 64.92, 52.19, 31.20, 31.14, 29.64.*
* impurities in the alphatic region
MS (MALDI) (*m/z*): obsvd. for $C_{432}H_{446}O_{12}$ [M^+]: 5815.8 (calcd. 5814.4)

Mp: > 300 °C

6.2.56. Synthesis of **111-3**

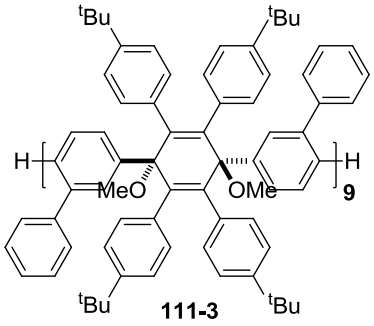

111-3

$C_{648}H_{668}O_{18}$
m.w.: 8744,23 g/mol

^{1}H NMR (500 MHz, $C_2D_2Cl_4$, 393 K) δ [ppm] = 7.70 – 7.08 (m, 6H), 7.05 – 6.77 (m, 16H), 6.70 (s, 8H), 6.49 (s, 4H), 3.85 (s, 6H), 1.20 – 1.04 (m, 36H).*

* peaks for t-butyl and methoxy groups contain several singlets due to unsymmetric built up. See trimer for explantion.

^{13}C NMR (126 MHz, $C_2D_2Cl_4$, 373 K) δ [ppm]: 149.08, 143.11, 142.30, 141.78, 140.22, 138.75, 136.39, 131.77, 129.72, 128.80, 127.53, 126.11, 123.68, 82.07, 52.60, 34.43, 32.30, 31.63, 30.07.*

* an absolute number of peaks cannot be reported due to the unsymmetric nature of the nonamer **111-3**.

MS (MALDI) (*m/z*): obsvd. for $C_{648}H_{668}O_{18}$ $[M\text{-}Me]^+$: 8731.7 (calcd. 8727.1).

Mp: > 300 °C.

6.3. X-ray chrystallographic structures

Details of the crystal data and a summary of the intensity data collection parameters for the following compounds are listed in the corresponding tables. In each case, suitable crystals were measured with STOE IPDS 2T diffractometer. Graphite-monochromated Mo Kα radiation was used. The structures were solved by direct methods with SIR-97 and refined by the full-matrix least-squares techniques against *F*2 (SHELXL-97). The intensities were corrected for Lorentz and polarization effects. The non-hydrogen atoms were refined anisotropically. Hydrogen atoms were refined using the riding model. The crystals structures were visualized using Mercury 3.3.

6.3.1. Crystal structures **25** *and* **38**

X-ray structure of **25**: CCDC *966738*. These data can be obtained from The Cambridge Crystallographic Data Cente *via* http://www.vddc.cam.ac.uk/data_request/cif.

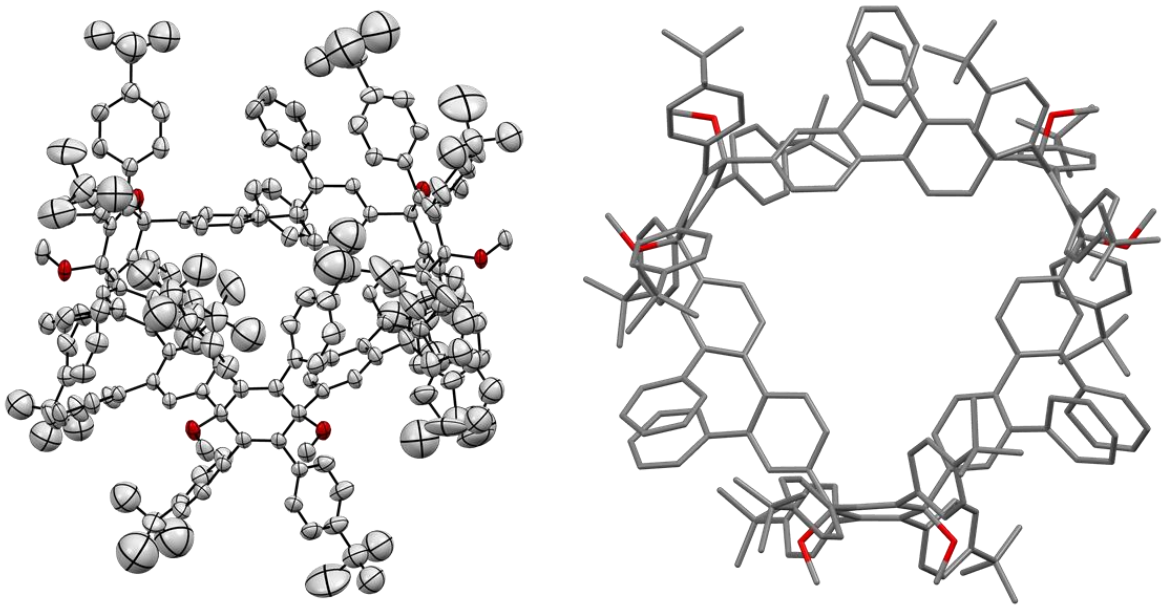

Figure 65: X-ray crystal structure of **25**. ORTEP drawing (left, front view) and wireframe model (right, top view). Hydrogen atoms and solvent molecules are omitted for clarity. Oxygen atoms are labeled in red.

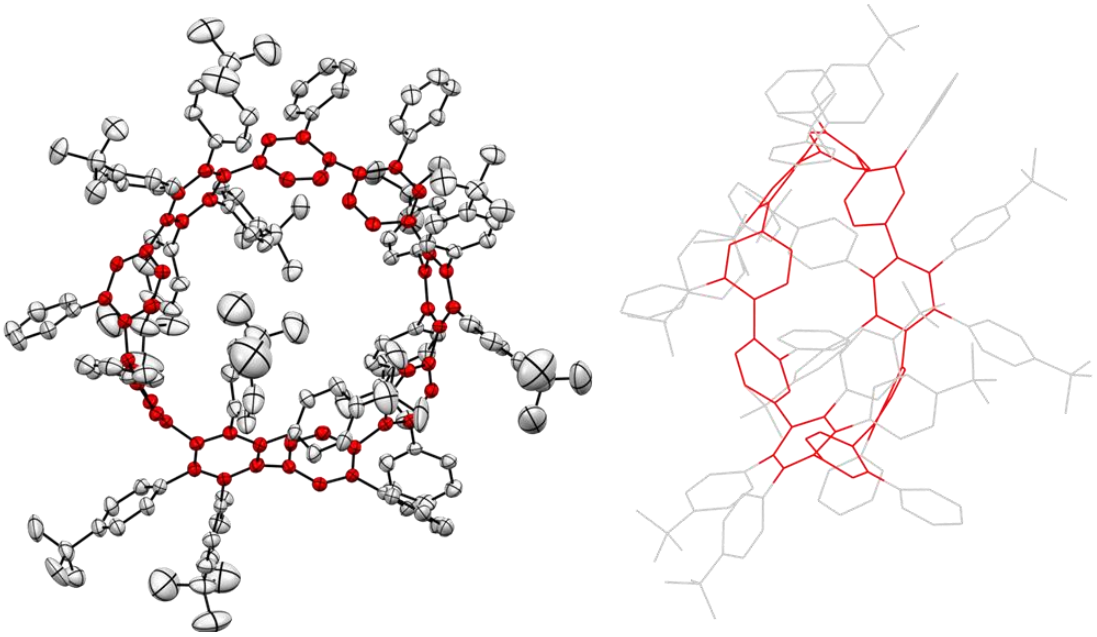

Figure 66: X-ray crystal structure of **38**. ORTEP drawing (left, front view) and wireframe model (right, top view). Hydrogen atoms and solvent molecules are omitted for clarity. The CPP ring is labeled in red.

Table S1: Crystallographic data and structure refinement details of **38** were obtained from dichloromethane/MeCN.

Compound	**38**	**25**
Molecular Formula	$C_{210}H_{204}$, $6CH_3CN$,$6CH_2CL_2$, H_2O	$C_{216}H_{222}O_6$, $4CH_2Cl_2$, $2H_2O$
Formula Weight	3322.7 $gmol^{-1}$	3216.76
Crystal Dimensions	0.2 x 0.2 x 0.4 mm	0.26 x 0.53 x 0.53 mm^3
Crystal color	colorless	Colorless
Crystal System	triclinic	monoclinic
Space Group	P -1	C 2/c
a	19.8160(7) Å	17.1642 (4) Å
b	21.5746(8) Å	38.0798(6) Å
c	26.3970(10) Å	35.9060 (8) Å
α	109.463(3)°	90.00
β	97.728(3)°	102.510(2)
γ	91.313(3)°	90.00
Cell Volume	10516.0(7) $Å^3$	22911.3(8) $Å^3$
Z value	2	4
$D_{calc.}$	1.049 gcm^{-3}	0.933 gcm^{-3}
F (000)	3538	6872.0
Temperature	-80 °C	-80 °C
Total number of Reflections	111671	97420
Unique number of Reflections (R_{int})	50418 (0.1313)	27616 (0.088)
Observed number of Reflections	12837	11357
Residuals: R_1 (I>2.00σ(I))	0.1030	0.1178
Residuals: R_1 (All Reflections)	0.2555	0.1896
wR_2 (All Reflections)	0.3059	0.3708
Goodness of Fit	0.781	1.038
Max Shift / Error	0.001 * e.s.d	0.001 * e.s.d.
Remark	Structure contains solvent molecules (CH_3CN, CH_2Cl_2) which are strongly disordered. The electron density was partially modulated with SQUEEZE.	Structure contains disordered solvent molecules that could not be localized. The Electron density was modulated with SQUEEZE.

A and B alerts in the checkCIF program were detected because (1) two dichloromethane molecules in the cavity of compound **38** are disordered and checkCIF program falsely recognized these two dichloromethanes as four molecules, resulting in Z value = 1 in spite of the crystal system being triclinic P -1; (2) *tert*-butyl groups were rotated; (3) many recrystallized solvents not only dichloromethane and acetonitrile but also water were included in the packing structure.

6.3.2. Crystal Structure of **76**

X-ray Crystal Structure of **76**: CCDC 1028674. These data can be obtained from The Cambridge Crystallographic Data Cente via www.vddc.cam.ac.uk/data_request/cif.

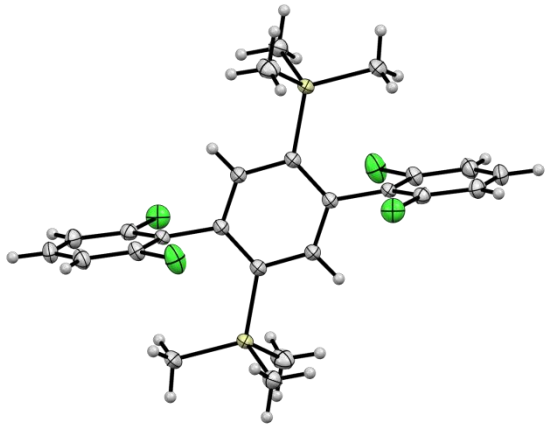

Table 1: Crystallographic data and structure refinement details **76**. Single crystals of **76** were obtained from DCM.

Compound	**76**
Molecular Formula	$C_{12}H_{13}Cl_2Si_1$
Formula Weight	256.23 $gmol^{-1}$
Crystal Dimensions	0.11x 0.16x 0.41 mm
Crystal color	clorless
Crystal System	triclinic
Space Group	P-1
a	8.1295(8)Å
b	8.2495(5)Å
c	11.1056(9)Å
α	81.138(4)Å
β	81.393(3)Å
γ	61.616(4)Å
Cell Volume	644.92(9) $Å^3$
Z value	2
$D_{calc.}$	1.32gcm^{-3}
Temperature	120 K
Total number of Reflections	8134
Unique number of Reflections (R_{int})	4083 (0.0006)
Observed number of Reflections	3340
Residuals: R_1 (I>2.00σ(I))	0.037
wR_2 (All Reflections)	0.042
Goodness of Fit	1.053
Max Shift / Error	0.0139

6.3.3. Crystal structure of **98.**

X-ray crystal structure of **98**. CCDC *1033268*. These data can be obtained from The Cambridge Crystallographic Data Cente *via* www.vddc.cam.ac.uk/data_request/cif.

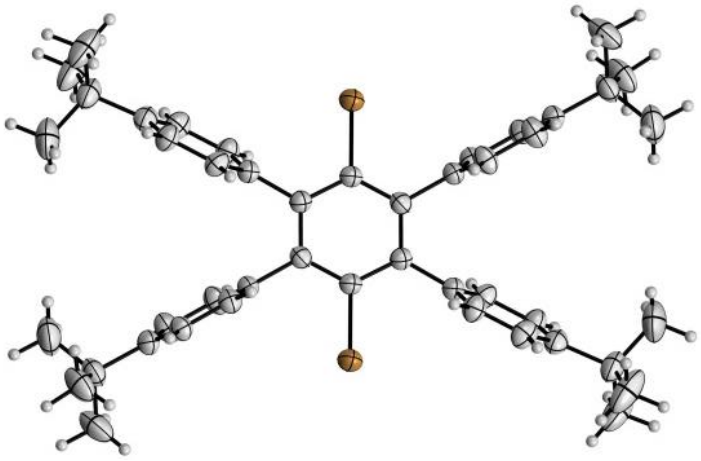

Figure 67: Crystal structure of compound **98**

Table 2: Crystallographic data and structure refinement details of **98**. Single crystals of **98** were obtained from DCM

Compound	**98**
Molecular Formula	$C_{46}H_{52}Br_2$
Formula Weight	764.69 $gmol^{-1}$
Crystal Dimensions	0.13 x 0.16 x 0.16 mm^3
Crystal color	colorless
Crystal System	monoclinic
Space Group	P 2_1/c
a	12.9767(9)Å
b	10.3514(6)Å
c	15.6662(9)Å
α	
β	ß = 105.739(5)°
γ	
Cell Volume	V = 2025.5(2)$Å^3$
Z value	2
$D_{calc.}$	1.254 gcm^{-3}
F (000)	796
Temperature	- 60 °C
Total number of Reflections	13702
Unique number of Reflections (R_{int})	4974 (0.052)
Observed number of Reflections	3376
Residuals: R_1 (I>2.00σ(I))	0.0383
Residuals: R_1 (All Reflections)	0.0726
wR_2 (All Reflections)	0.1010
Goodness of Fit	1.021
Max Shift / Error	0.001 * e.s.d

6.3.4 Crystal structure of **102**

X-ray crystal structur of **102**. CCDC *1028408.* These data can be obtained from The Cambridge Crystallographic Data Cente via www.vddc.cam.ac.uk/data_request/cif.

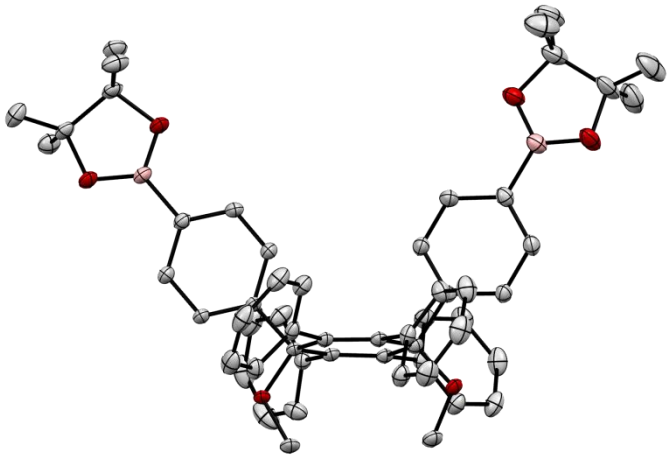

Figure 68: crystal structure of compound **102**.

Table 3: Crystallographic data and structure refinement details of **102**. Single crystals of **102** were obtained from DCM

Compound	**102**
Molecular Formula	$C_{56}H_{58}B_2O_6$
Formula Weight	848.86
Crystal color	colorless
Space Group	P-1
a	11.7260(3)
b	13.9324(4)
c	17.6031(4)
α	83.1779(15)
β	84.3768(15)
γ	70.1442(11)
Cell Volume	2680.60(12)
Z value	2
$D_{calc.}$	1.051 gcm^{-3}
F (000)	904.0
Temperature	120 K
Total number of Reflections	15600
Unique number of Reflections (R_{int})	11206
Observed number of Reflections	10129
Residuals: R_1 (I>2.00σ(I))	0.0632
wR_2 (All Reflections)	0.0732
Goodness of Fit	1.089

6.3.5 Crystal Structure of **108**

X-ray crystal structure: CCDC 1033267. These data can be obtained from The Cambridge Crystallographic Data Cente via www.vddc.cam.ac.uk/data_request/cif.

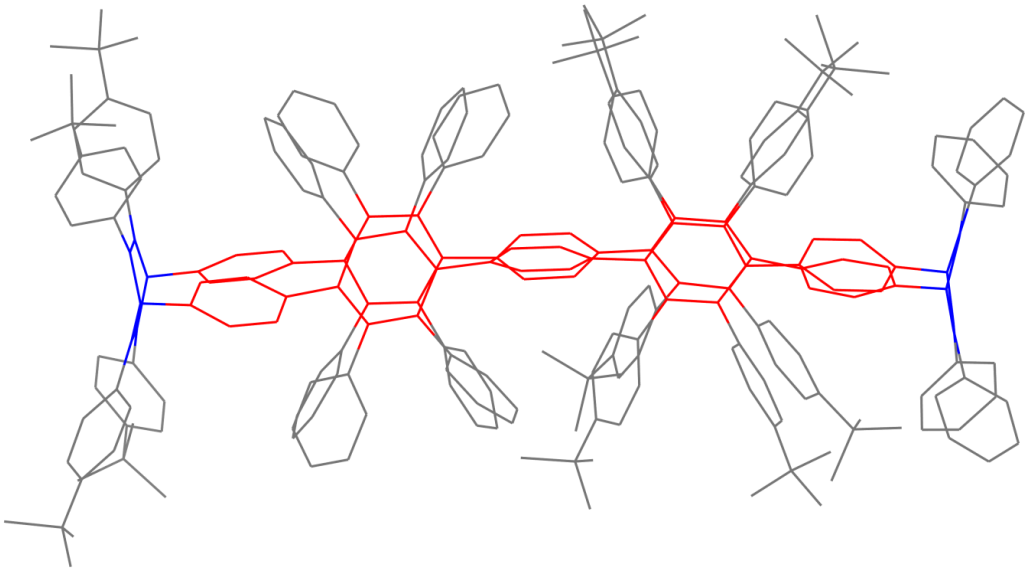

Figure 69: X-ray crystal structure of **108** in wireframe model (side view). Hydrogen atoms and solvent molecules are omitted for clarity. Pentaphenylenes are labeled in red, whereas the bridging cyclohexadiene units are labeled in blue.

Table S3: Crystallographic data and structure refinement details of **108**. Single crystals of **108** were obtained from dichloromethane/MeCN

Compound	**108**
Molecular Formula	$C_{264}H_{244}$+mCH_2CL_2+nCH_3CN+k*H_2O
Formula Weight	3416 $gmol^{-1}$
Crystal Dimensions	0.12 x 0.38 x 0.6 mm^3
Crystal color	Colorless
Crystal System	P 21/n
Space Group	monoklin
a	16.1937(15)Å
b	43.708(4)Å
c	33.799(3)Å
α	
β	92.792(1)°
γ	
Cell Volume	23894(7)$Å^3$
Z value	4
$D_{calc.}$	1.144 gcm^{-3}
F (000)	8704
Temperature	100 °C
Total number of Reflections	261715
Unique number of Reflections (R_{int})	56067 (0.1513)
Observed number of Reflections	21529
Residuals: R_1 (I>2.00σ(I))	0.1421
Residuals: R_1 (All Reflections)	0.2912
wR_2 (All Reflections)	0.3803
Goodness of Fit	1.675
Max Shift / Error	0.0001 * e.s.d.
Remark	Structure is disordered. Solvent molecules are disordered and amount of solvent could not be determined.

6.4 NMR Spectra

6.4.1. ^{1}H-NMR spectrum of **83**

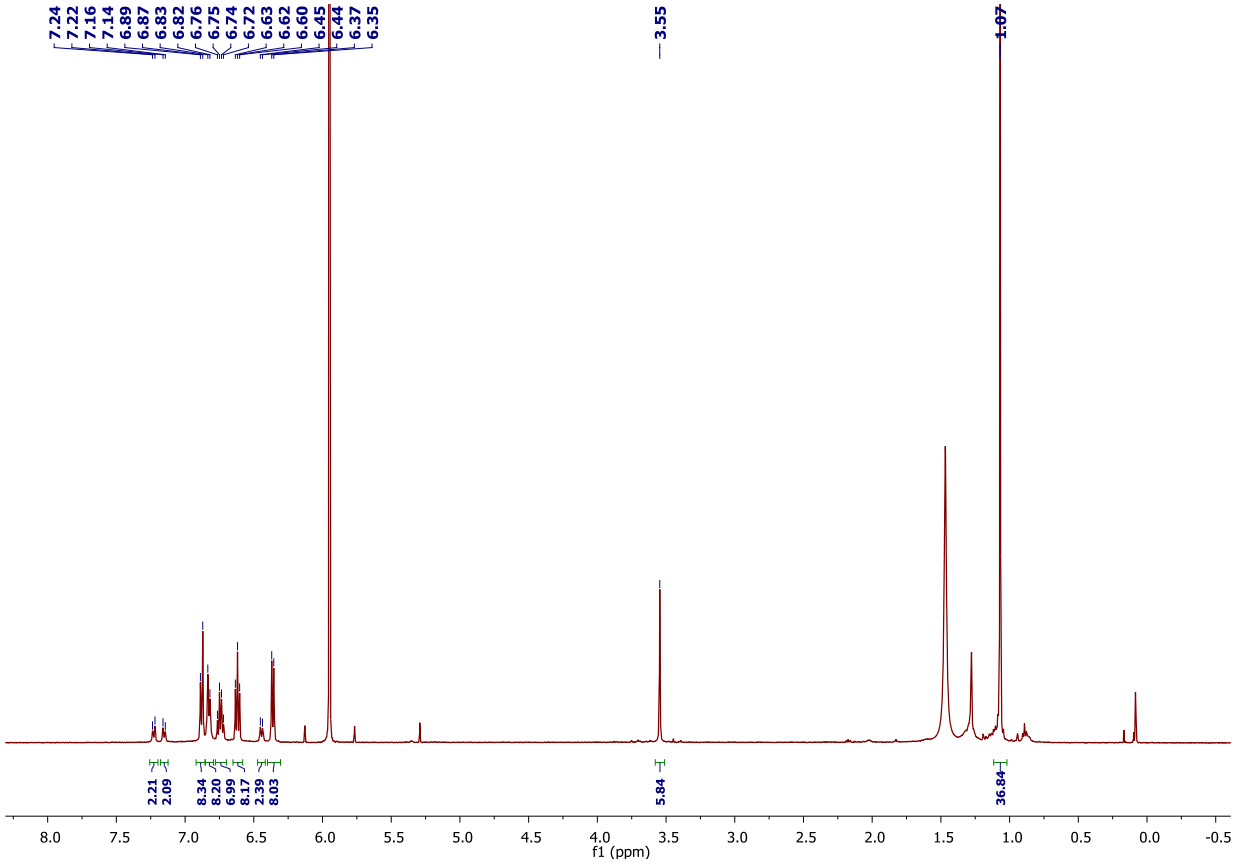

Figure 70: ^{1}H-NMR spectrum of triangular macrocycle recorded in $C_2D_2Cl_4$ at 60 °C.

6.4.2. COSY spectrum of compound **83**

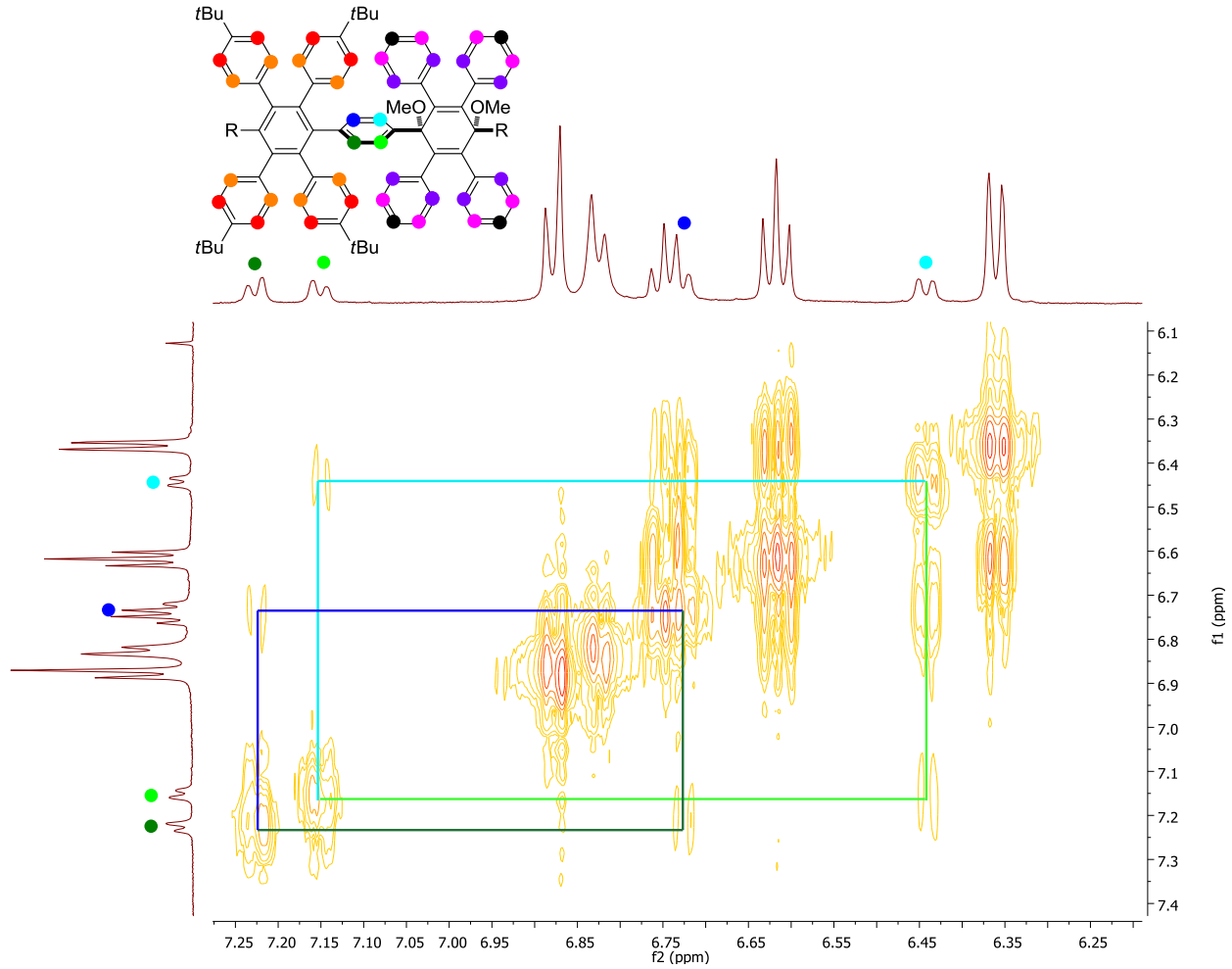

Figure 71: *ortho*-couplings for the phenylene ring in the COSY spectrum (80 °C, 500 MHz) of **83**. ^{4}J-couplings are highlighted.

6.5. Mass spectrometry

6.5.1 [15]PPC **62**

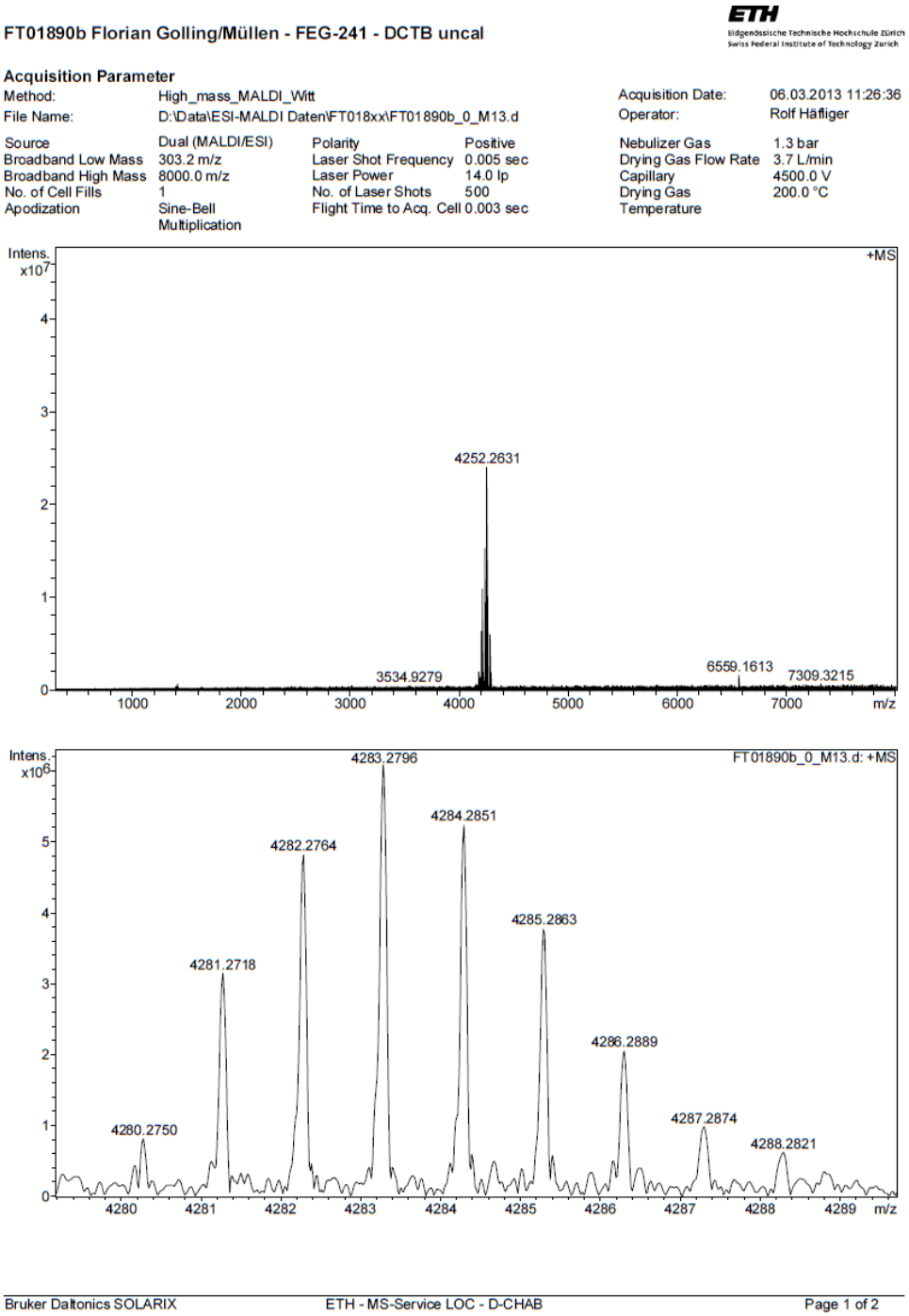

Figure 72: HR-MALDI spectrum of **62**. Theoretical mass: 4283.2796 g/mol. Found: 4283.2796 g/mol. The upper spectrum shows the monodemethoxylated product as main peak. The spectrum was recorded at the ETH Zurich by Rolf Häfliger.

6.5.2. Kinked [21] **67**

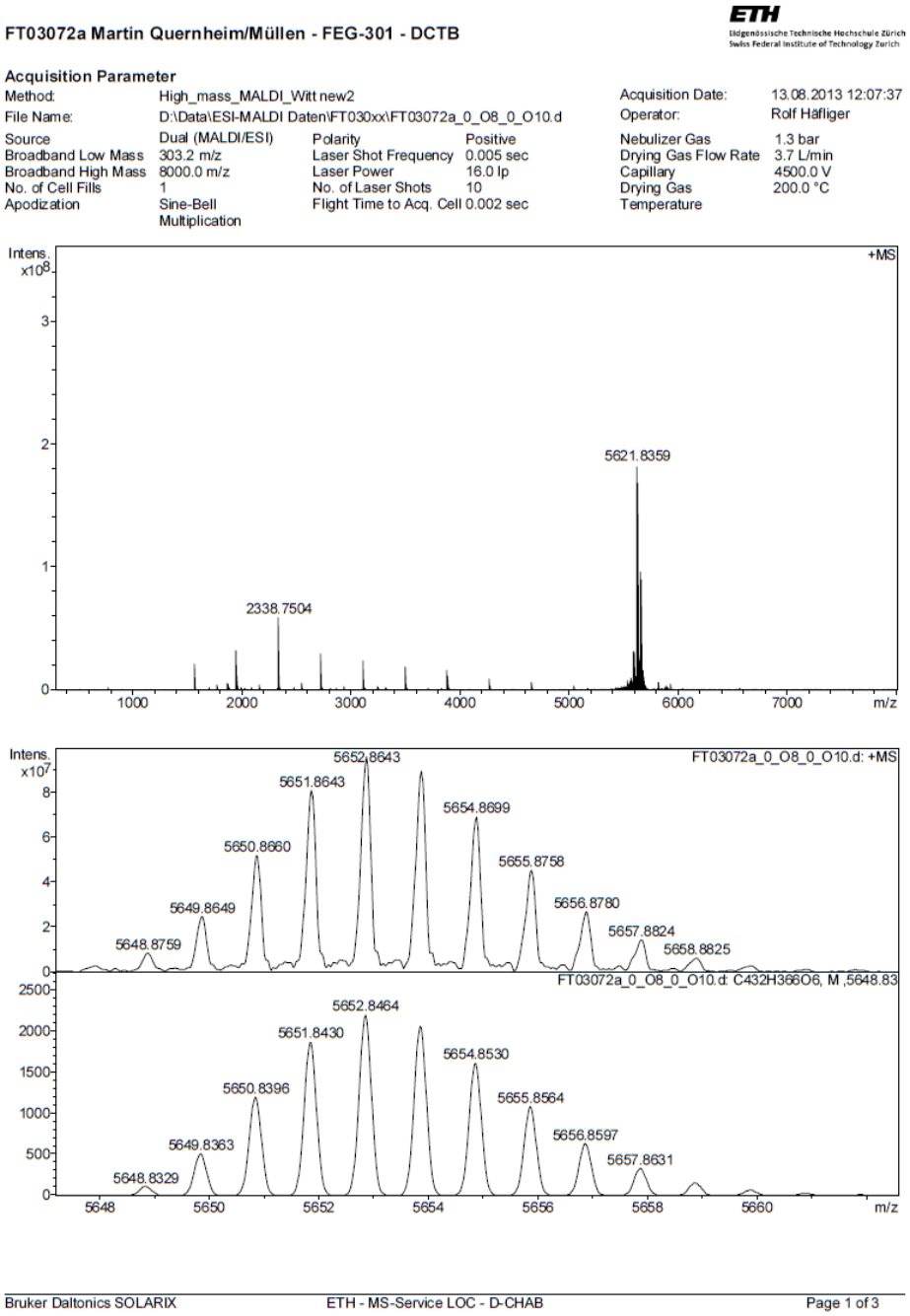

Figure 73: HR- MS spectrum of **67**. Theoretical mass: 5652.8464 g/mol. Found: 5652.8643 g/mol. The upper spectrum shows the monodemethoxylated product as main peak. The calibration standard can be observed in the upper spectrum from 1500 m/z to 4000 m/zThe spectrum was recorded at the ETH Zurich by Rolf Häfliger

6.5.3. [21]CPP based polyphenylene cylinder **68**

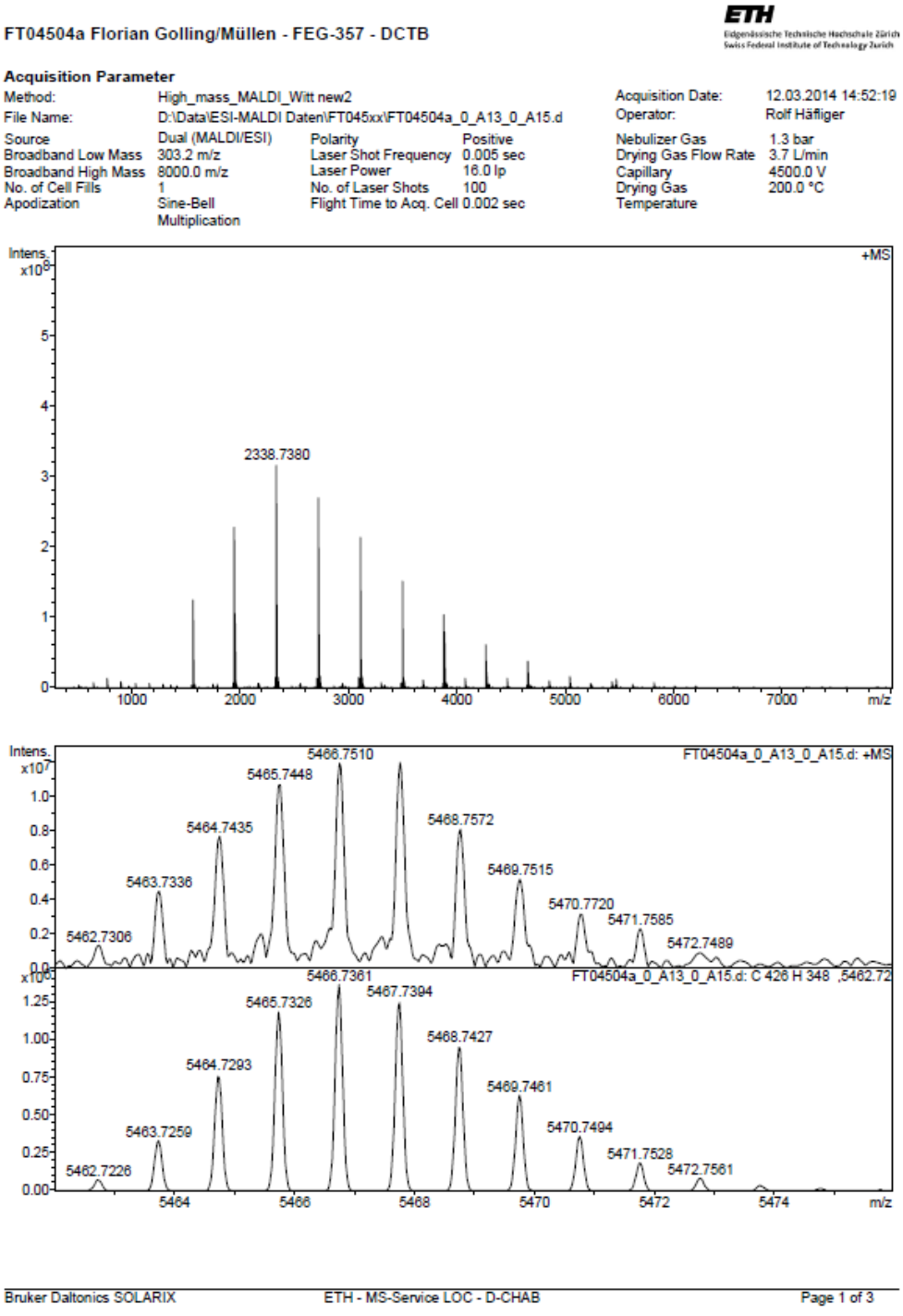

Figure 74: HR-MS of the [21]CPP based polyphenylene cylinder **68**

6.5.4. Triangular macrocycle **83**

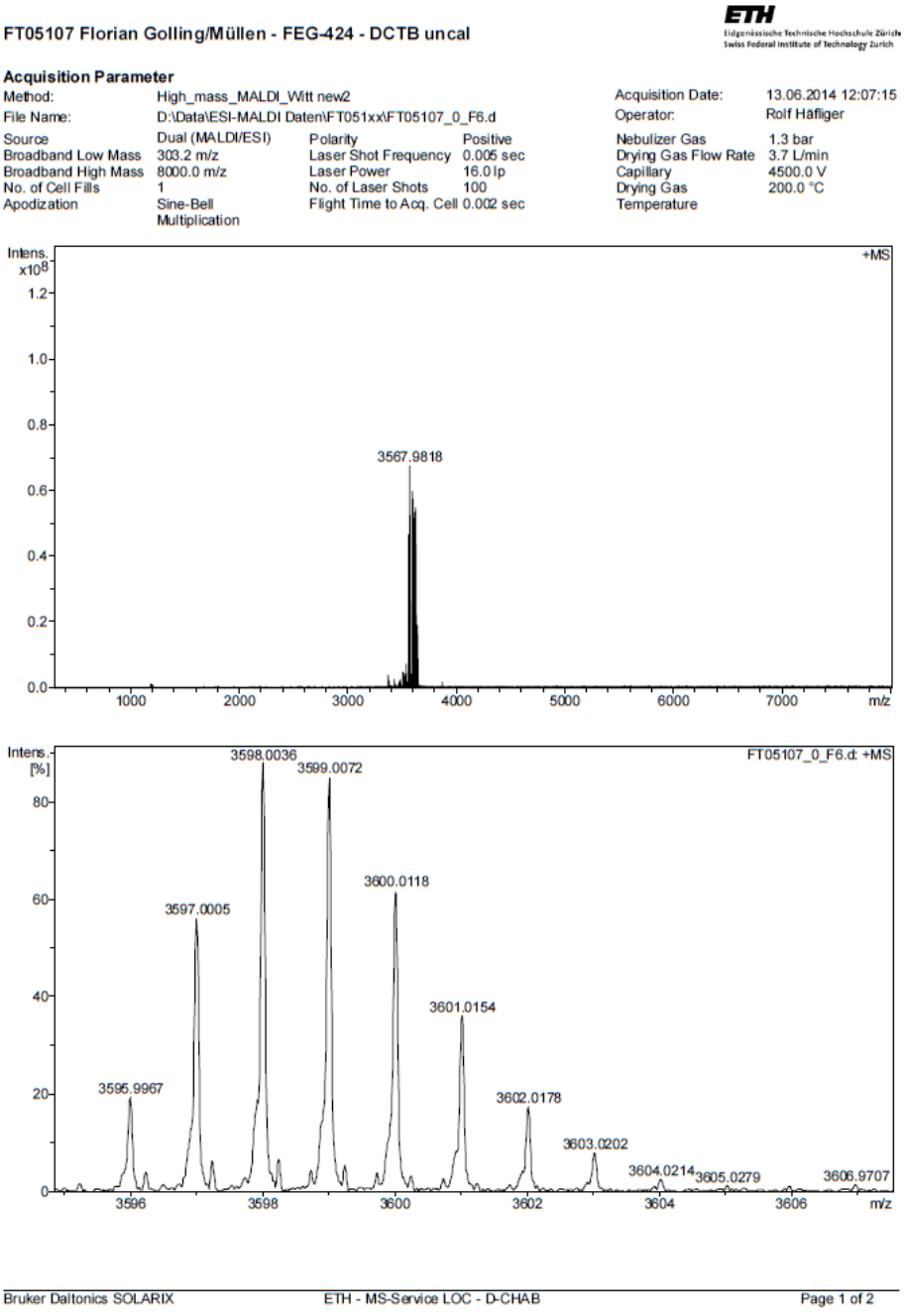

Figure 75: HR-MS spectrum of compound **83**. Several peaks for title compound observed due to methoxylation during ionization.

6.5.5. [12]PPC **84**

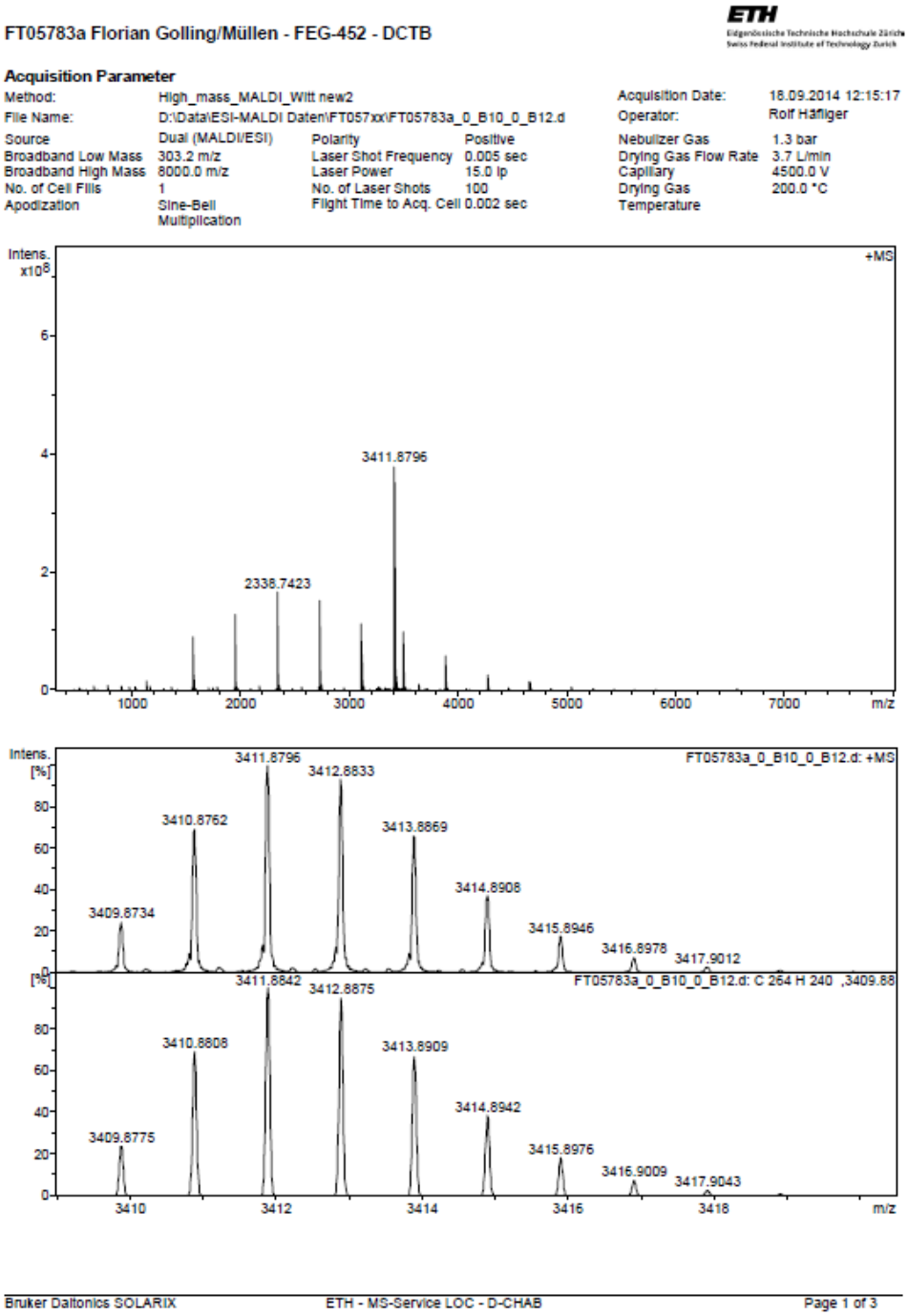

Figure 76: MALDI-TOF-MS measurement of compound **84**.

6.5.6. C_2-symmetric macrocycle **108**

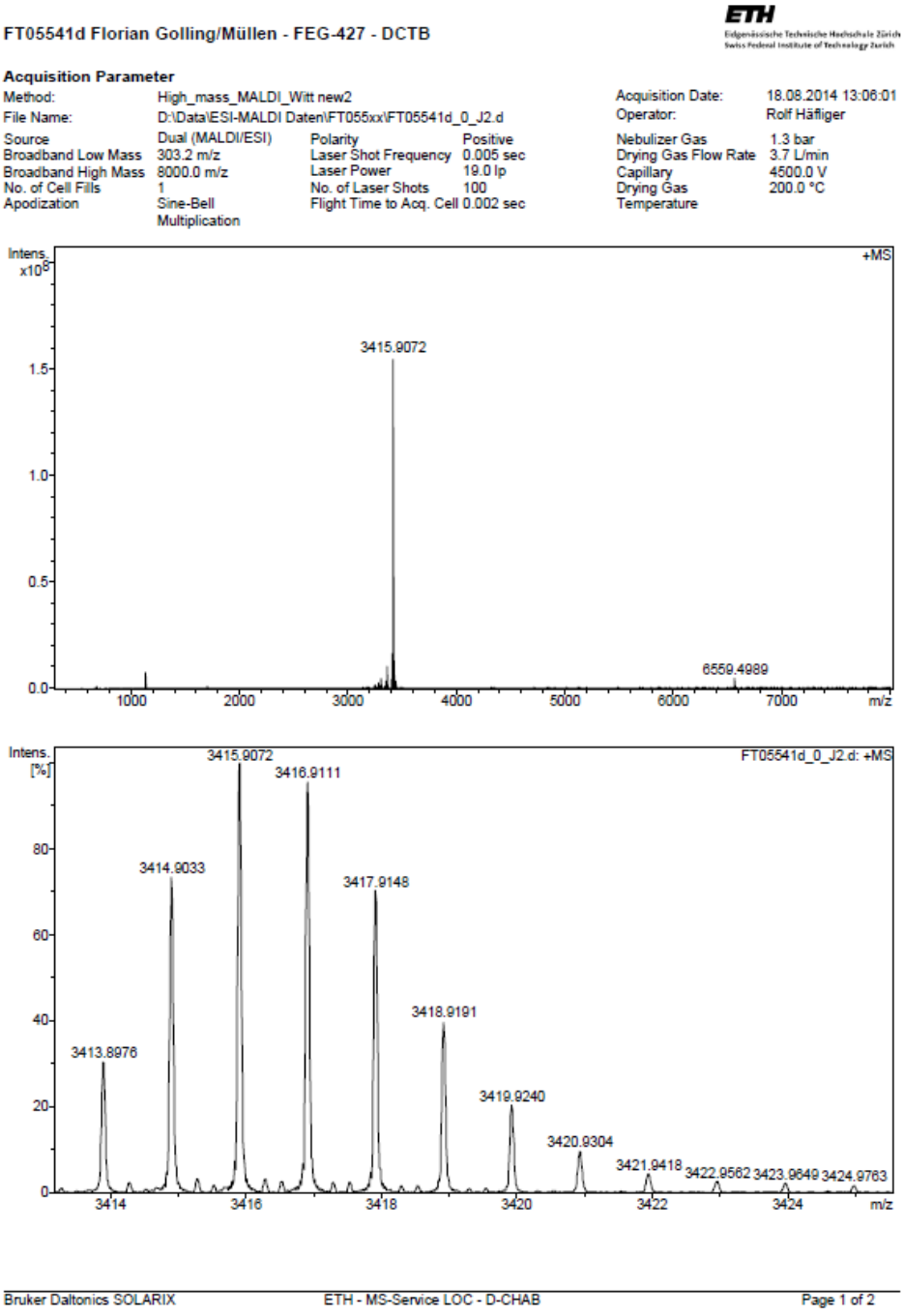

Figure 77: MALDI-MS spectrum of macrocycle **108**.

VII. Bibliography

[1] G. E. Moore, "Cramming More Components onto Integrated Circuits," Electronics, 1965, 114–1171965.

[2] A. Mishra, P. Bäuerle, A*ngew. Chem. Int. Ed. 2***012,** 5*1,* 2020-2067.

[3] X. Guo, M. Baumgarten, K. Müllen, P*rogress in Polymer Science 2***013,** 3*8,* 1832-1908.

[4] U. Mitschke, P. Bauerle, J. *Mater. Chem. 2***000,** 1*0,* 1471-1507.

[5] J. G. C. Veinot, T. J. Marks, A*cc. Chem. Res. 2***005,** 3*8,* 632-643.

[6] N. Thejo Kalyani, S. J. Dhoble, R*enewable and Sustainable Energy Reviews 2***012,** 1*6,* 2696-2723.

[7] B. O'Regan, M. Gratzel, N*ature 1***991,** 3*53,* 737-740.

[8] J. Roncali, P. Leriche, P. Blanchard, A*dv. Mater. 2***014,** n/a-n/a.

[9] Y. Sun, G. C. Welch, W. L. Leong, C. J. Takacs, G. C. Bazan, A. J. Heeger, N*at Mater 2***012,** 1*1,* 44-48.

[10] A. Facchetti, C*hem. Mater. 2***010,** 2*3,* 733-758.

[11] J. Mei, Y. Diao, A. L. Appleton, L. Fang, Z. Bao, J*ournal of the American Chemical Society 2***013,** 1*35,* 6724-6746.

[12] K. S. Novoselov, A. K. Geim, S. V. Morozov, D. Jiang, Y. Zhang, S. V. Dubonos, I. V. Grigorieva, A. A. Firsov, S*cience 2***004,** 3*06,* 666-669.

[13] A. Narita, X. Feng, Y. Hernandez, S. A. Jensen, M. Bonn, H. Yang, I. A. Verzhbitskiy, C. Casiraghi, M. R. Hansen, A. H. R. Koch, G. Fytas, O. Ivasenko, B. Li, K. S. Mali, T. Balandina, S. Mahesh, S. De Feyter, K. Müllen, N*at Chem 2***014,** 6, 126-132.

[14] A. J. Berresheim, M. Müller, K. Müllen, C*hem. Rev. 1***999,** 9*9,* 1747-1786.

[15] K. Müllen, A*CS Nano 2***014,** 8, 6531-6541.

[16] A. N. Abbas, G. Liu, A. Narita, M. Orosco, X. Feng, K. Müllen, C. Zhou, J. *Am. Chem. Soc. 2***014.**

[17] S. Iijima, T. Ichihashi, N*ature 1***993,** 3*63,* 603-605.

[18] S. Iijima, N*ature 1***991,** 3*54,* 56-58.

[19] D. S. Bethune, C. H. Klang, M. S. de Vries, G. Gorman, R. Savoy, J. Vazquez, R. Beyers, N*ature 1***993,** 3*63,* 605-607.

[20] R. Jasti, J. Bhattacharjee, J. B. Neaton, C. R. Bertozzi, J. *Am. Chem. Soc. 2***008,** 1*30,* 17646-17647.

[21] H. W. Kroto, J. R. Heath, S. C. O'Brien, R. F. Curl, R. E. Smalley, N*ature 1***985,** 3*18,* 162-163.

[22] D. Jariwala, V. K. Sangwan, L. J. Lauhon, T. J. Marks, M. C. Hersam, C*hem. Soc. Rev. 2***013,** 4*2,* 2824-2860.

[23] K. Nakada, M. Fujita, G. Dresselhaus, M. S. Dresselhaus, P*hysical Review B 1***996,** 5*4*, 17954-17961.

[24] K. I. Bolotin, K. J. Sikes, Z. Jiang, M. Klima, G. Fudenberg, J. Hone, P. Kim, H. L. Stormer, S*olid State Commun. 2***008,** 1*46*, 351-355.

[25] A. A. Balandin, S. Ghosh, W. Bao, I. Calizo, D. Teweldebrhan, F. Miao, C. N. Lau, N*ano Lett. 2***008,** 8, 902-907.

[26] S. Ghosh, I. Calizo, D. Teweldebrhan, E. P. Pokatilov, D. L. Nika, A. A. Balandin, W. Bao, F. Miao, C. N. Lau, A*ppl. Phys. Lett. 2***008,** 9*2*, -.

[27] H. Y. Chiu, V. V. Deshpande, H. W. C. Postma, C. N. Lau, C. Mikó, L. Forró, M. Bockrath, P*hys. Rev. Lett. 2***005,** 9*5*, 226101.

[28] C. Yu, L. Shi, Z. Yao, D. Li, A. Majumdar, N*ano Lett. 2***005,** 5, 1842-1846.

[29] E. Pop, D. Mann, Q. Wang, K. Goodson, H. Dai, N*ano Lett. 2***005,** 6, 96-100.

[30] P. Kim, L. Shi, A. Majumdar, P. L. McEuen, P*hys. Rev. Lett. 2***001,** 8*7*, 215502.

[31] X. Wang, L. Zhi, K. Müllen, N*ano Lett. 2***007,** 8, 323-327.

[32] S. Bae, H. Kim, Y. Lee, X. Xu, J.-S. Park, Y. Zheng, J. Balakrishnan, T. Lei, H. Ri Kim, Y. I. Song, Y.-J. Kim, K. S. Kim, B. Ozyilmaz, J.-H. Ahn, B. H. Hong, S. Iijima, N*at Nano 2***010,** 5, 574-578.

[33] Y. Hernandez, V. Nicolosi, M. Lotya, F. M. Blighe, Z. Sun, S. De, I. T. McGovern, B. Holland, M. Byrne, Y. K. Gun'Ko, J. J. Boland, P. Niraj, G. Duesberg, S. Krishnamurthy, R. Goodhue, J. Hutchison, V. Scardaci, A. C. Ferrari, J. N. Coleman, N*at Nano 2***008,** 3, 563-568.

[34] L. Chen, Y. Hernandez, X. Feng, K. Müllen, A*ngew. Chem. Int. Ed. 2***012,** 5*1*, 7640-7654.

[35] J. N. Coleman, A*dv. Funct. Mater. 2***009,** 1*9*, 3680-3695.

[36] S. Gilje, S. Han, M. Wang, K. L. Wang, R. B. Kaner, N*ano Lett. 2***007,** 7, 3394-3398.

[37] X. Li, Y. Zhu, W. Cai, M. Borysiak, B. Han, D. Chen, R. D. Piner, L. Colombo, R. S. Ruoff, N*ano Lett. 2***009,** 9, 4359-4363.

[38] F. Torrisi, T. Hasan, W. Wu, Z. Sun, A. Lombardo, T. S. Kulmala, G.-W. Hsieh, S. Jung, F. Bonaccorso, P. J. Paul, D. Chu, A. C. Ferrari, A*CS Nano 2***012,** 6, 2992-3006.

[39] B. C. Brodie Phil. Trans. 1859, 149, 249

[40] W. S. Hummers, R. E. Offeman, J. *Am. Chem. Soc. 1***958,** 8*0*, 1339-1339.

[41] L. Yanyu, J. Frisch, Z. Linjie, H. Norouzi-Arasi, F. Xinliang, J. P. Rabe, N. Koch, K. Mullen, N*anotechnology 2***009,** 2*0*, 434007 (434006 pp.)-434007 (434006 pp.).

[42] H. Ueta, M. Saida, C. Nakai, Y. Yamada, M. Sasaki, S. Yamamoto, S*urf. Sci. 2***004,** 5*60*, 183-190.

[43] J. Coraux, A. T. N'Diaye, C. Busse, T. Michely, N*ano Lett. 2***008,** 8, 565-570.

[44] A. L. Vázquez de Parga, F. Calleja, B. Borca, M. C. G. Passeggi, J. J. Hinarejos, F. Guinea, R. Miranda, P*hys. Rev. Lett. 2***008,** 1*00*, 056807.

[45] S. Marchini, S. Günther, J. Wintterlin, P*hysical Review B 2***007,** 7*6,* 075429.
[46] X. Li, W. Cai, J. An, S. Kim, J. Nah, D. Yang, R. Piner, A. Velamakanni, I. Jung, E. Tutuc, S. K. Banerjee, L. Colombo, R. S. Ruoff, S*cience 2***009,** 3*24,* 1312-1314.
[47] K. S. Novoselov, V. I. Falko, L. Colombo, P. R. Gellert, M. G. Schwab, K. Kim, N*ature 2***012,** 4*90,* 192-200.
[48] H. Yang, J. Heo, S. Park, H. J. Song, D. H. Seo, K.-E. Byun, P. Kim, I. Yoo, H.-J. Chung, K. Kim, S*cience 2***012,** 3*36,* 1140-1143.
[49] L. Britnell, R. V. Gorbachev, R. Jalil, B. D. Belle, F. Schedin, A. Mishchenko, T. Georgiou, M. I. Katsnelson, L. Eaves, S. V. Morozov, N. M. R. Peres, J. Leist, A. K. Geim, K. S. Novoselov, L. A. Ponomarenko, S*cience 2***012,** 3*35,* 947-950.
[50] L. Xie, H. Wang, C. Jin, X. Wang, L. Jiao, K. Suenaga, H. Dai, J. *Am. Chem. Soc. 2***011,** 1*33,* 10394-10397.
[51] M. G. Schwab, A. Narita, Y. Hernandez, T. Balandina, K. S. Mali, S. De Feyter, X. Feng, K. Müllen, J. *Am. Chem. Soc. 2***012,** 1*34,* 18169-18172.
[52] L. Dössel, L. Gherghel, X. Feng, K. Müllen, A*ngew. Chem. 2***011,** 1*23,* 2588-2591.
[53] X. Yang, X. Dou, A. Rouhanipour, L. Zhi, H. J. Räder, K. Müllen, J. *Am. Chem. Soc. 2***008,** 1*30,* 4216-4217.
[54] R. Denk, M. Hohage, P. Zeppenfeld, J. Cai, C. A. Pignedoli, H. Söde, R. Fasel, X. Feng, K. Müllen, S. Wang, D. Prezzi, A. Ferretti, A. Ruini, E. Molinari, P. Ruffieux, N*at Commun 2***014,** 5.
[55] J. Cai, P. Ruffieux, R. Jaafar, M. Bieri, T. Braun, S. Blankenburg, M. Muoth, A. P. Seitsonen, M. Saleh, X. Feng, K. Mullen, R. Fasel, N*ature 2***010,** 4*66,* 470-473.
[56] T. Ikegami, F. Nakanishi, M. Uchiyama, K. Ebihara, T*hin Solid Films 2***004,** 4*57,* 7-11.
[57] T. Guo, P. Nikolaev, A. Thess, D. T. Colbert, R. E. Smalley, C*hem. Phys. Lett. 1***995,** 2*43,* 49-54.
[58] M. Endo, T. Hayashi, Y-A. Kim, Pure Appl. Chem., 2006, Vol. 78, No. 9, pp. 1703-1713
[59] K. Hata, D. N. Futaba, K. Mizuno, T. Namai, M. Yumura, S. Iijima, S*cience 2***004,** 3*06,* 1362-1364.
[60] www.unidym.com/files/Unidym_Product_Sheet_SWNT.pdf
[61] M. Cinke, J. Li, B. Chen, A. Cassell, L. Delzeit, J. Han, M. Meyyappan, C*hem. Phys. Lett. 2***002,** 3*65,* 69-74.
[62] X. Lu, Z. Chen, C*hem. Rev. 2***005,** 1*05,* 3643-3696.
[63] S. Louie, in C*arbon Nanotubes, Vol. 80* (Eds.: M. Dresselhaus, G. Dresselhaus, P. Avouris), Springer Berlin Heidelberg, 2**001,** pp. 113-145.
[64] S. Hong, S. Myung, N*at Nano 2***007,** 2, 207-208.
[65] H. Zhang, B. Wu, W. Hu, Y. Liu, C*hem. Soc. Rev. 2***011,** 4*0,* 1324-1336.
[66] B. K. Sarker, S. Shekhar, S. I. Khondaker, A*CS Nano 2***011,** 5, 6297-6305.

[67] A. R. Harutyunyan, G. Chen, T. M. Paronyan, E. M. Pigos, O. A. Kuznetsov, K. Hewaparakrama, S. M. Kim, D. Zakharov, E. A. Stach, G. U. Sumanasekera, S*cience 2***009,** 3*26,* 116-120.

[68] L. Ding, A. Tselev, J. Wang, D. Yuan, H. Chu, T. P. McNicholas, Y. Li, J. Liu, N*ano Lett. 2***009,** 9*,* 800-805.

[69] G. Zhang, P. Qi, X. Wang, Y. Lu, X. Li, R. Tu, S. Bangsaruntip, D. Mann, L. Zhang, H. Dai, S*cience 2***006,** 3*14,* 974-977.

[70] S. Park, M. Vosguerichian, Z. Bao, N*anoscale 2***013,** 5*,* 1727-1752.

[71] S. J. Kang, C. Kocabas, T. Ozel, M. Shim, N. Pimparkar, M. A. Alam, S. V. Rotkin, J. A. Rogers, N*at Nano 2***007,** 2*,* 230-236.

[72] P. G. Collins, M. S. Arnold, P. Avouris, S*cience 2***001,** 2*92,* 706-709.

[73] S.-H. Hur, C. Kocabas, A. Gaur, O. O. Park, M. Shim, J. A. Rogers, J. *Appl. Phys. 2***005,** 9*8,* -.

[74] S. Kim, S. Kim, J. Park, S. Ju, S. Mohammadi, A*CS Nano 2***010,** 4*,* 2994-2998.

[75] K. Bradley, J.-C. P. Gabriel, G. Grüner, N*ano Lett. 2***003,** 3*,* 1353-1355.

[76] V. C. Parekh, P. C. Guha, J. Indian Chem. Soc. 1934, 11, 95–100

[77] R. Friederich, M. Nieger, F. Vögtle, C*hem. Ber. 1***993,** 1*26,* 1723-1732.

[78] S. Kammermeier, P. G. Jones, R. Herges, A*ngewandte Chemie International Edition in English 1***996,** 3*5,* 2669-2671.

[79] H. Takaba, H. Omachi, Y. Yamamoto, J. Bouffard, K. Itami, A*ngew. Chem. Int. Ed. 2***009,** 4*8,* 6112-6116.

[80] G. Fuhrmann, T. Debaerdemaeker, P. Bauerle, C*hem. Commun. 2***003,** 948-949.

[81] J. Krömer, I. Rios-Carreras, G. Fuhrmann, C. Musch, M. Wunderlin, T. Debaerdemaeker, E. Mena-Osteritz, P. Bäuerle, A*ngew. Chem. Int. Ed. 2***000,** 3*9,* 3481-3486.

[82] S. Yamago, Y. Watanabe, T. Iwamoto, A*ngew. Chem. Int. Ed. 2***010,** 4*9,* 757-759.

[83] C. Huang, Y. Huang, N. G. Akhmedov, B. V. Popp, J. L. Petersen, K. K. Wang, O*rg. Lett. 2***014,** 1*6,* 2672-2675.

[84] T. J. Sisto, M. R. Golder, E. S. Hirst, R. Jasti, J. *Am. Chem. Soc. 2***011,** 1*33,* 15800-15802.

[85] F. Sibbel, K. Matsui, Y. Segawa, A. Studer, K. Itami, C*hem. Commun. 2***013.**

[86] E. R. Darzi, T. J. Sisto, R. Jasti, J. *Org. Chem. 2***012,** 7*7,* 6624-6628.

[87] J. Xia, J. W. Bacon, R. Jasti, C*hem. Sci. 2***012,** 3*,* 3018-3021.

[88] T. Iwamoto, Y. Watanabe, Y. Sakamoto, T. Suzuki, S. Yamago, J. *Am. Chem. Soc. 2***011,** 1*33,* 8354-8361.

[89] S. Yamago, Y. Watanabe, T. Iwamoto, A*ngew. Chem. 2***010,** 1*22,* 769-771.

[90] E. Kayahara, V. K. Patel, S. Yamago, J. *Am. Chem. Soc. 2***014.**

[91] P. J. Evans, E. R. Darzi, R. Jasti, N*at Chem 2***014,** a*dvance online publication.*

[92] Y. Ishii, Y. Nakanishi, H. Omachi, S. Matsuura, K. Matsui, H. Shinohara, Y. Segawa, K. Itami, C*hem. Sci. 2***012,** 3*,* 2340-2345.

[93] E. Kayahara, Y. Sakamoto, T. Suzuki, S. Yamago, O*rg. Lett. 2***012,** 1*4,* 3284-3287.
[94] Y. Segawa, Scaron, Penel, S. Matsuura, H. Omachi, K. Itami, C*hem. Lett. 2***011,** *40,* 423-425.
[95] H. Omachi, S. Matsuura, Y. Segawa, K. Itami, A*ngew. Chem. 2***010,** 1*22,* 10400-10403.
[96] K. Matsui, Y. Segawa, K. Itami, O*rg. Lett. 2***012,** 1*4,* 1888-1891.
[97] H. Isobe, S. Hitosugi, T. Yamasaki, R. Iizuka, C*hem. Sci. 2***013,** 4, 1293-1297.
[98] S. Hitosugi, W. Nakanishi, H. Isobe, C*hem. Asian. J. 2***012,** 7, 1550-1552.
[99] S. Hitosugi, T. Yamasaki, H. Isobe, J. *Am. Chem. Soc. 2***012,** 1*34,* 12442-12445.
[100] S. Hitosugi, W. Nakanishi, T. Yamasaki, H. Isobe, N*at Commun 2***011,** 2, 492.
[101] T. Matsuno, S. Kamata, S. Hitosugi, H. Isobe, C*hem. Sci. 2***013,** 4, 3179-3183.
[102] H. Omachi, Y. Segawa, K. Itami, O*rg. Lett. 2***011,** 1*3,* 2480-2483.
[103] T. Matsuno, S. Sato, R. Iizuka, H. Isobe, C*hem. Sci. 2***015.**
[104] S. Hitosugi, K. Ohkubo, R. Iizuka, Y. Kawashima, K. Nakamura, S. Sato, H. Kono, S. Fukuzumi, H. Isobe, O*rg. Lett. 2***014.**
[105] H. Omachi, T. Nakayama, E. Takahashi, Y. Segawa, K. Itami, N*at Chem 2***013,** 5, 572-576.
[106] A. Yagi, G. Venkataramana, Y. Segawa, K. Itami, C*hem. Commun. 2***014,** 5*0,* 957-959.
[107] T. Iwamoto, E. Kayahara, N. Yasuda, T. Suzuki, S. Yamago, A*ngew. Chem. Int. Ed. 2***014,** 5*3,* n/a-n/a.
[108] J. Xia, M. R. Golder, M. E. Foster, B. M. Wong, R. Jasti, J. *Am. Chem. Soc. 2***012,** 1*34,* 19709-19715.
[109] T. J. Sisto, X. Tian, R. Jasti, J. *Org. Chem. 2***012,** 7*7,* 5857-5860.
[110] T. Nishiuchi, X. Feng, V. Enkelmann, M. Wagner, K. Müllen, C*hem. Eur. J. 2***012,** 1*8,* 16621-16625.
[111] A. Yagi, Y. Segawa, K. Itami, J. *Am. Chem. Soc. 2***012,** 1*34,* 2962-2965.
[112] Y. Ishii, S. Matsuura, Y. Segawa, K. Itami, O*rg. Lett. 2***014.**
[113] M. D. Watson, A. Fechtenkotter, K. Mullen, C*hem. Rev. 2***001,** 1*01,* 1267-1300.
[114] J. P. Hill, W. Jin, A. Kosaka, T. Fukushima, H. Ichihara, T. Shimomura, K. Ito, T. Hashizume, N. Ishii, T. Aida, S*cience 2***004,** 3*04,* 1481-1483.
[115] W. Pisula, X. Feng, K. Müllen, C*hem. Mater. 2***010,** 2*3,* 554-567.
[116] V. S. Iyer, M. Wehmeier, J. D. Brand, M. A. Keegstra, K. Müllen, A*ngewandte Chemie International Edition in English 1***997,** 3*6,* 1604-1607.
[117] S. M. Draper, D. J. Gregg, R. Madathil, J. *Am. Chem. Soc. 2***002,** 1*24,* 3486-3487.
[118] D. Wasserfallen, M. Kastler, W. Pisula, W. A. Hofer, Y. Fogel, Z. Wang, K. Müllen, J. *Am. Chem. Soc. 2***006,** 1*28,* 1334-1339.
[119] X. Feng, V. Marcon, W. Pisula, M. R. Hansen, J. Kirkpatrick, F. Grozema, D. Andrienko, K. Kremer, K. Mullen, N*at Mater 2***009,** 8, 421-426.

[120] V. S. Iyer, K. Yoshimura, V. Enkelmann, R. Epsch, J. P. Rabe, K. Müllen, A*ngew. Chem. Int. Ed. 1***998,** 3*7,* 2696-2699.
[121] L. Dossel, L. Gherghel, X. L. Feng, K. Mullen, A*ngew. Chem. Int. Ed. 2***011,** 5*0,* 2540-2543.
[122] Y. Fogel, L. Zhi, A. Rouhanipour, D. Andrienko, H. J. Räder, K. Müllen, M*acromolecules 2***009,** 4*2,* 6878-6884.
[123] A. A. O. Sarhan, C. Bolm, C*hem. Soc. Rev. 2***009,** 3*8,* 2730-2744.
[124] M. Grzybowski, K. Skonieczny, H. Butenschön, D. T. Gryko, A*ngew. Chem. Int. Ed. 2***013,** 5*2,* 9900-9930.
[125] H. Omachi, S. Matsuura, Y. Segawa, K. Itami, A*ngew. Chem. Int. Ed. 2***010,** 4*9,* 10202-10205.
[126] Y. Segawa, P. Senel, S. Matsuura, H. Omachi, K. Itami, C*hem. Lett. 2***011,** 4*0,* 423-425.
[127] J. Xia, R. Jasti, A*ngew. Chem. Int. Ed. 2***012,** 5*1,* 2474-2476.
[128] M. A. Petrukhina, L. T. Scott, John Wiley & Sons, Inc., Hoboken, NJ, USA, 2**011.**
[129] R. L. Viavattene, F. D. Greene, L. D. Cheung, R. Majeste, L. M. Trefonas, J. *Am. Chem. Soc. 1***974,** 9*6,* 4342-4343.
[130] F. H. Kohnke, A. M. Z. Slawin, J. F. Stoddart, D. J. Williams, A*ngewandte Chemie International Edition in English 1***987,** 2*6,* 892-894.
[131] A. Godt, V. Enkelmann, A.-D. Schlüter, A*ngewandte Chemie International Edition in English 1***989,** 2*8,* 1680-1682.
[132] R. Jasti, C. R. Bertozzi, C*hem. Phys. Lett. 2***010,** 4*94,* 1-7.
[133] H.-B. Li, A. J. Page, S. Irle, K. Morokuma, J. *Am. Chem. Soc. 2***012,** 1*34,* 15887-15896.
[134] J. C. Byers, A. G. Güell, P. R. Unwin, J. *Am. Chem. Soc. 2***014.**
[135] I. Ullah, R. A. Khera, M. Hussain, A. Villinger, P. Langer, T*etrahedron Lett. 2***009,** 5*0,* 4651-4653.
[136] A. Krasovskiy, F. Kopp, P. Knochel, A*ngew. Chem. Int. Ed. 2***006,** 4*5,* 497-500.
[137] A. Krasovskiy, P. Knochel, A*ngew. Chem. Int. Ed. 2***004,** 4*3,* 3333-3336.
[138] X. Yan, X. Cui, B. Li, L.-s. Li, N*ano Lett. 2***010,** 1*0,* 1869-1873.
[139] E. A. Krasnokutskaya, N. I. Semenischeva, V. D. Filimonov, P. Knochel, S*ynthesis 2***007,** 2*007,* 81-84.
[140] B. S. Nehls, F. Galbrecht, A. Bilge, D. J. Brauer, C. W. Lehmann, U. Scherf, T. Farrell, O*rganic & Biomolecular Chemistry 2***005,** 3, 3213-3219.
[141] F. Alonso, M. Yus, T*etrahedron 1***992,** 4*8,* 2709-2714.
[142] Y. Miyake, M. Wu, M. J. Rahman, M. Iyoda, C*hem. Commun. 2***005,** 411-413.
[143] M. J. Rahman, H. Shimizu, Y. Araki, H. Ikeda, M. Iyoda, C*hem. Commun. 2***013.**
[144] M. J. Rahman, J. Yamakawa, A. Matsumoto, H. Enozawa, T. Nishinaga, K. Kamada, M. Iyoda, J. *Org. Chem. 2***008,** 7*3,* 5542-5548.
[145] J. Trotter, A*cta Crystallographica 1***961,** 1*4,* 1135-1140.

[146] Y. Segawa, S. Miyamoto, H. Omachi, S. Matsuura, P. Šenel, T. Sasamori, N. Tokitoh, K. Itami, A*ngew. Chem. Int. Ed. 2***011,** 5*0,* 3244-3248.

[147] J. Wu, A. Fechtenkötter, J. Gauss, M. D. Watson, M. Kastler, C. Fechtenkötter, M. Wagner, K. Müllen, J. *Am. Chem. Soc. 2***004,** 1*26,* 11311-11321.

[148] A. Konishi, Y. Hirao, K. Matsumoto, H. Kurata, R. Kishi, Y. Shigeta, M. Nakano, K. Tokunaga, K. Kamada, T. Kubo, J. *Am. Chem. Soc. 2***013,** 1*35,* 1430-1437.

[149] A. Konishi, Y. Hirao, K. Matsumoto, H. Kurata, T. Kubo, C*hem. Lett. 2***013,** 4*2,* 592-594.

[150] Y. Avlasevich, C. Kohl, K. Mullen, J. *Mater. Chem. 2***006,** 1*6,* 1053-1057.

[151] K. Kawasumi, Q. Zhang, Y. Segawa, L. T. Scott, K. Itami, N*at Chem 2***013,** 5, 739-744.

[152] Y. Sakamoto, T. Suzuki, J. *Am. Chem. Soc. 2***013,** 1*35,* 14074-14077.

[153] L. Grill, M. Dyer, L. Lafferentz, M. Persson, M. V. Peters, S. Hecht, N*at Nano 2***007,** 2, 687-691.

[154] J. Cai, C. A. Pignedoli, L. Talirz, P. Ruffieux, H. Söde, L. Liang, V. Meunier, R. Berger, R. Li, X. Feng, K. Müllen, R. Fasel, N*at Nano 2***014,** a*dvance online publication.*

[155] M. Treier, C. A. Pignedoli, T. Laino, R. Rieger, K. Müllen, D. Passerone, R. Fasel, N*at Chem 2***011,** 3, 61-67.

[156] X. Feng, W. Pisula, K. Müllen, J. *Am. Chem. Soc. 2***007,** 1*29,* 14116-14117.

[157] R. Scholl, C. Seer, J*ustus Liebigs Annalen der Chemie 1***912,** 3*94,* 111-177.

[158] P. Rempala, J. Kroulík, B. T. King, J. *Org. Chem. 2***006,** *71,* 5067-5081.

[159] L. Zhai, R. Shukla, R. Rathore, O*rg. Lett. 2***009,** 1*1,* 3474-3477.

[160] D. J. Jones, B. Purushothaman, S. Ji, A. B. Holmes, W. W. H. Wong, C*hem. Commun. 2***012,** 4*8,* 8066-8068.

[161] F. E. Golling, M. Quernheim, M. Wagner, T. Nishiuchi, K. Müllen, A*ngew. Chem. Int. Ed. 2***014,** 5*3,* 1525-1528.

[162] M. Fujitsuka, D. W. Cho, T. Iwamoto, S. Yamago, T. Majima, P*CCP 2***012,** 1*4,* 14585-14588.

[163] M. Kastler, J. Schmidt, W. Pisula, D. Sebastiani, K. Müllen, J. *Am. Chem. Soc. 2***006,** 1*28,* 9526-9534.

[164] L.-C. Campeau, M. Parisien, A. Jean, K. Fagnou, J. *Am. Chem. Soc. 2***005,** 1*28,* 581-590.

[165] Y.-T. Wu, J. S. Siegel, C*hem. Rev. 2***006,** 1*06,* 4843-4867.

[166] A. C. Whalley, K. N. Plunkett, A. A. Gorodetsky, C. L. Schenck, C.-Y. Chiu, M. L. Steigerwald, C. Nuckolls, C*hem. Sci. 2***011,** 2, 132-135.

[167] T.-C. Wu, M.-K. Chen, Y.-W. Lee, M.-Y. Kuo, Y.-T. Wu, A*ngew. Chem. Int. Ed. 2***013,** 5*2,* 1289-1293.

[168] M.-K. Chen, H.-J. Hsin, T.-C. Wu, B.-Y. Kang, Y.-W. Lee, M.-Y. Kuo, Y.-T. Wu, C*hem. Eur. J. 2***014,** 2*0,* 598-608.

[169] M. Müller, V. S. Iyer, C. Kübel, V. Enkelmann, K. Müllen, A*ngew. Chem. 1***997,** 1*09,* 1679-1682.
[170] M. Müller, C. Kübel, F. Morgenroth, V. S. Iyer, K. Müllen, C*arbon 1***998,** 3*6,* 827-831.
[171] M. Müller, V. S. Iyer, C. Kübel, V. Enkelmann, K. Müllen, A*ngewandte Chemie International Edition in English 1***997,** 3*6,* 1607-1610.
[172] K. Harada, H. Hart, C. J. Frank Du, J. *Org. Chem. 1***985,** 5*0,* 5524-5528.
[173] H. Hart, G. C. Nwokogu, T*etrahedron Lett. 1***983,** 2*4,* 5721-5724.
[174] X. Yang, X. Dou, K. Müllen, C*hem. Asian. J. 2***008,** 3, 759-766.
[175] S. M. Bachrach, D. Stück, J. *Org. Chem. 2***010,** 7*5,* 6595-6604.
[176] Y. Segawa, H. Omachi, K. Itami, O*rg. Lett. 2***010,** 1*2,* 2262-2265.
[177] S. Yamaguchi, R.-Z. Jin, S. Ohno, K. Tamao, O*rganometallics 1***998,** 1*7,* 5133-5138.
[178] L. A. Jacob, B.-L. Chen, D. Stec, S*ynthesis 1***993,** 1*993,* 611-614.
[179] K. A. Walker, L. J. Markoski, J. S. Moore, S*ynthesis 1***992,** 1*992,* 1265-1268.
[180] F. Effenberger, A. Krebs, J. *Org. Chem. 1***984,** 4*9,* 4687-4695.
[181] M. C. Carreño, S. García-Cerrada, A. Urbano, C*hem. Eur. J. 2***003,** 9, 4118-4131.
[182] J. S. Moore, A*cc. Chem. Res. 1***997,** 3*0,* 402-413.
[183] in E*lectronic Materials: The Oligomer Approach,* Wiley-VCH Verlag GmbH, 2**007,** pp. I-XXII.
[184] K. S. Mali, J. Adisoejoso, E. Ghijsens, I. De Cat, S. De Feyter, A*cc. Chem. Res. 2***012,** 4*5,* 1309-1320.
[185] U. Scherf, K. Müllen, S*ynthesis 1***992,** 1*992,* 23-38.
[186] A. D. Schlüter, G. Wegner, A*cta Polym. 1***993,** 4*4,* 59-69.
[187] J. Sakamoto, M. Rehahn, G. Wegner, A. D. Schlüter, M*acromol. Rapid Commun. 2***009,** 3*0,* 653-687.
[188] Q. Zheng, S. K. Gupta, G. S. He, L.-S. Tan, P. N. Prasad, A*dv. Funct. Mater. 2***008,** 1*8,* 2770-2779.
[189] S. Setayesh, D. Marsitzky, K. Müllen, M*acromolecules 2***000,** 3*3,* 2016-2020.
[190] M. Rehahn, A.-D. Schlüter, G. Wegner, W. J. Feast, P*olymer 1***989,** 3*0,* 1054-1059.
[191] M. Rehahn, A.-D. Schlüter, G. Wegner, W. J. Feast, P*olymer 1***989,** 3*0,* 1060-1062.
[192] J. M. Batson, T. M. Swager, A*CS Macro Letters 2***012,** 1, 1121-1123.
[193] U. Scherf, K. Muellen, M*acromolecules 1***992,** 2*5,* 3546-3548.
[194] U. Scherf, K. Müllen, D*ie Makromolekulare Chemie, Rapid Communications 1***991,** 1*2,* 489-497.
[195] U. Scherf, K. Müllen, P*olymer 1***992,** 3*3,* 2443-2446.
[196] D. L. Gin, V. P. Conticello, R. H. Grubbs, J. *Am. Chem. Soc. 1***992,** 1*14,* 3167-3169.
[197] V. W. Kern, M. Seibel, H. O. Wirth, D*ie Makromolekulare Chemie 1***959,** 2*9,* 164-189.
[198] Y. Garmshausen, J. Schwarz, J. Hildebrandt, B. Kobin, M. Pätzel, S. Hecht, O*rg. Lett. 2***014,** 1*6,* 2838-2841.

[199] B. Hulsken, R. Van Hameren, J. W. Gerritsen, T. Khoury, P. Thordarson, M. J. Crossley, A. E. Rowan, R. J. M. Nolte, J. A. A. W. Elemans, S. Speller, N*at Nano 2***007,** 2, 285-289.

[200] R. Resel, J. *Phys.: Condens. Matter 2***008,** 2*0,* 184009.

[201] M. Rickhaus, A. P. Belanger, H. A. Wegner, L. T. Scott, J. *Org. Chem. 2***010,** 7*5,* 7358-7364.

[202] H.-B. Li, A. J. Page, S. Irle, K. Morokuma, C*hemPhysChem 2***012,** 1*3,* 1479-1485.

[203] L. Kraszkiewicz, M. Sosnowski, L. Skulski, S*ynthesis 2***006,** 2*006,* 1195-1199.

[204] H. A. Scarborough, W. A. Waters, J*ournal of the Chemical Society (Resumed) 1***927,** 89-97.

VIII Acknowledgements

I would like to thank my PhD advisor, Prof Dr. Klaus Müllen, for his continuous support throughout the past years. Our vivid discussions were inspiring and helped me to approach challenges from different perspectives. Plenty of new ideas originated from our meetings. It was a great pleasure to experience his passion, enthusiasm, curiosity for challenges in synthetic organic chemistry within the field of materials research. This spirit in conjunction with his reflective and critical questions was vital for the success of this work.
I would like to thank Dr. Tomohiki Nishiuchi as my former project leader, with whom I discussed synthetic as well as preparative challenges frequently. His synthetic experiences and his knowledge about cycloparaphenylenes were very valuable for the progress of this work.

I would like to acknowledge Dr. Markus Klapper and Prof. Xinliang Feng for their discussions and support.

I would like to thank Amelie Koch and Prof. Fytas for the fruitful collaboration, combining synthesis and dynamic light scattering.

I would like to thank Dr. Manfred Wagner for his fantastic help and valuable advices on NMR spectroscopy. I have learned a lot from you, Manfred. Besides the scientific Dr. Wagner, I also got to know him every Thursday, as the great soccer play "Manni". I have always enjoyed the soccer matches. Thanks to his passion, our AK Müllen soccer crew remained pretty much constant for roughly three years: Marco, Felix, Reinhardt, Dominic, Robert, Leo, Artem, Joe, Christoph, Martin, René, Brenton, Florian, Raphael, Ralf, Sebastian and Woody – I was a great time on the soccer pitch. Keep up the spirit!

I would like to thank Dr. Joachim Räder for his valuable advice on mass spectrometry measurements. I would also like to acknowledge Wen Zhang for measuring MS samples for me. I would especially thank Stefan Türk for measuring MALDI-MS samples and keeping the fantastic FD-MS spectrometer in such a great shape.

I would like to thank the crew of the chemical shop - Willi Lutz and Markus Thull - for their kind support with chemicals.

Thanks to Eva Deister for the synthesis of several starting materials. In this context, I would like to acknowledge my cooking students Barbara Heep and René Welker and my intern Stephan G. Wilke for their support.

I would like to thank my labmate Artem Skabeev, with whom I have enjoyed - in our small lab - *the bread and butter* of organic chemistry: "*bench time*"! Thanks for your valuable scientific discussions and insights either on my or your synthetic challenges, tedious purifications and troublesome reagents. It was a fantastic time!

Thanks to my office mates Jenny, Catarina, Katrin, Lisa, Eva, and Joe for the nice working atmosphere. Thanks to Leo for the interesting and inspiring conversations. I would especially thank Dr. Joseph Krumpfer for his helpful comments and valuable scientific discussions. I did learn a lot.

Last but definitely not least, I would like to thank the Müllen group for the great time. All the traditional activities throughout the years have made it a very exciting time.

Has there ever been a Thursday without Barbecue?

VIII. List of Publications

1. F. E. Golling, T. Schuster, C. Geidel, L. Mammen, D. Vollmer, K. Müllen, M. Klapper: "The Power of Perfluorinated Amphiphilic Polymers at Interfaces," *ACS Symposium Series* **2012**, *1106*, 111-126.

2. D. Joe, F. E. Golling, K. Friedemann, D. Crespy, M. Klapper, K. Müllen: "Anisotrop Supports in Metallocene-Catalyzed Polymerizations: Templates to Obtain Polyolefin Fibers," *Macromol. Mater. Eng.* **2014**, *299*, 1155-1162.

3. T. Schuster, F. E. Golling, J. W. Krumpfer, M. Wagner, R. Graf, A. A. Alsaygh, M. Klapper, K. Müllen: "Poly(isobutylene) Nanoparticles via Cationic Polymerization in Nonaquesous Emulsion," *Macromol. Rapid Commun.* **2014**, *DOI: 10.1002/marc.201400401*

4. F. E. Golling, M. Quernheim, M. Wagner, T. Nishiuchi, K. Müllen: „Concise Synthesis of 3D π-Extended Polyphenylene Cylinder, "*Angew. Chem. Int. Ed.* **2014**, *53*, 1525-1528.

5. M. Quernheim. F. E. Golling, W. Zhang, M. Wagner, J. Räder, T. Nishiuchi, K. Müllen: "The Precise Synthesis of Phenylene Extended Hexa-peri-hexabenzobronene Nanoring," *in preparation.*

6. F. E. Golling, A. Koch, G. Fytas, K. Müllen: "Rigid 1,4-Connected Cyclohexadiene Chains: Synthesis, Dynamic Light Scattering and DFT," *in preparation.*

7. F. E. Golling, M. Quernheim, M. Wagner, K. Müllen: "π-Extended [12]Cyclopara-phenylenes: from a Hexaphenylbenzene Cyclohexamer to its Unexpected C_2-symmetric Congener," *submitted.*

IX. Curriculum Vitae

Personal Details

Name	Florian Ernst Golling
Academic Title	Master of Science
Place of Birth	Gießen
Nationality	German

University Education

2008-2010 **M.Sc.** Technische Universität München & University of Toronto, Chemistry, Canada.
Thesis: "*Synthesis and Characterisation of New Siloxane-Bithiophene Telechels and their Alternating Copolymers*", Prof. Dr. Rieger, Chair for Macromolecular Chemistry, TU München.

2005-2008 **B.Sc.** Technische Universität München, Chemistry.
Thesis: „*Synthesis of Monoliths for Affinity Chromatography to Separate Bacteria",* Prof. Dr. Nießner, Institute for Analytical Chemistry, TU München.

School Education

1996-2008 **Abitur,** Stadtgymnasium Dortmund, Dortmund.

2002-2003 11th grade: Stay at Ridley College, St. Catharines, Canada.

1992-1996 Landgrafen Grundschule, Dortmund.

Presentations

July 2014 Student Seminar Prague, Czech Republic (Graduate School „MAINZ“) **Talk***: „Synthesis of Polyphenylene Cylinders: Precursors for a Bottom-Up Approach toward size-defined CNTs?”*, July 24-28, 20 min.

Aug 2013 Student Seminar Stockholm, Schweden (Graduate School „MAINZ“) **Talk***: „A Bottom-up Approach toward the Synthesis of size-defined CNTs”*, August 8-12, 20 min.

March 2012 8th Ziegler-Natta Colloquium, Kanazawa, Japan, March 27-30. **Talk**: „*Perfluorinated Emulsions for the Synthesis of Polyolefins”* 28.03.2012, 11:35-11.55.

Poster

Nov 2013 Retreat of the Graduate School „MAINZ“, Bad Dürkheim, November 18-20. **Title** „*Synthesis of Polyphenylene Cylinders: Precursors for the Bottom-up Synthesis of CNTs?*“ (19. November 2013).

Feb 2012 Makromolekulares Kolloquium, Freiburg, 23.02.2012 - 25.02.2012, **Title**: *„Design and Use of Fluorous Amphiphilic Polymers”*, (February 23).

Aug 2011 ACS Conference Denver, USA. **Title**: „*Design and Use of Fluorous Amphiphilic Polymers for Nanoparticles Formation*“; Section: „*Colloids“*(August 29).

Summer School

May 2013 Organic Electronics Summer School, Biarritz, France. May 29 – June 1.